OF 361

ANALYSIS OF THE SOCORRO HYDRO-GEOTHERMAL SYSTEM; CENTRAL NEW MEXICO

by

Margaret W. Barroll

Submitted in Partial Fulfillment of
the Requirements for the Degree of
Doctor of Philosophy

NEW MEXICO INSTITUTE OF MINING AND TECHNOLOGY
Socorro, New Mexico, 87801

November, 1989

ABSTRACT

Analysis of geothermal and hydrogeologic data from the Socorro area provides new insight into both the geothermal regime and ground-water flow system. New geothermal data from the Socorro geothermal area, originally obtained by industry investigators, further delineate a known geothermal high in the Socorro mountain block and reveal a profound geothermal low west of the mountain block in La Jencia Basin. Anomalously low heat flows in La Jencia Basin suggest ground-water downflow, but hydrologic and geothermal evidence indicate that infiltration of surface recharge is not significant in this area. We conclude that eastward flowing ground water is forced to flow down beneath a claystone aquitard in eastern La Jencia Basin, thus reducing near-surface heat flows. High heat flows in the Socorro mountain block occur in areas where relatively permeable volcanic rocks outcrop at the surface. We conclude that ground water flows upward in these locations where the claystone aquitard is missing, probably enhanced by subsurface barriers to horizontal flow, thus elevating near-surface heat flows. Upper crustal magma in the Socorro area (suggested by seismic evidence) may also contribute heat to the system.

A coherent, though very simple model of the Socorro hydrothermal system has been developed, in which upper crustal heat is redistributed by ground-water flow, without anomalous heat sources. Finite difference modeling of ground-water flow and heat transport was applied to an idealized two-dimensional cross-section of the Socorro hydrogeologic system. The modeling results demonstrate that the ground-water flow pattern that we have suggested is consistent with the hydrogeology of the Socorro area, and this hydrologic system could produce the geothermal anomalies observed in the Socorro area. Analysis of the heat balance of the Socorro system is also consistent with the hypothesis that anomalous crustal heat

sources need not play a substantial role in the Socorro geothermal system. It is possible, though, that substantial amounts of anomalous heat are hidden, advected out of the system by hydrologic underflow.

Acknowledgements

I thank my adviser, Dr. Marshall Reiter, for suggesting this study and for his help and encouragement. I also thank the other members of my advisory committee: Dr. Allan Gutjahr, Dr. Fred Phillips, Dr. Allan Sanford and Dr. John Schlue. I especially thank my husband, Hans Hartse, for his support and encouragement during this long process.

I acknowledge the N. M. Bureau of Mines and Mineral Resources for its generous support, and New Mexico Tech for use of computer facilities. I acknowledge the following individuals and organizations who originally acquired the data used in this study, and gave me permission to use and present this data, or who shared their copies of data with me: D. Blackwell, C. Chapin, J. Ni, R. Osburn, M. Reiter, A. Sanford, C. Swanberg, Chevron Resources Co., GeothermEx, Inc.; Phillips Petroleum Co., Sunoco Energy Devel. Co., and Thermal Power Company. I also thank a large number of other individuals who helped me track down obscure data. I thank Maureen Wilks for making measurements of the Ur and Th content of rock samples. Drafting was done by Becky Titus, Irean Rae, and Ellen Limburg.

I also thank Dr. Richard Chamberlin, Dr Geraldo Gross, Dr. Robert Lee and Dr. William Stone for many helpful discussions.

Table of Contents

List of Figures

Plates

Plates and plate captions located in back sleeve.

List of Tables

INTRODUCTION

The Socorro geothermal area (Figure 1 and Plate 1) is located in central New Mexico, within the Rio Grande rift, at the edge of the extensive Oligocene Mogollon-Datil volcanic field. Warm springs issue from the east edge of the Socorro mountain block (Figure 1), a Pliocene horst separating the Socorro Basin and La Jencia Basin. (In this discussion the "Socorro mountain block" includes parts of the Socorro-Lemitar-Chupadera mountain block, but we are most interested in the area between Socorro Canyon and Nogal Canyon; Figure 1.) Thermal waters are also found in the Blue Canyon Well, which is located west of the thermal springs, within the Socorro mountain block (BCW in Figure 3 and Plate 1; Summers, 1976). High air temperatures are observed in mine shafts within the Socorro mountain block. Extremely high temperature gradients have been measured within the mountain block, including a heat-flow measurement of 490 $mW\ m^{-2}$ (Reiter and Smith, 1977; Sanford, 1977), substantially higher than typical heat flows in the Rio Grande rift $75 - 100\ mW\ m^{-2}$ (Reiter et al., 1986). In 1976 the United States Geological Survey designated an area of 362 km^2 in and around Socorro as the Socorro Peak Known Geothermal Resource Area (Chapin et al., 1978). The extent of the geothermal anomalies near Socorro, and the source of the observed anomalous heat has been a subject of inquiry for a number of years. Summaries of previous investigations of the Socorro geothermal area are found in Chapin et al. (1978) and Hawkins and Stephens (1980).

Seismic data indicate that there is magma in the crust in the immediate vicinity of Socorro, both at mid-crustal levels ($\approx$20 km depth) and at upper crustal levels (possibly as shallow as 5 km depth) (Rinehart et al., 1979; Sanford, 1983). The mid-crustal magma body is extensive, $\approx$1700 km^2 in area, underlying most of the Socorro area. The southern boundary of the body is near Socorro Canyon

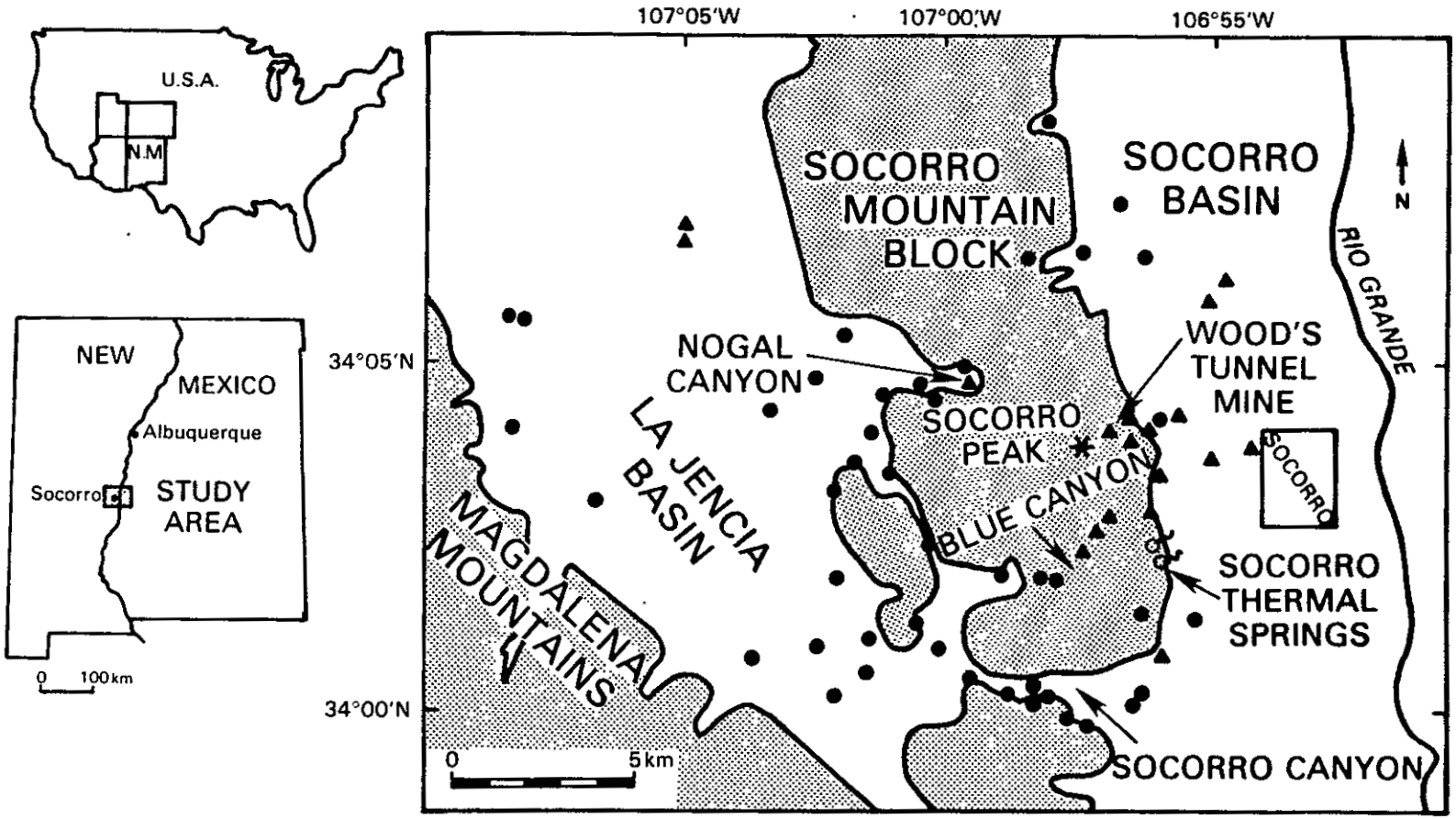

Fig. 1. Location map: Socorro geothermal study area, with data site locations. Triangles: data from previous studies. Circles: new geothermal data from industry sources. Socorro mountain block, as discussed in the present study, includes parts of the Lemitar and Chupadera mountain ranges, as well as Socorro Peak.

(Figure 1). Smaller, shallower magma bodies are suggested by seismically anomalous upper crustal volumes, and by local microearthquake swarms (Sanford, 1983). It has been suggested that upper crustal magma may contribute heat to the Socorro geothermal system (Chapin et al., 1978).

A number of investigators have suggested that subsurface temperatures within and near the Socorro mountain block are probably influenced by ground-water flow (Summers, 1976; Reiter and Smith, 1977; Sanford, 1977; Chapin et al., 1978). Harder et al. (1980) suggested that many geothermal anomalies along the Rio Grande rift are produced by forced convection (advection). It is possible that the geothermal anomalies observed at Socorro are the result of ground-water flow redistributing heat in a relatively normal geothermal regime (Reiter and Smith, 1977), and this possibility is the focus of this study.

In this study, we investigate the geothermal regime and subsurface hydrogeology of the Socorro area. A large set of geothermal data, originally obtained by industry investigators, is presented. These data, combined with geothermal data obtained by Reiter and Smith (1977) and Sanford (1977), describe the local geothermal regime in some detail. Important sources of geologic information about the Socorro area are unpublished lithologic logs by Chapin and Osburn, drillers logs, and an extensive study by Chamberlin (1980). Important sources of hydrologic and hydrogeologic information are studies by Anderholm (1987), Stone (1977) and Gross and Wilcox (1983). The geothermal data in conjunction with hydrogeologic information suggest certain subsurface hydrologic phenomena: downflow in La Jencia Basin and upflow in the Socorro mountain block. We propose a model for the Socorro hydrothermal system based on these findings. The model involves heat redistribution in the crust by ground-water flow, without the need of anomalous upper-crust heat sources.

Finite difference techniques are applied to the proposed model. Idealized cross-sections representing the Socorro hydrothermal system are modeled using a two-dimensional, steady-state code developed for this study. Hydrologic modeling verifies that the hydrologic system we propose is consistent with the hydrogeology of the Socorro area. Modeling of conductive and advective heat transport indicates that the geothermal anomalies observed in the Socorro area could be produced by this hydrologic flow system.

This study parallels work done by a number of other investigators such as Kilty et al. (1979), Severini and Huntley (1983) and Ingebritsen, (1989). These investigators have studied systems in which advection of heat by ground-water flow produces significant geothermal effects.

TERRESTRIAL HEAT FLOW

The study of terrestrial heat flow is the study of heat flow from the earth's interior. Heat flow (q_z) is defined by

$$q_z = -k_\Theta \frac{dT}{dz}$$

where k_Θ is the thermal conductivity of the medium, and z denotes vertical distance. In order to determine heat flow, measurements of both subsurface vertical temperature gradient and subsurface thermal conductivity are required.

Heat-flow data often give information relating to deep subsurface thermal and tectonic processes. In many cases, however, near surface disturbances are the dominant influence on near surface heat flows. Near surface heat sources, such as upper crustal magma may cause very high surface heat flow, masking the heat flow from deeper depths.

Hydrologic flow systems can also perturb near surface heat flows by advecting heat. The effect of vertical ground-water flow is illustrated in Figure 2. Hydrologic upflow elevates near surface temperature gradients and reduces deeper temperature gradients (Fig. 2b). Hydrologic downflow reduces temperature gradients near the surface (Fig. 2c).

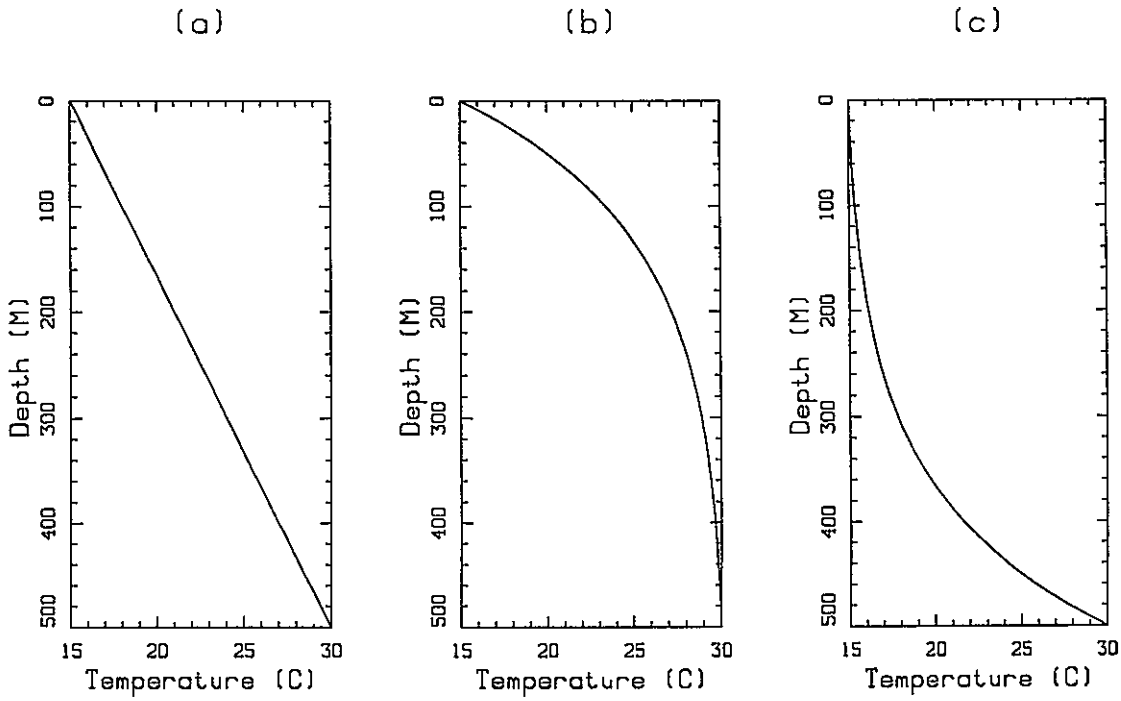

Fig. 2. Influence of vertical fluid flow on subsurface temperature. (a) undisturbed temperatures; (b) temperatures disturbed by fluid upflow; (c) temperatures disturbed by fluid downflow.

PREVIOUS STUDIES: SOCORRO GEOTHERMAL SYSTEM

Geothermal studies by Sanford (1977) and Reiter and Smith (1977) presented temperature logs from 18 sites in the Socorro area (Figures 1 and 3). The following discussion is taken from those two works. These investigators recorded subsurface temperatures from wells that ranged in depth from 20 to 110 m. High temperature gradients were measured at sites in the eastern part of the Socorro mountain block, in Blue Canyon and near Wood's Tunnel. A well drilled in Precambrian rock deep within Wood's Tunnel mine was collared $\approx$128 m below land surface, and extended to a total depth of $\approx$195 m below land surface. Extremely high temperature gradients were measured in this well: $130 - 287\ ^{o}C/km$. The thermal conductivity of core from the well was measured, and the heat flow in the well was determined to be $\approx$490 $mW\ m^{-2}$ (Reiter and Smith, 1977). Heat flows of $\approx$280 $mW\ m^{-2}$ were estimated in Blue Canyon (Sanford, 1977).

Temperature gradients were found to be much lower in adjacent Socorro Basin ($\approx 20 - 60\ ^{o}C/km$, neglecting gradients at depths less than 30 m). Temperature gradients in the basin appear to be somewhat higher at locations closest to the Socorro mountain block. Sanford (1977) suggested that the substantial decrease of temperature gradients east of the Socorro mountain block is caused by southward ground-water flow in Socorro Basin.

Both Sanford (1977) and Reiter and Smith (1977) have suggested the possibility that ground-water flow through the Socorro mountain block could advect heat out of the mountain block, masking anomalous heat sources. Alternatively, these investigators indicated that upward ground-water flow would advect heat to the surface, and such upward flow could enhance the influence of an anomalous heat source or else upflow would bring up heat from depth associated with the background geothermal gradient.

OVERVIEW OF GEOTHERMAL DATA, PRESENT STUDY

NEAR SURFACE HEAT FLOW

This study employs data from a number of industry geothermal well sites as well as data from Reiter and Smith (1977) and Sanford (1977). The locations of these sites and the numbering system employed in this study are shown in Figure 3 and Plate 1. The industry data set consists of subsurface temperature profiles from 49 industrial geothermal wells, and drill cuttings from most of those wells. These wells were drilled between 1978 and 1980. The wells range in depth from about 75 to 600 m, and are typically $\approx$150 m deep. Several different companies were involved in drilling and logging temperatures in these wells, and little information is available concerning well construction. Chapin (unpublished) and Osburn (unpublished) made lithologic logs for most of these wells from drill cuttings, and we have used these logs extensively in this study. We have also included temperature logs from the sites presented by Reiter and Smith (1977), and Sanford (1977). Drill cuttings and lithologic logs (by Foster, unpublished) were available for a number of these sites (mostly wells from Sanford, 1977).

Thermal conductivities (k_Θ) were measured using the steady-state method described by Reiter and Hartman (1971), applied to drill cuttings by the technique described by Sass et al. (1971). In addition to our own laboratory measurements, some k_Θ measurements made by industry investigators were available. See Appendix C for further discussion of thermal conductivity measurement.

Heat flows were determined at sites from which temperature data have been obtained at depths greater than 30 m, and thermal conductivity data exist or can be estimated (see Appendix B for a more detailed discussion of heat-flow determination). The heat-flow determinations are plotted and contoured in Figure 4, and

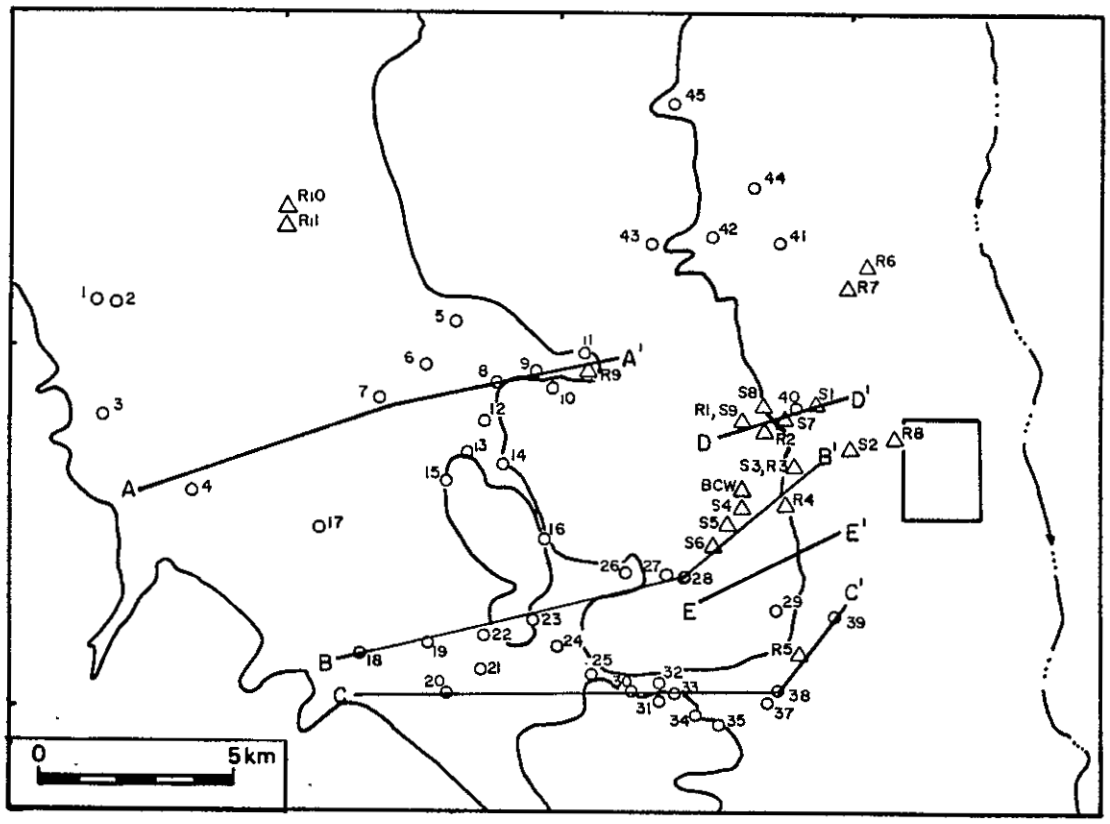

Fig. 3. Map of the Socorro Geothermal area. Wells shown with circles are from the industrial geothermal data set obtained between 1978 and 1980. Wells shown with triangles are from earlier studies. Numbers or letters and numbers are for well identification. Identification codes beginning with R are from Reiter and Smith (1977). Identification codes beginning with S are from Sanford (1977). Locations of cross sections are shown by lines AA', BB', CC', DD', and EE'.

presented more fully in Table 1. In many cases, heat flow varies somewhat with depth within a well. If heat flow did not vary greatly, and if the temperature depth profile did not seem extremely perturbed, we took either a mean value or the value of heat flow from the deeper part of the well. The uncertainty of most heat-flow determinations is $\approx 10-20$ percent (see Appendices A and B, and Table 1).

Some wells have extremely distorted temperature depth profiles. Temperature logs from most of the deeper wells are extremely perturbed; these logs have isothermal zones and negative gradients occasionally occur. Such extreme features in a temperature depth profile suggest fluid flow in the borehole. Similar profiles were observed at the Beoware Geothermal field, Nevada; Smith (1983) suggested that these temperature disturbances were produced by thermal fluids welling up in the well bore annulus. It is difficult to determine a representative temperature gradient for such wells. We calculated an average geothermal gradient and estimated heat flow for disturbed wells from the bottom hole temperature of the well and an estimated surface temperature (see Appendix B and Table 1). These heat-flow estimates are denoted by astericks in Figure 4, and are not considered as reliable as the other data.

The heat-flow data in Figure 4 show not only great variability, but also interesting trends. High heat flows are found in parts of the Socorro mountain block. Extremely high heat flows are found in the vicinity of Wood's Tunnel (490 $mW\ m^{-2}$, Reiter and Smith, 1977), and in Blue Canyon and Socorro Canyon ($225-260\ mW\ m^{-2}$). It is uncertain whether these high heat flows are part of a continuous zone (as contoured in Figure 4) or several discrete anomalous areas. Heat flows elsewhere in the Socorro mountain block are more typical of Rio Grande rift values ($75-100\ mW\ m^{-2}$), although there are a few scattered low

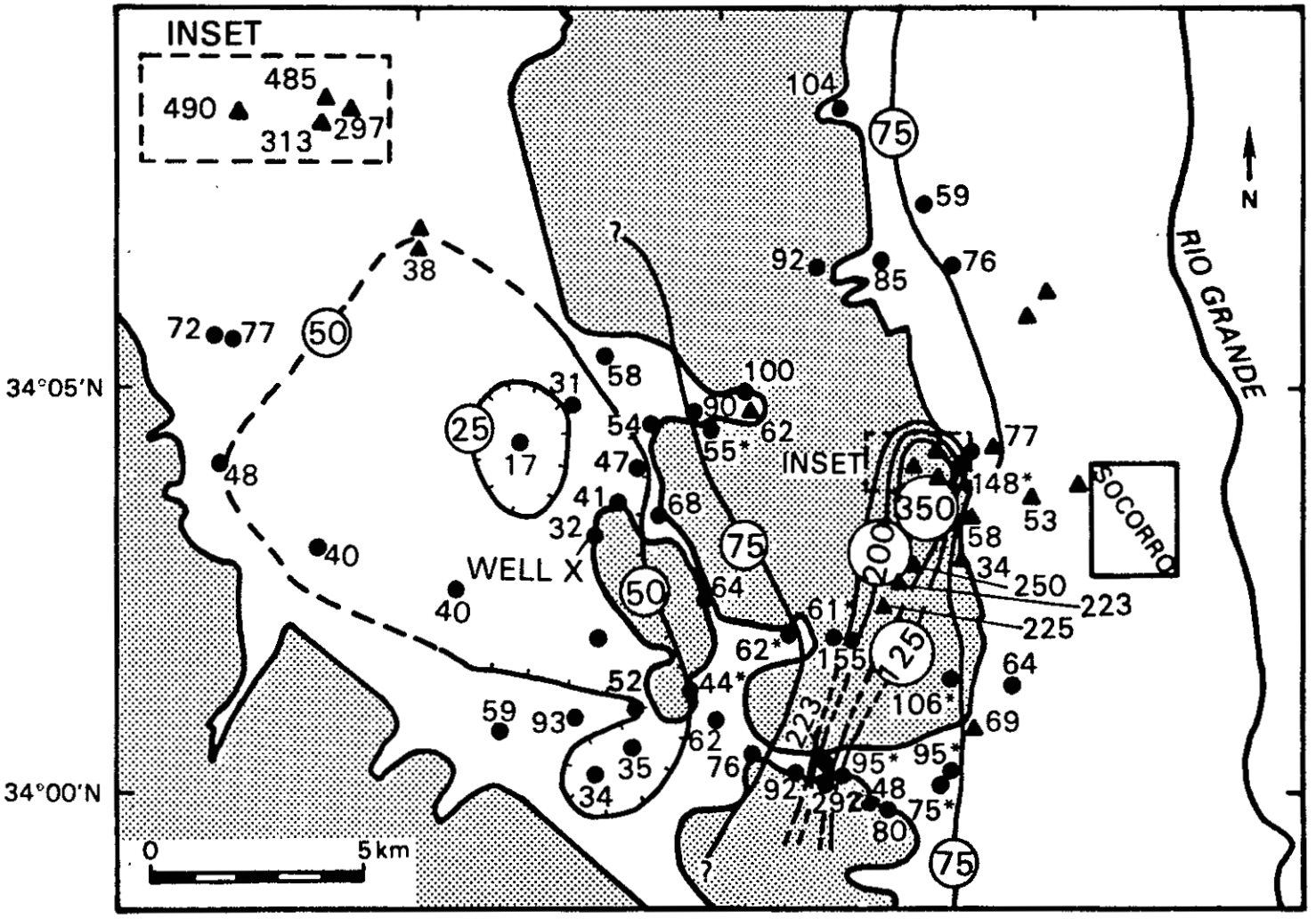

Fig. 4. Heat-flow contour map. Heat flows given in $mW\ m^{-2}$ (1 $HFU = 41.84\ mW\ m^{-2}$). Note magnified inset of Wood's Tunnel area. The uncertainties of the heat-flow determinations range from 10% to 20%, except for heat-flow estimates (indicated by *) which have higher uncertainty. Circled numbers are contour labels and contours are dashed where data is sparse. Note that contour interval varies between 25 and 150 $mW\ m^{-2}$ depending on location.

TABLE 1

HEAT FLOW: SOCORRO GEOTHERMAL AREA

Well Number	Depth Interval (m)	(m)	$\Gamma \pm \Delta\Gamma$ $\frac{^\circ C}{km}$		k_Θ $\frac{W}{m^\circ C}$	$q_i \pm \Delta q_i$ $\frac{mW}{m^2}$		$q \pm \Delta q$ $\frac{mW}{m^2}$	
1	21.3	97.5	38.9	.3	1.86	72	10	72	10
2	15	89	39.5	.9	1.95	77	13	77	13
3	15.2	27.4	64.5	.5	1.73	112	15		
	27.4	45.7	39.6	2.5	1.79	71	17		
	45.7	85.3	26.9	.2	1.79	48	9	48^D	9
4	21.3	39.6	29.0	.4	1.60	46	6		
	39.6	61.0	16.7	.4	1.60	27	4		
	67.1	94.5	23.2	.3	1.60	37	4	40	5
5	30.5	91.4	24.8	.1	1.54	38	7		
	94.5	149.4	33.7	.3	1.73	58	6	58^D	6
6	61.0	149.4	16.9	.1	1.86	31	3	31	3
7	21.3	45.7	10.5	.4	1.81	19	5		
	64.0	73.2	2.9	.2	1.81	5.2	2		
	76.2	106.7	9.4	.3	1.81	17	4	17^D	4
8	18.3	88.4	25.6	.2	1.86	48	5		
	97.5	146.3	32.1	.1	1.86	60	6	54	6
9	27.4	100.6	46.3	.3	1.72	80	10		
	103.6	140.2	57.6	.3	1.72	99	13	90	12
10	54.9	243.8	51.5	.2	1.53	79	9		
	268.2	347.5	13.2	.3	1.87	25	3		
	347.5	585.2	32.1	.4	1.70	55	6		
	0.0	591.3	32.8*		1.68			55*	

TABLE 1 (Continued)

Well Number	Depth Interval (m)		$\Gamma \pm \Delta\Gamma$ $\frac{^\circ C}{km}$		k_Θ $\frac{W}{m^\circ C}$	$q_i \pm \Delta q_i$ $\frac{mW}{m^2}$		$q \pm \Delta q$ $\frac{mW}{m^2}$	
11	24.4	61.0	20.4	.2	1.65	34	4		
	64.0	91.4	42.4	1.2	1.65	70	9		
	94.5	128.0	54.9	.2	1.66	91	9		
	128.0	149.4	62.4	.6	1.66	104	10	100[D]	10
12	15.2	76.2	24.1	.2	1.74	42	5		
	82.3	149.4	29.9	.2	1.74	52	6	47	5
13	30.5	152.4	23.0	.3	1.77	41	5	41	5
14	27.4	143.3	42.5	.1	1.59	68	7	68	7
15	91.4	579.1	18.3	.1	1.74	32	3	32	3
16	12.2	152.4	39.7	.2	1.60	64	6	64	6
17	30.0	60.0	25.1	1.5	1.60	40	8	40	8
18	30.5	64.0	36.0	.2	1.48	53	9		
	67.1	91.4	43.3	.3	1.48	64	11	59	10
19	170.7	219.5	39.5	.4					
	249.9	408.4	44.9	.3	2.1	93	12	93	12
20	21.3	94.5	14.2	.2	1.65	23	4		
	94.5	109.7	20.6	.5	1.65	34	6	34[D]	6
21	18.3	42.7	-.9	.8	1.38	1.2			
	61.0	137.2	28.5	.4	1.23	35	4	35[D]	4
22	51.8	88.4	16.2	.2	1.61	26	3		
	106.7	149.4	30.7	.3	1.71	52	5	52[D]	5

TABLE 1 (continued)

Well Number	Depth Interval (m)	(m)	$\Gamma \pm \Delta\Gamma$ $\frac{^oC}{km}$		k_Θ $\frac{W}{m^oC}$	$q_i \pm \Delta q_i$ $\frac{mW}{m^2}$		$q \pm \Delta q$ $\frac{mW}{m^2}$	
23	85.3	335.3	37.8	.2	1.49	56	6		
	353.6	463.3	26.7	.5	1.67	45	5		
	487.7	579.1	13.6	.3	1.77	24	3		
	0.0	585.2	27.9*		1.58			44*	
24	18.3	57.9	36.0	.4	1.6	58	6		
	61.0	137.2	41.1	.2	1.6	66	6	62	6
25	33.5	79.2	49.0	.2	1.6	78	10		
	82.3	149.4	42.0	.5	1.79	75	12	76	10
26	182.9	371.9	60.9	.3	1.58	96	12		
	378.0	408.4	33.1	.6	1.60	53	7		
	414.5	524.3	.5	.4	1.60	0.8			
	530.4	554.7	24.6	1.4	1.58	39	7		
	0.0	573.0	39.1*		1.59			62*	
27	18.3	371.9	50.1	.2	1.58	79	9		
	408.4	530.4	32.3	.4	1.54	50	6		
	542.5	585.2	.9	1.8	1.89	1.7			
	0.0	585.2	38.6*		1.58			61*	
28	18.3	67.1	94.5	1.1	1.75	165	18		
	79.2	121.9	80.2	.7	1.78	143	17	155	19
29	36.6	85.3	60.3	1.5	1.58	95			
	97.5	140.2	40.6	.5	1.58	64			
	0.0	146.3	66.4*		1.6			106*	
30	36.6	140.2	53.8	.4	1.71	92	9	92	9
31	12.2	54.9	159.5	2.1	1.83	292	32	292	32

TABLE 1 (Continued)

Well Number	Depth Interval (m)	(m)	$\Gamma \pm \Delta\Gamma$ $\frac{^\circ C}{km}$		k_Θ $\frac{W}{m^\circ C}$	$q_i \pm \Delta q_i$ $\frac{mW}{m^2}$		$q \pm \Delta q$ $\frac{mW}{m^2}$	
32	9.1	42.7	176.6	3.0	1.78	314	44		
	45.7	73.2	139.1	.8	1.6	223	22	223[D]	22
33	18.3	48.8	97.8	.7	1.45	142	20		
	48.8	88.4	74.6	.7	1.45	108	15		
	91.4	118.9	42.5	.6	1.45	62	9		
	140.2	152.4	5.5	.7	1.45	8	1		
	0.0	152.4	65.8*		1.45			95*	
34	24.4	85.3	31.1	.2	1.49	46	7		
	106.7	146.3	33.4	.2	1.49	50	8	48	6
35	27.4	88.4	44.5	.3	1.66	74	7		
	91.4	137.2	51.6	.2	1.66	86	8	80	8
36	21.3	70.1	48.6	.9	1.81	88	11	88	11
37	79.2	115.8	41.0	1.4	1.57	64	10		
	121.9	256.0	63.5	.4	1.58	100	12		
	256.0	298.7	85.4	1.9	1.57	134	16		
	317.0	408.4	11.7	.7	1.54	18	3		
	0.0	399.3	48.0*		1.57			75*	
38	19.8	42.7	71.9	1.1	1.70	122	24		
	48.8	85.3	58.6	.4	1.49	87	10		
	91.4	115.8	43.7	.8	1.49	65	8		
	121.9	140.2	65.6	2.7	1.54	101	23		
	0.0	141.7	61*		1.56			95*	
39	36.6	79.3	36.8	.7	1.75	64	8	64	8

TABLE 1 (Continued)

Well Number	Depth Interval (m)	(m)	$\Gamma \pm \Delta\Gamma$ $\frac{^oC}{km}$		k_Θ $\frac{W}{m^oC}$	$q_i \pm \Delta q_i$ $\frac{mW}{m^2}$		$q \pm \Delta q$ $\frac{mW}{m^2}$	
40	12.2	42.7	118.0	2.8	1.51	178	27		
	48.8	85.3	97.1	1.9	1.69	164	23		
	85.3	115.8	66.6	2.5	1.79	119	19		
	0.0	121.9	89*		1.66			148*	
41	21.3	51.8	47.0	.3	1.71	80	15		
	57.9	97.5	41.9	.2	1.71	72	13	76	14
42	18.2	76.2	53.4	.1	1.59	85	14	85	14
43	15.2	152.4	55.1	.5	1.68	92	9	92	9
44	12.2	24.4	54.1	.7	1.51	82	14		
	27.4	67.1	38.5	.2	1.52	59	10	59[D]	10
45	9.1	73.2	72.5	.2	1.43	104	9	104	9
46	15.2	33.5	71.1	.5	1.58	112	13		
	33.5	82.3	59.6	.1	1.58	94	10		
	82.3	125.0	55.8	.1	1.58	88	10	91[D]	10
47	24.4	76.2	23.7	.1	1.46	35	5	35	5
48	24.4	85.3	37.1	.6	1.89	70	15	70	15
49	21.3	91.4	26.7	.7	1.86	50	7	50	7

Table 1. Heat-Flow Determinations: Socorro Geothermal Area. Well numbers correspond to numbers in Figure 3 and Plate 1. This table gives temperature gradient and the standard deviation of the temperature gradient (Γ and $\Delta\Gamma$), thermal conductivity (k_Θ) and heat flow and uncertainty in heat flow (q_i and Δq_i) for listed depth intervals in each well. The final column ($q \pm \Delta q$) gives the best value of heat flow for each well, and the estimated uncertainty (see Appendix B). Heat-flow values marked by an asterick are heat-flow estimates made using maximum recorded temperatures, total well thermal conductivities and estimated surface temperatures as described in Appendix B. Heat-flow values marked by a "D" are taken from the deeper part of the well.

values ($34 - 62\ mW\ m^{-2}$).

Extremely low heat flows are found in La Jencia Basin. Heat flows are less than $50\ mW\ m^{-2}$ in most of the part of La Jencia Basin included in this study, and a number of heat flows are near or below $30\ mW\ m^{-2}$. These heat-flow values are far below typical Rio Grande rift heat flows ($\approx 75 - 90\ mW\ m^{-2}$; Reiter et al., 1986). Many of the heat flows measured in La Jencia Basin are lower than typical values for cool, stable continental areas ($35 - 65\ mW\ m^{-2}$, Lachenbruch and Sass, 1977). A profoundly low heat-flow anomaly occurs at and near Well 7 in eastern La Jencia Basin. The near-surface heat flow at Well 7 is $17\ mW\ m^{-2}$ (determined from a somewhat distorted temperature-depth profile; see Appendix B), and heat flows of 31, 32, 41 and $47\ mW\ m^{-2}$ occur nearby. In the southernmost part of La Jencia Basin, heat flows of $34\ mW\ m^{-2}$ and $35\ mW\ m^{-2}$ are observed. Heat flows at the borders of La Jencia Basin, near the Magdalena and Socorro mountain blocks are usually somewhat higher. Along the Magdalena mountain front, heat flows range from 40 to $77\ mW\ m^{-2}$, still somewhat low for the Rio Grande rift.

Industry geothermal data from Socorro Basin are consistent with the data presented by Sanford (1977) and Reiter and Smith (1977). Heat flows in Socorro Basin are rather low, increasing somewhat with proximity to the Socorro mountain block.

Heat flows in the Socorro geothermal area vary greatly over very short horizontal distances. The high heat flows at Wood's Tunnel are only $\approx 10\ km$ from the lowest heat flows of La Jencia Basin, and less than $\approx 5\ km$ from areas of low to average heat flow in the Socorro Basin. The high heat flows of Socorro Canyon are only $\approx 5\ km$ from heat flows of $\approx 35\ mW\ m^{-2}$ in La Jencia Basin. Because heat flows change dramatically over such short distances, the phenomena

controlling the heat-flow anomalies must be very shallow, i. e., in the upper crust.

The extremely low heat flows in La Jencia Basin suggest the presence of downward ground-water flow. Hydrologic perturbations are also suggested by the variation of heat flow with depth in many of the wells in the Socorro area. High heat flows ($>100\ mW\ m^{-2}$) are only observed at depths shallower than 200 m, which is consistent with the hypothesis that the high gradients are a result of hydrologic upflow (See Figure 2). Unfortunately, deep data have not been obtained from the areas of highest heat flow. The highest heat flows ($>200\ mW\ m^{-2}$) are observed only in wells of relatively shallow depth, less than 100 m (except at the Wood's Tunnel site which is deeper than 100 m, but almost entirely above the water table).

SUBSURFACE GEOLOGIC AND TEMPERATURE DATA

As part of this study, we have made generalized geologic cross sections (Plates 2,3 and 4 and Figs. 10 and 13) through the study area at locations indicated on Figure 3 (AA',BB',CC', DD' and EE'). The cross sections are constructed using information from cross sections in Chamberlin (1980) and from lithologic logs from the geothermal wells of this study. We have had access to lithologic logs of geothermal wells made by C. Chapin, G. Osburn, R. Foster, as well as driller's logs from a number of wells. More detailed discussion of the origins, stratigraphic and structural relationships and hydrologic characteristics of the different geologic units is found in the following Geology and Hydrogeology sections.

Subsurface temperature contours from geothermal well data are superimposed on the generalized geology of these cross sections (except for cross section EE'). Temperature contours show the large variation in the subsurface geothermal

regime that occurs over relatively short horizontal distances. Some of the deepest wells included in the cross sections (26 and 27) have distorted temperature profiles indicative of borehole flow, and therefore, some of the temperatures measured within these wells may not represent formation temperatures. Temperature profiles in these wells are suggestive of fluid upflow from sources near the bottom of the well, and we suggest that in these cases the bottom hole temperatures are the most reliable. Estimated "corrected" subsurface temperatures are calculated for two of these wells (by assuming linear temperature variation between the maximum recorded temperature and an estimated surface temperature) and "corrected" temperature contours are indicated by dotted lines in Plate 3, cross section BB'. (See Appendix B and Table 1 for more information on estimated heat flows and surface temperatures from greatly distorted temperature-depth profiles.)

Temperatures below the bottom of a well are extrapolated from the bottom hole temperature using the most representative temperature gradient of that well. Where this procedure appears to be highly uncertain, we have dashed the temperature contours.

Subsurface temperature data from these cross-sections (AA',BB' and CC') show the same trends as the surface heat-flow data. Subsurface temperatures are elevated within the Socorro mountain block and depressed in La Jencia Basin. Cross-sections BB' and CC' show the anomalously high subsurface temperatures found in certain locations of the Socorro mountain block. The most elevated subsurface temperatures occur in upfaulted blocks of volcanic rock (wells S4, S5, S6 and BCW in cross-section BB', wells 31 and 32 in CC'). The anomalously low subsurface temperatures and temperature gradients of La Jencia Basin are most clearly shown in cross section AA'. The most depressed subsurface temperatures occur in and near a thick claystone unit (Wells 7, 15 and 6). Before we discuss

these cross-sections further, it is necessary to present some information on the geology and hydrology of the Socorro area.

GEOLOGY AND HYDROGEOLOGY

GEOLOGY

The Tertiary geologic history of the Socorro area can be briefly summarized in accordance with Chamberlin (1980) Chapin et al. (1978), and Bruning (1973). Extensive volcanism covered much of southeastern New Mexico in early Tertiary times. The north-eastern extremity of the Oligocene Datil-Mogollon volcanic field is the Socorro Cauldron which formed about 27 ma (Figure 5), during the early stages of the development of the Rio Grande rift. The Datil-Mogollon volcanic field consists of numerous interlocking and overlapping cauldrons which produced voluminous ash-flows. Large down-dropped cauldron structures were filled with thick volcanic and volcaniclastic deposits; such deposits were considerable thinner outside of cauldrons. For purposes of discussion all cauldron-related volcanic units and any pre-cauldron Tertiary volcanic rocks are referred to as "early Tertiary" volcanic rocks in this study.

Cauldron volcanism subsided in early Miocene times and a broad sedimentary basin developed, the Popatosa basin. Sedimentary units possibly in excess of 1000 m were deposited; these are now known as the Popatosa Formation. The lower Popatosa Formation consists of mudflows, volcaniclastic materials and other sedimentary rocks (now very well indurated). The upper Popatosa Formation consists of sediments associated with the playa lake which formed in the central part of the Popatosa basin. The playa lake was centered, approximately, at the location of the present day Socorro mountain block; a thick claystone unit was deposited in

this area. Fanglomerates were deposited near sediment source areas, such as the present Magdalena Mountains. Volcanism recrudesced in late Miocene times; volcanic flows and domes became interbedded with Popatosa lacustrine sediments. A hydrothermal system was probably active at this time. The existence of this hydrothermal system is indicated by extensive potassium metasomatism observed in lower Popatosa rocks and early Tertiary volcanic rocks (Chapin et al., 1978).

Block faulting disrupted the Popatosa basin between 7-4 Ma, producing the present topography. The Socorro-Lemitar mountain block, an intra-graben horst, was upfaulted out of central Lake Popatosa. The Magdalena Mountains, already relatively high, were elevated further. The existence of recent fault scarps in the Socorro area indicates that block faulting continues into present times. Sedimentary deposits eroded from these mountain blocks have been deposited in Socorro and La Jencia basins. The Sierra Ladrones Formation is composed of these sediments, ancestral Rio Grande deposits in the Socorro Basin, and basaltic lavas that were erupted in the Socorro area about 4 Ma (Bachman and Mehnert, 1978). The Popatosa Formation and Sierra Ladrones Formation (and interbedded volcanic units) comprise the Santa Fe group. More recent sedimentary deposits are referred to as "post Santa Fe Alluvium". In this study volcanic rocks from the late Miocene and the more recent basalts are referred to as "late Tertiary" volcanic rocks.

Figure 5 is a generalized geologic map of the study area. The outlines of the mountain blocks as drawn generally correspond to the limits of surface exposure of upper Popatosa Formation and older rocks that comprise the mountain block. Units older than the upper Popatosa Formation are represented by patterns. A generalized geologic column for the Socorro area, showing the units of interest in this study, is shown in Figure 6. More detailed geology and geologic history can be found in Bruning (1973), Chapin et al. (1978), and Chamberlin (1980).

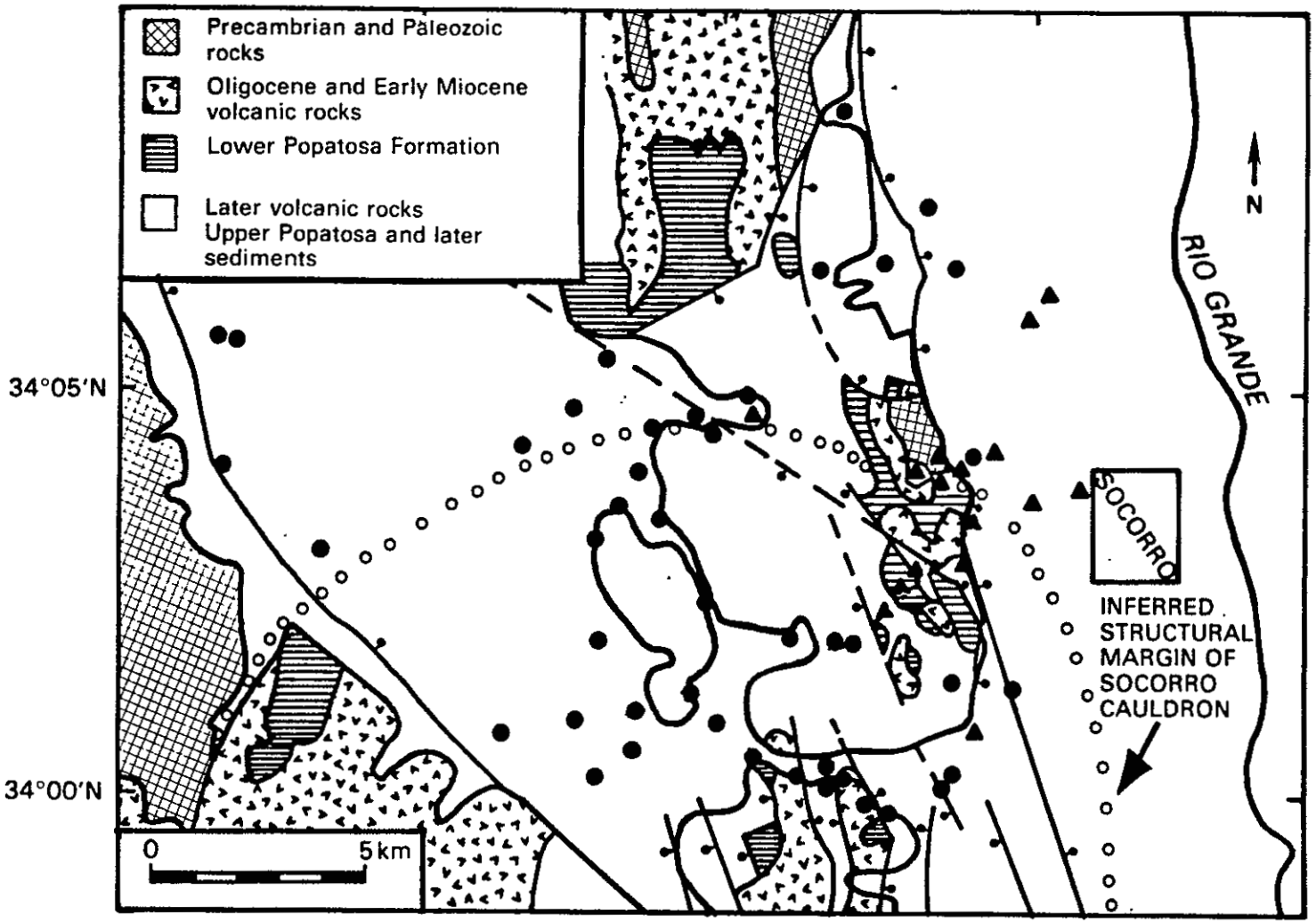

Fig. 5. Generalized geologic map of the study area showing features of interest, after Chapin et al., 1978. Note outcrops of Precambrian, Paleozoic and early Tertiary volcanic rocks, and Lower Popatosa formation in the Socorro mountain block. Some faults included with downthrown sides marked. Outlines of mountain blocks roughly corespond to the limits of Popatosa and pre-Popatosa outcrop.

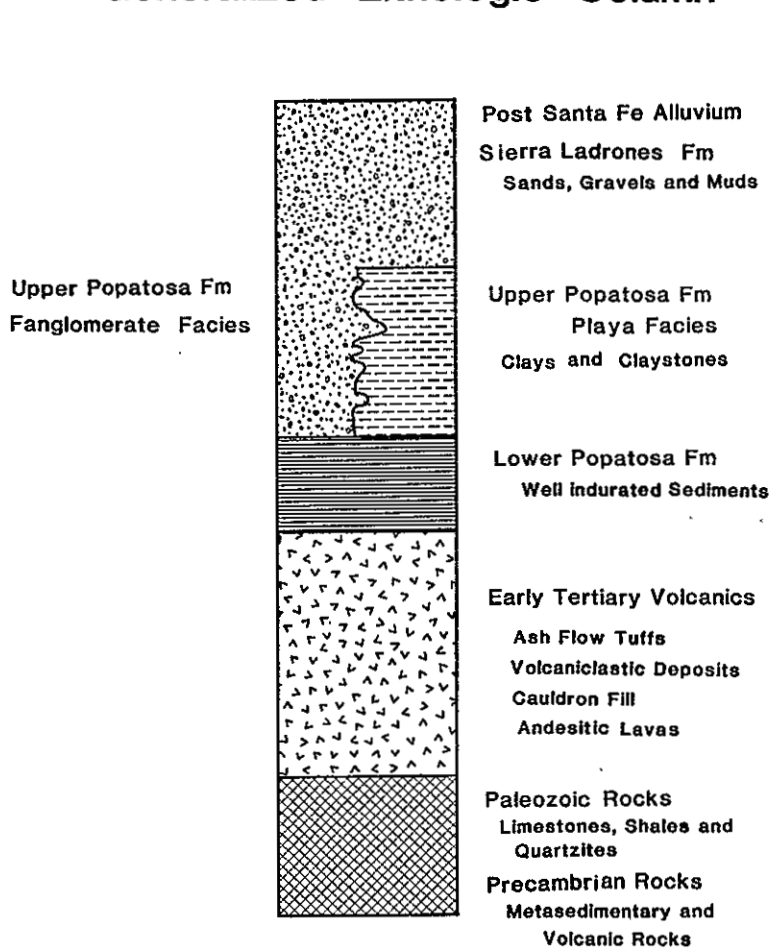

Fig. 6. Generalized geologic column of the Socorro area. Summarized from Chamberlin (1980) and Chapin et al (1978).

The Socorro area is structurally complex. Pliocene block faulting cuts across older cauldron structures. Block faulting exposes Precambrian and Paleozoic rocks at the surface in the Socorro mountain block north of the northern boundary of the Socorro caldera. Within the caldera, in the southern Socorro-Lemitars mountains, thick early Tertiary volcanic rocks and Popatosa claystones are exposed at the surface while Precambrian and Paleozoic rocks are buried at unknown depths beneath the surface (see Figure 5). Similarly, in the Magdalena Mountains, Early Tertiary volcanic rocks are exposed within caldera boundaries in the southern part of the range, and Precambrian rocks are exposed at the surface north of caldera boundaries. The geologic structure of the Socorro area is more fully detailed in Chapin et al. (1978), Chamberlin (1980), and Eggleston et al., (1983).

HYDROGEOLOGY

The Socorro area is semi-arid, receiving ~24 centimeters of precipitation a year in the town of Socorro, and roughly twice that amount in the Magdalena Mountains (Gabin and Lesperance, 1977; Hawkins and Stephens, 1981). Most precipitation occurs in the late summer in the form of violent thunderstorms. Recharge occurs predominantly in and near the mountain blocks, especially the Magdalena Mountains. (Anderholm, 1987). Dewey estimated that the total recharge to La Jencia Basin from the Magdalena Mountains is an order of magnitude greater than the total recharge in and near the Socorro mountain block (Anderholm, 1987). The large difference in total recharge is probably a result of the difference in precipitation, the much larger total area of the Magdalena Mountains, and the lower potential evapotranspiration in the Magdalena Mountains, caused by cooler air temperatures (Gabin and Lesperance, 1977).

A generalized sketch of water table elevation data, based on Stone (1977), is shown in Figure 7. Subsurface flow directions, at least at shallow depths, can be estimated assuming that horizontal ground-water flow is roughly perpendicular to water level contours. Note that the water table elevation is much higher in La Jencia Basin than in the Socorro Basin, and therefore ground water tends to flow from La Jencia Basin into the Socorro Basin.

The Socorro Basin is part of the Rio Grande drainage in which ground water generally flows from north to south. The Socorro Basin is separated from La Jencia Basin by the Socorro mountain block. Ground water in La Jencia Basin recharges in and near the Magdalena Mountains, and flows (roughly) south-west to north-east in the basin subsurface (Stone, 1977). Some ground water flows through the Socorro mountain block into the Socorro Basin. Figure 8 illustrates the flow of ground water through La Jencia Basin and the Socorro mountain block, as suggested by Gross (1981). Flow through Socorro mountain block is thought to occur (for the most part) in early Tertiary volcanic rocks, perhaps preferentially through more permeable fractured zones such as Socorro and Nogal Canyons (Anderholm, 1987). It has been suggested by a number of investigators that the movements of fluids in and near the Socorro mountain block is largely controlled by fractures (Chapin et al., 1978; Hawkins and Stephens, 1981).

There appear to be three basic types of hydrologic units in this area (see Figure 6). Firstly, there are poorly consolidated sediments which have a high matrix permeability: gravels, sands, and muds of the late Tertiary Sierra Ladrones Formation and post Santa Fe alluvium, and the fanglomerate facies of the Popatosa Formation. The principle aquifer of the Socorro area is composed of relatively unconsolidated sediments of this type (Anderholm, 1987).

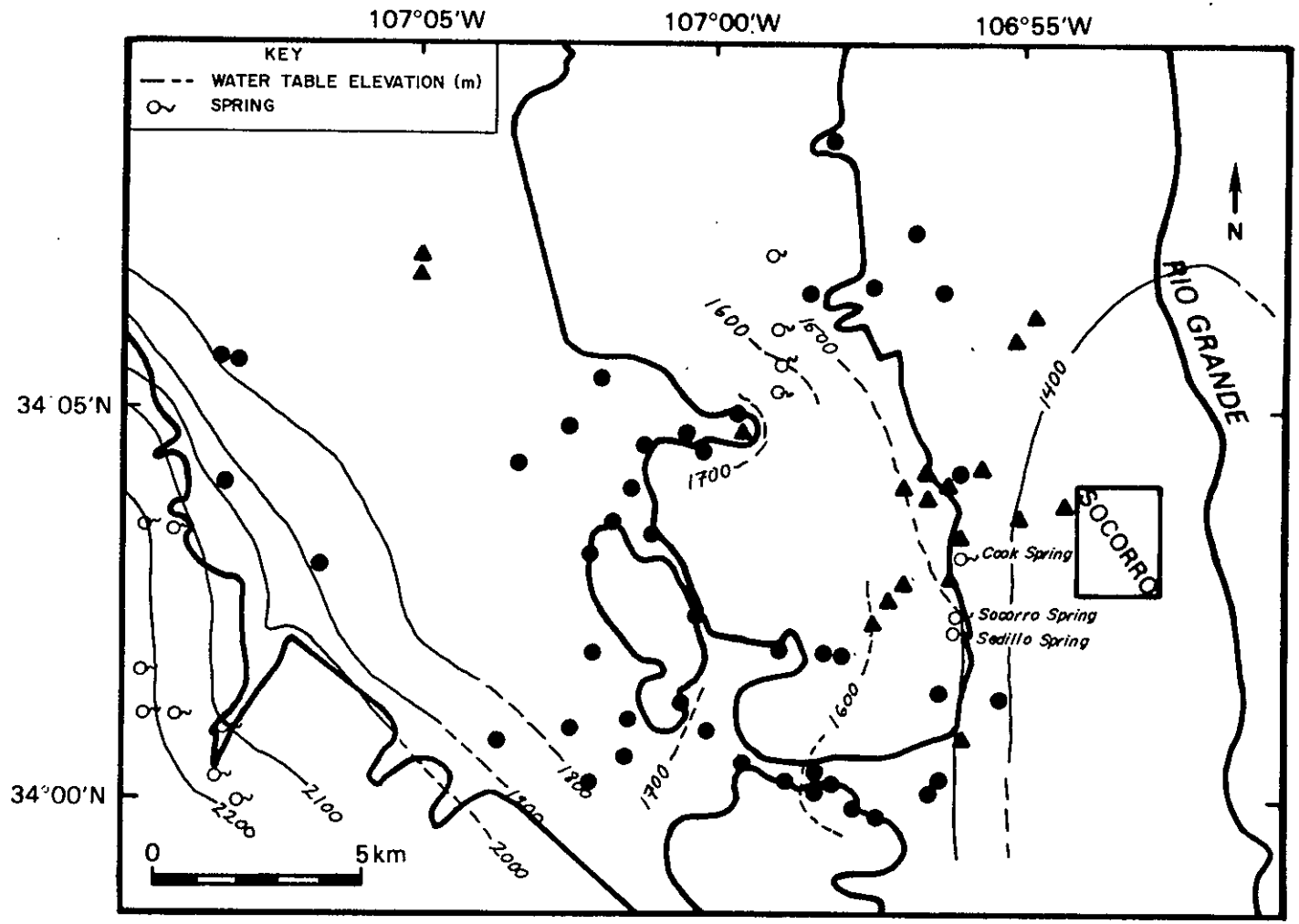

Fig. 7. Generalized water-level contour map of the Socorro area, after Stone (1977).

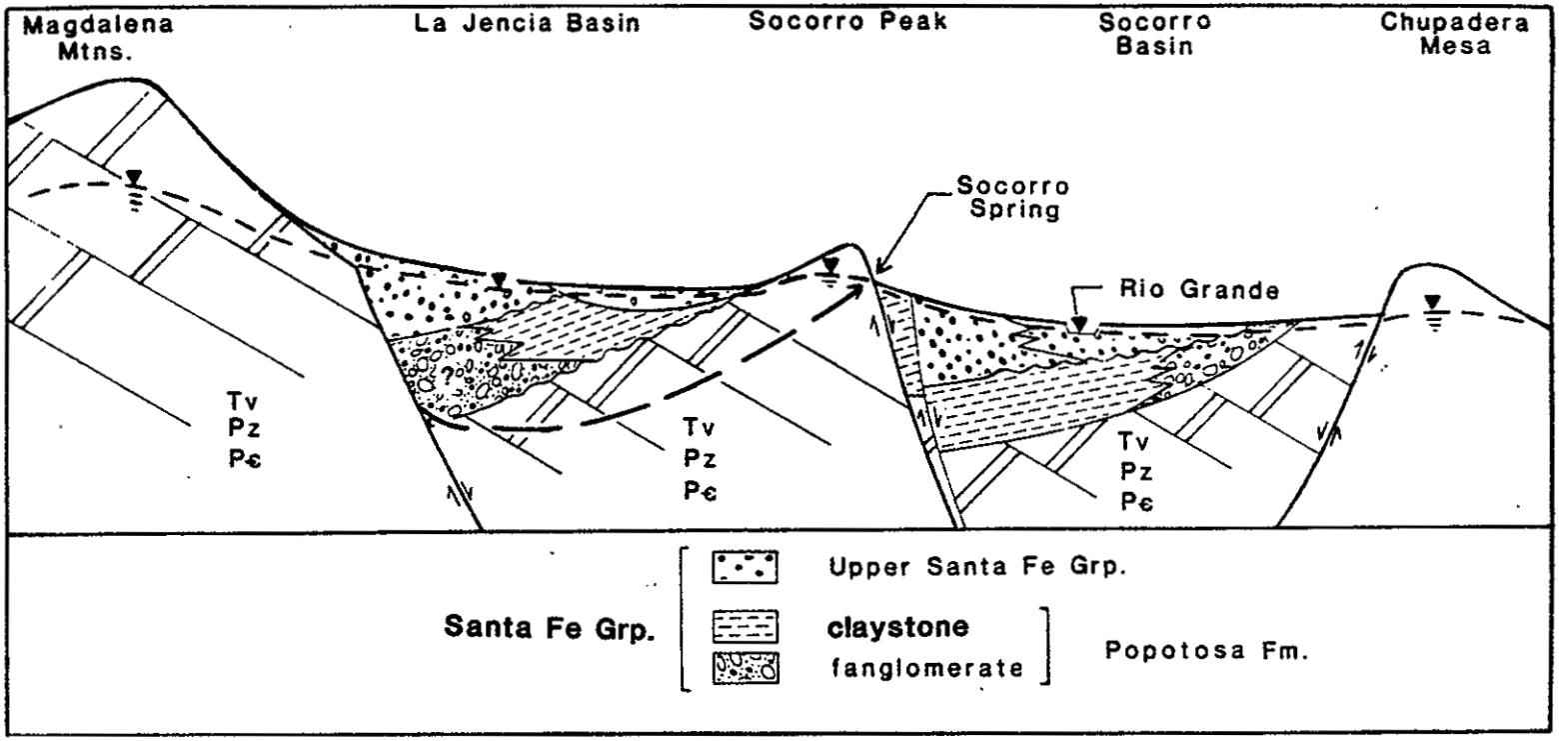

Fig. 8. Generalized hydrogeologic cross section through the Socorro geothermal area, after Gross and Wilcox (1983).

Secondly, there are a number of different types of hard rock which may have relatively high fracture permeabilities: Tertiary volcanic rocks, highly indurated sedimentary rocks, and Paleozoic and Precambrian rocks (Chapin et al., 1978; Anderholm, 1987). Early Tertiary volcanic rocks comprise a secondary aquifer in the Socorro area. These rocks may have served as a reservoir for an ancient (late Miocene?) geothermal system and are thought to transmit water through the Socorro mountain block at the present time (Chapin et al., 1978; Anderholm, 1987). Thermal and non-thermal springs issue from fractures in the well-indurated sedimentary rocks of the Lower Popatosa formation, which indicates that this unit, where fractured, has a relatively high permeability (Chamberlin, 1980). Precambrian and Paleozoic rocks may also have substantial fracture permeability, especially near fracture zones (Anderholm, 1987).

The third major hydraulic unit in the Socorro area consists of clays and moderately indurated upper Popatosa Formation playa claystones. The matrix permeability of clayey material is naturally low (Freeze and Cherry, 1979), and the fracture permeability of clays and claystones is also probably very low. Upper Popatosa claystones become ductile when wet, and therefore it appears likely that any fractures that form in the claystone below the water table would heal. Popatosa claystones are thought to act as an aquitard in the Socorro area (Anderholm, 1987; Chapin, et al., 1978).

The stratigraphic and structural relationships of these units are illustrated in Figures 6 and 12 and Plates 2, 3 and 4. Gravels, sands and muds of the principle aquifer overlie the clays and fanglomerates of the upper Popatosa Formation. In the study area, upper Popatosa claystones are found in the subsurface of eastern La Jencia Basin and in the Socorro mountain block while upper Popatosa fanglomerate facies are found in the subsurface of western La Jencia Basin and in the

Magdalena Mountains (Bruning, 1973). The approximate location of the transition between claystone and fanglomerate of the upper Popatosa Formation in La Jencia Basin is shown in Plates 2,3 and 4. This transition probably involves a gradational change between claystones and fanglomerates, as well as intertonguing of units. The fanglomerates near the transition contain quite a bit of mud and clay. It is possible that faulting in central La Jencia Basin juxtaposes upper Popatosa claystone to the east against sands, gravels and muds to the west (Bruning, 1973; Osburn, personal communication). Late Tertiary volcanic rocks occur locally amongst upper Popatosa and younger units.

The secondary aquifer (composed of lower Popatosa Formation rocks and early Tertiary volcanic units) underlies the upper Popatosa Formation. The thickness of the early Tertiary volcanic rock is probably quite great (at least 1.5 km) within the Socorro Cauldron (Chapin et at., 1978).

Upper Popatosa claystones are exposed at the surface in the upfaulted Socorro mountain block. Early Tertiary volcanics rocks and Precambrian rocks are exposed in upfaulted sub-blocks (Figures 5, 9 and 10). Along the faults bounding the eastern side of the Socorro mountain block, upfaulted Tertiary volcanics and fractured, well-indurated sediments are juxtaposed against wedges of relatively impermeable upper Popatosa claystones (Figure 10; Chamberlin (1980).

Thermal springs are found at the eastern edge of the Socorro mountain block (Figures 1, 7 and 10). The spring waters are very dilute, and show no signs of interaction with deep reservoir rocks (Hall, 1960; Gross and Wilcox, 1983). Instead, it appears that these waters are heated in a relatively shallow aquifer associated with early Tertiary volcanics. The waters of the Socorro thermal springs are thought to originate in the Magdalena mountains and travel eastward in the subsurface through the Socorro mountain block (as shown is Fig 8), although a

KEY TO LITHOLOGIC UNITS

Post Santa Fe Alluvium
Sierra Ladrones Fm
Upper Popatosa Fm Fanglomerate Facies

Upper Popatosa Fm Playa Facies
Clays and Claystones

Lower Popatosa Fm
Well indurated Sedimentary Rocks

Early Tertiary Volcanic
and Volcaniclastic rocks
(Includes late Tertiary Volcanic rocks in a few locations)

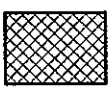

Paleozoic rocks
Precambrian rocks

Fig. 9. Key to lithologic units for Figures 10 and 13 and Plates 2, 3, and 4. Information from Chamberlin et al (1980) and Chapin et al (1978). A copy of this figure is included in the sleeve holding the plates.

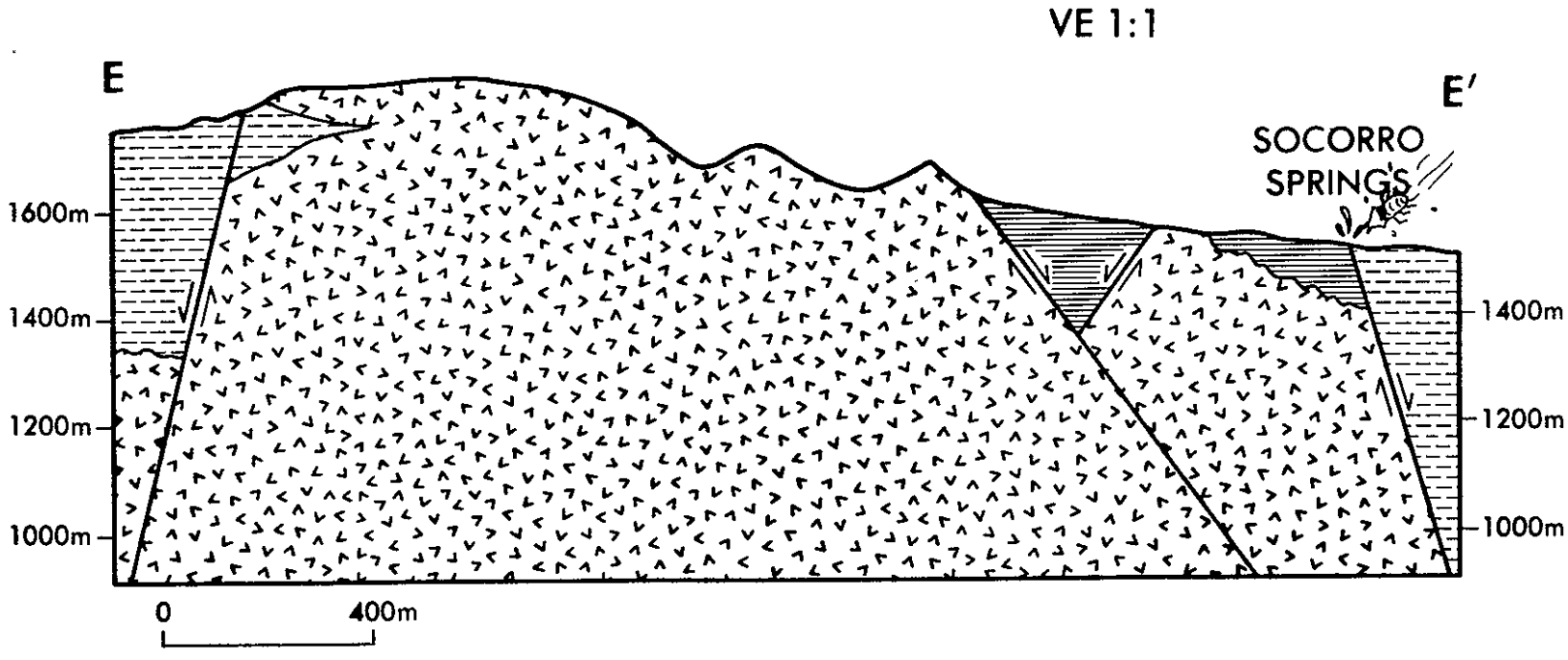

Fig. 10. Generalized geologic cross section EE' of Socorro Springs (note isopod). Key to litholgic symbols in Figure 9. Cross section location found in Figure 3.

component of local recharge is likely (Hall, 1960; Gross and Wilcox, 1983). The springs are fault controlled; they issue from fractured early Tertiary volcanic rocks near an outcrop of low permeability claystones which are faulted down against the more permeable rocks (Figure 10; Gross and Wilcox, 1983; Chapin, et al., 1978). It has been suggested that the springs discharge at this location because the eastward flow of heated waters in the Tertiary volcanics is blocked by the down-faulted claystones, thus forcing the waters to flow upward to the surface. (Chapin et al., 1978).

Ground water in the Magdalena Mountains and throughout La Jencia Basin is generally of the $Ca-HCO_3$ type, while waters discharged from the Socorro thermal springs and Blue Canyon Well are of the $Na-HCO_3$ type (Summers, 1972; Gross and Wilcox, 1980). Hall (1963) suggests that the chemical change is caused by ion exchange in the rhyolitic tuffs underlying the Popatosa Formation, as the waters pass through the Socorro mountain block. Ion exchange may be enhanced by above-normal subsurface temperatures (Gross and Wilcox, 1983).

HYDROTHERMAL INTERPRETATION

LA JENCIA BASIN

The low heat flows in La Jencia Basin are almost certainly caused by hydrologic downflow. The easiest way to obtain downward ground-water flow is by surficial recharge, i. e., downward percolation of direct precipition or runoff. However, in the semi-arid Socorro area, low precipitation and high potential evapotranspiration make direct recharge from rainfall a rare event (Wallace and Renard, 1967). The primary source of recharge is probably transmission losses from flow events, which in the case of La Jencia Basin predominantly occur close

to the Magdalena Mountains in western La Jencia Basin (Anderholm, 1987). Heat flows observed in western La Jencia Basin near the Magdalana Mountains are somewhat low (Figure 3), and we suggest that hydrologic recharge may have perturbed and reduced heat flows in this area.

It seems unlikely, however, that infiltration of recharge is a major factor in producing the lowest observed heat flows ($17 - 32\ mW\ m^{-2}$) in the eastern part of La Jencia Basin. The sites are more than 5 kilometers from the Magdalena mountain front, while Dewey suggested that most recharge occurs within one kilometer of the mountain front (Anderholm, 1987). These sites are fairly close to the Socorro mountain block, but recharge in and near the Socorro mountain block is probably quite small (about one-tenth the recharge to La Jencia Basin from the Magdalena Mountains). In addition, any infiltration in eastern and central La Jencia Basin would be impeded by low permeability clays at and near the surface (Anderholm, 1987).

The strongest argument against significant infiltration of recharge in eastern La Jencia Basin is found in the geothermal data. The low heat-flow sites in this area are wells drilled in clays and claystones (which in some cases are overlain by gravel). Heat flow is constant with depth in most of these wells, though in some cases the heat flow is somewhat different in the overlying gravel or there is some minor distortion somewhere in the temperature depth profile. Well 15 was drilled in 600 m of upper Popatosa formation (mostly claystones) in eastern La Jencia Basin and demonstrates constant (low) heat flow with depth ($32\ mW\ m^{-2}$; see Figure 11). If there were significant vertical ground-water flow in the Popatosa claystones, the heat flow would vary systematically with depth (see Figure 2). Therefore infiltration of recharge from the surface is not the dominant influence on subsurface temperatures in eastern La Jencia Basin, although it may contribute to

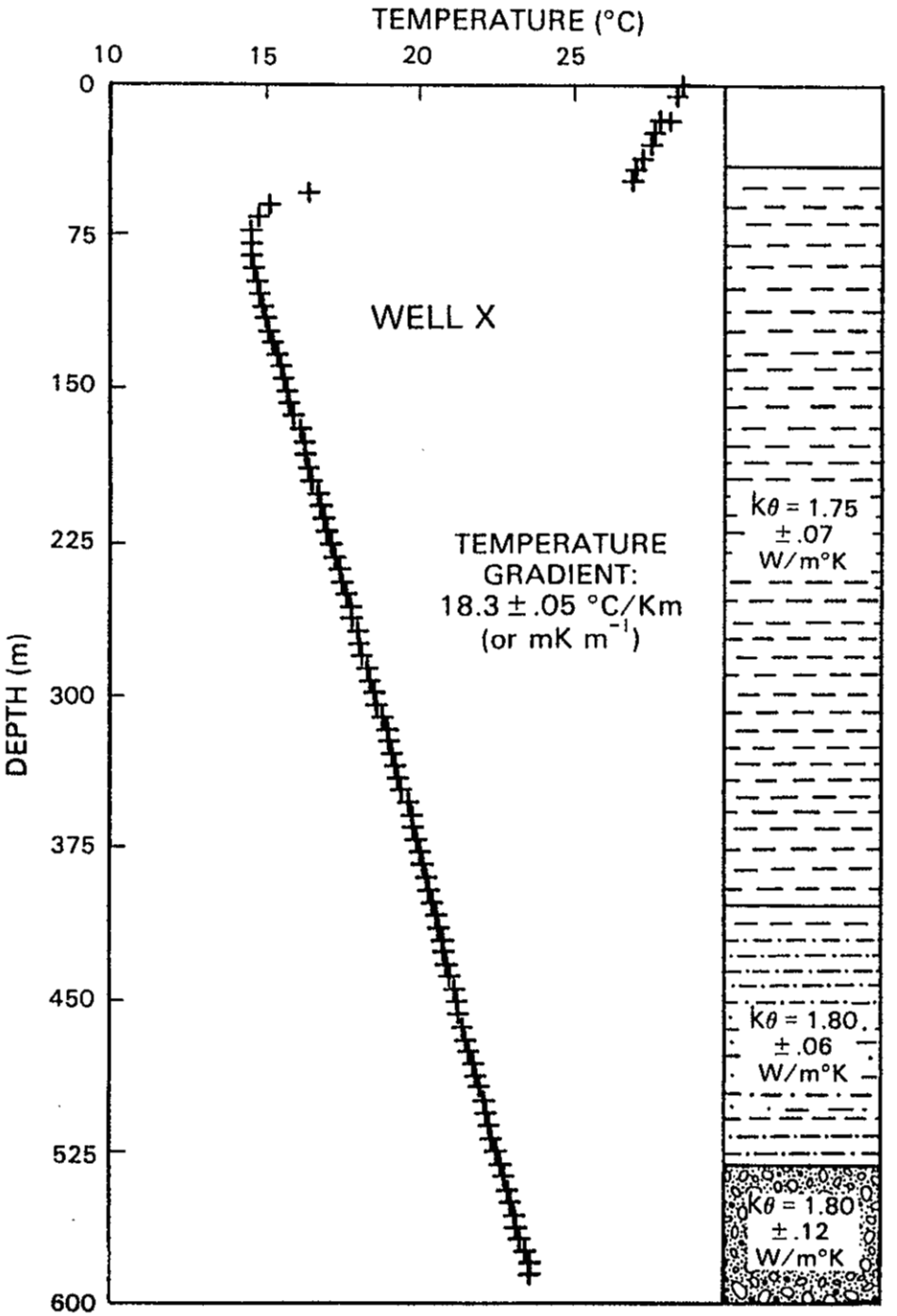

Fig. 11. Temperature-depth profile of Well X, located in Figure 2, in eastern La Jencia Basin. Discontinuity at ~50 *m* probably denotes level of water in well, (not necessarily water table). Heat flow 32 ±2 $mW\ m^{-2}$. Lithology after Chapin, (unpublished lithologic logs): 38 *m* −403 *m*: claystones; 403 *m* −533 *m*: claystones and sandstone; 533 *m* −610 *m*: sandstone.

low temperature gradients in some locations (especially in surficial gravels).

The heat-flow profile of Well 15 (Figure 11) is constant with depth, indicating that vertical ground-water flow between the surface and the bottom of this well is negligible. Since the magnitude of the conductive heat flow at this site, and other nearby sites, is much lower than normal there must be another process influencing the subsurface temperature regime, besides direct infiltration of recharge. We suggest that the near surface temperature regime is perturbed by ground-water flow elsewhere, adjacent to and/or below the Popatosa claystones.

We hypothesize that the low heat flows of eastern La Jencia Basin are produced by eastward flowing ground water (that recharged in or near the Magdalena Mountains) that is forced to flow down beneath the relatively impermeable east basin claystones into more permeable materials below. Figure 12 is a schematic east-west cross section of Socorro area hydrogeology which illustrates this hypothesis. Recharge occurs in and near the Magdalena Mountains, and the ground water flows roughly eastward through gravels, fanglomerates and Tertiary volcanics of western La Jencia Basin. In central La Jencia Basin the lithology of the upper Popatosa changes from permeable fanglomerate to low permeability clays and claystones which extend from near (or at) the surface down to depths of (possibly) 1000 m. Ground water flows downward near the fanglomerate/ claystone transition into more permeable material below, i. e., fractured well-indurated sedimentary rocks and fractured volcanic rocks of the secondary aquifer.

This hypothesis is best supported by the Nogal Canyon cross-section (AA', Plate 2). In this cross-section the transition between upper Popatosa fanglomerate facies and Upper Popatosa playa (claystone) facies appears to occur near Well 7. Well 7, drilled in gravels and mud, has the lowest heat flow observed in the Socorro area. (Temperatures in this well appear somewhat perturbed and therefore

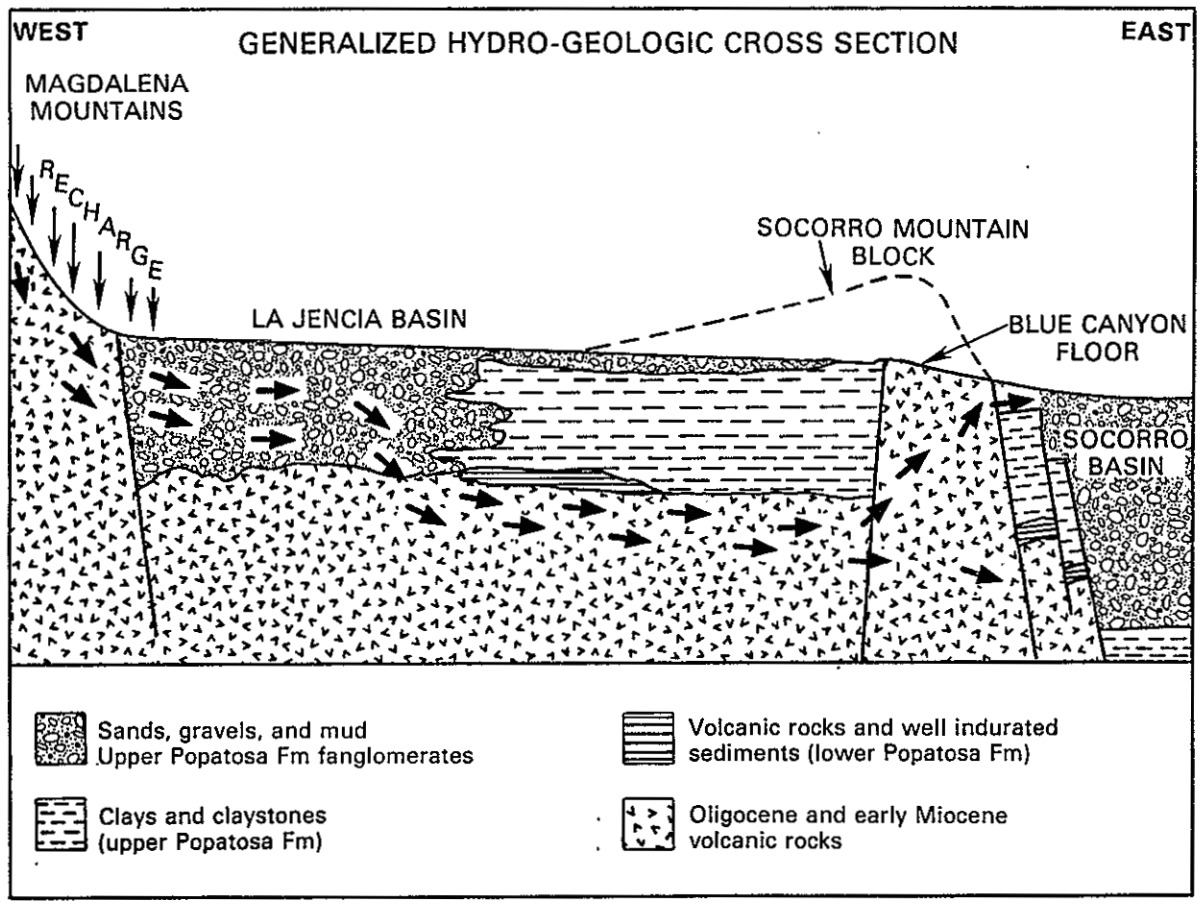

Fig. 12. Generalized hydrogeologic cross-section through La Jencia Basin and the Socorro mountain block. Arrows denote hydrologic recharge and postulated ground-water flow path. Geology based on Chamberlin (1980), Chapin, Osburn and Foster (unpublished lithologic logs). Ground-water flow system based on Stone (1977), Anderholm (1987), Gross and Wilcox (1983) and ideas developed in the present study.

we do not regard this as one of our most reliable data sites.) Well 15 (Figure 11) is also located near the transition, but in the claystone aquitard, and, as discussed above, has a very low but constant heat flow. (Well 15 is actually somewhat off the cross-section and therefore not as close to Well 7 as it appears in cross-section AA'.) We suggest that eastward flowing ground water is forced to flow downward in the vicinity of Well 7, beneath the claystone aquitard observed in Well 15. Heat is advected downward by the ground water, reducing surface heat flows in this area.

The transition between the fanglomerate and the playa (claystone) facies of the upper Popatosa is a transition between an unconfined aquifer and an aquifer confined beneath the claystone aquitard. A question raised by our hypothesis is: Why is eastward flowing water in the unconfined aquifer forced to flow down under the aquitard instead of up and over the aquitard? The most likely answer is that the claystone aquitard extends above the level of the water table in the unconfined aquifer of western La Jencia Basin, and the unconfined ground water does not have sufficient potential energy to flow up and over the claystone. West of the fanglomerate/ claystone transition the water table elevation is probably $\approx$1740 m (data are sparse, but the water table in La Jencia Basin seems to be very flat; (Stone, 1977; Anderholm, 1987)). East of the transition, the elevation of the top of the claystone aquitard is $\approx$1775 m in Well 6, $\approx$1755 m in Well 13, and $\approx$1766 m in Well 15. Unconfined water west of the transition will not have sufficient energy to flow up over the aquitard.

The Blue Canyon and Socorro Canyon cross sections (BB' and CC', plates 3 and 4) also pass through La Jencia Basin. These cross sections include the transition between fanglomerate and claystone in the upper Popatosa Formation. Depression of subsurface temperatures and temperature gradients can be observed at the transition in the Socorro Canyon cross section. However, the depression of subsurface temperatures near the transition does not appear to be as profound in the Socorro Canyon cross-section as it appears in the Nogal Canyon cross section. The Blue Canyon cross section does not appear to show any depression of isotherms near the fanglomerate/ claystone transition. Perhaps not all of the ground water in this area is forced to flow beneath the claystone; note that the top of the claystone in Well 22 is fairly deep.

SOCORRO MOUNTAIN BLOCK

The high heat flows of the Socorro Mountain Block are probably greatly influenced by ground-water flow (although upper crustal magma may also contribute heat). Hydrologic upflow in the Socorro mountain block has been suggested by many investigators (Chapin et al., 1978; Reiter and Smith, 1977). Comparing Figures 4 and 5, we note that zones of high heat flow in Socorro and Blue canyons are coincident with outcrops of relatively permeable Tertiary volcanic rocks. High heat flows occur in upfaulted blocks from which the Popatosa claystone aquitard has been eroded away. The coincidence of elevated subsurface temperatures and upfaulted Tertiary volcanics is most clearly illustrated in cross section BB' of Blue Canyon (Plate 3). Elevated temperatures occur in wells S5, S4 and BCW in upfaulted Tertiary volcanic rocks, and also in Well S6 which is in claystone overlying upfaulted volcanics.

We suggest that the absence of a claystone aquitard in upfaulted blocks of volcanics allows ground water, previously confined beneath the Popatosa claystone, to flow upward, thus elevating heat flows. The ground-water flow path is illustrated in the right hand side of Figure 12, i. e., ground water flows eastward in the Tertiary volcanics below the Popatosa claystones, and upward in the upfaulted block of Tertiary volcanics. This hypothesis is consistent with the ideas presented by Witcher (1988) who found that "tectonic and erosional stripping of Cenozoic and Mesozoic aquitards has exposed discharge windows which channel outflow of thermal water" providing discharge sites "for most of the region's convective systems". In the Socorro area, thermal waters discharge only at the thermal springs (Socorro, Sedillo and Cook springs). We suggest that the same phenomena (fluid upflow in a hydrologic window) elevates heat flow regardless of whether fluid discharge occurs or not.

Subsurface temperatures in Socorro Canyon (cross-section CC', Plate 4) are elevated in part (although not all) of the upfaulted blocks of Tertiary volcanic and Lower Popatosa Formation rocks. Temperatures are much lower in adjacent claystones, west and east of the upfaulted volcanics. Anderholm (1983) suggested upflow of geothermal water occurs where the Tertiary volcanic aquifer is near the surface in Socorro Canyon, This is consistent with the hypothesis presented in this study, and is supported by the elevated heat flows observed in Socorro Canyon. Heat flows greater than 200 $mW\,m^{-2}$ are found in wells 31 and 32, and the temperature profile in Well 33 is extremely curved, suggesting the influence of hydrologic upflow (either in the well bore or in the formation).

Heat flows are also somewhat elevated in upfaulted early Tertiary volcanic rocks in Nogal Canyon (AA', Plate 2). Early Tertiary rocks are upfaulted within 150 m of the surface in the eastern part of cross section AA'. We suggest that

ground water flows up from under the thick claystone of eastern La Jencia Basin, in the upfaulted volcanic rocks, even though the volcanic rocks do not outcrop at the surface.

A number of causes probably contribute to hydrologic upflow in the upfaulted Tertiary volcanic rocks. Water confined under the thick claystone aquitard may be overpressured, and flow upward naturally where the confining layer is absent (or where the base of the confining layer is higher in elevation such as in Nogal Canyon). Thermal bouyancy may also contribute to hydrologic upflow. Water confined beneath the claystone aquitard may be heated by either the natural geothermal gradient, or by anomalous crustal heat sources, increasing its thermal bouyancy and enhancing upflow.

In addition, we suggest that downfaulted blocks of claystone east of the upfaulted Tertiary volcanic hydraulic windows act to enhance the upflow of ground water in these areas. At the Socorro thermal springs, a similarly located claystone block outcrops and thermal waters discharge at the surface (see Figure 10). Elsewhere in the Socorro mountain block, claystone blocks are buried in the subsurface east of Tertiary volcanic outcrops (Chamberlin, 1980). We suggest that ground water flows up and over the claystone blocks (without surface discharge), elevating near-surface heat flows (Figure 12). The possibility that such subsurface flow barriers promote upflow is most clearly demonstrated in the cross section through Blue Canyon (BB', Plate 3). Subsurface temperatures are elevated in the upfaulted block of volcanic rocks as observed in wells S6, S5, S4 and BCW (Blue Canyon Well). Between BCW and Well R4, faulting has placed low permeability claystones against the volcanic aquifer. We do not known the exact depth of the down-dropped claystone block in this area; two cross sections by Chamberlin (1980), one south of our cross section and one to the north, place the top of the

claystone at $\approx$1450 m, and $\approx$1220 m, elevation respectively. The water table elevation in this area is higher that the top of the claystone; the water level in Blue Canyon Well is $\approx$1524 m, and Socorro and Sedillo springs discharge at 1524 m (Summers, 1976). This evidence indicates that ground water in the upfaulted volcanic rocks has sufficient potential energy to flow over the subsurface claystone barrier.

Claystone also exists in the subsurface east of the outcropping Tertiary volcanics in Socorro Canyon. It is less certain that ground water flows up over claystone in this area. The lithologic log of Well 35 (no lithologic information exists from Well 34) and cross sections by Chamberlin (1980) indicate that the top of the claystone is very close to the surface: between 1570 and 1610 m elevation. Evidence from geothermal wells 31 and 32 indicates that water table in the upfaulted volcanic block is probably about 1585 m elevation. It is possible that some ground water flows up and over the claystone aquitard along the interface between upfaulted volcanic rocks and downfaulted claystones in or near Socorro Canyon.

SOCORRO PEAK - WOOD'S TUNNEL

We now address the problem of the exceptionally high heat flows in the Wood's Tunnel area east of Socorro Peak. The Wood's Tunnel site is in a structural position similar to the other high heat-flow sites of the Socorro mountain block, i. e., in an upfaulted block from which Popatosa claystones have been eroded away. Wood's Tunnel, however, is outside of the Socorro cauldron, and the highest heat flow (490 $mW\ m^{-2}$) is measured in Precambrian rocks instead of Tertiary volcanics (Fig. 13). High heat flows are also observed in nearby volcanic rocks and sediments which overlie shallow Precambrian rocks (see Figs. 4, 5 and

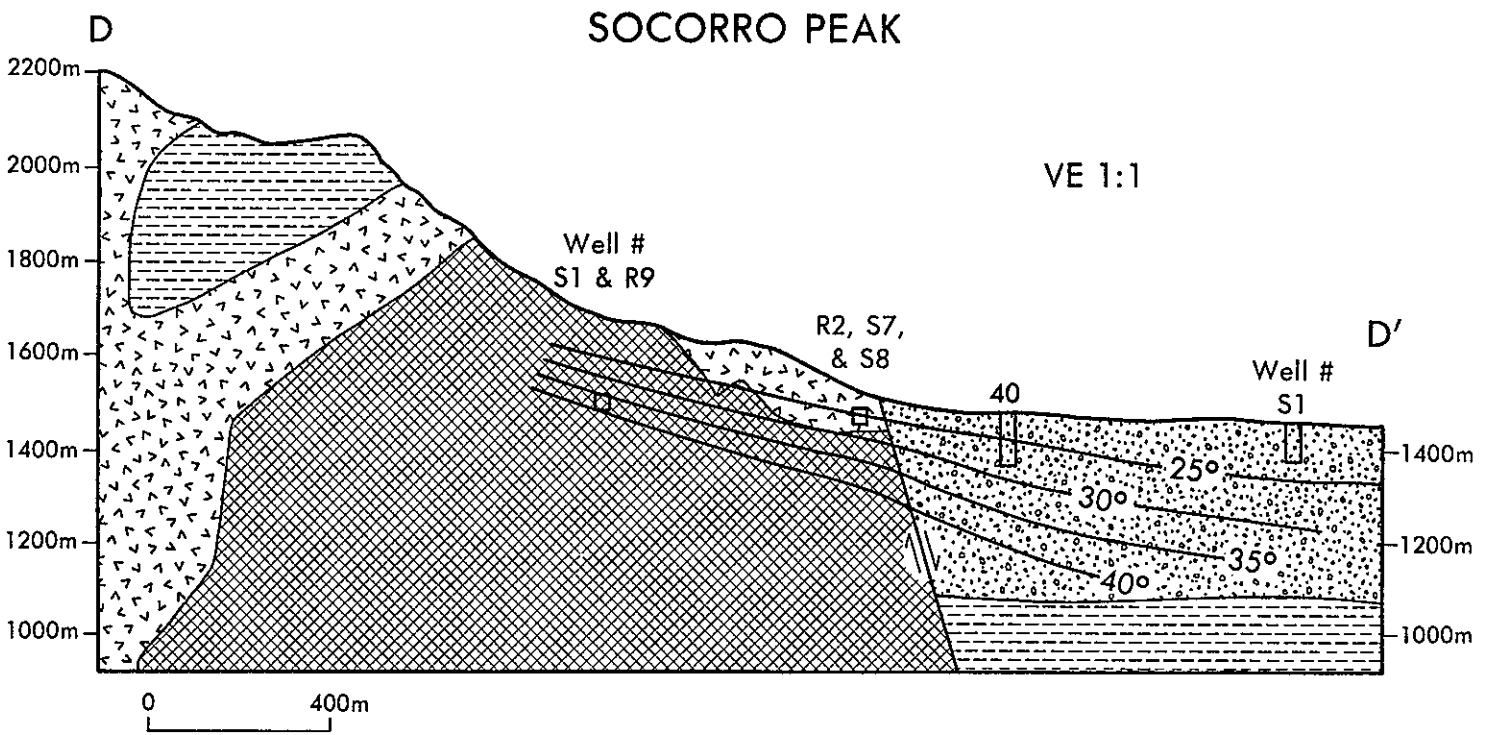

Fig. 13. Generalized geologic and geothermal cross section DD' of the Socorro Peak-Wood's Tunnel area. Temperatures are in degrees celsius. Cross section location shown in Figure 3 and key to lithology shown in Figure 9. Geology is from Chamberlin's cross section BB', (1980).

13).

Anderholm (1987) suggested that Precambrian rocks may transmit water in densely fractured or weathered zones. Wood's Tunnel is near two major fault zones: the ring fracture zone of the Socorro cauldron, and the range front fault zone of the Socorro mountain block. We suggest that the fracture permeability of the Precambrian rocks in this area may be quite high, and that hydrologic upflow elevates heat flows in this area, as it does in Blue Canyon and Socorro Canyon. Core from Wood's Tunnel is riddled with fractures, and the seismic quality factor ("Q") in this location is anomalously low for Precambrian rock, suggesting the presence of "open or saturated pores or fractures" (Carpenter, 1985). Evidence indicates that there is a vertical hydraulic head gradient in this area consistent with upward ground-water flow; Sanford (1977) observed that the water level in a well near Wood's Tunnel rose when that well was deepened. We hypothesize that hydrologic upflow may contribute to the high heat flows observed at and near Wood's Tunnel.

Thermal refraction may also elevate heat flows at Wood's Tunnel. Heat is conducted preferentially through material of higher thermal conductivity. The thermal conductivity of the Precambrian rock at Wood's Tunnel is approximately twice that of the surrounding younger rock, therefore we anticipate a substantial thermal refraction effect.

NUMERICAL MODELING

INTRODUCTION

The purpose of numerical modeling in this study is to simulate, in the first order, the hydrogeothermal system hypothesized for the Socorro area. We wish to determine whether the hydrogeology of the Socorro area could, indeed, produce the hydrologic phenomena that we have suggested, and whether such a hydrological system could, in turn, produce geothermal anomalies of the magnitude observed in the Socorro area.

A two-dimensional, steady-state, finite difference model has been developed to simulate hydraulic heads and temperatures. The density and viscosity of water are assumed constant with respect to temperature and, therefore, the possible effects of free convection are not considered. Hydraulic heads are modeled first, and the hydraulic head field is used to determine fluid velocities. The fluid velocities are incorporated into the conductive/ advective solution for temperatures (see Appendix D for a more complete description).

The model system (Fig. 14) represents an idealized W-E cross-section from central La Jencia Basin, through the Socorro mountain block, and into Socorro Basin (similar to the cross-section in Figure 12). The cross section of the model system is assumed to be parallel to ground-water flow in La Jencia Basin and the Socorro mountain block. Ground-water flow in the Socorro Basin is largely perpendicular to the model system and therefore the model does not simulate hydrogeothermal conditions east of the Socorro mountain block. The model extends into the Socorro Basin solely to avoid boundary condition constraints at the

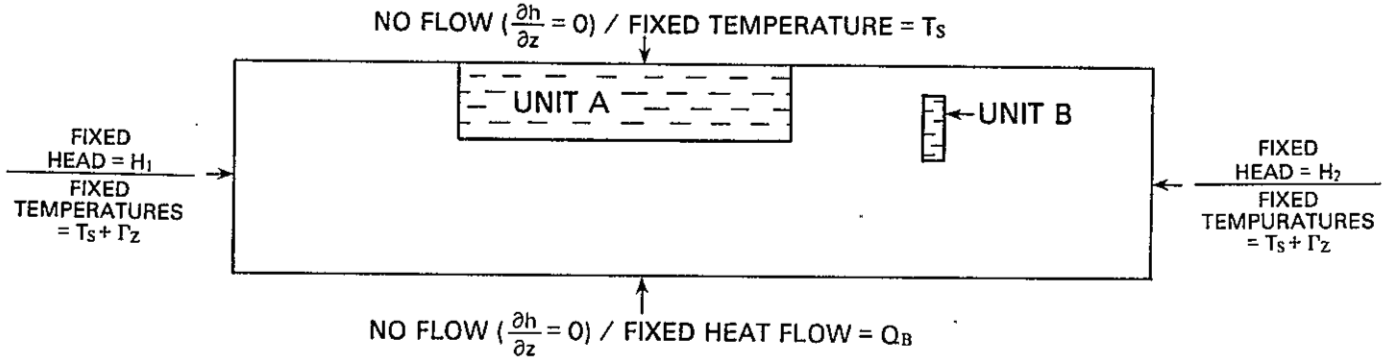

Fig. 14. Base model for numerial simulation: consists of two types of hydrologic unit: the aquitard (units A and B) and the aquifer (everything else). k_H of aquitard units A and B is $1 \times 10^{-9}\ m\ s^{-1}$; k_{HA} (hydraulic conductivity of aquifer system) is $2 \times 10^{-7}\ m\ s^{-1}$ (chosen to be consistent with appropriate values from Freeze and Cherry, 1979; and Hawkins and Stephens, 1980); k_Θ: homogeneous: $1.5\ W\ (m^\circ C)^{-1}$ (from laboratory measurements). Boundary conditions: $H_1 = 1770\ m$, $H_2 = 1390\ m$ (correspond to observed water table elevations), $T_S = 15^\circ C$, $\Gamma = 40\ mK\ m^{-1}$ (approximately consistent with observed temperature gradients), $Q_B = 90\ mW\ m^{-2}$ (consistent with background heat flow in Rio Grande rift south of Socorro). System dimensions: Horizontal: 14 km, vertical: 3 km; depth of base of unit A: 1.05 km, depth of top of unit B: 300 km, depth of of base of unit B: 1.35 km. Grid spacing: $\Delta x = \Delta y = 150\ m$.

eastern front of the Socorro mountain block, because hydrologic and geothermal conditions in this area are highly uncertain and, if specified in the model, would exert substantial influence on model results. Further discussion of the boundary conditions of the system can be found in Figure 7, and Appendix E.

BASE MODEL

A simple base model which simulates the most important hydrologic elements of the Socorro geothermal system is shown in Figure 14. Thermal conductivity is constant (1.5 $W\ m^o\ C^{-1}$) throughout this system, a reasonable assumption for geologic materials found in the Socorro area (except for Precambrian rock). The hydrogeology of the model has been greatly simplified, and consists of only two basic units. Low permeability clays and claystones comprise an aquitard, which is given an hydraulic conductivity (k_H) of $10^{-9}\ m\ s^{-1}$. The primary sedimentary aquifer and the secondary volcanic aquifer of the Socorro area are combined into one with k_H of $2 \times 10^{-7}\ m\ s^{-1}$.

One large aquifer block (unit A, Figure 14) extends from the top of the model (which corresponds to the water table) to 1000 m depth. Unit A represents the clays and claystones of eastern La Jencia Basin and the western part of the Socorro mountain block. (Modeled here as a vertical discontinuity, the western edge of the claystone is a transition from the permeable fanglomerate facies to low permeability claystone facies of the upper Popatosa formation. The transition may involve gradational change and intertonguing of the different units.) The more permeable hydrologic window to the right of unit A represents upfaulted Tertiary volcanic rocks. A smaller aquitard block (unit B), east of the hydrologic window, represents the wedge of Popatosa claystone downfaulted into the subsurface on the eastern side of the Socorro mountain block (more claystone undoubtedly exists

east of this wedge in the subsurface but at unknown, probably great depths, and is not included in this model; Sanford, 1981).

The base model has been constructed with a flat, impermeable bottom boundary, at sufficient depth to allow a reasonable thickness (2 km) of Lower Popatosa Formation and Tertiary volcanic rocks within Socorro Cauldron. No topography has been introduced into the impermeable basement of the base model because we are not sure what form that topography should take. When included, basement topography exerts considerable influence on model results, as will be discussed later.

The results from the base model system are shown in Figure 15. The hydraulic head field (Figure 15, bottom) shows distortion due to the presence of the aquitard units. Ground-water flow is perpendicular to the hydrologic head contours, and therefore we can state that fluid, in the model system, flows downward under the upstream edge of unit A, upward from under the aquitard into the hydrologic window between units A and B, and up and over unit B.

The temperature field is distorted by fluid flow (Figure 15, middle). Subsurface temperatures are elevated in the hydrologic window and depressed near the upstream edge of unit A. Surface heat flows generated by the base model are shown in Figure 15 (top). Surface heat flows are reduced from a background value of 90 $mW\,m^{-2}$ to as low as 15 $mW\,m^{-2}$ in and near the upstream end of unit A. Surface heat flows are elevated in the more permeable hydrologic window to about 110 $mW\,m^{-2}$, with a maximum of 177 $mW\,m^{-2}$.

There appear to be two components of upward fluid flow in the hydrologic window. The maximum heat flow of 177 $mW\,m^{-2}$ occurs at a spike directly above the upstream edge of unit B. It appears that the heat-flow spike is caused by a very local upflow of fluid associated with unit B. This spike does not appear

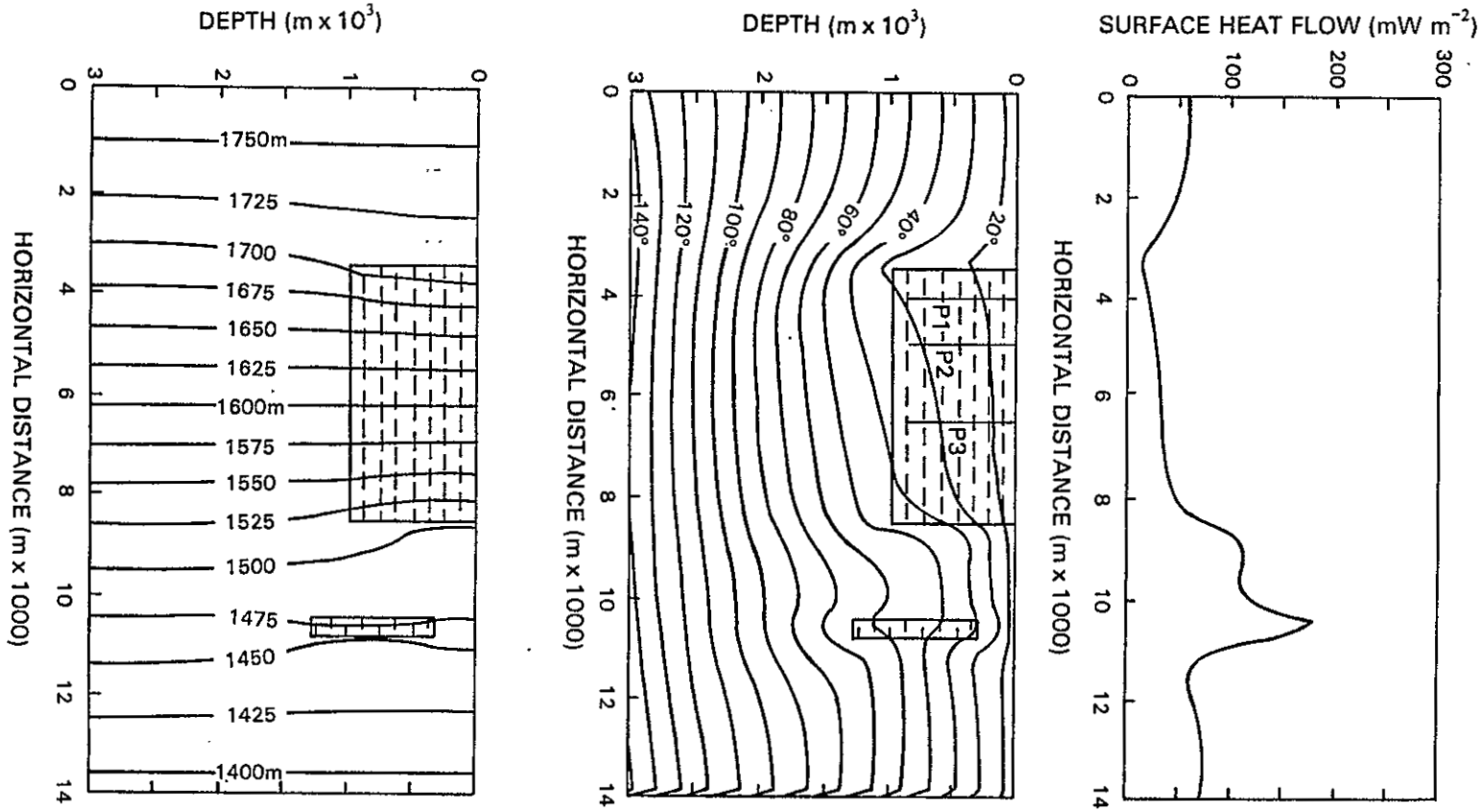

Fig. 15. Numerical simulation results for base model. Lower part: Hydraulic head field (m) (Vertical Exaggeration, 2.6:1). Middle part: Temperature field ($^{\circ}C$) (Vertical Exaggeration, 2.6:1). Upper part: Surface heat flow ($mW\ m^{-2}$). P1, P2 and P3 in middle figure indicates the locations from which the model generated temperature-depth profiles of Figure 9 were taken. Net hydrologic flux through system: $1.3 \times 10^{-5}\ m\ s^{-1}$. Area marked with dashes represent low permeability units.

in models from which unit B is absent (such as the Nogal Canyon model depicted in Figure 20), strongly suggesting that the spike is a result of unit B forcing additional fluid upflow in the hydrologic window. Heat flows are somewhat elevated throughout the hydrologic window (to $\approx$110 $mW\ m^{-2}$) as the result of upflow of ground water from underneath the unit A Popatosa aquitard. This broader heat-flow anomaly occurs whether unit B is present or not (see Figure 20), suggesting that this anomaly is not related to unit B. Instead, it appears that this anomaly is caused by fluid upwelling in the hydrologic window caused by the absence of unit A. Since we have not included thermal bouyancy in the model, it seems most likely that the fluid beneath unit A is overpressured and flows upward naturally where the confining layer (unit A) is absent. Examination of the hydraulic head field in the lower part of Figure 15 shows that hydraulic heads are greater beneath the right side of unit A than in the overlying claystones, and so the fluid confined beneath unit A is overpressured.

The results from the base model are qualitatively in agreement with observed heat flows in the Socorro area. The upstream edge of unit A corresponds to the transition between Upper Popatosa fanglomerates and claystones in central La Jencia Basin. We predicted that this transition could produce downward groundwater flow, and this is the result produced by our numerical model. Depressed subsurface temperatures and heat flows occur in the model near the upstream end of unit A (Fig. 15) correspond to those observed in central La Jencia Basin. We also suggested that hydrologic upflow occurs in the upfaulted volcanics rocks of the Socorro mountain block, elevating subsurface temperatures and surface heat flows. This model has shown that upflow is likely occur in such a hydrologic window, and that elevated subsurface temperatures and heat flows would result. These preliminary results are very promising, although the actual magnitude of the

high heat flows in the Socorro Mountain block are not reproduced in this model.

The base model not only simulates the surface heat-flow profile, but also simulates important features of the observed subsurface temperature field. For example, as mentioned earlier, temperatures measured in Popatosa claystone in eastern La Jencia Basin increase linearly with depth, yielding constant but very low heat flows. This is best demonstrated by the temperature-depth profile of Well 15 (Fig. 11). The temperature gradient measured in Well 15 is constant ($18.3\ ^{o}C/km$) to 600 m depth, in (predominantly) Popatosa claystones. Numerically generated profiles, produced by the base model within the upstream half of unit A are shown in Figure 16. The locations of these profiles within this base model are shown in the middle part of Figure 15, and the location of P1 or P2 ought to correspond to Well 15 in eastern La Jencia Basin. These model-generated temperature-depth profiles demonstrate constant, low temperature gradients to at least 600 m depth ($15 - 23\ ^{o}C/km$), just as is observed in Well 15 in eastern La Jencia Basin (Fig. 11).

We consider the successful simulation of the subsurface temperature field in eastern La Jencia Basin to be an important argument in favor of our model of hydrologic flow in La Jencia Basin. The existence of low heat flows in La Jencia Basin only suggests hydrologic downflow of some sort. The existence of *constant*, low heat flow to depths of 600 m is more difficult to explain. The fact that our base model also produces constant, low heat flows to such depth (in the corresponding part of the model) strongly suggests that our model of flow is likely to be correct, that is; that ground water is forced to flow downward near the transition between upper Popatosa fanglomerates and claystones in central La Jencia Basin. Ground water is forced to flow down beneath Popatosa claystones into more permeable materials below.

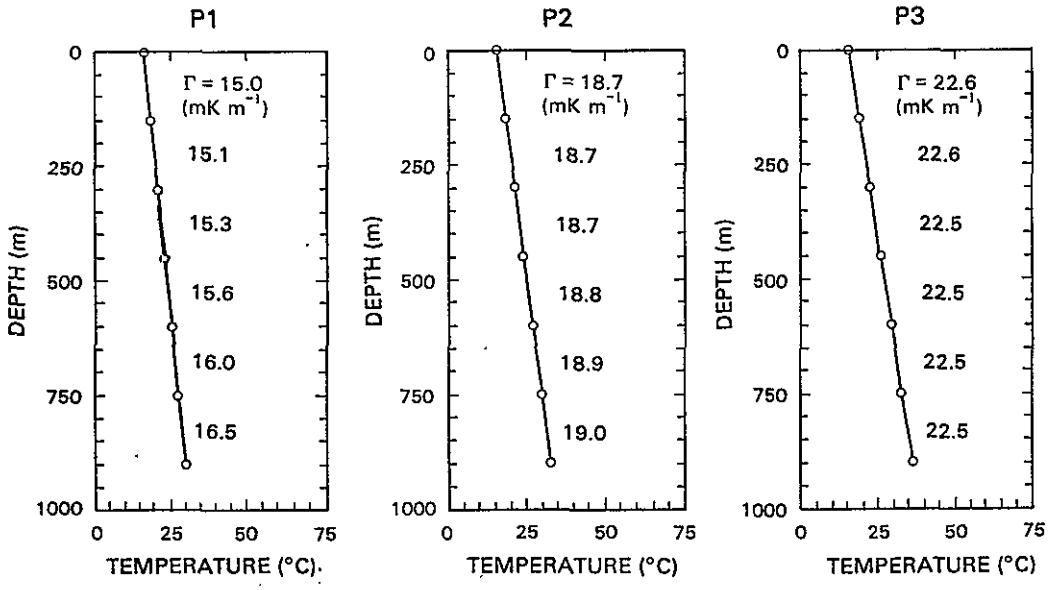

Fig. 16. Numerically simulated temperature-depth profiles, base model. Temperature gradients given for each interval in $^{\circ}C/km$ (or $mK\ m^{-1}$). Locations of profiles P1, P2 and P3 shown in middle part of Figure 15.

The outputs from the base model are very similar to the subsurface head and temperature fields and the surface heat-flow profiles produced by almost all of the models generated as part of this study. For the most part, only the magnitude of the surface heat-flow anomalies varied from model to model. Ground-water flow patterns and subsurface temperature-depth profiles at given locations within the model do not vary greatly between models. Similar geothermal anomalies occur in corresponding locations in each of the models. Key features of the models presented in this study are compared in Table 2. Table 2 lists the maximum and minimum heat flow of each of the models presented in the following sections as well as the net hydraulic flux through each system, as discussed in the following section.

GROUND WATER FLUX CONSTRAINTS

An important constraint on the geothermal model is the net ground-water flux through the system. We assume that the source of most of the ground water in the Socorro hydrothermal system is recharge in and near the Magdalena Mountains. Anderholm (1987) cites an estimate by Dewey of recharge to La Jencia Basin from the Magdalena Mountains of 0.162 $m^3 s^{-1}$ (4150 acre-ft/yr). As a first order approximation, we assume that this recharge is spread evenly along the 15-20 km of mountain front which faces La Jencia Basin. The result is an average flux entering the system per horizontal distance perpendicular to the direction of flow of 8.1×10^{-6} to 1.1×10^{-5} $m^2\ s^{-1}$. This quantity is an estimate for the total flux into the two dimensional cross-section of our numerical model.

This estimate of net hydrologic inflow is highly uncertain. The accuracy of the recharge estimate is unknown and there are other possible components of inflow to the system. Some recharge occurs in the Socorro mountain block, and

Table 2, Comparison of Selected Models

Model		Q_H $m^2\ s^{-1} \times 10^{-5}$	q_{min} $mW\ m^{-2}$	q_{max} $mW\ m^{-2}$
Base Model	$(k_{HA} = 2 \times 10^{-7})$	1.3	14.6	177
Vary k_{HA}				
A	$(k_{HA} = 10 \times 10^{-7})$	6.3	14.5	282
B	$(k_{HA} = 5 \times 10^{-7})$	3.2	11.7	227
D	$(k_{HA} = 1 \times 10^{-7})$	0.63	22.3	105
Vary q_B				
$q_B = 180\ mW\ m^{-2}$		1.3	16.3	190
Aquitard	Geometry			
Blue C.		1.2	20.2	272
Socorro C.		1.3	17.7	224
Nogal C.		0.92	18.9	117
Basement	Topography			
Pib		1.3	14.6	300
Pib22		1.1	18.1	241
Anisotropic	k_H			
$\frac{k_{HZ}}{k_{HZ}} =$	10 in Tv	1.3	16.1	199
Estimated Q_H from recharge: $0.81 - 1.1 \times 10^{-5}\ m^2\ s^{-1}$				

Table 2. Comparison of Selected Models. This table contains abbreviated descriptions and results from the models discussed in the text and depicted in Figs. 15, 18, 19, 20, 21, 22, 23 and 24. Q_H is the net hydraulic flux through the model, q_{min} and q_{max} are the minimum and maximum surface heat flows produced by the model.

there may be ground-water underflow entering the system from the west, through the Magdalena mountain block. The hydrologic inflow estimate assumes that the recharge and subsurface hydrologic flow are evenly distributed along the 15 - 20 km of Magdalena mountain front facing La Jencia Basin. Flow may be concentrated in more permeable pathways in La Jencia Basin and the Socorro mountain block, so that flow through certain cross sections may be higher than through others. There are also likely to be components of flow perpendicular to the system, which the present model cannot consider.

The net flux (Q_H) through the numerical model system is determined by integrating the volumetric flux (determined by Darcy's law) over the right-hand boundary of the model system.

$$Q_H = \sum_i k_i \frac{\partial h}{\partial x} \Delta z$$

where k_i is the hydraulic conductivity of the i^{th} grid block, x and z are the horizontal and vertical coordinates, and the summation includes all the grid blocks on the right-hand boundary of the model. Q_H is not an input parameter for the numerical model but is controlled by head boundary conditions and the k_H distribution.

The base model described above has a net ground-water flux of $1.3 \times 10^{-5}\ m^2 s^{-1}$. We consider this value to be not unreasonably high in view of the above uncertainties (estimated average influx from recharge in Magdalena Mountains is 8.1×10^{-6} to $1.1 \times 10^{-5}\ m^2 s^{-1}$).

The horizontal fluid flow rate (Darcy velocity) through the aquifer system of the base model is typically $4 \times 10^{-9}\ m\ s^{-1}$. Assuming a porosity of 0.30 (30 percent), the seepage velocity is $1.3 \times 10^{-8}\ m\ s^{-1}$, indicating that the residence time for water in this system (14 km horizontal distance) is on the order of 30,000

years. (Note that the system and this residence time do not include recharge of ground water in and near the Magdalena Mountains. If the extra distance between the recharge areas and the western end of the model system is included, we estimate the residence time to be 36,000 to 42,000 years).

The maximum vertical Darcy velocity in the base model system is $\approx 5 \times 10^{-9}\ m\ s^{-1}$ upward. The maximum vertical velocity occurs in the hydrologic window at the upstream edge of unit B.

SELECTED ADDITIONAL MODELS

VARIATION OF AQUIFER HYDRAULIC CONDUCTIVITY

The hydraulic conductivity of the aquifer system (k_{HA}) is one of the most important factors in our model. For a given aquifer/aquitard geometry, ground-water flow rates are controlled by the k_{HA}. Figure 17 shows surface heat-flow profiles produced by the base model when k_{HA} is varied (also see Table 2). Increasing k_{HA} produces more pronounced heat-flow anomalies, most by notably elevating the heat flow in the hydraulic window between units A and B. When k_{HA} is increased by a factor of five over the base model value, the maximum surface heat flow generated by the model is increased from 180 $mW\ m^{-2}$ to 280 $mW\ m^{-2}$. The ground-water flux through the high k_{HA} model is very large: six times that of the hydrologic input estimated to derive from the Magdalena Mountains, and therefore this model is probably not very realistic.

The models discussed above simulate the shape of the heat-flow profile observed near Socorro fairly well. High heat flows are produced by the model in the correct location (i. e., at the hydrologic window) and low heat flow are produced at the left hand edge of unit A, as desired. The anomalously low heat-flows

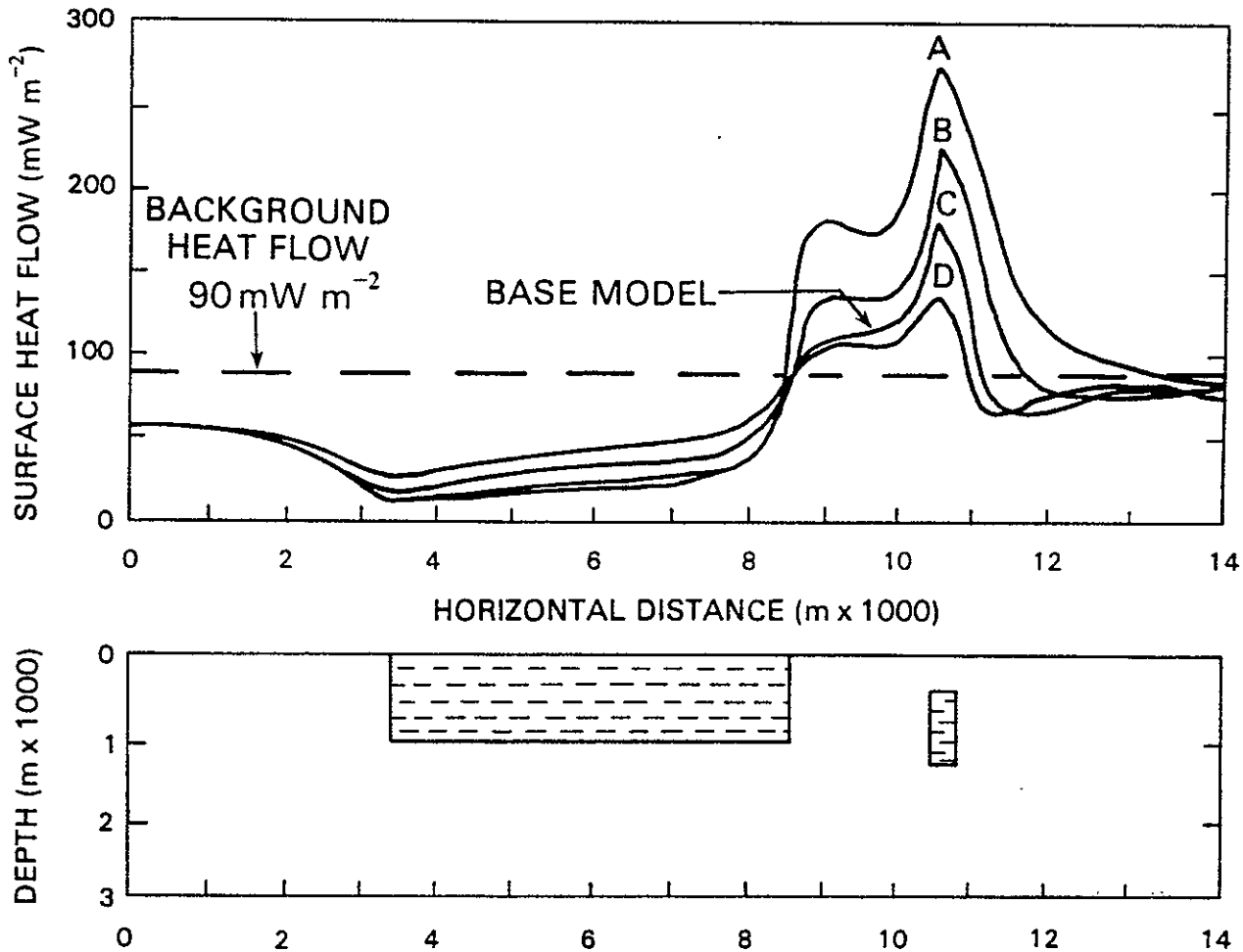

Fig. 17. Variation of aquifer hydraulic conductivity. Numerical simulation results for base model with different k_{HA}. All model parameters same as base model, listed in caption of Figure 14, except k_{HA}. A: $k_{HA} = 10 \times 10^{-7}$ m s^{-1}; B: $k_{HA} = 5 \times 10^{-7}$ m s^{-1}; C: $k_{HA} = 2 \times 10^{-7}$ m s^{-1}; and D: $k_{HA} = 1 \times 10^{-7}$ m s^{-1}.

produced by these models ($\approx$15 $mW\ m^{-2}$) are comparable to heat flows observed in La Jencia Basin. The high heat flow of Socorro Canyon and Blue Canyon ($\approx$220 $-$290 $mW\ m^{-2}$), and Socorro Peak (490 $mW\ m^{-2}$) have not been reproduced, except by models with excessively high fluid fluxes (Models A and B in Table 2). It may be that we have not matched the high heat flows of the Socorro mountain block because free convection effects are not modeled, or it may be that we need to make other adjustments to the model.

One simple adjustment to the model is to change the basal heat flow. We find, however, that the base model is relatively insensitive to basal heat flow. A system identical to the base model, with a basal heat flow (q_B) of 180 $mW\ m^{-2}$ (instead of 90 $mW\ m^{-2}$), produces a maximum surface heat flow of 190 $mW\ m^{-2}$ (instead of 177 $mW\ m^{-2}$) (see Table 2). Increasing the model's basal heat flow above the typical background heat flow of the Rio Grande rift (75 $-$100 $mW\ m^{-2}$, Reiter et al., 1986) is roughly equivalent to introducing an anomalous heat source below the base of the model. The insensitivity of the base model to anomalous basal heat indicates that anomalous heat is swept out of the model by fluid flow. This model does not, however, include free convection effects, which could be very important in the case of anomalous basal heat flow. Free convection would probably produce stronger fluid upflow, and might bring more heat to the surface within the system.

VARIATION OF AQUITARD GEOMETRY

The size and shape of the aquitard units in the model has a great influence on the hydraulic flux through the model and also on the magnitude of the geothermal anomalies produced by the model. Altering aquifer/aquitard geometry is one way to enhance the geothermal anomalies produced by a model without increasing the

net hydrologic flux through that system. Unit B is an important factor in producing the maximum heat flow in the hydrologic window of the base model. In the base model, unit B extends from 0.3 km to 1.05 km. Deepening the base of unit B increases fluid upflow in the hydrologic window and enhances the geothermal anomaly observed there. However, if the base of unit B extends all the way down to the base of the model, almost all hydrologic flow is choked off, and almost no geothermal anomalies result.

SIMULATION OF OBSERVED HEAT FLOWS

Figure 18 illustrates a model in which the aquitard geometry has been adjusted in order to reproduce the heat-flow profile observed in Blue Canyon (cross section BB'). In this model, unit B extends from 0.3 km to 1.95 km, and unit A extends somewhat further to the left than it does in the base model. Heat flows observed in Blue Canyon are denoted by crosses (heat-flow determinations) and stars (heat-flow estimates).

Net fluid flux through this model is slightly less than the base model ($1.2 \times 10^{-6}\ m^2\ s^{-1}$ compared to $1.3 \times 10^{-5}\ m^2\ s^{-1}$). However, the maximum heat flow produced by this model is much higher than in the base model ($272\ mW\ m^{-2}$ as opposed to $177\ mW\ m^{-2}$). The deepening of unit B appears to causes a a greater quantity of water to flow upward, producing very high heat flows. The heat flows generated by the model depicted in Figure 18 compare favorable with observed surface heat flows, but it should be noted that these models are poorly constrained, non-unique, and do not include possible free convection effects. We do not suggest that the geometry of aquifers and aquitards shown in Figure 18, nor the values of hydraulic conductivity used in this model, are those necessarily occurring in Blue Canyon. Instead, we wish to show that it

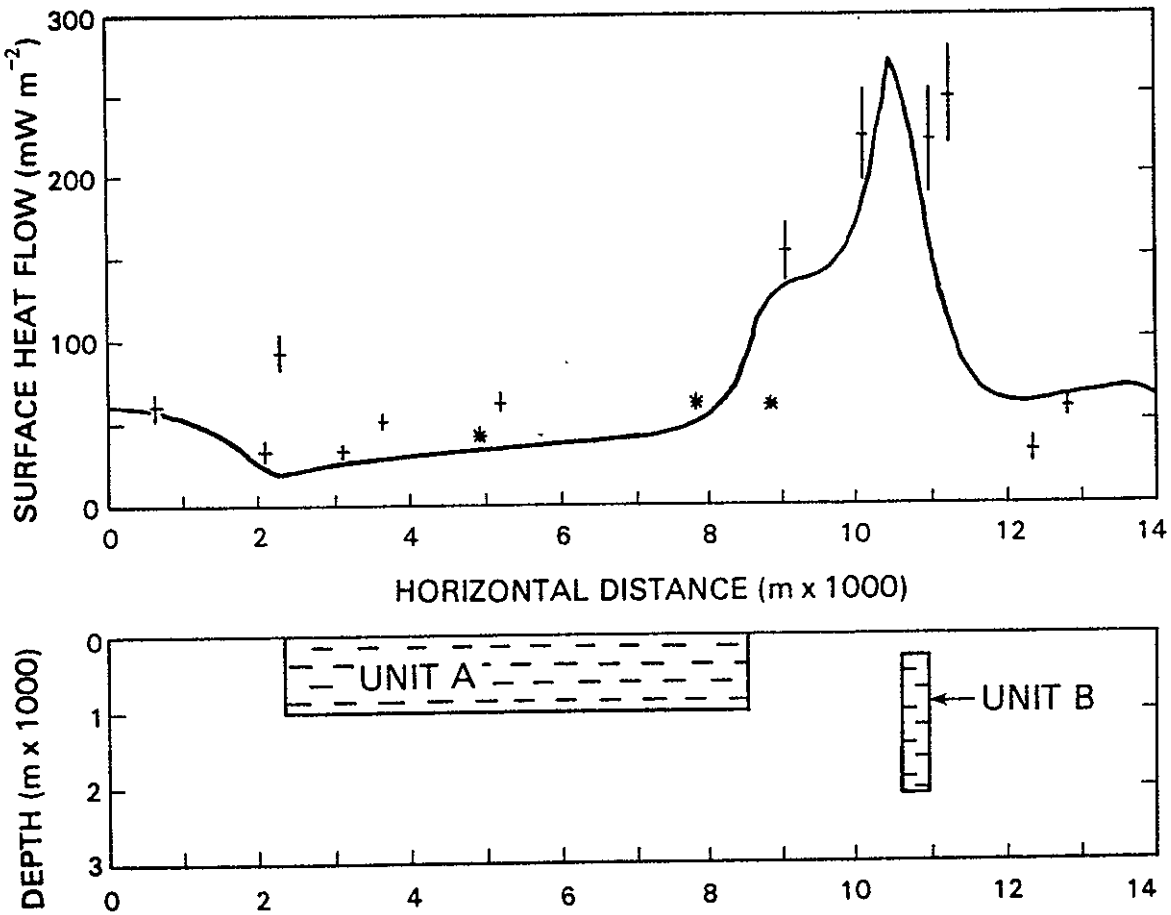

Fig. 18. Heat-flow profile generated using a variation of thee base model compared to observed heat flows from Blue Canyon (cross section BB' in Figure 3). Crosses represent heat-flow determinations with error bars and stars represent more uncertain heat-flow estimates from sites in Blue Canyon. This model is similar to the base model of Figure 14, except that the base of unit B aquitard is 0.9 *km* deeper and unit A aquitard extends further to the left.

is possible to reproduce the near-surface heat flows observed in the Socorro area using this type of hydrothermal model.

A similar model has been used to simulate heat flows in Socorro Canyon (Figure 19). In the Socorro Canyon model, unit B extends from 0.3 km to 1.95 km depth and unit A does not extent as far to the left as in the base model. The heat-flow profile generated by the model matches the temperatures observed in Socorro Canyon (cross section CC', Fig. 3) fairly well.

The hydrogeology of Nogal Canyon appears to be somewhat different than Blue and Socorro canyons. The Tertiary volcanic aquifer does not outcrop but Tertiary volcanic rocks are closer to the surface in an area of somewhat elevated heat flows than in cooler areas further west. A simple model which simulates the heat flows observed at Nogal Canyon is shown in Figure 20. The bottom boundary of this model is shallower than in the base model because it is possible that much of the flow to and near Nogal Canyon occurs outside of Socorro the cauldron (see Fig. 5), where the Tertiary volcanic aquifer is relatively thin. No equivalent of unit B is included in the Nogal Canyon model because no evidence suggests that a subsurface flow barrier of this type exists in this part of Nogal Canyon. Nevertheless, the model-generated surface heat flows are elevated above the area where the aquifer approaches the surface.

The net fluid flux through each of the three model systems described in this section is listed in Table 2. These flux values are roughly consistent with the flux we have estimated for the Socorro hydrothermal system.

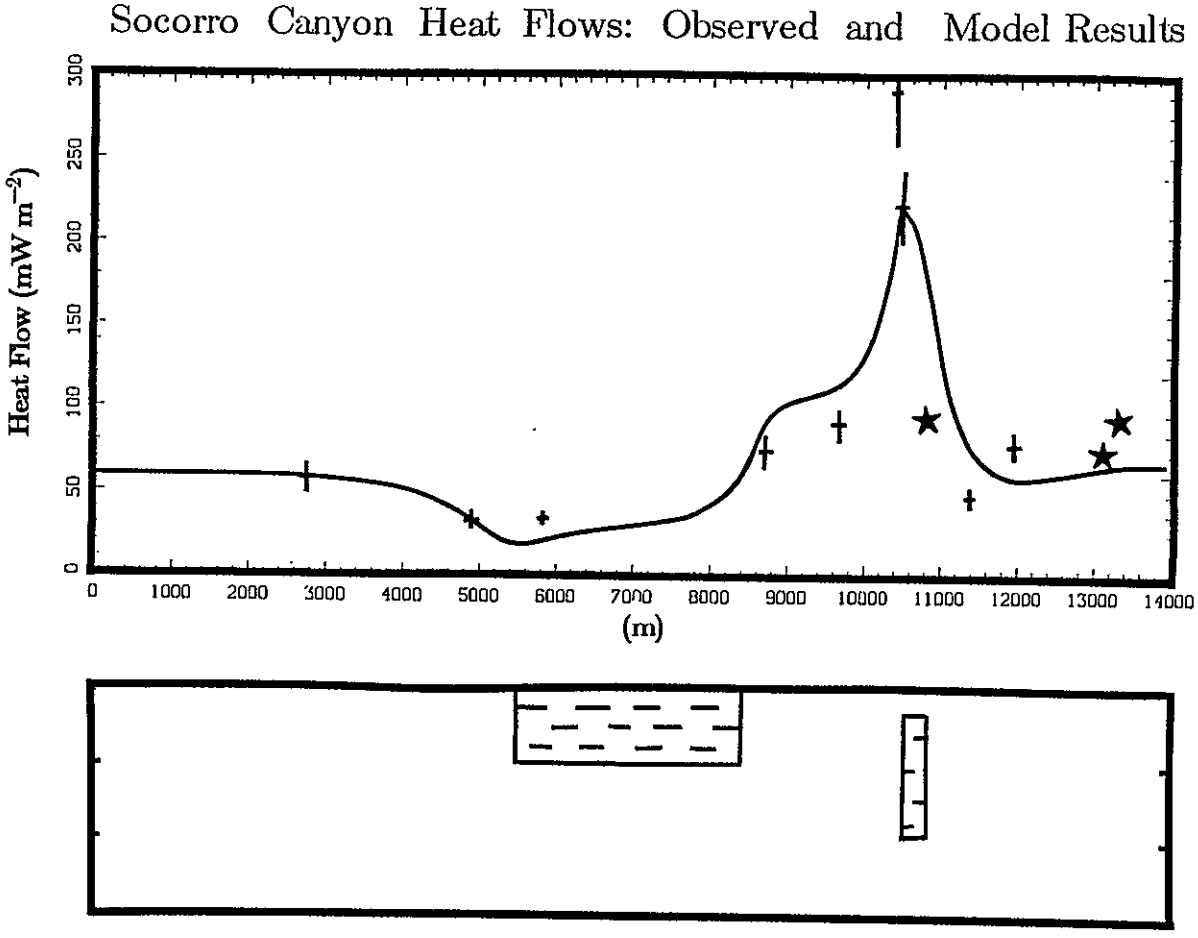

Fig. 19. Numerically generated surface heat-flow profile from variation of base model compared to observed heat flows from Socorro Canyon (cross section CC' in Figure 3). Crosses represent heat-flow determinations with error bars and stars represent more uncertain heat-flow estimates from sites in Socorro Canyon. This model is similar to the base model of Figure 14, except that the base of unit B aquitard is 0.9 *km* deeper and unit A aquitard does not extend as far to the left.

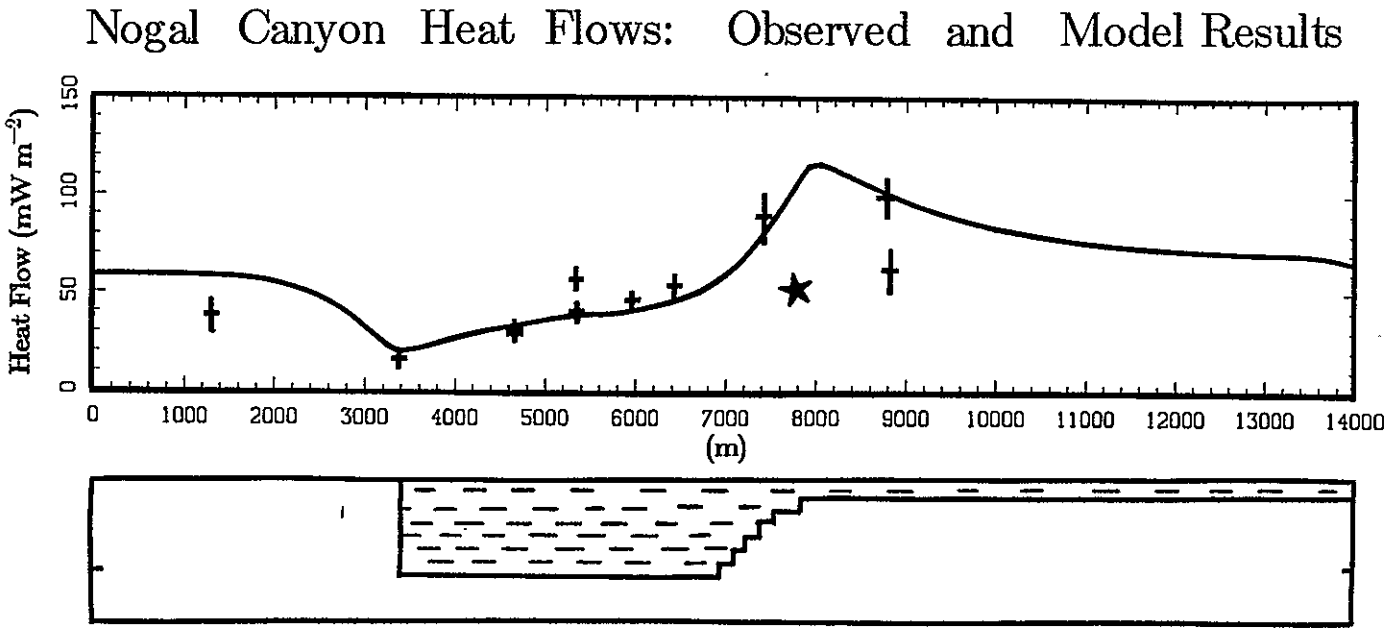

Fig. 20. Numerically generated surface heat flow profile from variation of base model compared to observed heat flows from Nogal Canyon (cross section AA' in Figure 3). Crosses represent heat flow determinations with error bars and stars represent more uncertain heat flow estimates from sites in Nogal Canyon.

BASEMENT TOPOOGRAPHY

Surface heat-flow profiles of some of the previously discussed models are manipulated by changing the depth to which unit B extends. Another technique that increases the positive heat-flow anomaly without increasing the hydrologic flux through the system is the introduction of topographic relief in the impermeable basement. If we assume that Paleozoic or Precambrian rocks (at depth) approximate an impermeable basement for the Socorro hydrothermal system (which is not necessarily true), then it is reasonable to expect some topography in the basement. Offsets in the Paleozoic/ Precambrian surface are probably associated with cauldron margins, resurgent domes within cauldrons, and more recent block faulting (Chamberlin, 1980). It is likely that the surface of the bedrock is tilted, probably dipping to the west in most of the study area (Chamberlin, 1980).

A relatively simple system (Model Pib) which demonstrates the influence of basement topography is shown in Figure 21. In this model, an upfaulted block of impermeable basement intrudes into the base of the model, below the upfaulted hydrologic window. The surface heat-flow profile produced by this model is also shown in Figure 21. The shape of the heat-flow profile produced by this model is similar to that of the base model, however the maximum heat flow produced by this model is much higher (260 $mW\ m^{-2}$), while the hydraulic flux is somewhat lower than in the base model (Table 2). It appears that the basement block causes more ground water to flow upward in the hydrologic window, thus further elevating heat flows.

A more complex system (Model Pib22) is shown in Figure 22. In this case the basement and the base of the unit A aquitard are both given a westward dip. Again, the model-generated heat-flow profile has not changed very much. The maximum surface heat flow produced by this model is higher than the base model

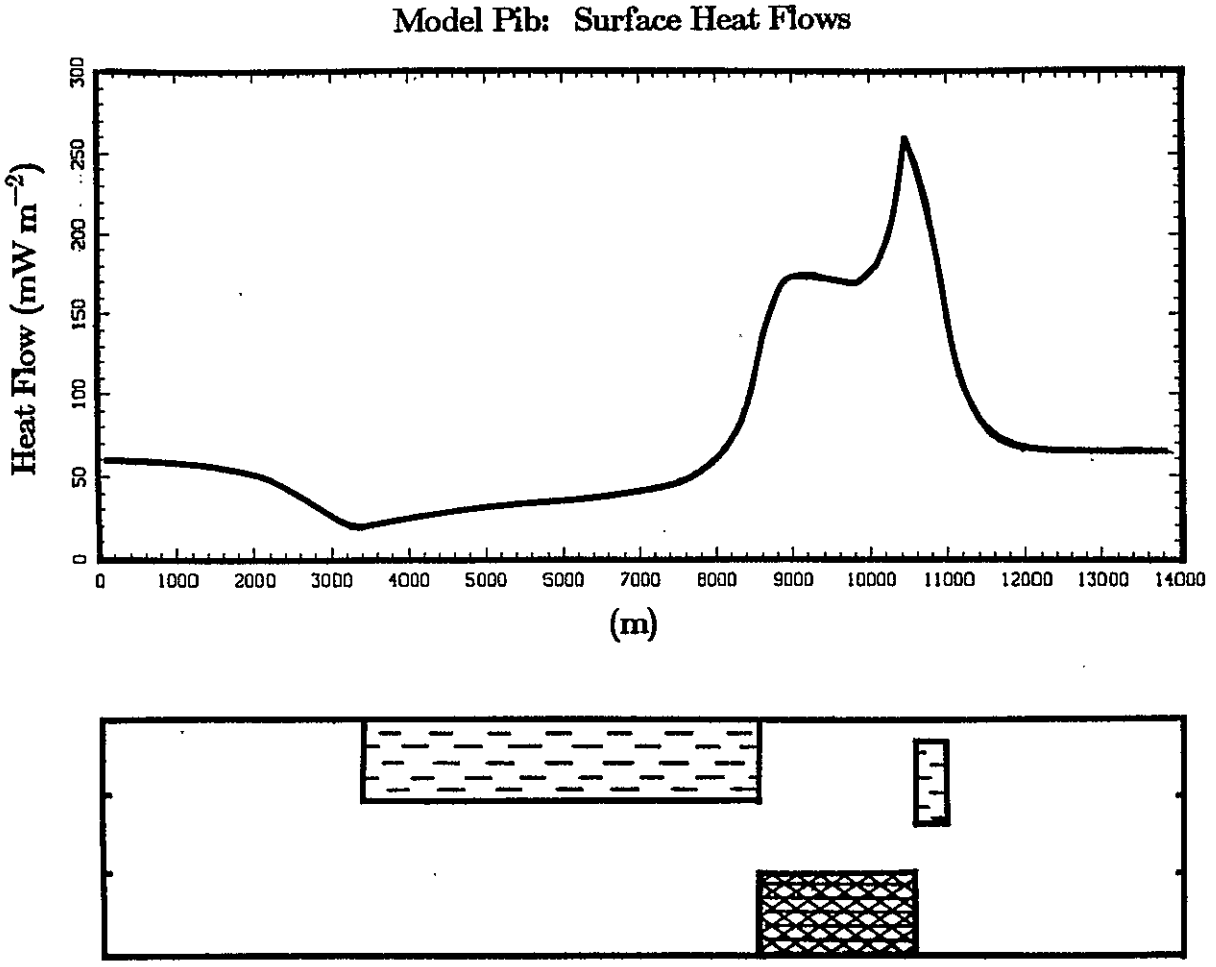

Fig. 21. Numerically generated surface heat-flow profile of model Pib. Units A and B are the same as in the base model but a block representing basement topography has been added (cross hatched area, $k_H = 10^{-17}\ m\ s^{-1}$).

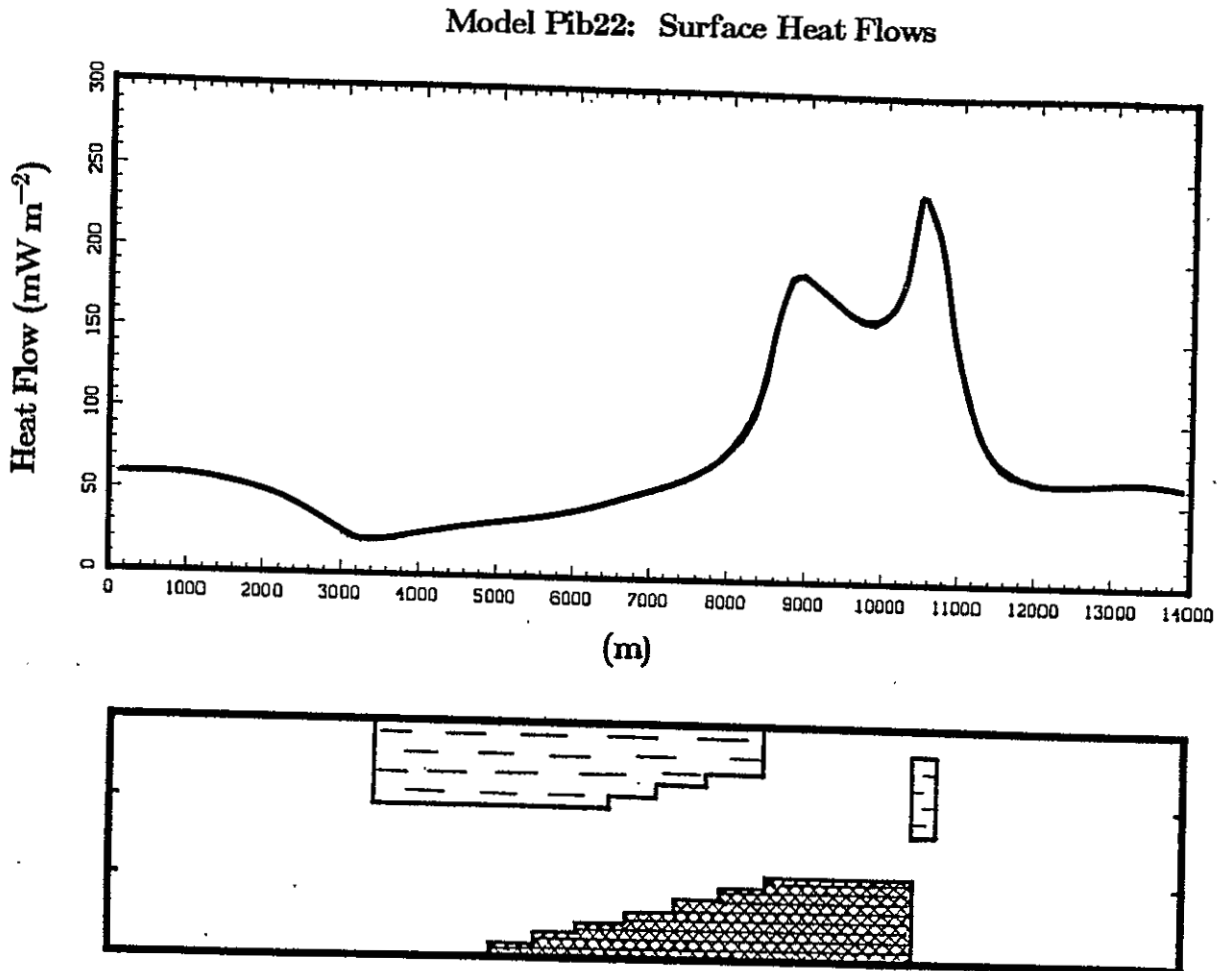

Fig. 22. Numerically generated surface heat-flow profile of model Pib22. Unit B is the same as in the base model. The bottom right side of unit A now slopes down to the left, representing west dip. The hatchured area ($k_H = 10^{-17}\ m\ s^{-1}$). represents basement topography, also dipping west.

(Table 2), but not as high as Pib, perhaps because some more hydrologic upflow occurs to the right of the hydrologic window (due to the dipping basement) and so less upflow occurs in the hydrologic window itself. The net hydrologic flow through this system is the same as through Pib.

THERMAL REFRACTION

Thermal conductivity (k_Θ) variation is also important in the Socorro geothermal system. As mentioned previously, the k_Θ of the Precambrian rock at Wood's Tunnel (Fig. 13) is twice that of surrounding materials, and the fracture hydraulic conductivity of the Precambrian rock in this area may be fairly high. We suggest that the extremely high heat flows of Wood's Tunnel may be caused be a combination of hydrologic upflow and thermal refraction. We have modeled such a system, and have compared the results with results from base model in Figure 23. The new model combines the heterogeneous k_H distribution of the base model with a new heterogeneous k_Θ distribution. The hash-marked high k_Θ area in Figure 23 represents Precambrian rocks. The change in thermal conductivity distribution has no effect on the hydraulic model. The net hydraulic flux through this system is the same as in the base model: $1.3 \times 10^{-5}\ m^2 s^{-1}$.

The maximum surface heat flow generated by this model is in the hydrologic window, as before. In this model the hydrologic window is also a high k_Θ zone, and the maximum heat flow is almost twice as high as that produced by the base model ($300\ mW\ m^{-2}$ compared to $180\ mW\ m^{-2}$). These results compare favorably with observations in the Socorro area. The highest heat flows measured in the Socorro area are in and near Precambrian rock. The heat flow observed at Wood's Tunnel ($490\ mW\ m^{-2}$) is almost twice the magnitude of the high heat flows observed in Blue and Socorro Canyons ($\approx 220 - 290\ mW\ m^{-2}$). We

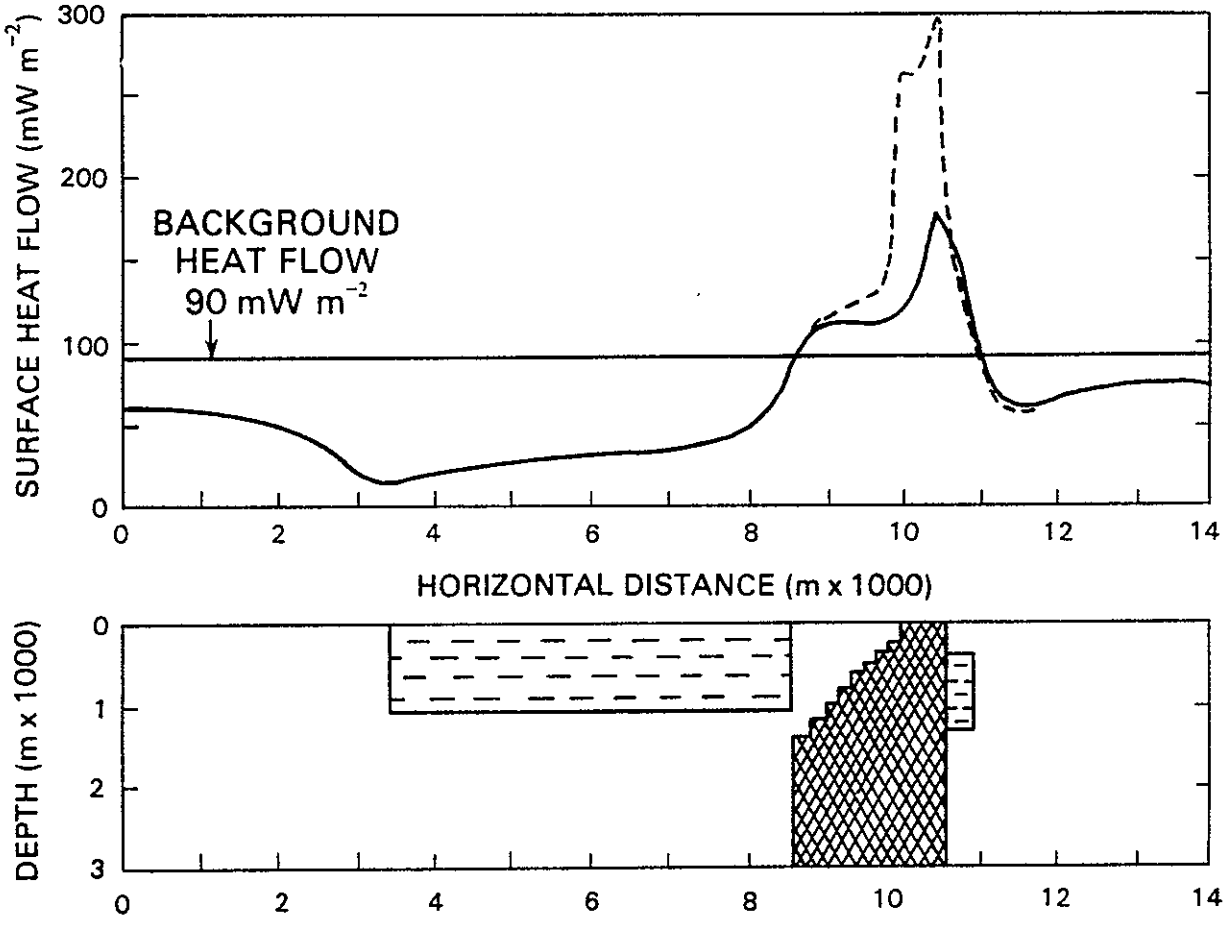

Fig 23. Numerical simulation results for heterogeneous thermal conductivity, compared with base model results. k_Θ of the hatchured area is 3 $W(m^\circ K)^{-1}$, k_Θ of the rest of the system is 1.5 $W(m^\circ K)^{-1}$. Hydraulic conductivity distribution is the same as the base model, described in caption of Figure 14.

conclude that the extremely high heat flow of the Wood's Tunnel area could be caused by a combination of ground-water upflow and thermal refraction. We conclude that the highest heat flows in the Socorro area are found near Wood's Tunnel because of the effect of thermal refraction in the upfaulted, high k_Θ Precambrian rocks.

ANISOTROPY

The models previously presented all have isotropic hydrologic conductivity distributions. We suggest that vertical cooling fractures in volcanic rocks in the Socorro area could cause these volcanic rocks to have greater vertical hydraulic conductivity (k_{HZ}) than horizontal (k_{HX}). The geothermal anomalies in Blue and Socorro canyons occur in volcanic rocks, therefore enhanced k_{HZ} in these rocks could be an important effect. Figure 24 illustrates a model which is, in most respects, identical to the base model except that in the parts of the system representing volcanic rocks k_{HZ} is 10 times k_{HX}. (The distribution of k_{HX} in this model is the same as the base model, only k_{HZ} in the volcanic rocks differs). The total hydrologic flux through this model is about the same as the base model (Table 2).

In the anisotropic model, heat-flow anomalies occur in the same locations as in the base model, but The shape of the surface heat-flow profile in the hydrologic window is somewhat different. The heat-flow profile of the base model has a single peak with a "shoulder" on its left side, above the hydrologic window. The anisotropic model has a double peak. The new peak (173 $mW\ m^{-2}$) is at the left hand edge of the hydrologic window, indicating that upflow of the ground water from confinement beneath the unit A aquitard has been greatly enhanced. The heat-flow peak at the upstream edge of unit B has been increased by anisotropy

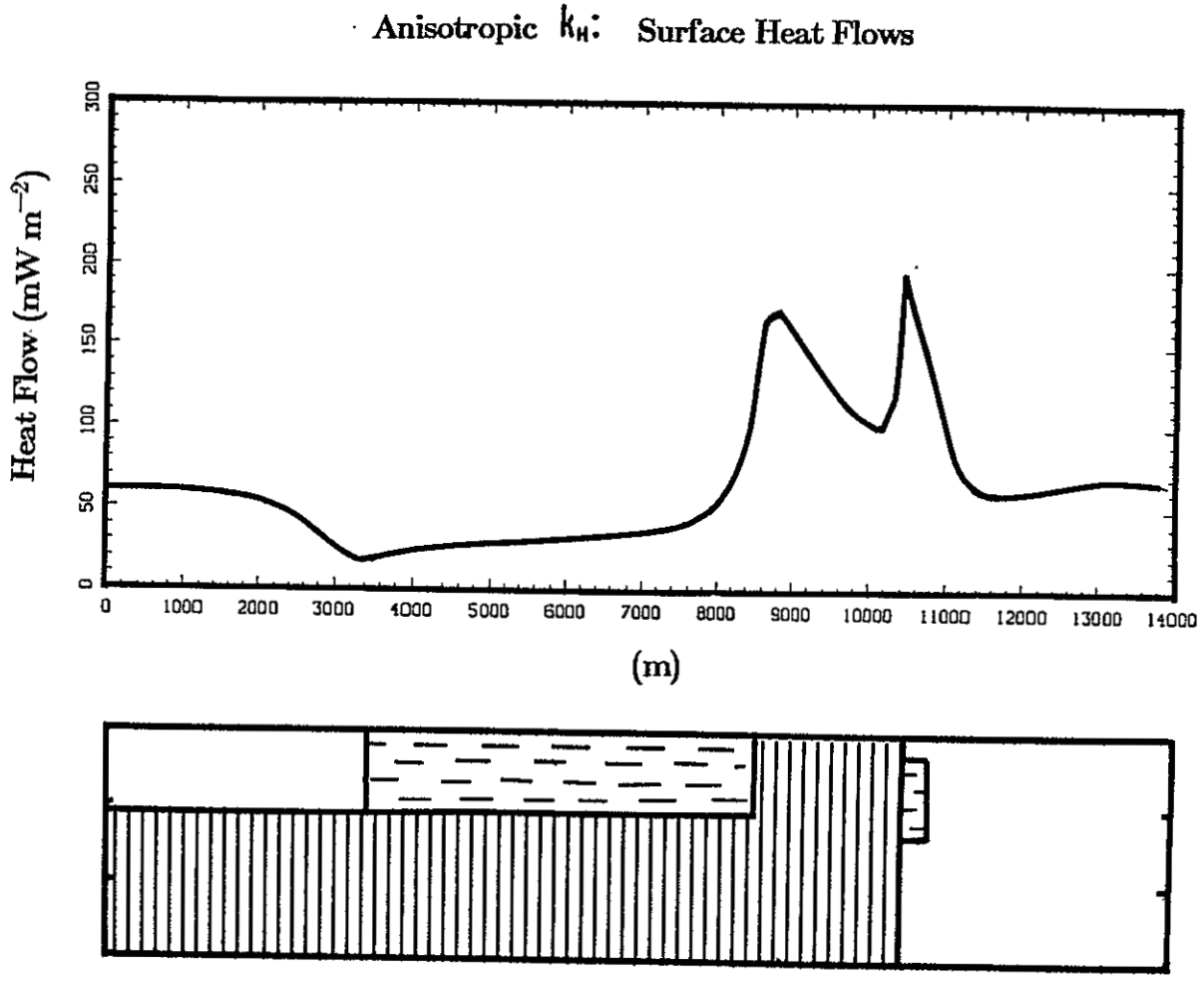

Fig 24. Numerical simulation results for anistropic hydraulic conductivity. Area with vertical stripes has $k_{HZ} = 2 \times 10^{-6}$ and $k_{HX} = 2 \times 10^{-7}$. The remainder of the model has the same parameters as the base model.

also, but only by $\approx 22\ mW\ m^{-2}$, whereas the heat flow at the left edge of the window has been increased by $\approx 63\ mW\ m^{-2}$.

The net effect of anisotropy is to produce more uniformly elevated heat flows in the hydrologic window, instead of a dominant heat-flow peak near unit B. This is caused by enhanced hydrologic outflow throughout the hydrologic window. We expect that the influence of thermal bouyancy, if included in the model, would be similar. The relatively high temperatures of fluid beneath the unit A aquitard would cause that water to be more bouyant, increasing the vertical hydraulic head gradient and thereby increasing upward flow. We do not know what the magnitude of this effect would be.

HEAT BALANCE

Heat balance calculations are described in some detail in Appendix F. An initial heat budget calculation was performed including the heat conducted out of the surface of an "area of interest" (Q_{out}) and the heat convected out of the area by the thermal springs (Q_S) (Figure 25a). We estimate that this heat could be provided by an average basal heat flow of $76 - 82\ mW\ m^{-2}$. Reiter et al. (1986) suggest a background heat flow of $77\ mW\ m^{-2}$ for the Albuquerque-Belen Basin (north of Socorro, within the Rio Grande rift) and $95\ mW\ m^{-2}$ for the Rio Grande rift south of Socorro. Therefore, a background heat flow of $76 - 82\ mW\ m^{-2}$ would be at the low end of the range. Thus, the observed surface heat output at the Socorro geothermal system does not, of itself, suggest the necessity of anomalous crustal heat sources in the Socorro area. Ingebritsen et al. (1989) came to similar conclusions for part of the Cascade Range, based on heat budget analysis; they found that ground-water circulation sweeps sufficient heat out of recharge areas to account for the anomalous heat observed in nearby discharge

areas.

Heat advected out of the system in the subsurface has not been considered in the simple heat balance calculations described above. The volume and temperature of hydrologic underflow leaving the system is not known, but underflow into the Socorro Basin could advect substantial amounts of heat out of the Socorro mountain block and out of the system, masking the effect of thermal sources (Figure 25b). For example, if underflow is equal to the difference between local recharge (as described in Appendix F) and spring discharge, and the underflow undergoes a temperature increase of $20^{o}\,C$ between entering and leaving the system, that flow would carry $\approx 13\ MW$ out of the system. If this extra heat is included in the heat balance, a higher average heat flow of 120 $mW\,m^{-2}$ is required, which would be somewhat high for this part of the Rio Grande rift.

SUGGESTIONS FOR FURTHER RESEARCH

There are two directions that further investigation of the Socorro hydrogeothermal system can take: field studies and additional modeling. Field studies are important because the hydrologic parameters of the Socorro area are very poorly constrained. One of the most important units is the Tertiary volcanic aquifer, about which we have almost no quantitative information. Testing of the Blue Canyon Well might yield important constraints on the hydrologic properties of the volcanic aquifer near the surface. It would be necessary to drill and test deeper wells to determine the properties of the volcanic aquifer at depth, beneath the claystone aquitard. The total thickness of the volcanic aquifer might be determined by analysis of seismic data, such as the COCORP profile through La Jencia Basin (de Voogd et al., 1988).

HEAT BALANCE (SIMPLIFIED)

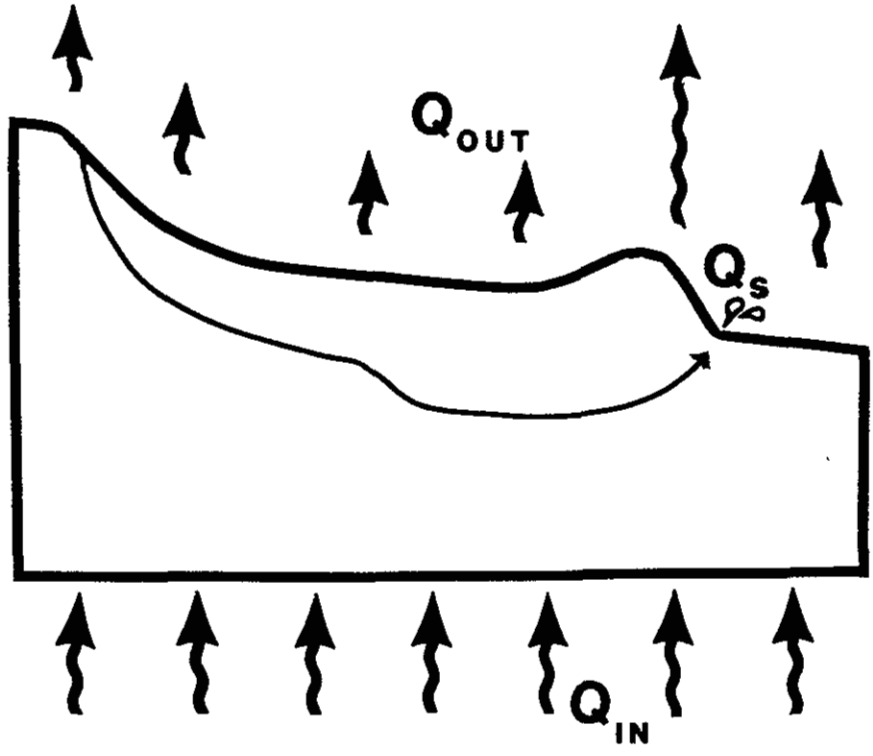

$$Q_{IN} = Q_{OUT} + Q_s$$

Fig. 25a. Simplified heat balance. This figure represents a generalized cross section from the Magdalena Mountains to Socorro Basin. Long thin line represents ground water flowing from the Magdelena Mountains to discharge at the Socorro thermal springs. Fat arrows represent conductive heat flow. Q_{out} is the net heat conducted out of the top surface of the system, Q_{in} is the net heat conducted into the base of the system, Q_s is the heat convected out of the system by the thermal springs.

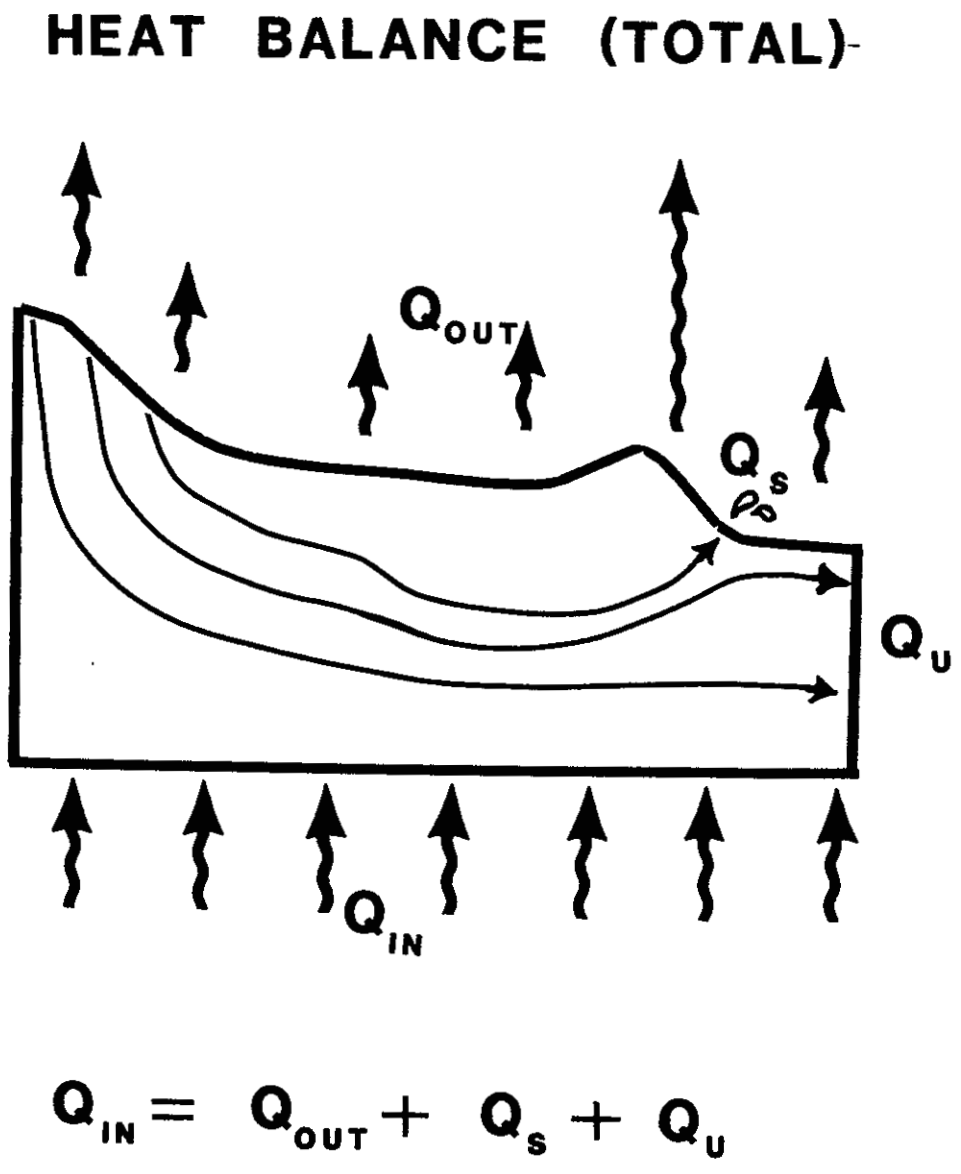

Fig. 25b. More complete heat balance. Q_s is the heat convected out of the system by hydrologic underflow.

Forced convective heat transport in a steady-state, two-dimensional system was modeled in this study. Thermal bouyancy could be incorporated into the model, in order to determine whether or not free convection is likely to be important in the system. We do not anticipate that thermal bouyancy will change the model results in any important way. Thermal bouyancy will probably enhance upflow in the hydrologic window, much as occurs in the anisotropic model (Figure 24), and lead to somewhat more elevated heat flows in that part of the model.

The next improvement to the model is to include thermal spring discharge in the model. The model upper boundary conditions for hydraulic head and temperature will have to be altered. The location of spring discharge must be given a constant head (or possibly a fixed fluid flow) boundary condition to allow spring discharge. In order to model a thermal spring, the surface temperature at the location of spring discharge can not be fixed. Instead, an energy flux boundary condition must be applied at this location. In order to model a thermal spring of the discharge and temperature observed in the Socorro area (as well as modeling the near surface heat flows), additional constraints on the model may be found, for example: the depth to which ground water flows may be more closely constrained.

Hydrogeochemical modeling is another promising avenue for research. Ion exchange processes in the secondary volcanic aquifer have been discussed, but not modeled. The model of fluid flow and temperatures presented in this study could probably be used as a basis for modeling the hydrogeochemical evolution of ground water in the Socorro system.

CONCLUSIONS

Heat flow in the Socorro geothermal area varies profoundly over very short distances, which suggests causes in the uppermost crust. Heat flow trends correlate with hydrogeologic controls on ground-water flow. It is most likely that the subsurface geothermal regime in the Socorro area is strongly influenced by subsurface hydrology.

Geothermal evidence suggests certain hydrologic flow patterns in the Socorro area. Extremely low heat flows occur in eastern La Jencia Basin where a fanglomerate aquifer changes into a claystone aquitard. We conclude that ground water is forced to flow down from the fanglomerate aquifer into more permeable materials beneath the claystone aquitard, reducing surface heat flows. Ground water is confined beneath this aquitard in eastern La Jencia Basin and western parts of the Socorro mountain block.

High heat flows occur in the Socorro mountain block where the aquitard has been eroded away from upfaulted blocks and relatively permeable volcanics rocks are exposed at the surface. We conclude that ground water flows upward in these upfaulted permeable rocks, causing elevated heat flows, and that subsurface hydrologic barriers probably act to enhance ground-water upflow in these areas. The highest heat flows are observed in and near highly fractured Precambrian rocks. We suggest that it is possible that the permeability of the Precambrian rocks is sufficiently high to allow hydrologic upflow to elevate heat flows in this area. In addition, thermal refraction caused by the relatively high thermal conductivity of the Precambrian rocks contributes to the high heat flows in this area.

Finite difference, steady-state modeling supports these conclusions. We modeled hydraulic heads in simple systems incorporating the most important features of the Socorro hydrothermal system. The numerical models show that

fluid flow in accordance with our predictions is consistent with the hydrogeology of the Socorro area. Subsurface temperature modeling of the systems incorporates heat conduction and advection of heat by hydrologic flow. The results of temperature modeling support the conclusion that a reasonable subsurface ground-water flow system could produce geothermal anomalies of the magnitudes and locations observed in the Socorro area. Basal heat input into the numerical models is a constant 90 $mW\,m^{-2}$, which is generally consistent with heat flows observed elsewhere in the Rio Grande rift. Therefore it appears that anomalously high heat input is not required to produce the geothermal anomalies observed in the Socorro area. Numerical modeling suggests that it is possible for ground-water flow to sweep anomalous heat out of the system, but the models do not include free convection, which could be very important in the case of anomalous heat sources.

Heat balance estimates suggest that the surface heat output in Socorro (conductive heat flow and advective thermal spring discharge) could be accounted for by an input background heat flow of $76 - 82\ mW\,m^{-2}$. Again, it appears that anomalous heat sources are not required to account for the heat observed at the surface in the Socorro area. The heat balance estimates neglect heat swept out of the system by hydrologic underflow, and therefore are minimum values. We conclude that if there are anomalous heat sources in the upper crust of the Socorro area, the heat from these bodies does not cause anomalous heat output at the surface in the Socorro geothermal area. These estimates of background heat flow from heat balance calculations are minimum values. Heat balance calculations including estimated underflow show that considerable amounts of anomalous heat could be swept out of the system by underflow into the Socorro Basin.

References

Anderholm, S. K., Hydrogeology of the Socorro and La Jencia basins, Socorro county, New Mexico, **Field Conf. Guideb. N. M. Geol. Soc., 34,** 303-310, 1983.

Anderholm, S. K., Hydrogeology of the Socorro and La Jencia basins, Socorro county, New Mexico, **U. S. Geol. Surv. Water-Resources Invest. Rep. 84-4342,** 62 pp., 1987.

Bachman, G. O. and H. H. Mehnert, New K-Ar dates and the late Pliocene to Holocene geomorphic history of the central Rio Grande region, **Geol. Soc. Am. Bull., 88,** 1251-1266, 1978.

Bruning, J. E., Origin of the Popatosa Formation north-central Socorro County, N. M., **Open File Report, N. M. Bur. Mines and Miner. Resour., 38,** 132 pp., 1973.

Carpenter, P. J., Apparent Q for upper crustal rocks of the central Rio Grande rift, **J. Geophys. Res., 90,** 8661-8674, 1985.

Carslaw, H. S., and Jaeger, J. C., **Conduction of Heat in Solids** Oxford Univ. Press, Oxford, 510 pp., second ed., 1959.

Chamberlin, R. M., Cenozoic stratigraphy and structure of the Socorro Peak volcanic center, central New Mexico, **Open File Report, N. M. Bur. Mines and Miner. Resour., 118,** 532 pp., 1980.

Chapin, C. E., R. M. Chamberlin, G. R. Osburn, D. W. White, and A. R. Sanford, Exploration framework of the Socorro Geothermal Area, New Mexico, in **Field Guide to Selected Cauldrons and Mining Districts of the Datil-Mogollon Volcanic Field, Spec. Publ. N. M. Geol. Soc., 7,** 114-129, 1978.

Clark, N. J., and W. K. Summers, Records of wells and springs in the Socorro and Magdalena area, Socorro County, New Mexico, 1968, **N. M. Bur. of Mines and Miner. Resour., Circ. 115,** 51 pp., 1971.

de Voogd, B., L. Serpa, and L. Brown, Crustal extension and magmatic processes; COCORP profiles from Death Valley and the Rio Grande rift, **Geol. Soc. Am. Bull., 100,** 1550-1567, 1988.

de Vries, B. A., Thermal properties of soils, in **Physics of Plant Environments,** edited by W. R. van Wijk, pp. 211-235, North-Holland, Amsterdam, 1963.

Domenico, P. A., and V. V. Palciauskas, Theoretical analysis of forced convective heat transfer in regional ground-water flow, **Geol. Soc. Am. Bull., 84,** 3803-3814, 1973.

Eggleston, T. L., G. R. Osburn, and C. E. Chapin, Third day road log from Socorro to San Antonio, Nogal Canyon, Chupadera Mountains, Luis Lopez manganese district, and the MCA mine, **Field Conf. Guideb. N. M. Geol. Soc., 34,** 61-83, 1983.

Freeze, R. A. and J. A. Cherry, **Groundwater** Prentice-Hall, Englewood Cliffs, New Jersey, 1979.

Gabin, V. L. and L. E. Lesperance, **New Mexico climatological data, precipitation, temperature, evaporation and wind, monthly and annual means 1850-1975,** W. K. Summers and Assoc., Socorro, N. M., 436 pp., 1977.

Gross, G. W. and R. Wilcox, Groundwater circulation in the Socorro geothermal area, **State-Coupled Low Temperature Geothermal Resource Assessment Program, Fiscal Year 1980, Final Technical Rep.,** edited by L. Icerman, A. Starkey, and N. Trentman, pp. 2-95 to 2-189, N. M. S. U., Las Cruces, N. M., 1981.

Gross, G. W. and R. Wilcox, Groundwater circulation in the Socorro geothermal area, **Field Conf. Guideb. N. M. Geol. Soc., 34,** 311-318, 1983.

Hall, F. R., Springs in the vicinity of Socorro, N. M., **Field Conf. Guideb. N. M. Geol. Soc., 14,** 160-179, 1963.

Harder, V., P. Morgan, and C. A. Swanberg, Geothermal resources in the Rio Grande rift: origins and potential, **Trans. Geothermal Resour. Counc., 4,** 61-64, 1980.

Hawkins D. B. and Stephens, D. B., Geothermal Data Availability for Computer Simulation in the Socorro Peak KGRA, Socorro County, N. M., in **State-Coupled Low Temperature Geothermal Resource Assessment Program, Fiscal Year 1980, Final Technical Rep.,** edited by L. Icerman, A. Starkey, and N. Trentman, pp. 2-11 to 2-89, N. M. S. U., Las Cruces, N. M., 1981.

Ibrahim, A-B. K., 1962, Relation between compressional wave velocity and aquifer porosity, **M.S. Thesis,** Geoscience Dept., New Mexico Instit. of Mining and Technology, 59 pp., 1962.

Ingebritsen, S. E., D. R. Sherrod, and R. H. Mariner, Heat flow and hydrothermal circulation in the Cascade Range, north-central Oregon, **Science, 243,** 1458-1462, 1989.

Kilty, K. and D. S. Chapman, Convective heat transfer in selected geologic situations, **Groundwater, 18,** 386-394, 1980.

Lachenbruch, A. H. and J. H. Sass, Heat flow in the United States and the thermal regime of the crust, in **The Nature and Physical Properties of the Earth's Crust,** edited by J. G. Heacock, pp. 626-675, AGU, Washington, D. C., 1977.

Minier, J. D., A geothermal study in west-central New Mexico, **Ph.D. Dissertation,** New Mexico Instit. of Mining and Technology, Socorro, New Mexico, 1987.

Morris, D. A. and A. I. Johnson, Summary of hydrologic and physical properties of rock and soil materials as analyzed by the hydrologic laboratory of the U. S. Geological Survey -- 1948-1960. **U. S. Geological Survey Water Supply Paper 1839-D,** 1967.

Reiter, M. and H. Hartman, A new steady-state method for determining thermal conductivity, **J. Geophys. Res., 76,** 7047-7051, 1971.

Reiter, M., and R. Smith, Subsurface temperature data in the Socorro Peak, KGRA, New Mexico, **Geotherm. Energy Mag., 5,** 37-41, 1977.

Reiter, M., R. E. Eggleston, B. R. Broadwell, and J. Minier, Estimates of terrestrial heat flow from deep petroleum tests along the Rio Grande rift in central and southern New Mexico, **J. Geophys. Res., 91,** 6225-6245, 1986.

Rinehart, E. J., A. R. Sanford, and R. M. Ward, Geographic extent and shape of an extensive magma body at mid-crustal depths in the Rio Grande rift near Socorro, New Mexico, in **Rio Grande Rift: Tectonics and Magmatism** , edited by R. E. Riecker, pp. 237-251, AGU, Washington, D. C., 1979.

Sanford, A. S., Temperature gradient and heat flow measurements in the Socorro, N. M. area, 1965-1968, **Geophysics Open File Rep. 15,** 19 pp., N. M. Inst. of Min. and Technol., Socorro, 1977.

Sanford, A. S., Magma bodies in the Rio Grande rift in central New Mexico, **Field Conf. Guideb. N. M. Geol. Soc., 34,** 123-125, 1983.

Sanford, A. S., Seismic measurements of the Tertiary fill in the Rio Grande depression west of Socorro, N. M., **State-Coupled Low Temperature Geothermal Resource Assessment Program, Fiscal Year 1980, Final Technical Rep.,** edited by L. Icerman, A. Starkey, and N. Trentman, pp. 2-1 to 2-10, N. M. S. U., Las Cruces, N. M., 1981.

Sass, J. H., A. H. Lachenbruch, and R. J. Munroe, Thermal conductivity of rocks from measurements on fragments and its applications to heat flow determinations, **J. Geophys. Res., 76,** 3391-3401, 1971.

Severini, A. P., and D. Huntley, Heat convection in Warm Springs Valley, Virginia, **Groundwater, 21,** 726-732, 1983.

Shearer, C. R., A regional terrestrial heat-flow study in Arizona, **Ph.D. Dissertation,** New Mexico Instit. of Mining and Technology, Socorro, New Mexico, 184 pp., 1979.

Smith, C., Thermal hydrology and heat flow of Beoware geothermal area, Nevada, **Geophysics, 48,** 618-626, 1983.

Stone, W. J., Preliminary hydrologic maps of the Socorro Peak area, **N. M. Bur. Mines and Miner. Resour. Open File Maps,** 4 sheets, 1977.

Summers, W. K., Catalogue of themal waters in New Mexico, **N. M. Bur. Mines and Miner. Resour. Hydrologic Rep. 4,** 80 pp., 1976.

Witcher, J. C., Geothermal resources of southwestern New Mexico and southeastern Arizona, **Field Conf. Guideb. N. M. Geol. Soc., 39,** 191-197, 1988.

Woodside, W. and J. H. Messmer, Thermal conductivity of Porous Media. I. Unconsolidated Sands, **Journal of Applied Physics, 32,** 1688-1706, 1961.

Appendix A

Temperature-Depth and Thermal Conductivity data

This appendix presents heat production data, well location data, temperature-depth data, plots and thermal conductivity data k_Θ from 49 industry geothermal wells. Table A1 contains the site elevation, latitude and longitude, and depth of each industry geothermal well. The following pages contain temperature-depth plots from the industry geothermal data set, and tables of temperature depth data and thermal conductivity data from each of these wells. (Note: the location of well 40 is somewhat uncertain.)

All temperatures were measured by the industrial operators several months or more after the well was drilled. Thermal conductivity values were either measured in the lab as part of this study or measured by the operator. In a few cases, neither samples nor any measurement of k_Θ are available, and in these cases we estimated k_Θ from measurements in similar lithology in other wells.

The following thermal conductivity data are presented:

Depth Int	Depth interval (in meters) from which the $k_{\Theta M}$ values were measured
Lith	Lithology of the interval based on lithologic logs by Chapin or Osburn, driller's logs, and/or our own observation of the samples.
$k_{\Theta M}$	Matrix thermal conductivity (mean value)
SSD	Sample standard deviation of $k_{\Theta M}$ (no entry if there are fewer than 3 measurements)
N	Number of measurements (0 indicated no sample)

Φ	In-situ porosity: estimated using values in Table C1 unless measurement noted.
$\Delta\Phi$	Estimated uncertainty in Φ
k_Θ	In-situ thermal conductivity
Δk_Θ	Uncertainty in k_Θ due to uncertainty in Φ and $k_{\Theta M}$

The following abbreviations are used in summarizing lithology:

B	Boulders
G	Gravel
S	Sand
SS	Sandstone
M	Mud
MS	Mudstone
C	Clay
CS	Claystone
(p)	Upper Popatosa Formation claystone
Conglom	Indurated comglomerate rock
Bas And	Basaltic Andesite
TV	Tertiary volcanic rocks
W Tuff	Welded Tuff

Sedimentary materials are described by listing components in descending order of importance: e.g. C,S & G would be a sandy clay with some gravel.

Thermal conductivty measurement is described in Appendix C, and heat-flow determination is described in Appendix B.

TABLE A1: Well Locations

Well Number	Depth (M)	Elevation (M)	Location					
			Latitude			Longitude		
				min	sec		min	sec
1	98	1875	34	05	57	107	07	56
2	89	1871	34	05	57	107	07	44
3	87	2014	34	04	19	107	07	57
4	96	1950	34	03	18	107	06	25
5	154	1756	34	05	45	107	01	55
6	154	1780	34	05	05	107	02	23
7	116	1801	34	04	50	107	03	12
8	150	1737	34	04	46	107	01	06
9	146	1716	34	04	55	107	00	36
10	610	1743	34	04	50	107	00	18
11	154	1682	34	05	06	106	59	42
12	151	1756	34	04	14	107	01	24
13	152	1780	34	03	50	107	01	40
14	147	1780	34	03	35	107	01	05
15	610	1804	34	03	20	107	02	05
16	154	1728	34	02	34	107	00	24
17	60	1860	34	02	50	107	03	55
18	91	1938	34	00	52	107	03	37
19	415	1856	34	01	00	107	02	30
20	115	1856	34	00	18	107	02	10
21	140	1804	34	00	42	107	01	35
22	152	1829	34	01	09	107	01	35
23	610	1725	34	01	27	107	00	45
24	140	1707	34	01	00	107	00	15
25	152	1701	34	00	32	106	59	42

TABLE A1, Continued

Well Number	Depth (M)	Elevation (M)	Location					
			Latitude			Longitude		
				min	sec		min	sec
26	610	1725	34	02	04	106	59	05
27	610	1707	34	02	02	106	58	13
28	151	1676	34	02	02	106	58	00
29	146	1570	34	01	28	106	56	26
30	115	1643	34	00	22	106	59	05
31	61	1634	34	00	08	106	58	35
32	73	1622	34	00	22	106	58	31
33	152	1622	34	00	11	106	58	18
34	152	1622	33	59	56	106	57	55
35	146	1590	33	59	50	106	57	43
36	72	1585	33	58	22	106	57	22
37	440	1579	34	00	13	106	56	38
38	123	1582	34	00	18	106	56	35
39	79	1509	34	01	18	106	55	37
40	117	1470	34	03	46	106	56	15
			34	04	10	106	56	15
41	98	1494	34	06	44	106	56	25
42	79	1536	34	06	50	106	57	04
43	152	1603	34	06	48	106	58	32
44	70	1500	34	07	30	106	56	53
45	76	1634	34	08	40	106	58	38
46	134	1588	34	10	52	106	57	23
47	76	1487	34	13	20	106	56	28
48	91	1472	34	05	17	106	50	15
49	91	1408	33	59	23	106	50	37

Table A1. Locations of industy geothermal sites. Latitude North and Longitude West are accurate to ≈5". Location of Well 40 is questionable, the operator plotted it at two different locations.

Heat Production

The concentrations Uranium and Thorium in Socorro area Precambrian and Tertiary volcanic rocks were measured by M. Wilks using Instrument Neutron Activation. The results are found in Table A2. In general, we observe that the Tertiary volcanics have greater radiogenic heat production from U and Th than the Precambrian rocks. We do not consider radiogenic heat production to be important in the Socorro area, compared with the strong hydrothermal effects that are observed. The modeling done in this study does not include radiogenic heat production.

Concentration of U and Th were measured by Neutron Activation. A is the sum of the heat production from U and Th, calculated using 6.19 $\times 10^{-8}$ $cal\ cm^{-3}s^{-1}$ for U and 1.66 $\times 10^{-8}$ $cal\ cm^{-3}s^{-1}$ for Th.

Table A2: Heat Production from Uranium and Thorium

Sample	U (ppm)	Th (ppm)	A (HGU)
Wood's Tunnel, P€	0.87	2.89	1.0
	0.70	2.73	0.9
Well 10, TV (Lemitar Tuff)	4.31	19.03	5.8
Well 23, TV (Luis Lopez Fm.)	3.48	14.6	4.5

(TV =Tertiary volcanics, P€ =Precambrian)

Well Number: 1

Subsurface Temperatures

z (m)	T (^{o}C)	z (m)	T (^{o}C)	z (m)	T (^{o}C)	z (m)	T (^{o}C)
3.0	17.97	27.4	17.14	51.8	18.07	76.2	18.95
6.1	17.28	30.5	17.23	54.9	18.21	79.2	19.15
9.1	16.56	33.5	17.39	57.9	18.31	82.3	19.28
12.2	16.31	36.6	17.49	61.0	18.42	85.3	19.37
15.2	16.47	39.6	17.61	64.0	18.49	88.4	19.49
18.3	16.68	42.7	17.71	67.1	18.60	91.4	19.62
21.3	16.83	45.7	17.84	70.1	18.69	94.5	19.75
24.4	16.98	48.8	17.95	73.2	18.82	97.5	19.86

Thermal Conductivities

Depth Int (m)	(m)	Lith	$k_{\Theta M} \pm SSD$ $\left(\frac{W}{m^{o}C}\right)$		N	$\Phi \pm \Delta\Phi$		$k_{\Theta} \pm \Delta k_{\Theta}$ $\left(\frac{W}{m^{o}C}\right)$	
3.0	49.0	Soil,B & S	3.13 *	0.00	1	0.30	0.05	1.92	0.25
49.0	61.0	MS,S & G	3.13 *	0.00	1	0.30	0.10	1.92	0.40
61.0	98.0	S & M	3.67 *	0.37	4	0.40	0.05	1.79	0.21

Comments:

Lithologic logs: Chapin and driller's log

* k_{Θ}: operator values (ok)

Well Number: 2

Subsurface Temperatures

z (m)	T ($^\circ C$)	z (m)	T ($^\circ C$)	z (m)	T ($^\circ C$)	z (m)	T ($^\circ C$)
6.1	15.28	24.4	16.72	54.9	17.90	85.3	19.08
9.1	15.24	30.5	17.13	61.0	18.11	89.0	19.22
12.2	15.74	36.6	17.26	67.1	18.34		
15.2	16.17	42.7	17.43	73.2	18.60		
18.3	16.35	48.8	17.68	79.2	18.86		

Thermal Conductivities

Depth Int (m)	(m)	Lith	$k_{\Theta M}$ $\left(\frac{W}{m^\circ C}\right)$	$\pm$ SSD	N	Φ	$\pm \Delta\Phi$	k_Θ $\left(\frac{W}{m^\circ C}\right)$	$\pm \Delta k_\Theta$
0.0	59.0	G	3.20	0.30	6	0.30	0.05	1.95	0.21
59.0	91.0	M & S	3.22	0.25	6	0.30	0.10	1.95	0.39

Comments:
Lithologic log: Chapin

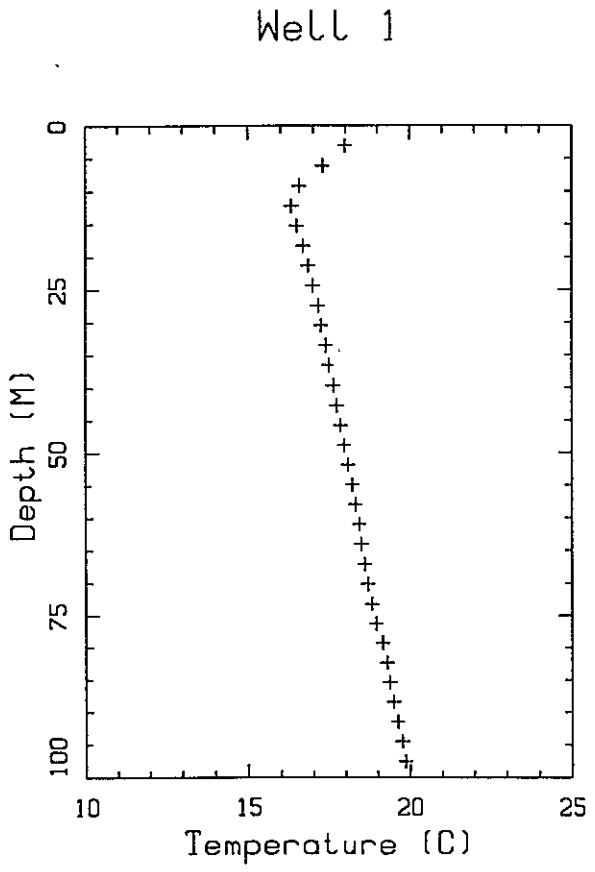
Well 1
Depth (M)
0
25
50
75
100
10
15
20
25
Temperature (C)

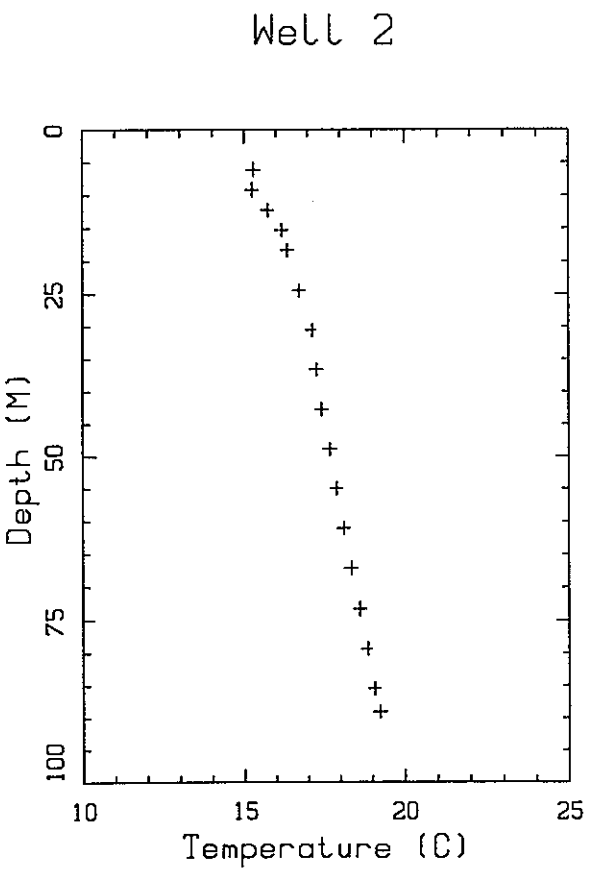
Well 2
Depth (M)
0
25
50
75
100
10
15
20
25
Temperature (C)

Well Number: 3

Subsurface Temperatures

z (m)	T (°C)	z (m)	T (°C)	z (m)	T (°C)	z (m)	T (°C)
3.0	16.71	27.4	15.95	51.8	16.79	76.2	17.44
6.1	15.81	30.5	16.00	54.9	16.86	79.2	17.52
9.1	15.27	33.5	16.22	57.9	16.94	82.3	17.60
12.2	14.99	36.6	16.30	61.0	17.01	85.3	17.68
15.2	15.16	39.6	16.47	64.0	17.10	87.2	17.68
18.3	15.35	42.7	16.57	67.1	17.19		
21.3	15.55	45.7	16.61	70.1	17.27		
24.4	15.74	48.8	16.71	73.2	17.36		

Thermal Conductivities

Depth Int (m)	(m)	Lith	$k_{\Theta M} \pm SSD$ $\left(\frac{W}{m^\circ C}\right)$		N	$\Phi \pm \Delta\Phi$		$k_\Theta \pm \Delta k_\Theta$ $\left(\frac{W}{m^\circ C}\right)$	
0.0	30.0	G	2.70 *	0.00	1	0.30	0.05	1.73	0.21
30.0	83.0	MS & S	2.85 *	0.12	3	0.30	0.10	1.79	0.32
85.0	87.0	MS & S	2.73 *	0.00	1	0.30	0.10	1.74	0.35

Comments:
Lithologic logs: Chapin and driller's log
* k_Θ: operator values (ok)

Well Number: 4

Subsurface Temperatures

z (m)	T ($^{\circ}C$)	z (m)	T ($^{\circ}C$)	z (m)	T ($^{\circ}C$)	z (m)	T ($^{\circ}C$)
3.0	17.36	27.4	15.65	51.8	16.19	76.2	16.68
6.1	15.72	30.5	15.73	54.9	16.24	79.2	16.74
9.1	14.94	33.5	15.81	57.9	16.30	82.3	16.82
12.2	14.89	36.6	15.91	61.0	16.36	85.3	16.89
15.2	15.11	39.6	16.00	64.0	16.42	88.4	16.96
18.3	15.30	42.7	16.05	67.1	16.48	91.4	17.04
21.3	15.46	45.7	16.09	70.1	16.55	94.5	17.11
24.4	15.56	48.8	16.15	73.2	16.60	96.0	17.15

Thermal Conductivities

Depth Int (m)		Lith	$k_{\Theta M} \pm SSD$ $\left(\frac{W}{m^{\circ}C}\right)$		N	$\Phi \pm \Delta\Phi$		$k_{\Theta} \pm \Delta k_{\Theta}$ $\left(\frac{W}{m^{\circ}C}\right)$	
27.0	96.0	S & M	3.04 *	0.11	5	0.40	0.05	1.60	0.18

Comments:

Lithologic logs: Chapin and driller's log

* k_{Θ}: operator values (ok)

Well 3

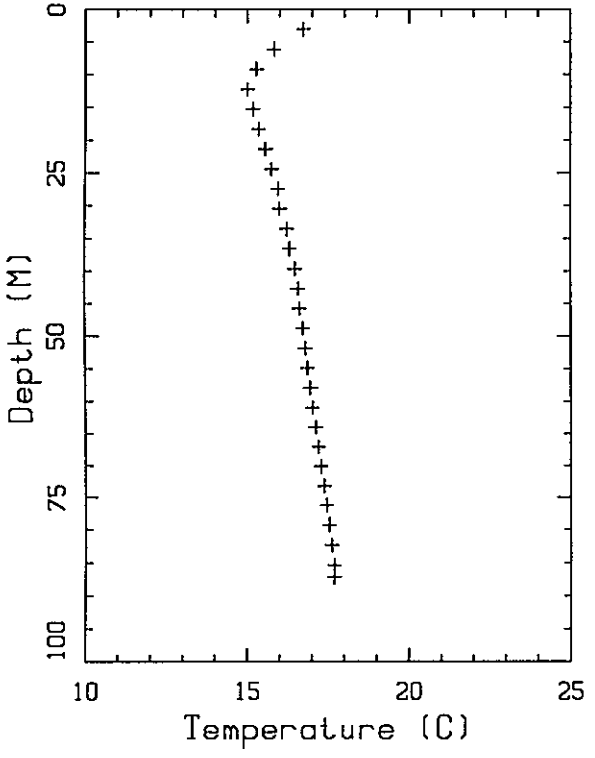
Depth (M)
0
25
50
75
100
10
15
20
25
Temperature (C)

Well 4

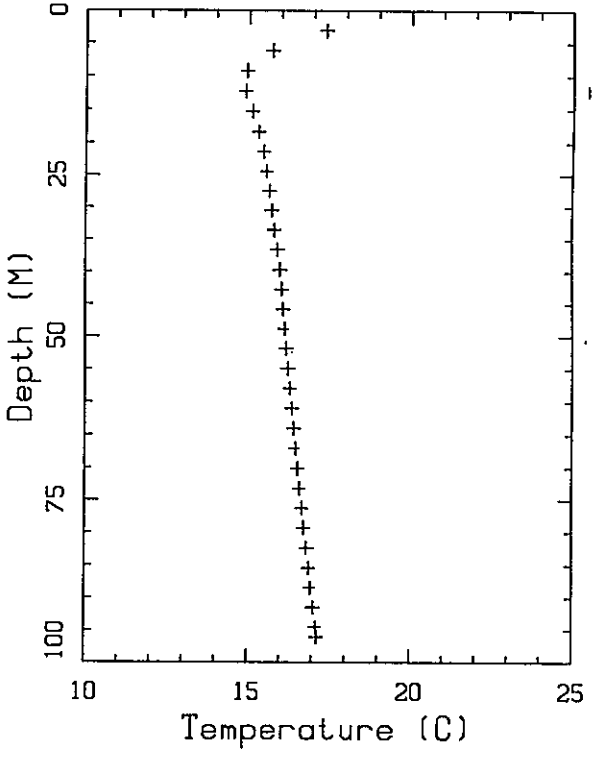
Depth (M)
0
25
50
75
100
10
15
20
25
Temperature (C)

Well Number: 5

Subsurface Temperatures

z (m)	T (°C)	z (m)	T (°C)	z (m)	T (°C)	z (m)	T (°C)
3.0	17.25	45.7	16.90	88.4	17.97	131.1	19.40
6.1	15.43	48.8	16.99	91.4	18.05	134.1	19.51
9.1	15.77	51.8	17.06	94.5	18.16	137.2	19.62
12.2	16.09	54.9	17.14	97.5	18.29	140.2	19.71
15.2	16.27	57.9	17.22	100.6	18.38	143.3	19.79
18.3	16.30	61.0	17.28	103.6	18.46	146.3	19.87
21.3	16.36	64.0	17.36	106.7	18.59	149.4	20.05
24.4	16.41	67.1	17.43	109.7	18.66	152.1	21.06
27.4	16.48	70.1	17.50	112.8	18.76		
30.5	16.53	73.2	17.57	115.8	18.91		
33.5	16.61	76.2	17.65	118.9	19.01		
36.6	16.69	79.2	17.75	121.9	19.09		
39.6	16.75	82.3	17.81	125.0	19.21		
42.7	16.82	85.3	17.88	128.0	19.31		

Thermal Conductivities

Depth Int (m)	(m)	Lith	$k_{\Theta M} \pm SSD$ $\left(\frac{W}{m^\circ C}\right)$		N	$\Phi \pm \Delta\Phi$		$k_\Theta \pm \Delta k_\Theta$ $\left(\frac{W}{m^\circ C}\right)$	
37.0	91.0	C & G (p?)	2.28		1	0.30	0.10	1.54	0.28
91.0	152.0	G & C (p?)	2.49	0.31	4	0.30	0.05	1.63	0.16

Comments:
Lithologic log: Osburn and Chapin

Well Number: 6

Subsurface Temperatures

z (m)	T ($^\circ C$)	z (m)	T ($^\circ C$)	z (m)	T ($^\circ C$)	z (m)	T ($^\circ C$)
3.0	15.74	48.8	16.52	94.5	17.13	140.2	17.91
6.1	15.45	51.8	16.49	97.5	17.18	143.3	17.97
9.1	15.85	54.9	16.51	100.6	17.23	146.3	18.03
12.2	16.03	57.9	16.54	103.6	17.27	149.4	18.09
15.2	16.13	61.0	16.59	106.7	17.32	152.4	18.15
18.3	16.18	64.0	16.63	109.7	17.37	153.6	18.16
21.3	16.23	67.1	16.67	112.8	17.43		
24.4	16.29	70.1	16.71	115.8	17.47		
27.4	16.31	73.2	16.76	118.9	17.53		
30.5	16.31	76.2	16.82	121.9	17.59		
33.5	16.36	79.2	16.87	125.0	17.64		
36.6	16.45	82.3	16.93	128.0	17.69		
39.6	16.55	85.3	16.98	131.1	17.74		
42.7	16.55	88.4	17.03	134.1	17.80		
45.7	16.59	91.4	17.09	137.2	17.86		

Thermal Conductivities

Depth Int (m)	(m)	Lith	$k_{\Theta M}$ $\pm$ *SSD* $\left(\frac{W}{m^\circ C}\right)$		N	Φ $\pm$ $\Delta\Phi$		k_Θ $\pm$ Δk_Θ $\left(\frac{W}{m^\circ C}\right)$	
6.0	152.0	CS &G (p)	2.46	0.22	6	0.20	0.05	1.86	0.19

Comments:
Lithologic log: Osburn

Well 5
Depth (M)
0
25
50
75
100
125
150
175
10
15
20
25
Temperature (C)

Well 6
Depth (M)
0
25
50
75
100
125
150
175
10
15
20
25
Temperature (C)

Well Number: 7

Subsurface Temperatures

z (m)	T ($^\circ C$)	z (m)	T ($^\circ C$)	z (m)	T ($^\circ C$)	z (m)	T ($^\circ C$)
3.0	18.21	36.6	16.18	70.1	16.33	103.6	16.59
6.1	16.53	39.6	16.20	73.2	16.34	106.7	16.62
9.1	15.59	42.7	16.22	76.2	16.33	109.7	16.54
12.2	15.58	45.7	16.26	79.2	16.37	112.8	16.52
15.2	15.77	48.8	16.23	82.3	16.39	115.8	16.74
18.3	15.91	51.8	16.24	85.3	16.40		
21.3	16.00	54.9	16.26	88.4	16.44		
24.4	16.03	57.9	16.18	91.4	16.48		
27.4	16.08	61.0	16.18	94.5	16.51		
30.5	16.12	64.0	16.31	97.5	16.53		
33.5	16.15	67.1	16.32	100.6	16.55		

Thermal Conductivities

Depth Int (m)	(m)	Lith	$k_{\Theta M} \pm SSD$ $\left(\frac{W}{m^\circ C}\right)$		N	$\Phi \pm \Delta\Phi$		$k_\Theta \pm \Delta k_\Theta$ $\left(\frac{W}{m^\circ C}\right)$	
12.0	116.0	CS,MS &G	2.89 *	0.44	9	0.30	0.10	1.81	0.38

Comments:

Lithologic logs: Chapin and driller's log

* k_Θ: values from our lab and from the operator (ok)

Well Number: 8

Subsurface Temperatures

z (m)	T (°C)	z (m)	T (°C)	z (m)	T (°C)	z (m)	T (°C)
3.0	17.05	45.7	17.06	88.4	18.15	131.1	19.48
6.1	15.44	48.8	17.13	91.4	18.25	134.1	19.57
9.1	15.83	51.8	17.19	94.5	18.34	137.2	19.66
12.2	16.07	54.9	17.27	97.5	18.41	140.2	19.77
15.2	16.17	57.9	17.34	100.6	18.50	143.3	19.88
18.3	16.30	61.0	17.41	103.6	18.60	146.3	19.97
21.3	16.39	64.0	17.48	106.7	18.69	149.4	20.06
24.4	16.49	67.1	17.57	109.7	18.78	150.3	20.09
27.4	16.57	70.1	17.64	112.8	18.88		
30.5	16.67	73.2	17.73	115.8	18.98		
33.5	16.74	76.2	17.80	118.9	19.08		
36.6	16.80	79.2	17.89	121.9	19.17		
39.6	16.87	82.3	17.97	125.0	19.28		
42.7	16.99	85.3	18.06	128.0	19.36		

Thermal Conductivities

Depth Int (m)	(m)	Lith	$k_{\Theta M} \pm SSD$ $\left(\frac{W}{m^\circ C}\right)$		N	$\Phi \pm \Delta\Phi$		$k_\Theta \pm \Delta k_\Theta$ $\left(\frac{W}{m^\circ C}\right)$	
6.0	152.0	CS &G (p)	2.45	0.25	8	0.20	0.05	1.86	0.19

Comments:
Lithologic log: Osborn

Well 7

Depth (M)
0
25
50
75
100
125
150
175
10
15
20
25
Temperature (C)

Well 8

Depth (M)
0
25
50
75
100
125
150
175
10
15
20
25
Temperature (C)

Well Number: 9

Subsurface Temperatures

z (m)	T ($^\circ C$)	z (m)	T ($^\circ C$)	z (m)	T ($^\circ C$)	z (m)	T ($^\circ C$)
3.0	16.21	39.6	17.97	76.2	19.64	112.8	21.54
6.1	15.84	42.7	18.05	79.2	19.81	115.8	21.70
9.1	16.12	45.7	18.27	82.3	19.92	118.9	21.89
12.2	16.41	48.8	18.40	85.3	20.07	121.9	22.07
15.2	16.64	51.8	18.55	88.4	20.24	125.0	22.23
18.3	16.84	54.9	18.67	91.4	20.38	128.0	22.42
21.3	16.99	57.9	18.76	94.5	20.51	131.1	22.58
24.4	17.14	61.0	18.91	97.5	20.69	134.1	22.78
27.4	17.40	64.0	19.05	100.6	20.84	137.2	22.93
30.5	17.60	67.1	19.22	103.6	21.01	140.2	23.09
33.5	17.69	70.1	19.35	106.7	21.16	143.3	23.23
36.6	17.88	73.2	19.48	109.7	21.34	146.3	23.29

Thermal Conductivities

Depth Int (m)	(m)	Lith	$k_{\Theta M} \pm SSD$ $\left(\frac{W}{m^\circ C}\right)$	N	$\Phi \pm \Delta\Phi$		$k_\Theta \pm \Delta k_\Theta$ $\left(\frac{W}{m^\circ C}\right)$	
18.0	140.0	G & M (p?)	2.69	2	0.30	0.05	1.72	0.21
140.0	152.0	Basalt	1.79	2	0.20	0.05	1.44	0.14

Comments:
Lithologic logs: Osburn and Chapin

Well 9

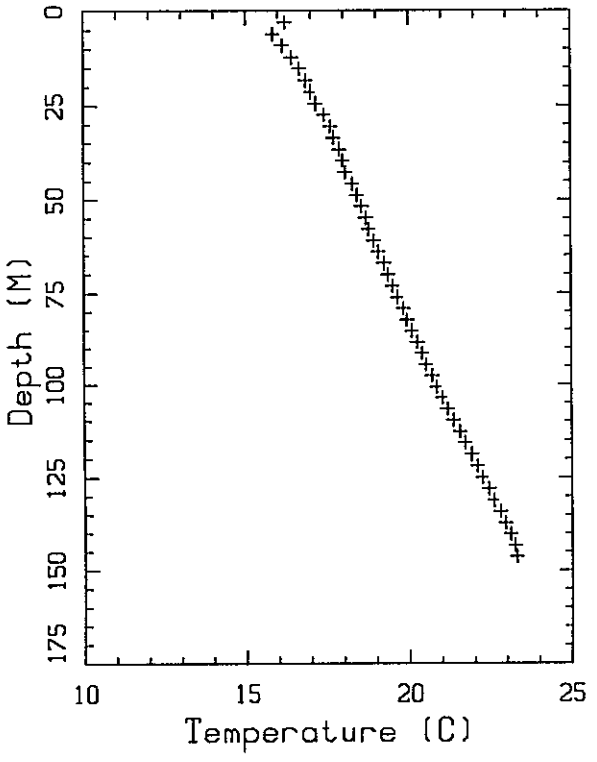

Well Number: 10

Subsurface Temperatures

z (m)	T (°C)	z (m)	T (°C)	z (m)	T (°C)	z (m)	T (°C)
0.0	24.50	158.5	21.50	310.9	27.40	463.3	31.60
6.1	24.70	164.6	21.90	317.0	27.50	469.4	31.80
12.2	24.50	170.7	22.30	323.1	27.50	475.5	32.00
18.3	24.50	176.8	22.50	329.2	27.60	481.6	32.20
24.4	16.15	182.9	22.90	335.3	27.70	487.7	32.40
30.5	15.60	189.0	23.20	341.4	27.80	493.8	32.60
36.6	15.65	195.1	23.50	347.5	27.90	499.9	32.80
42.7	15.80	201.2	23.85	353.6	28.20	506.0	33.00
54.9	16.40	207.3	24.10	359.7	28.40	512.1	33.20
61.0	16.70	213.4	24.50	365.8	28.50	518.2	33.40
67.1	16.90	219.5	24.80	371.9	28.60	524.3	33.50
73.2	17.20	225.6	25.10	378.0	28.80	530.4	33.70
79.2	17.50	231.6	25.40	384.0	29.00	536.4	33.90
85.3	17.80	237.7	25.70	390.1	29.20	542.5	34.10
91.4	18.18	243.8	25.90	396.2	29.40	548.6	34.30
97.5	18.50	249.9	26.10	402.3	29.60	554.7	34.40
103.6	18.70	256.0	26.40	408.4	29.80	560.8	34.60
109.7	19.00	262.1	26.60	414.5	30.00	566.9	34.90
115.8	19.30	268.2	26.80	420.6	29.20	573.0	35.10
121.9	19.70	274.3	26.90	426.7	30.50	579.1	35.30
128.0	20.00	280.4	27.00	432.8	30.60	585.2	35.50
134.1	20.52	286.5	27.10	438.9	30.80	591.3	35.60
140.2	20.60	292.6	27.20	445.0	31.00		
146.3	21.00	298.7	27.20	451.1	31.20		
152.4	21.30	304.8	27.30	457.2	31.40		

Well Number: 10

Thermal Conductivities

Depth Int (m)		Lith	$k_{\Theta M}$ $\left(\frac{W}{m^\circ C}\right)$	$\pm$ SSD	N	Φ	$\pm \Delta\Phi$	k_Θ $\left(\frac{W}{m^\circ C}\right)$	$\pm \Delta k_\Theta$
76.0	114.0	Basalt	1.62	0.07	3	0.20	0.10	1.33	0.17
114.0	168.0	SS	1.97	0.09	3	0.25	0.05	1.47	0.13
191.0	229.0	Mudflow	2.36	0.19	5	0.20	0.05	1.80	0.18
229.0	434.0	W Tuff	2.47	0.10	6	0.20	0.05	1.87	0.19
434.0	518.0	Bas And	1.79	0.10	4	0.20	0.05	1.44	0.12
518.0	610.0	W Tuff	2.58	0.16	8	0.20	0.05	1.93	0.19

Comments:
Lithologic log: Chapin

Well 10

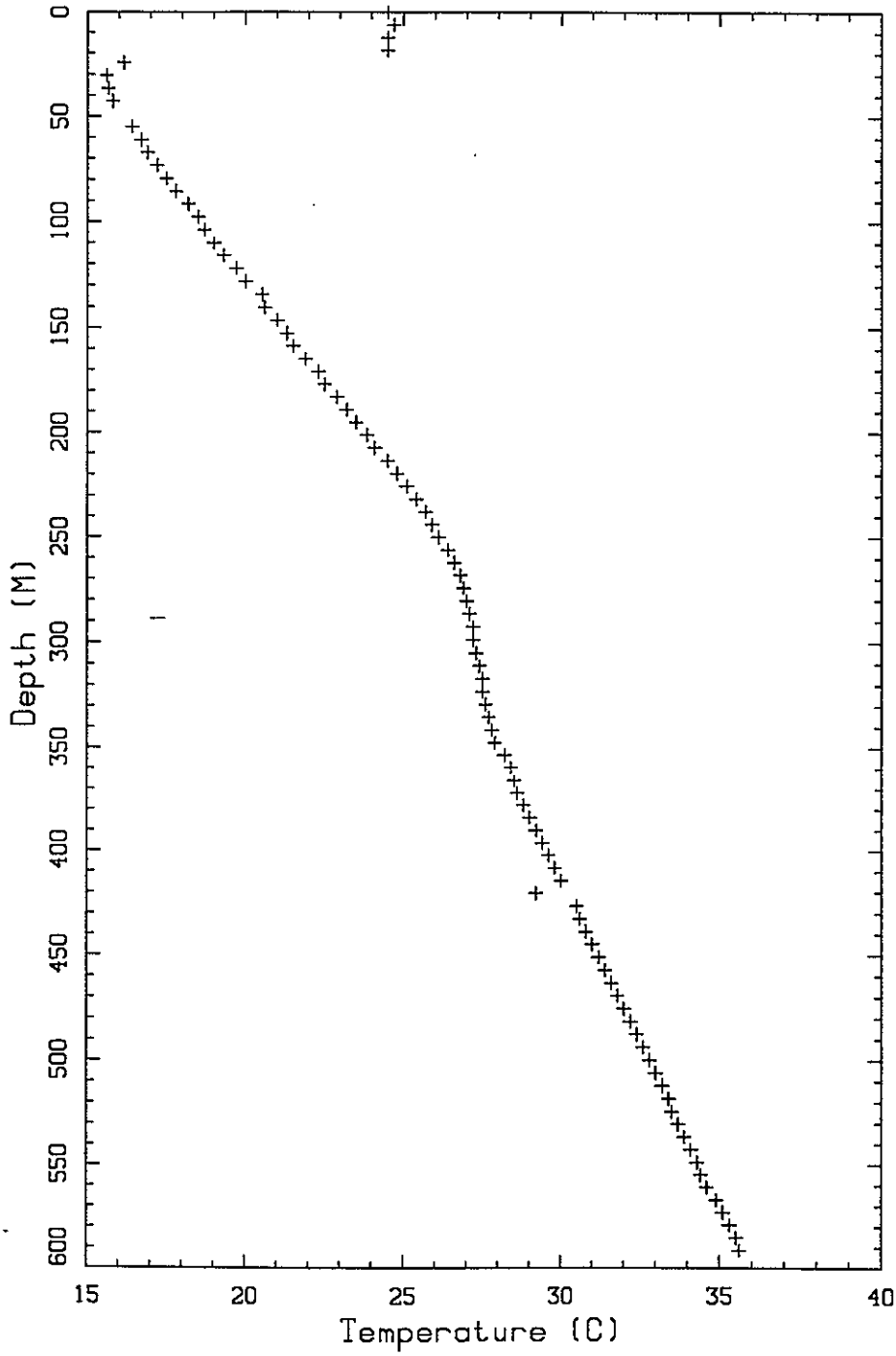
Depth (M)
0
50
100
150
200
250
300
350
400
450
500
550
600
15
20
25
30
35
40
Temperature (C)

Well Number: 11

Subsurface Temperatures

z (m)	T (^{o}C)	z (m)	T (^{o}C)	z (m)	T (^{o}C)	z (m)	T (^{o}C)
6.1	16.49	48.8	17.68	91.4	19.18	134.1	21.59
9.1	16.84	51.8	17.76	94.5	19.36	137.2	21.77
12.2	17.08	54.9	17.81	97.5	19.51	140.2	21.95
15.2	17.13	57.9	17.89	100.6	19.69	143.3	22.16
18.3	17.13	61.0	17.95	103.6	19.86	146.3	22.32
21.3	17.17	64.0	18.04	106.7	20.01	149.4	22.55
24.4	17.21	67.1	18.12	109.7	20.18	152.4	22.71
27.4	17.25	70.1	18.21	112.8	20.36	153.6	22.76
30.5	17.32	73.2	18.32	115.8	20.52		
33.5	17.38	76.2	18.48	118.9	20.68		
36.6	17.45	79.2	18.60	121.9	20.85		
39.6	17.51	82.3	18.72	125.0	21.03		
42.7	17.57	85.3	18.88	128.0	21.20		
45.7	17.64	88.4	19.03	131.1	21.39		

Thermal Conductivities

Depth Int (m)	(m)	Lith	$k_{\Theta M}$ $\pm$ SSD $\left(\frac{W}{m^{o}C}\right)$		N	Φ $\pm$ $\Delta\Phi$		k_{Θ} $\pm$ Δk_{Θ} $\left(\frac{W}{m^{o}C}\right)$	
0.0	73.0	Basalt	2.12		2	0.20	0.05	1.65	0.18
73.0	154.0	CS (p)	2.13	0.14	5	0.20	0.05	1.66	0.15

Comments:
Lithologic log: Osburn

Well Number: 12

Subsurface Temperatures

z (m)	T (°C)	z (m)	T (°C)	z (m)	T (°C)	z (m)	T (°C)
3.0	17.15	45.7	17.13	88.4	18.20	131.1	19.47
6.1	15.70	48.8	17.19	91.4	18.29	134.1	19.56
9.1	16.04	51.8	17.24	94.5	18.38	137.2	19.67
12.2	16.32	54.9	17.33	97.5	18.47	140.2	19.76
15.2	16.41	57.9	17.41	100.6	18.55	143.3	19.84
18.3	16.47	61.0	17.47	103.6	18.65	146.3	19.94
21.3	16.52	64.0	17.57	106.7	18.76	149.4	20.03
24.4	16.60	67.1	17.63	109.7	18.84	151.2	20.05
27.4	16.68	70.1	17.71	112.8	18.89		
30.5	16.73	73.2	17.79	115.8	18.98		
33.5	16.84	76.2	17.88	118.9	19.10		
36.6	16.91	79.2	17.97	121.9	19.20		
39.6	16.98	82.3	18.04	125.0	19.29		
42.7	17.08	85.3	18.13	128.0	19.38		

Thermal Conductivities

Depth Int (m)	(m)	Lith	$k_{\Theta M}$ $\pm$ SSD $\left(\frac{W}{m^\circ C}\right)$		N	Φ $\pm$ $\Delta\Phi$		k_Θ $\pm$ Δk_Θ $\left(\frac{W}{m^\circ C}\right)$	
0.0	152.0	CS &S (p)	2.47	0.12	4	0.25	0.05	1.74	0.17

Comments:
Lithologic log: Osburn

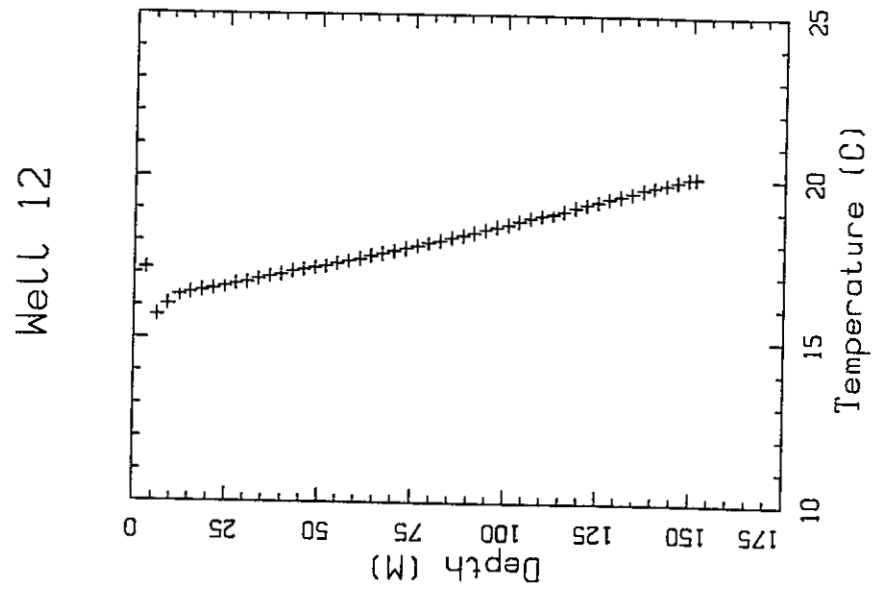
Well 12
Depth (M)
0
25
50
75
100
125
150
175
Temperature (C)
10
15
20
25

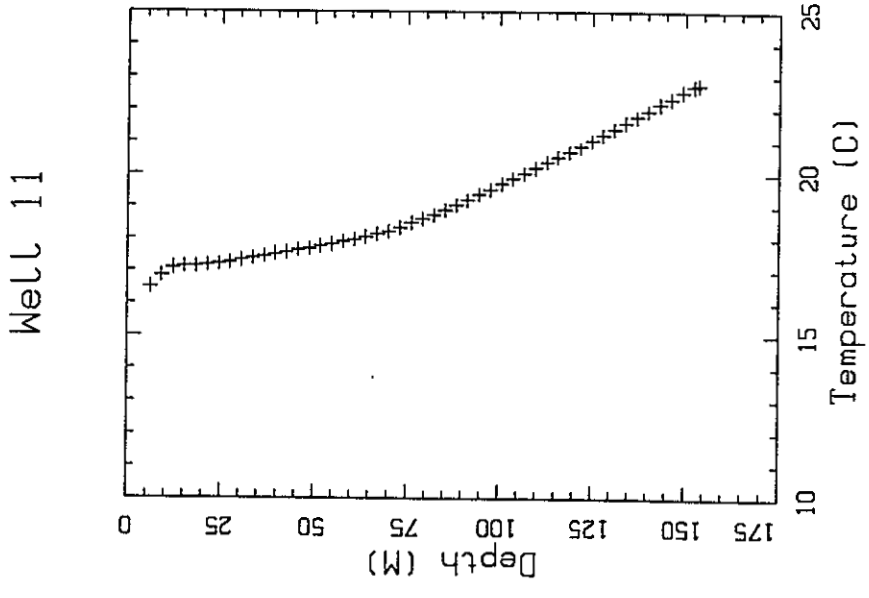
Well 11
Depth (M)
0
25
50
75
100
125
150
175
Temperature (C)
10
15
20
25

Well Number: 13

Subsurface Temperatures

z (m)	T ($^\circ C$)	z (m)	T ($^\circ C$)	z (m)	T ($^\circ C$)	z (m)	T ($^\circ C$)
3.0	17.06	30.5	16.22	85.3	17.45	140.2	18.72
6.1	16.45	36.6	16.33	91.4	17.61	146.3	18.83
9.1	16.06	42.7	16.45	97.5	17.72	152.4	18.95
12.2	15.83	48.8	16.56	103.6	18.06		
15.2	16.00	54.9	16.72	109.7	18.00		
18.3	15.95	61.0	16.83	115.8	18.11		
21.3	16.06	67.1	17.00	121.9	18.28		
24.4	16.33	73.2	17.11	128.0	18.39		
27.4	16.22	79.2	17.28	134.1	18.56		

Thermal Conductivities

Depth Int (m)	(m)	Lith	$k_{\Theta M} \pm SSD$ $\left(\frac{W}{m^\circ C}\right)$		N	$\Phi \pm \Delta\Phi$		$k_\Theta \pm \Delta k_\Theta$ $\left(\frac{W}{m^\circ C}\right)$	
12.0	116.0	CS-(p)	2.37	0.15	3	0.20	0.05	1.81	0.18
116.0	152.0	S & G	2.60		2	0.30	0.05	1.68	0.20

Comments:
Lithologic logs: Chapin, driller's log

Well Number: 14

Subsurface Temperatures

z (m)	T ($^\circ C$)	z (m)	T ($^\circ C$)	z (m)	T ($^\circ C$)	z (m)	T ($^\circ C$)
3.0	15.64	42.7	18.21	82.3	19.87	121.9	21.53
6.1	15.91	45.7	18.34	85.3	19.99	125.0	21.63
9.1	16.34	48.8	18.48	88.4	20.15	128.0	21.80
12.2	16.64	51.8	18.59	91.4	20.34	131.1	21.94
15.2	16.78	54.9	18.70	94.5	20.42	134.1	22.07
18.3	16.98	57.9	18.84	97.5	20.47	137.2	22.21
21.3	17.15	61.0	18.96	100.6	20.62	140.2	22.35
24.4	17.35	64.0	19.09	103.6	20.78	143.3	22.49
27.4	17.51	67.1	19.21	106.7	20.91	146.3	22.59
30.5	17.69	70.1	19.34	109.7	21.03	146.6	22.61
33.5	17.81	73.2	19.46	112.8	21.19		
36.6	17.94	76.2	19.61	115.8	21.35		
39.6	18.07	79.2	19.73	118.9	21.45		

Thermal Conductivities

Depth Int (m)	(m)	Lith	$k_{\Theta M} \pm SSD$ $\left(\frac{W}{m^\circ C}\right)$		N	$\Phi \pm \Delta\Phi$		$k_\Theta \pm \Delta k_\Theta$ $\left(\frac{W}{m^\circ C}\right)$	
0.0	152.0	CS (p)	2.02	0.25	6	0.20	0.05	1.59	0.17

Comments:
Lithologic log: Osburn

Well 13

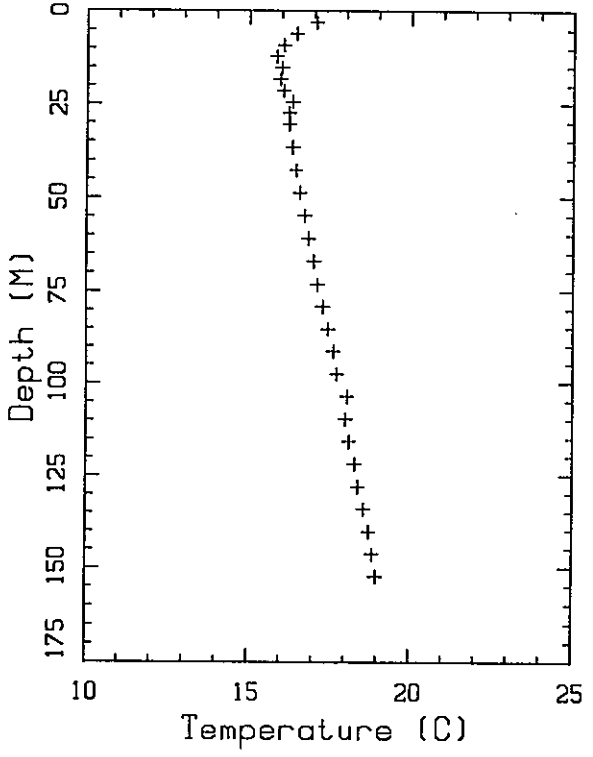

Well 14

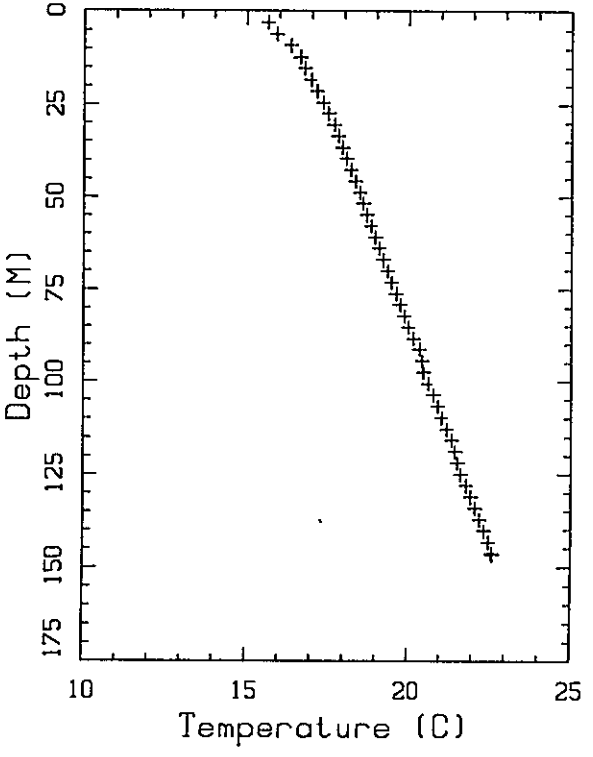

Well Number: 15

Subsurface Temperatures

z (m)	T (^{o}C)	z (m)	T (^{o}C)	z (m)	T (^{o}C)	z (m)	T (^{o}C)
0.0	28.50	152.4	15.72	304.8	18.61	457.2	21.28
6.1	28.34	158.5	15.78	310.9	18.78	463.3	21.39
18.3	28.11	164.6	15.89	317.0	18.95	469.4	21.50
18.3	27.78	170.7	16.11	323.1	19.00	475.5	21.61
24.4	27.61	176.8	16.22	329.2	19.11	481.6	21.78
30.5	27.50	182.9	16.28	335.3	19.22	487.7	21.89
36.6	27.22	189.0	16.39	341.4	19.28	493.8	22.00
42.7	27.00	195.1	16.50	347.5	19.39	499.9	22.11
48.8	26.89	201.2	16.72	353.6	19.61	506.0	22.22
54.9	16.39	207.3	16.78	359.7	19.72	512.1	22.28
61.0	15.11	213.4	16.89	365.8	19.78	518.2	22.39
67.1	14.72	219.5	17.00	371.9	19.89	524.3	22.50
73.2	14.50	225.6	17.11	378.0	20.00	530.4	22.67
79.2	14.50	231.6	17.28	384.0	20.11	536.4	22.78
85.3	14.50	237.7	17.39	390.1	20.22	542.5	22.89
91.4	14.61	243.8	17.50	396.2	20.28	548.6	23.00
97.5	14.72	249.9	17.61	402.3	20.39	554.7	23.11
103.6	14.78	256.0	17.72	408.4	20.50	560.8	23.17
109.7	14.89	262.1	17.78	414.5	20.61	566.9	23.28
115.8	15.00	268.2	18.00	420.6	20.72	573.0	23.50
121.9	15.11	274.3	18.00	426.7	20.78	579.1	23.61
128.0	15.22	280.4	18.11	432.8	20.89	585.2	23.61
134.1	15.39	286.5	18.28	438.9	21.00		
140.2	15.50	292.6	18.39	445.0	21.11		
146.3	15.61	298.7	18.50	451.1	21.22		

Well Number: 15

Thermal Conductivities

Depth Int (m)	(m)	Lith	$k_{\Theta M}$ $\left(\frac{W}{m^\circ C}\right)$	$\pm$ *SSD*	N	Φ	$\pm \Delta\Phi$	k_Θ $\left(\frac{W}{m^\circ C}\right)$	$\pm \Delta k_\Theta$
61.0	404.0	CS (p)	2.10	0.16	15	0.15	0.05	1.74	0.16
404.0	533.0	CS,SS (p)	2.26	0.03	5	0.20	0.05	1.74	0.17
533.0	610.0	SS	2.58	0.14	6	0.25	0.05	1.80	0.18

Comments:
Lithologic logs: Chapin
Porosity of CS measured in our lab

Well 15

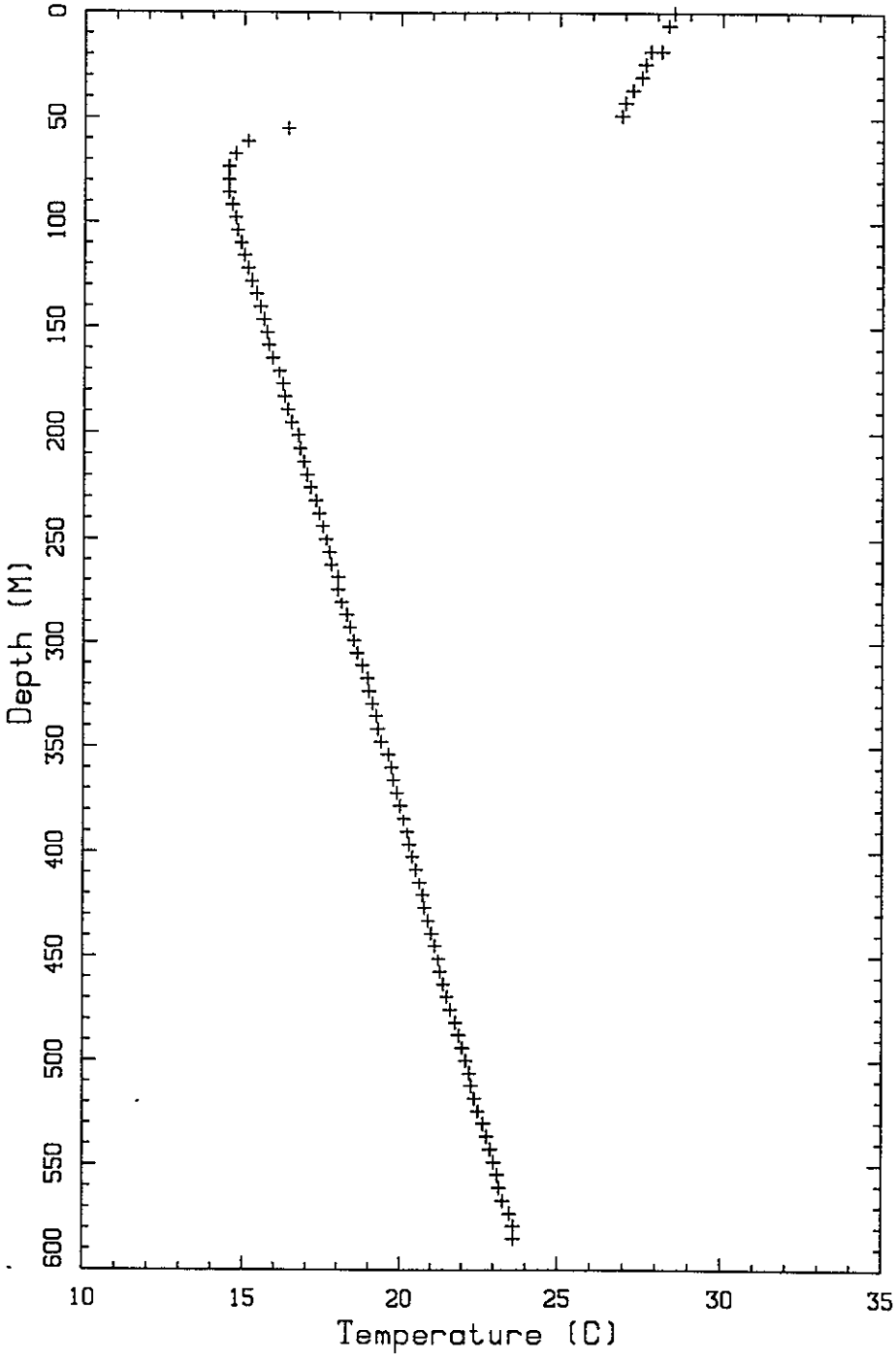
Depth (M)
0
50
100
150
200
250
300
350
400
450
500
550
600
10
15
20
25
30
35
Temperature (C)

Well Number: 16

Subsurface Temperatures

z (m)	T ($^\circ C$)	z (m)	T ($^\circ C$)	z (m)	T ($^\circ C$)	z (m)	T ($^\circ C$)
3.0	17.56	30.5	17.22	85.3	19.33	140.2	21.61
6.1	15.67	36.6	17.50	91.4	19.56	146.3	21.89
9.1	16.17	42.7	17.72	97.5	19.83	152.4	22.11
12.2	16.45	48.8	17.95	103.6	20.00		
15.2	16.56	54.9	18.22	109.7	20.28		
18.3	16.72	61.0	18.45	115.8	20.56		
21.3	16.89	67.1	18.67	121.9	20.83		
24.4	17.00	73.2	18.89	128.0	21.11		
27.4	17.11	79.2	19.11	134.1	21.34		

Thermal Conductivities

Depth Int (m)	(m)	Lith	$k_{\Theta M} \pm SSD$ $\left(\frac{W}{m^\circ C}\right)$		N	$\Phi \pm \Delta\Phi$		$k_\Theta \pm \Delta k_\Theta$ $\left(\frac{W}{m^\circ C}\right)$	
6.0	140.0	CS (p)	2.03	0.14	8	0.20	0.05	1.60	0.14

Comments:
Lithologic logs: Chapin, driller's log

Well Number: 17

Subsurface Temperatures

z (m)	T ($^\circ C$)	z (m)	T ($^\circ C$)	z (m)	T ($^\circ C$)	z (m)	T ($^\circ C$)
0.0	30.00	20.0	15.11	40.0	15.90	60.0	16.30
5.0	15.22	25.0	15.19	45.0	16.00		
10.0	14.80	30.0	15.54	50.0	16.14		
15.0	15.01	35.0	15.72	55.0	16.22		

Thermal Conductivities

Depth Int (m)	(m)	Lith	$k_{\Theta M} \pm SSD$ $\left(\frac{W}{m^\circ C}\right)$	N	$\Phi \pm \Delta\Phi$	$k_\Theta \pm \Delta k_\Theta$ $\left(\frac{W}{m^\circ C}\right)$	
0.0	60.0	S & M?		0		1.60	0.20

Comments:
Temps measured in water well
No lithologic log, no samples
k_Θ value from well #4.

Well 16

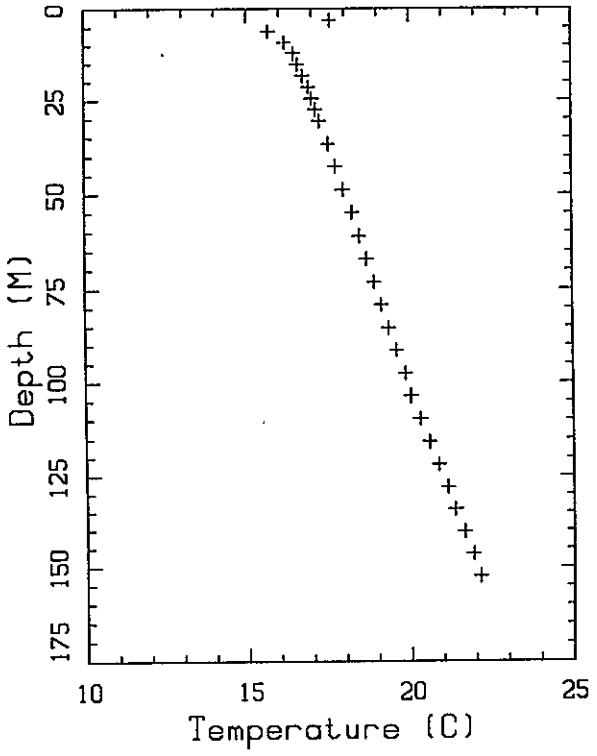

Well 17

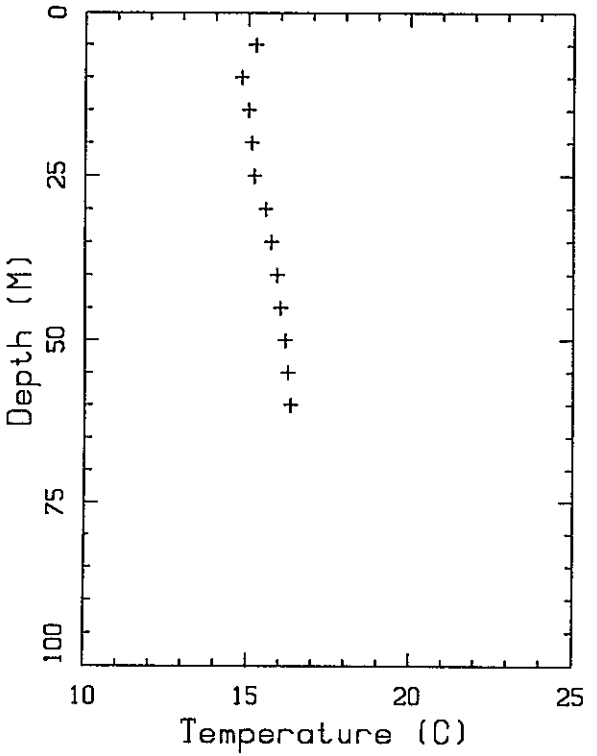

Well Number: 18

Subsurface Temperatures

z (m)	T (°C)	z (m)	T (°C)	z (m)	T (°C)	z (m)	T (°C)
3.0	17.70	30.5	16.58	57.9	17.56	85.3	18.69
6.1	16.78	33.5	16.67	61.0	17.67	88.4	18.84
9.1	15.54	36.6	16.79	64.0	17.77	91.4	18.95
12.2	15.70	39.6	16.91	67.1	17.90		
15.2	15.96	42.7	17.01	70.1	18.03		
18.3	16.11	45.7	17.12	73.2	18.17		
21.3	16.24	48.8	17.24	76.2	18.31		
24.4	16.36	51.8	17.35	79.2	18.43		
27.4	16.33	54.9	17.45	82.3	18.56		

Thermal Conductivities

Depth Int (m)	(m)	Lith	$k_{\Theta M} \pm SSD$ $\left(\frac{W}{m^\circ C}\right)$	N	$\Phi \pm \Delta\Phi$		$k_\Theta \pm \Delta k_\Theta$ $\left(\frac{W}{m^\circ C}\right)$	
21.0	91.0	MS,S & G	2.16 *	0.16	8	0.30	0.10	1.48	0.23

Comments:
Lithologic logs: Chapin and driller's log
* k_Θ: values from our lab and from the operator (ok)

Well 18

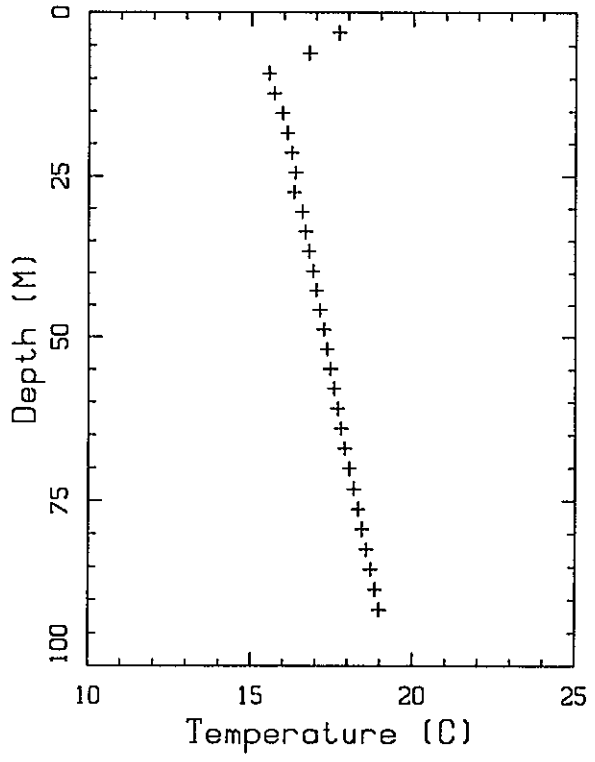

Well Number: 19

Subsurface Temperatures

z (m)	T (°C)	z (m)	T (°C)	z (m)	T (°C)	z (m)	T (°C)
3.0	28.29	79.2	21.01	155.4	22.14	304.8	28.16
6.1	27.69	82.3	20.86	158.5	22.85	310.9	28.41
9.1	27.46	85.3	20.78	164.6	22.60	317.0	28.70
12.2	26.14	88.4	20.75	170.7	22.76	323.1	29.03
15.2	25.74	91.4	20.72	176.8	23.04	329.2	29.36
18.3	25.27	94.5	20.71	182.9	23.24	335.3	29.61
21.3	24.57	97.5	20.70	189.0	23.49	341.4	29.85
24.4	24.30	100.6	20.70	195.1	23.74	347.5	30.11
27.4	24.20	103.6	20.73	201.2	23.95	353.6	30.32
30.5	24.01	106.7	20.77	207.3	24.24	359.7	30.54
33.5	23.82	109.7	20.78	213.4	24.44	365.8	30.82
36.6	23.66	112.8	20.84	219.5	24.71	371.9	31.08
39.6	23.53	115.8	20.90	225.6	24.80	378.0	31.45
42.7	23.35	118.9	20.95	231.6	25.05	384.0	31.67
45.7	23.18	121.9	21.00	237.7	25.23	390.1	31.91
48.8	23.00	125.0	21.06	243.8	25.40	396.2	32.20
51.8	22.79	128.0	21.09	249.9	25.61	402.3	32.51
54.9	22.62	131.1	21.11	256.0	25.92	408.4	32.79
57.9	22.46	134.1	21.55	262.1	26.14	414.5	33.03
61.0	21.55	137.2	21.59	268.2	26.39		
64.0	21.45	140.2	21.66	274.3	26.64		
67.1	21.39	143.3	21.76	280.4	26.99		
70.1	21.23	146.3	21.87	286.5	27.35		
73.2	21.15	149.4	22.36	292.6	27.77		
76.2	21.09	152.4	22.04	298.7	27.88		

Well Number: 19

Thermal Conductivities

Depth Int (m)	(m)	Lith	$k_{\Theta M} \pm SSD$ $\left(\frac{W}{m^\circ C}\right)$	N	$\Phi \pm \Delta\Phi$		$k_\Theta \pm \Delta k_\Theta$ $\left(\frac{W}{m^\circ C}\right)$	
292.0	433.0	G & CS	3.58 *	0.19	7	0.30	0.05	2.10	0.25

Comments:

Lithologic logs: Chapin and driller's log

* k_Θ: operator values (ok)

Well 19

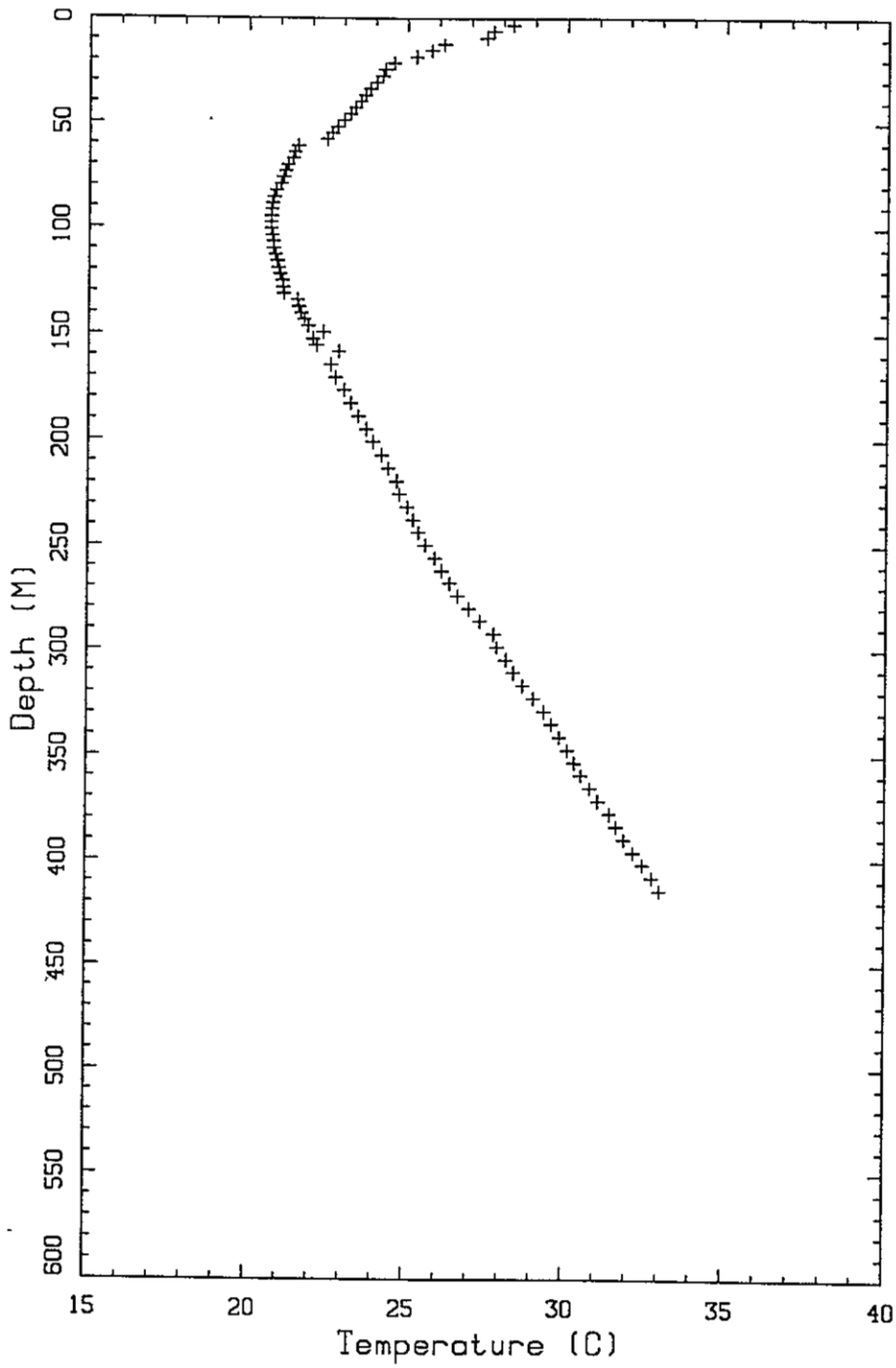
Depth (M)
0
50
100
150
200
250
300
350
400
450
500
550
600
15
20
25
30
35
40
Temperature (C)

Well Number: 20

Subsurface Temperatures

z (m)	T ($^\circ C$)	z (m)	T ($^\circ C$)	z (m)	T ($^\circ C$)	z (m)	T ($^\circ C$)
3.0	19.69	36.6	17.56	70.1	17.99	103.6	18.57
6.1	17.51	39.6	17.58	73.2	18.03	106.7	18.63
9.1	16.86	42.7	17.62	76.2	18.09	109.7	18.70
12.2	16.95	45.7	17.66	79.2	18.15	112.8	18.80
15.2	17.10	48.8	17.70	82.3	18.18	115.2	18.79
18.3	17.20	51.8	17.73	85.3	18.25		
21.3	17.30	54.9	17.78	88.4	18.30		
24.4	17.36	57.9	17.83	91.4	18.32		
27.4	17.44	61.0	17.87	94.5	18.38		
30.5	17.47	64.0	17.89	97.5	18.45		
33.5	17.52	67.1	17.96	100.6	18.52		

Thermal Conductivities

Depth Int (m)	(m)	Lith	$k_{\Theta M} \pm SSD$ $\left(\frac{W}{m^\circ C}\right)$	N	$\Phi \pm \Delta\Phi$		$k_\Theta \pm \Delta k_\Theta$ $\left(\frac{W}{m^\circ C}\right)$	
34.0	116.0	MS & S	2.52 *	0.11	5	0.30	0.10	1.65	0.28

Comments:
Lithologic logs: Chapin and driller's log
* k_Θ: operator values (ok)

Well Number: 21

Subsurface Temperatures

z (m)	T ($^{\circ}C$)	z (m)	T ($^{\circ}C$)	z (m)	T ($^{\circ}C$)	z (m)	T ($^{\circ}C$)
3.0	18.90	42.7	17.67	82.3	18.52	121.9	19.67
6.1	17.80	45.7	17.71	85.3	18.60	125.0	19.77
9.1	17.60	48.8	17.80	88.4	18.68	128.0	19.86
12.2	17.80	51.8	17.86	91.4	18.74	131.1	19.96
15.2	17.80	54.9	17.90	94.5	18.83	134.1	20.08
18.3	17.70	57.9	17.95	97.5	18.91	137.2	20.19
21.3	17.68	61.0	18.02	100.6	19.01	140.2	20.25
24.4	17.64	64.0	18.08	103.6	19.11		
27.4	17.64	67.1	18.14	106.7	19.20		
30.5	17.64	70.1	18.23	109.7	19.28		
33.5	17.64	73.2	18.29	112.8	19.38		
36.6	17.65	76.2	18.37	115.8	19.48		
39.6	17.66	79.2	18.44	118.9	19.58		

Thermal Conductivities

Depth Int (m)	(m)	Lith	$k_{\Theta M} \pm SSD$ $\left(\frac{W}{m^{\circ}C}\right)$	N	$\Phi \pm \Delta\Phi$		$k_{\Theta} \pm \Delta k_{\Theta}$ $\left(\frac{W}{m^{\circ}C}\right)$	
0.0	61.0	G	1.96 *	1	0.30	0.05	1.38	0.15
61.0	152.0	CS &G (p)	1.67 *	2	0.30	0.05	1.23	0.12

Comments:

Lithologic log: Osburn

* No samples, operator values of k_{Θ} (probably low)

Well 20

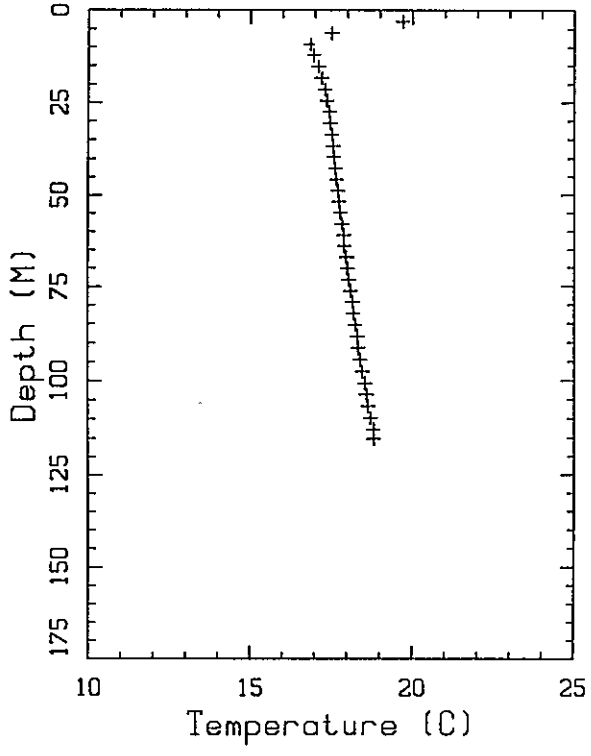

Well 21

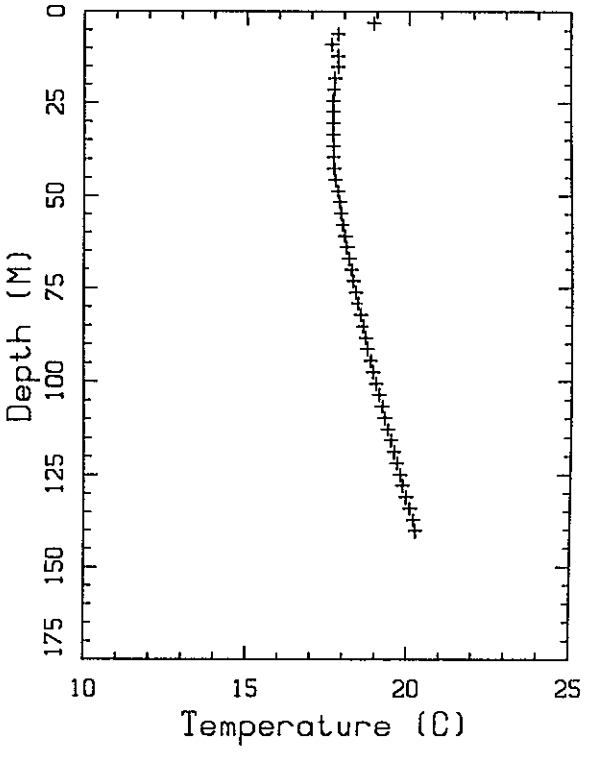

Well Number: 22

Subsurface Temperatures

z (m)	T ($^\circ C$)	z (m)	T ($^\circ C$)	z (m)	T ($^\circ C$)	z (m)	T ($^\circ C$)
3.0	17.13	45.7	17.79	88.4	18.38	131.1	19.53
6.1	16.44	48.8	17.77	91.4	18.44	134.1	19.62
9.1	16.64	51.8	17.79	94.5	18.50	137.2	19.67
12.2	16.88	54.9	17.82	97.5	18.58	140.2	19.77
15.2	17.11	57.9	17.88	100.6	18.64	143.3	19.88
18.3	17.17	61.0	17.92	103.6	18.70	146.3	19.98
21.3	17.21	64.0	17.97	106.7	18.77	149.4	20.08
24.4	17.25	67.1	18.03	109.7	18.86	151.5	20.15
27.4	17.34	70.1	18.08	112.8	18.95		
30.5	17.49	73.2	18.13	115.8	19.03		
33.5	17.69	76.2	18.17	118.9	19.11		
36.6	17.69	79.2	18.22	121.9	19.21		
39.6	17.63	82.3	18.27	125.0	19.30		
42.7	17.71	85.3	18.32	128.0	19.40		

Thermal Conductivities

Depth Int (m)	(m)	Lith	$k_{\Theta M} \pm SSD$ $\left(\frac{W}{m^\circ C}\right)$		N	$\Phi \pm \Delta\Phi$		$k_\Theta \pm \Delta k_\Theta$ $\left(\frac{W}{m^\circ C}\right)$	
0.0	98.0	G & C	2.44		1	0.30	0.05	1.61	0.19
98.0	152.0	CS (p)	2.21	0.22	4	0.20	0.05	1.71	0.15

Comments:
Lithologic log: Osburn

Well 22

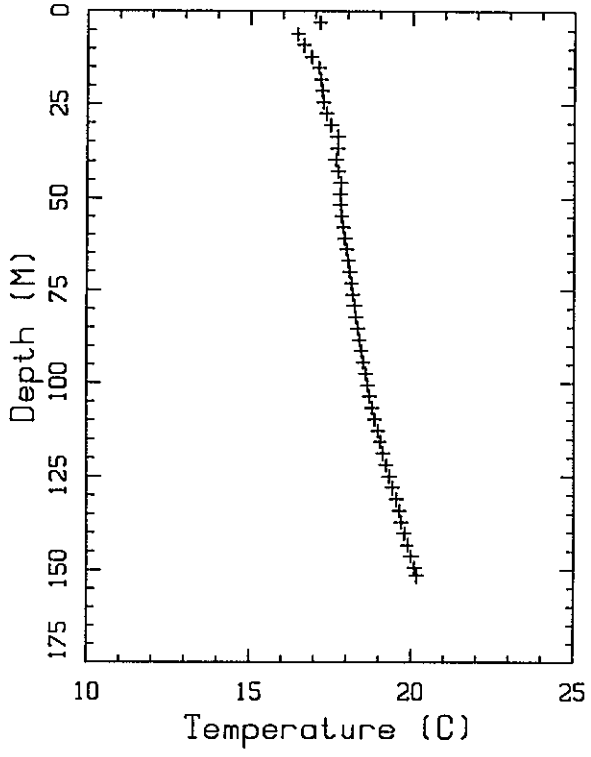

Well Number: 23

Subsurface Temperatures

z (m)	T (°C)	z (m)	T (°C)	z (m)	T (°C)	z (m)	T (°C)
0.0	39.00	152.4	20.72	304.8	26.39	457.2	30.89
6.1	39.00	158.5	20.89	310.9	26.61	463.3	31.00
12.2	38.39	164.6	21.22	317.0	26.89	469.4	31.11
18.3	37.78	170.7	21.50	323.1	27.11	475.5	31.11
24.4	37.50	176.8	21.72	329.2	27.28	481.6	31.28
30.5	37.23	182.9	21.89	335.3	27.50	487.7	31.39
36.6	36.89	189.0	22.11	341.4	27.61	493.8	31.50
42.7	36.61	195.1	22.28	347.5	27.78	499.9	31.61
48.8	36.39	201.2	22.61	353.6	28.00	506.0	31.72
54.9	20.89	207.3	22.78	359.7	28.28	512.1	31.78
61.0	18.11	213.4	23.50	365.8	28.50	518.2	31.89
67.1	17.61	219.5	23.22	371.9	28.72	524.3	32.00
73.2	17.61	225.6	23.50	378.0	28.89	530.4	32.06
79.2	18.00	231.6	23.78	384.0	29.00	536.4	32.11
85.3	18.11	237.7	24.00	390.1	29.22	542.5	32.22
91.4	18.28	243.8	24.22	396.2	29.39	548.6	32.28
97.5	18.50	249.9	24.39	402.3	29.50	554.7	32.39
103.6	18.72	256.0	24.72	408.4	29.72	560.8	32.50
109.7	18.89	262.1	24.89	414.5	29.78	566.9	32.50
115.8	19.22	268.2	25.22	420.6	30.00	573.0	32.61
121.9	19.50	274.3	25.39	426.7	30.22	579.1	32.61
128.0	19.72	280.4	25.61	432.8	30.28	585.2	32.72
134.1	20.00	286.5	25.78	438.9	30.50		
140.2	20.22	292.6	26.00	445.0	30.61		
146.3	20.39	298.7	26.22	451.1	30.78		

Well Number: 23

Thermal Conductivities

Depth Int (m)	(m)	Lith	$k_{\Theta M}$ $\left(\frac{W}{m^\circ C}\right)$	$\pm$ SSD	N	Φ	$\pm \Delta\Phi$	k_Θ $\left(\frac{W}{m^\circ C}\right)$	$\pm \Delta k_\Theta$
84.0	404.0	CS (p)	1.86	0.13	38	0.20	0.05	1.49	0.13
404.0	450.0	Mudflow	2.52	0.09	4	0.20	0.05	1.90	0.19
450.0	610.0	Rhyodacite	2.31	0.28	11	0.20	0.05	1.77	0.18

Comments:
Lithologic log: Chapin
Porosity of CS measured in our lab

- Well 23 -

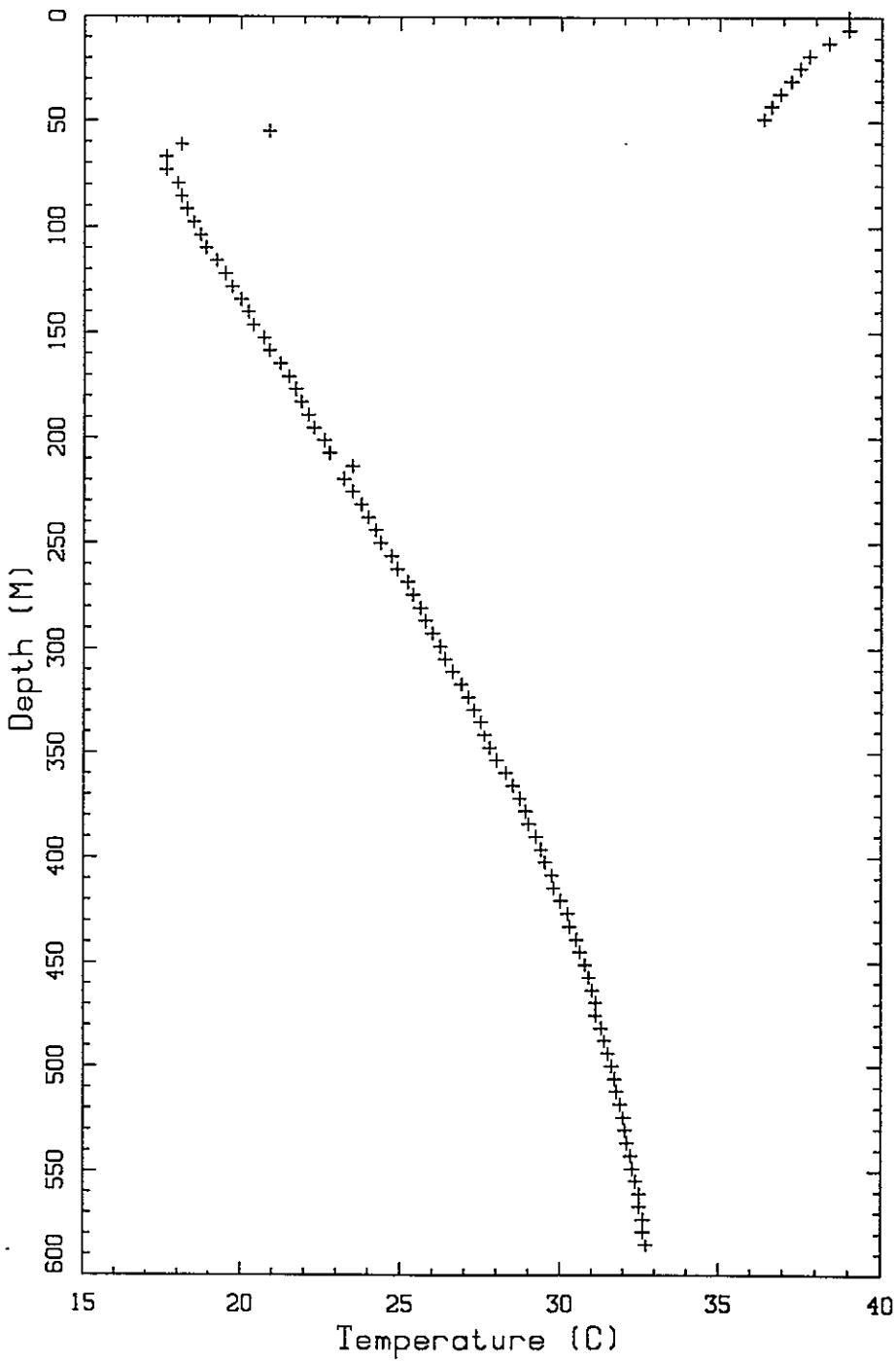
Depth (M)
0
50
100
150
200
250
300
350
400
450
500
550
600
15
20
25
30
35
40
Temperature (C)

Well Number: 24

Subsurface Temperatures

z (m)	T (°C)	z (m)	T (°C)	z (m)	T (°C)	z (m)	T (°C)
6.1	16.52	42.7	18.43	79.2	19.74	115.8	21.28
9.1	16.75	45.7	18.54	82.3	19.90	118.9	21.41
12.2	17.24	48.8	18.66	85.3	20.03	121.9	21.55
15.2	17.45	51.8	18.75	88.4	20.12	125.0	21.67
18.3	17.55	54.9	18.90	91.4	20.27	128.0	21.78
21.3	17.64	57.9	18.97	94.5	20.40	131.1	21.91
24.4	17.77	61.0	19.04	97.5	20.50	134.1	22.03
27.4	17.91	64.0	19.15	100.6	20.64	137.2	22.15
30.5	18.02	67.1	19.30	103.6	20.75	140.2	22.27
33.5	18.14	70.1	19.43	106.7	20.87		
36.6	18.25	73.2	19.51	109.7	21.02		
39.6	18.33	76.2	19.65	112.8	21.14		

Thermal Conductivities

Depth Int (m)	(m)	Lith	$k_{\Theta M} \pm SSD$ $\left(\frac{W}{m^\circ C}\right)$		N	$\Phi \pm \Delta\Phi$		$k_\Theta \pm \Delta k_\Theta$ $\left(\frac{W}{m^\circ C}\right)$	
30.0	152.0	CS (p)	2.03	0.25	4	0.20	0.05	1.60	0.14
Comments: Lithologic log: Osburn									

Well Number: 25

Subsurface Temperatures

z (m)	T ($^\circ C$)	z (m)	T ($^\circ C$)	z (m)	T ($^\circ C$)	z (m)	T ($^\circ C$)
3.0	18.07	45.7	19.35	88.4	21.38	131.1	23.25
6.1	16.54	48.8	19.50	91.4	21.51	134.1	23.36
9.1	16.91	51.8	19.64	94.5	21.66	137.2	23.47
12.2	17.37	54.9	19.80	97.5	21.74	140.2	23.60
15.2	17.73	57.9	19.96	100.6	21.90	143.3	23.70
18.3	17.86	61.0	20.10	103.6	22.06	146.3	23.82
21.3	18.00	64.0	20.25	106.7	22.28	149.4	23.96
24.4	18.14	67.1	20.39	109.7	22.42	152.4	24.16
27.4	18.31	70.1	20.57	112.8	22.54		
30.5	18.53	73.2	20.69	115.8	22.64		
33.5	18.76	76.2	20.83	118.9	22.74		
36.6	18.92	79.2	21.00	121.9	22.87		
39.6	19.04	82.3	21.25	125.0	23.00		
42.7	19.19	85.3	21.28	128.0	23.13		

Thermal Conductivities

Depth Int (m)	(m)	Lith	$k_{\Theta M} \pm SSD$ $\left(\frac{W}{m^\circ C}\right)$	N	$\Phi \pm \Delta\Phi$		$k_\Theta \pm \Delta k_\Theta$ $\left(\frac{W}{m^\circ C}\right)$	
0.0	37.0	CS?	1.80 *	1	0.20	0.05	1.45	0.14
91.0	152.0	CS?	2.34 *	2	0.20	0.05	1.79	0.21

Comments:
No Lithologic log
* No samples, operator values of k_Θ (probably low)

Well 24

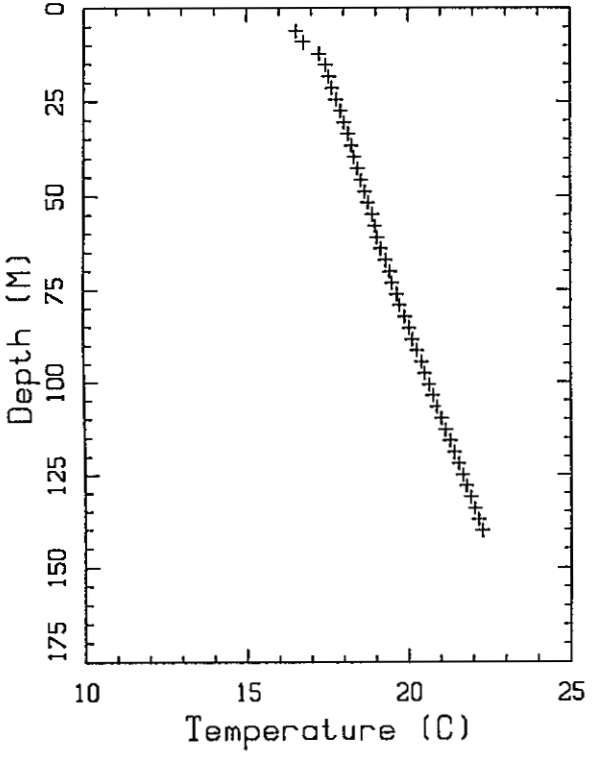

Well 25

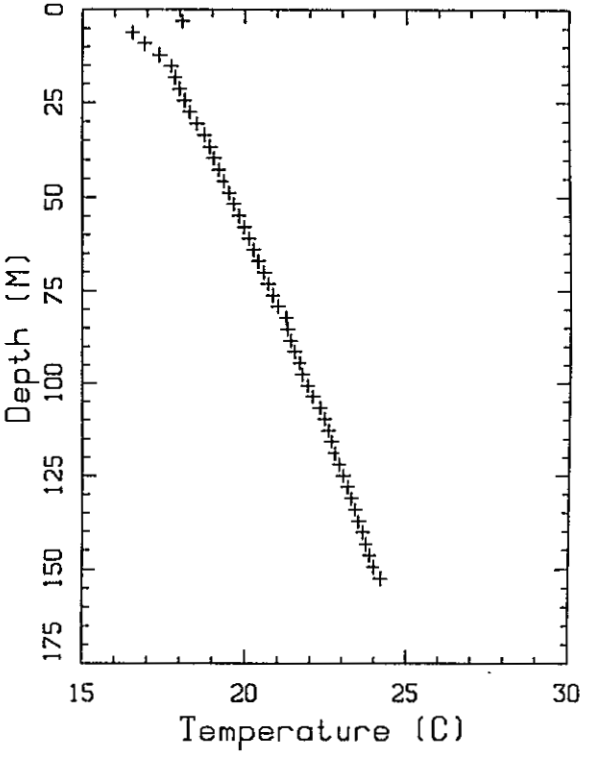

Well Number: 26

Subsurface Temperatures

z (m)	T (°C)	z (m)	T (°C)	z (m)	T (°C)	z (m)	T (°C)
0.0	29.89	158.5	26.50	317.0	32.78	475.5	37.61
6.1	31.61	164.6	26.28	323.1	33.22	481.6	37.61
12.2	31.78	170.7	24.39	329.2	33.50	487.7	37.61
18.3	31.89	176.8	24.39	335.3	33.89	493.8	37.61
24.4	31.72	182.9	24.72	341.4	34.28	499.9	37.50
30.5	31.72	189.0	25.00	347.5	34.61	506.0	37.50
36.6	31.50	195.1	25.28	353.6	35.00	512.1	37.50
42.7	31.39	201.2	25.78	359.7	35.39	518.2	37.61
48.8	31.22	207.3	26.11	365.8	35.73	524.3	37.61
54.9	30.89	213.4	26.39	371.9	36.11	530.4	37.78
61.0	30.72	219.5	26.89	378.0	36.39	536.4	38.00
67.1	30.50	225.6	27.28	384.0	36.61	542.5	38.11
73.2	30.22	231.6	27.61	390.1	36.78	548.6	38.28
79.2	29.89	237.7	28.00	396.2	37.00	554.7	38.39
85.3	29.61	243.8	28.28	402.3	37.23	560.8	38.73
91.4	29.39	249.9	28.72	408.4	37.39	566.9	38.73
97.5	29.22	256.0	29.11	414.5	37.39	573.0	38.78
103.6	29.00	262.1	29.50	420.6	37.50		
109.7	28.78	268.2	29.89	426.7	37.50		
115.8	28.61	274.3	30.39	432.8	37.61		
121.9	28.39	280.4	30.72	438.9	37.61		
128.0	28.00	286.5	31.11	445.0	37.61		
134.1	27.78	292.6	31.50	451.1	37.61		
140.2	27.39	298.7	31.89	457.2	37.61		
146.3	27.56	304.8	32.28	463.3	37.61		
152.4	26.89	310.9	32.50	469.4	37.61		

Well Number: 26

Thermal Conductivities

Depth Int (m)	(m)	Lith	$k_{\Theta M} \pm SSD$ $\left(\frac{W}{m^\circ C}\right)$	N	$\Phi \pm \Delta\Phi$		$k_\Theta \pm \Delta k_\Theta$ $\left(\frac{W}{m^\circ C}\right)$	
9.0	375.0	CS (p)	2.00 *	0	0.20	0.05	1.58	0.17
375.0	539.0	CS,SS (p)	2.20 *	0	0.25	0.05	1.60	0.18
539.0	567.0	CS (p)	2.00 *	0	0.20	0.05	1.58	0.17
567.0	610.0	CS,SS (p)	2.20 *	0	0.25	0.05	1.60	0.18

Comments:

Lithologic logs: Chapin

* No samples available, $k_{\Theta M} \pm SSD$ measured in similar lithology, different well

Well 26

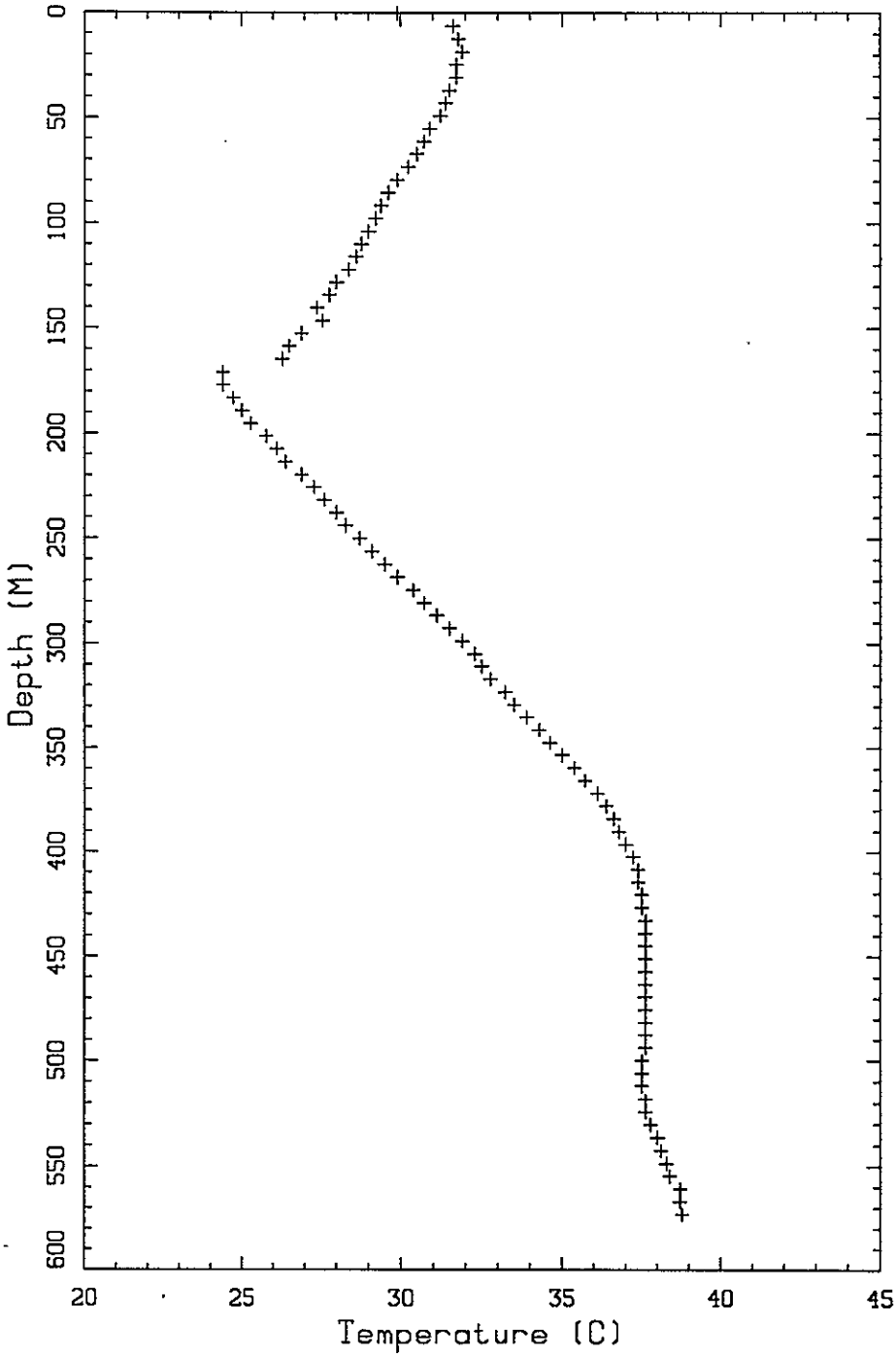
Depth (M)
0
50
100
150
200
250
300
350
400
450
500
550
600
20
25
30
35
40
45
Temperature (C)

Well Number: 27

Subsurface Temperatures

z (m)	T (°C)	z (m)	T (°C)	z (m)	T (°C)	z (m)	T (°C)
0.0	30.00	152.4	21.50	298.7	28.89	445.0	35.11
6.1	29.72	158.5	21.72	304.8	29.22	451.1	35.39
12.2	14.89	164.6	22.00	310.9	29.39	457.2	35.50
18.3	15.00	170.7	22.39	317.0	29.72	463.3	35.73
24.4	15.28	176.8	22.72	323.1	30.00	469.4	35.89
30.5	15.50	182.9	23.00	329.2	30.28	475.5	36.11
36.6	15.78	189.0	23.39	335.3	30.61	481.6	36.28
42.7	16.00	195.1	23.72	341.4	30.89	487.7	36.50
48.8	16.28	201.2	24.00	347.5	31.11	493.8	36.73
54.9	16.50	207.3	24.28	353.6	31.39	499.9	36.78
61.0	16.78	213.4	24.72	359.7	31.72	506.0	37.00
73.2	17.39	219.5	25.00	365.8	32.00	512.1	37.23
79.2	17.72	225.6	25.28	371.9	32.28	518.2	37.39
85.3	18.00	231.6	25.61	378.0	32.50	524.3	37.50
91.4	18.28	237.7	25.89	384.0	32.72	530.4	37.73
97.5	18.50	243.8	26.22	390.1	33.00	536.4	37.78
103.6	18.78	249.9	26.50	396.2	33.22	542.5	37.89
109.7	19.22	256.0	26.78	402.3	33.50	548.6	38.00
115.8	19.50	262.1	27.11	408.4	33.78	554.7	38.11
121.9	19.89	268.2	27.50	414.5	34.00	560.8	38.11
128.0	20.22	274.3	27.78	420.6	34.22	566.9	38.11
134.1	20.50	280.4	28.00	426.7	34.39	573.0	38.00
140.2	20.89	286.5	28.28	432.8	34.61	579.1	38.00
146.3	21.11	292.6	28.61	438.9	34.89	585.2	38.00

Well Number: 27

Thermal Conductivities

Depth Int (m)	(m)	Lith	$k_{\Theta M} \pm SSD$ $\left(\frac{W}{m^\circ C}\right)$	N	$\Phi \pm \Delta\Phi$		$k_\Theta \pm \Delta k_\Theta$ $\left(\frac{W}{m^\circ C}\right)$	
27.0	494.0	CS (p)	2.00 *	0	0.20	0.05	1.58	0.17
494.0	533.0	Bas And	1.80 *	0	0.20	0.05	1.45	0.15
533.0	610.0	W Tuff	2.50 *	0	0.20	0.05	1.89	0.23

Comments:

Lithologic log: Chapin

Only contaminated samples available

* k_Θ measured in similar lithology, different well

Well 27

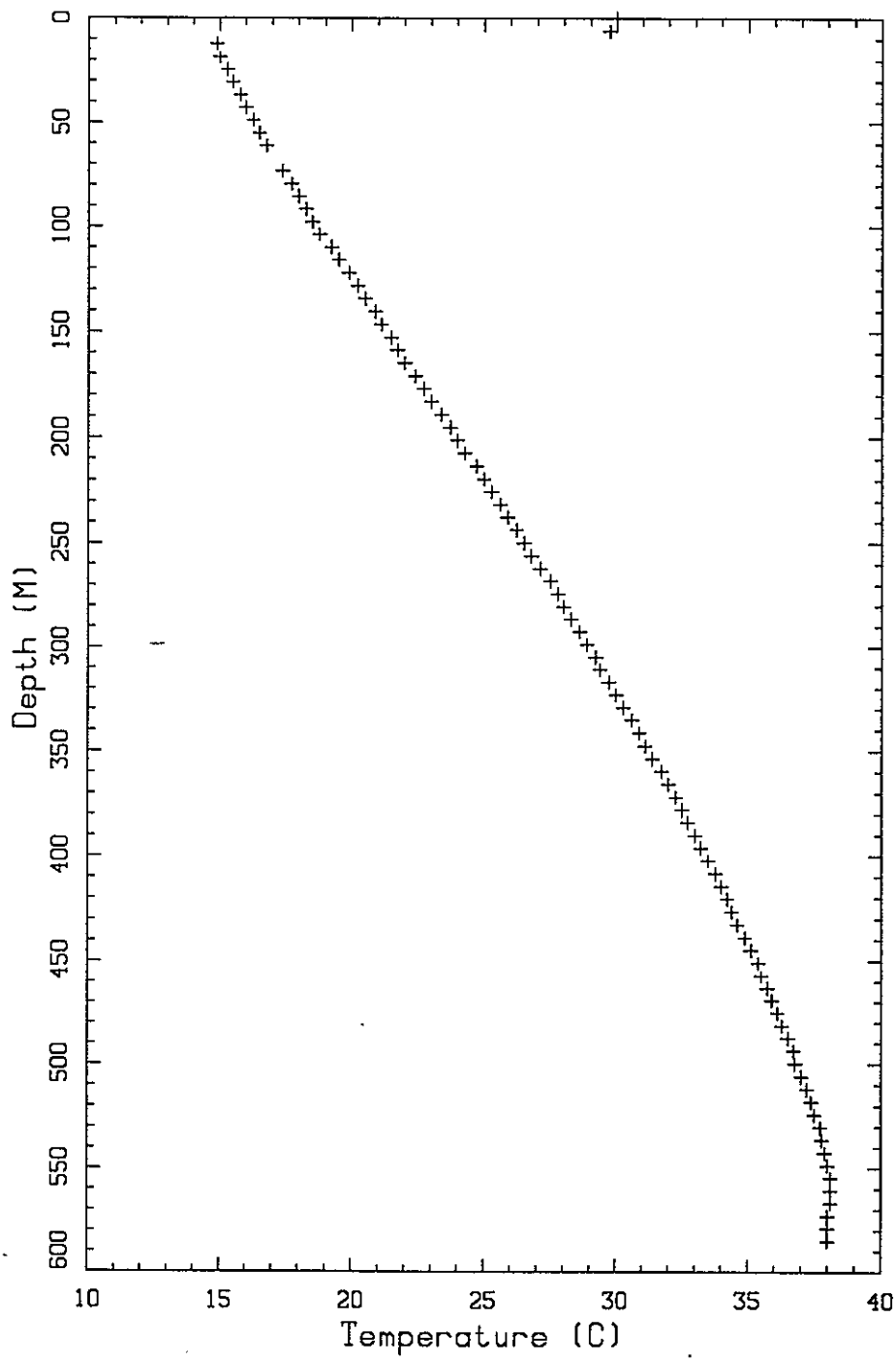
Depth (M)
0
50
100
150
200
250
300
350
400
450
500
550
600
10
15
20
25
30
35
40
Temperature (C)

Well Number: 28

Subsurface Temperatures

z (m)	T ($^\circ C$)	z (m)	T ($^\circ C$)	z (m)	T ($^\circ C$)	z (m)	T ($^\circ C$)
9.1	16.56	48.8	20.56	91.4	24.22	134.1	27.42
12.2	16.96	54.9	21.15	97.5	24.71	140.2	27.84
18.3	17.58	61.0	21.68	103.6	25.20	146.3	28.20
24.4	18.22	67.1	22.22	109.7	25.64	150.9	28.65
30.5	18.90	73.2	22.71	115.8	26.13		
36.6	19.43	79.2	23.17	121.9	26.61		
42.7	20.02	85.3	23.67	128.0	27.04		

Thermal Conductivities

Depth Int (m)	(m)	Lith	$k_{\Theta M}$ $\pm$ *SSD* $\left(\frac{W}{m^\circ C}\right)$		N	Φ $\pm$ $\Delta\Phi$		k_Θ $\pm$ Δk_Θ $\left(\frac{W}{m^\circ C}\right)$	
0.0	85.0	CS (p)	2.27	0.25	5	0.20	0.05	1.75	0.18
85.0	98.0	CS &S (p)	2.60		2	0.25	0.05	1.95	0.23
98.0	116.0	CS (p)	2.03		2	0.20	0.05	1.60	0.18
116.0	128.0	CS &S (p)	2.78	0.36	3	0.25	0.05	1.90	0.25
128.0	152.0	CS (p)	2.33		2	0.20	0.05	1.78	0.21

Comments:

Lithologic log: Chapin

Well Number: 29

Subsurface Temperatures: "Instrument acting goofy"

z (m)	T (°C)	z (m)	T (°C)	z (m)	T (°C)	z (m)	T (°C)
6.1	17.96	42.7	22.29	91.4	46.72	140.2	27.16
9.1	17.94	48.8	22.58	97.5	25.44	146.3	27.33
12.2	18.52	54.9	22.80	103.6	25.68		
15.2	37.13	61.0	23.28	109.7	25.96		
18.3	19.72	67.1	44.55	115.8	26.20		
24.4	39.63	73.2	24.10	121.9	50.33		
30.5	21.22	79.2	24.47	128.0	26.72		
36.6	21.93	85.3	24.82	134.1	26.92		

Well Number: 29

Subsurface Temperatures: Spikes removed: data highly suspect

z (m)	T (°C)	z (m)	T (°C)	z (m)	T (°C)	z (m)	T (°C)
6.1	17.96	42.7	22.29	85.3	24.82	134.1	26.92
9.1	17.94	48.8	22.58	97.5	25.44	140.2	27.16
12.2	18.52	54.9	22.80	103.6	25.68	146.3	27.33
18.3	19.72	61.0	23.28	109.7	25.96		
30.5	21.22	73.2	24.10	115.8	26.20		
36.6	21.93	79.2	24.47	128.0	26.72		

Thermal Conductivities

Depth Int (m)	(m)	Lith	$k_{\Theta M} \pm SSD$ $\left(\frac{W}{m^\circ C}\right)$		N	$\Phi \pm \Delta\Phi$		$k_\Theta \pm \Delta k_\Theta$ $\left(\frac{W}{m^\circ C}\right)$	
0.0	146.0	TV?	0.00	0.00	0	0.00	0.00	1.60	0.40

Comments:
No lithologic log
No samples

Well 28

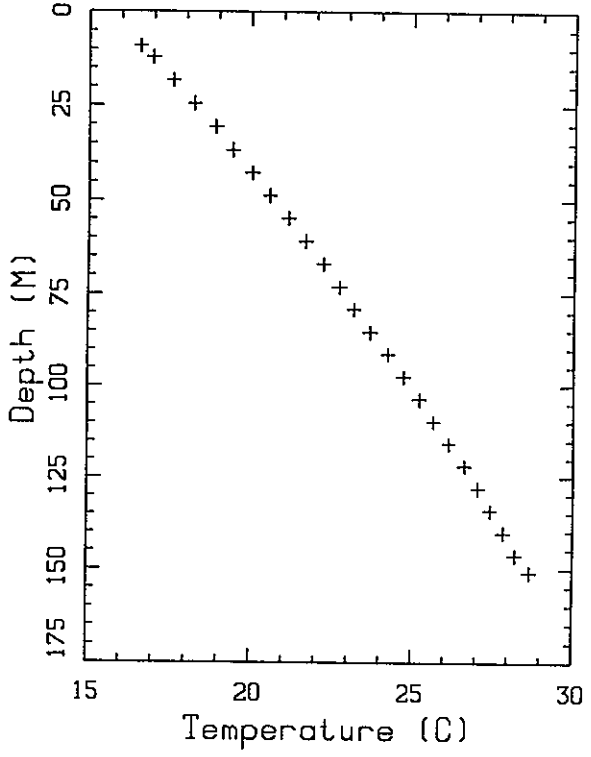

Well 29

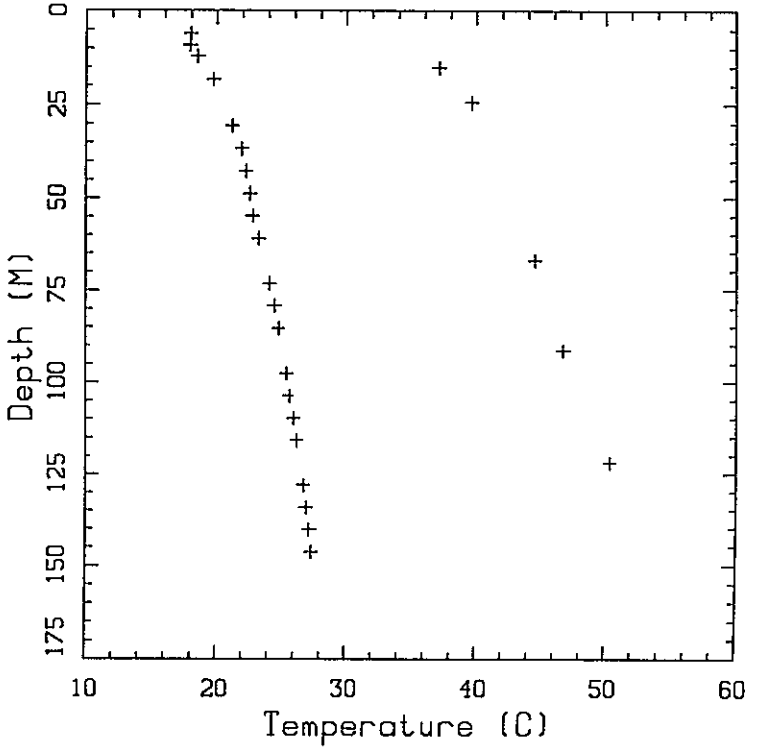

Well Number: 30

Subsurface Temperatures

z (m)	T ($^\circ C$)	z (m)	T ($^\circ C$)	z (m)	T ($^\circ C$)	z (m)	T ($^\circ C$)
3.0	20.67	27.4	18.89	70.1	21.00	109.7	23.22
6.1	17.56	30.5	18.78	73.2	21.17	115.8	23.50
9.1	17.67	36.6	19.11	79.2	21.45	121.9	23.78
12.2	18.17	42.7	19.61	85.3	21.78	128.0	24.11
15.2	18.28	48.8	19.89	91.4	22.17	134.1	24.50
19.8	18.50	54.9	20.22	97.5	22.50	140.2	24.72
24.4	18.78	61.0	20.56	103.6	22.89	144.8	24.95

Thermal Conductivities

Depth Int (m)	(m)	Lith	$k_{\Theta M} \pm SSD$ $\left(\frac{W}{m^\circ C}\right)$		N	$\Phi \pm \Delta\Phi$		$k_\Theta \pm \Delta k_\Theta$ $\left(\frac{W}{m^\circ C}\right)$	
9.0	146.0	CS (p)	2.22	0.07	7	0.20	0.05	1.71	0.15

Comments:
Lithologic logs: Chapin, driller's log

Well Number: 31

Subsurface Temperatures

z (m)	T ($^{\circ}C$)	z (m)	T ($^{\circ}C$)	z (m)	T ($^{\circ}C$)	z (m)	T ($^{\circ}C$)
6.1	19.05	30.5	22.25	54.9	26.00		
12.2	19.08	36.6	23.17	61.0	27.37		
18.3	20.25	42.7	24.12				
24.4	21.27	48.8	25.00				

Thermal Conductivities

Depth Int (m)	(m)	Lith	$k_{\Theta M}$ $\left(\frac{W}{m^{\circ}C}\right)$	$\pm$ SSD	N	Φ	$\pm \Delta\Phi$	k_{Θ} $\left(\frac{W}{m^{\circ}C}\right)$	$\pm \Delta k_{\Theta}$
9.0	55.0	Conglom	2.41	0.06	4	0.20	0.05	1.83	0.18

Comments:
Lithologic Log: Chapin

Well 30

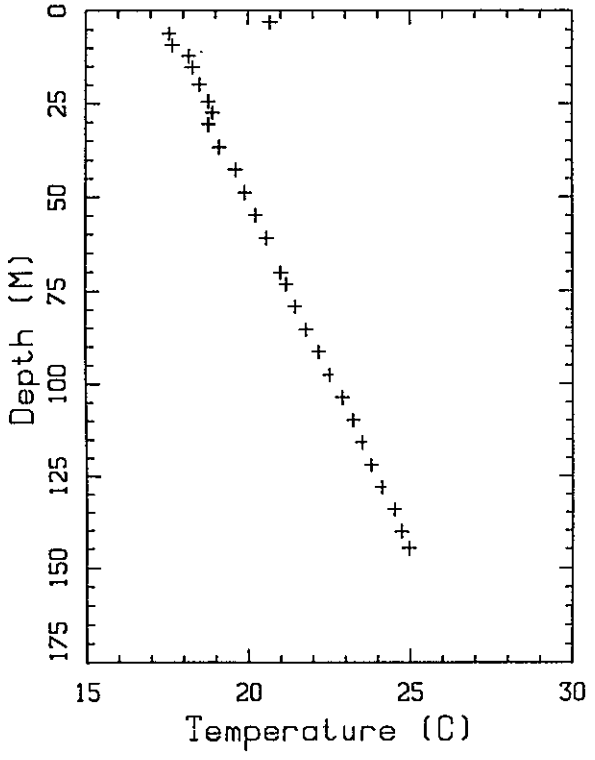

Well 31

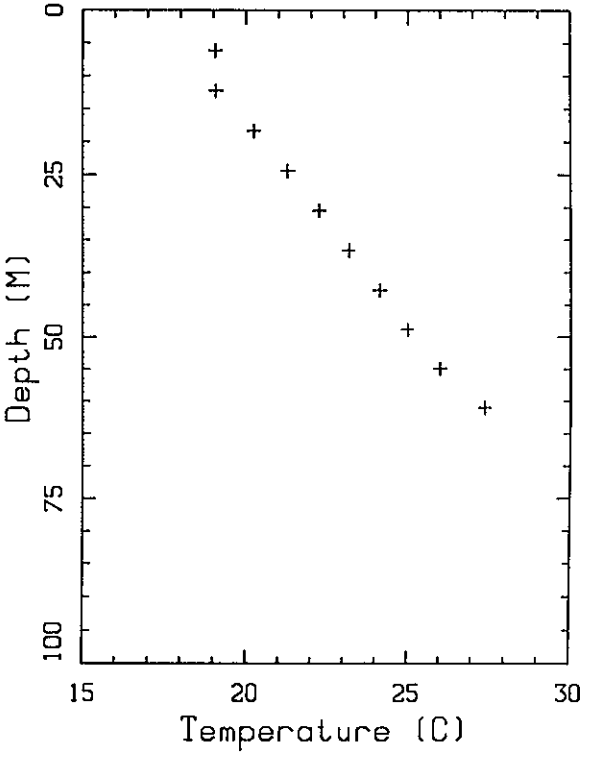

Well Number: 32

Subsurface Temperatures

z (m)	T ($^\circ C$)	z (m)	T ($^\circ C$)	z (m)	T ($^\circ C$)	z (m)	T ($^\circ C$)
3.0	19.91	21.3	22.00	39.6	25.34	57.9	27.84
6.1	18.57	24.4	22.53	42.7	25.81	61.0	28.28
9.1	19.91	27.4	23.22	45.7	26.17	64.0	28.72
12.2	20.68	30.5	23.94	48.8	26.56	67.1	29.13
15.2	21.14	33.5	24.41	51.8	26.98	70.1	29.56
18.3	21.56	36.6	24.91	54.9	27.44	73.2	29.93

Thermal Conductivities

Depth Int (m)	(m)	Lith	$k_{\Theta M}$ $\left(\frac{W}{m^\circ C}\right)$	$\pm$ SSD	N	Φ	$\pm \Delta\Phi$	k_Θ $\left(\frac{W}{m^\circ C}\right)$	$\pm \Delta k_\Theta$
15.0	45.0	CS	2.33 *	0.00	2	0.20	0.05	1.78	0.21
45.0	73.0	Rhyolite	2.03 *	0.16	5	0.20	0.05	1.60	0.14

Comments:

Lithologic logs: Chapin and driller's log

* k_Θ: values from our lab and from the operator (ok)

Well Number: 33

Subsurface Temperatures

z (m)	T ($^\circ C$)	z (m)	T ($^\circ C$)	z (m)	T ($^\circ C$)	z (m)	T ($^\circ C$)
3.0	17.50	45.7	22.18	88.4	25.42	131.1	27.01
6.1	17.54	48.8	22.46	91.4	25.54	134.1	27.07
9.1	18.22	51.8	22.70	94.5	25.66	137.2	27.12
12.2	18.78	54.9	22.93	97.5	25.82	140.2	27.16
15.2	19.15	57.9	23.20	100.6	25.95	143.3	27.19
18.3	19.49	61.0	23.45	103.6	26.09	146.3	27.21
21.3	19.79	64.0	23.68	106.7	26.23	149.4	27.22
24.4	20.09	67.1	23.90	109.7	26.31	152.4	27.23
27.4	20.41	70.1	24.13	112.8	26.47		
30.5	20.69	73.2	24.37	115.8	26.59		
33.5	21.04	76.2	24.57	118.9	26.70		
36.6	21.33	79.2	24.79	121.9	26.80		
39.6	21.62	82.3	24.97	125.0	26.87		
42.7	21.88	85.3	25.20	128.0	26.94		

Thermal Conductivities

Depth Int (m)	(m)	Lith	$k_{\Theta M} \pm SSD$ $\left(\frac{W}{m^\circ C}\right)$	N	$\Phi \pm \Delta\Phi$		$k_\Theta \pm \Delta k_\Theta$ $\left(\frac{W}{m^\circ C}\right)$	
6.0	152.0	TV?	1.80 *	0.15	4	0.20	0.05	1.45	0.15

Comments:
No lithologic log
* No samples, operator values of k_Θ (probably low)

Well 32

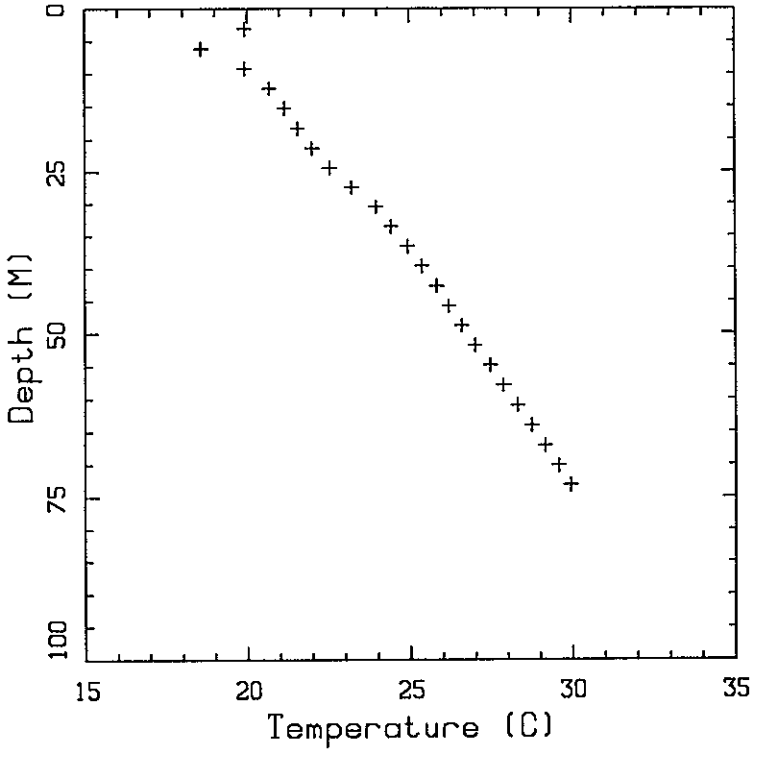

Well 33

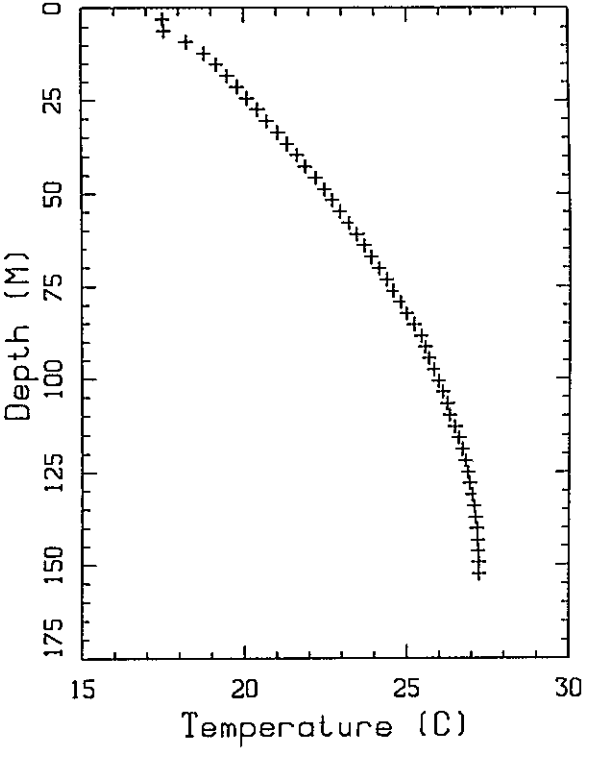

A64

Well Number: 34

Subsurface Temperatures

z (m)	T (°C)	z (m)	T (°C)	z (m)	T (°C)	z (m)	T (°C)
3.0	18.82	45.7	19.82	88.4	21.14	131.1	22.38
6.1	17.67	48.8	19.92	91.4	21.20	134.1	22.49
9.1	18.09	51.8	20.01	94.5	21.26	137.2	22.59
12.2	18.54	54.9	20.11	97.5	21.34	140.2	22.69
15.2	18.75	57.9	20.20	100.6	21.42	143.3	22.78
18.3	18.86	61.0	20.28	103.6	21.50	146.3	22.87
21.3	19.01	64.0	20.39	106.7	21.58	149.4	22.96
24.4	19.14	67.1	20.47	109.7	21.66	152.4	23.01
27.4	19.22	70.1	20.56	112.8	21.75		
30.5	19.33	73.2	20.65	115.8	21.86		
33.5	19.42	76.2	20.76	118.9	21.96		
36.6	19.52	79.2	20.84	121.9	22.07		
39.6	19.61	82.3	20.92	125.0	22.18		
42.7	19.74	85.3	21.06	128.0	22.29		

Thermal Conductivities

Depth Int (m)	(m)	Lith	$k_{\Theta M} \pm SSD$ $\left(\frac{W}{m^\circ C}\right)$	N	$\Phi \pm \Delta\Phi$		$k_\Theta \pm \Delta k_\Theta$ $\left(\frac{W}{m^\circ C}\right)$	
0.0	152.0	TV?	1.87 *	0.26	3	0.20	0.05	1.49	0.16

Comments:
No lithologic log
* No samples, operator values of k_Θ (probably low)

Well Number: 35

Subsurface Temperatures

z (m)	T ($^\circ C$)	z (m)	T ($^\circ C$)	z (m)	T ($^\circ C$)	z (m)	T ($^\circ C$)
3.0	21.00	39.6	19.94	76.2	21.54	112.8	23.39
6.1	17.77	42.7	20.07	79.2	21.68	115.8	23.56
9.1	18.07	45.7	20.21	82.3	21.83	118.9	23.71
12.2	18.45	48.8	20.31	85.3	21.98	121.9	23.86
15.2	18.63	51.8	20.42	88.4	22.12	125.0	24.03
18.3	18.78	54.9	20.59	91.4	22.29	128.0	24.20
21.3	18.98	57.9	20.71	94.5	22.44	131.1	24.33
24.4	19.16	61.0	20.82	97.5	22.59	134.1	24.47
27.4	19.36	64.0	20.98	100.6	22.77	137.2	24.65
30.5	19.54	67.0	21.13	103.6	22.94	140.2	24.84
33.5	19.67	70.1	21.28	106.7	23.09	143.3	24.90
36.6	19.79	73.2	21.38	109.7	23.21	146.3	25.05

Thermal Conductivities

Depth Int (m)	(m)	Lith	$k_{\Theta M}$ $\pm$ *SSD* $\left(\frac{W}{m^\circ C}\right)$		N	Φ $\pm$ $\Delta\Phi$		k_Θ $\pm$ Δk_Θ $\left(\frac{W}{m^\circ C}\right)$	
12.0	152.0	CS (p)	2.13	0.19	6	0.20	0.05	1.66	0.15

Comments:
Lithologic log: Osburn

Well 34
Depth (M)
0
25
50
75
100
125
150
175
15
20
25
30
Temperature (C)

Well 35
Depth (M)
0
25
50
75
100
125
150
175
15
20
25
30
Temperature (C)

Well Number: 36

Subsurface Temperatures

z (m)	T ($^\circ C$)	z (m)	T ($^\circ C$)	z (m)	T ($^\circ C$)	z (m)	T ($^\circ C$)
3.0	20.80	21.3	18.63	48.8	20.08		
6.1	17.75	24.4	18.80	54.9	20.30		
9.1	17.34	27.4	18.97	61.0	20.56		
12.2	17.69	30.5	19.19	67.1	20.88		
15.2	18.20	36.6	19.51	70.1	21.09		
18.3	18.37	42.7	19.80	71.6	21.15		

Thermal Conductivities

Depth Int (m)	(m)	Lith	$k_{\Theta M}$ $\left(\frac{W}{m^\circ C}\right)$	$\pm$ SSD	N	Φ	$\pm \Delta\Phi$	k_Θ $\left(\frac{W}{m^\circ C}\right)$	$\pm \Delta k_\Theta$
0.0	41.0	G	2.56	0.19	3	0.30	0.05	1.66	0.17
41.0	69.0	Tuff	2.62	0.18	4	0.20	0.05	1.95	0.20

Comments:
Lithologic Log: Chapin

Well 36

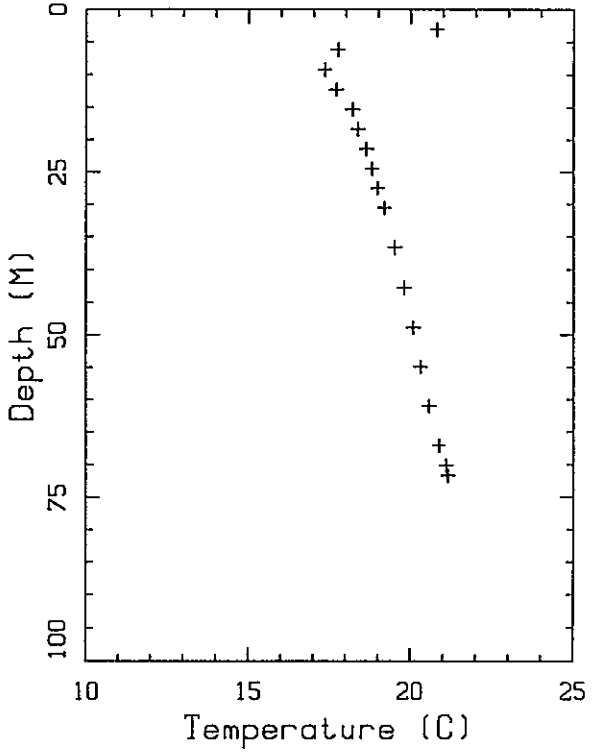

Well Number: 37

Subsurface Temperatures

z (m)	T ($^{\circ}C$)	z (m)	T ($^{\circ}C$)	z (m)	T ($^{\circ}C$)	z (m)	T ($^{\circ}C$)
0.0	37.00	109.7	22.11	219.5	28.78	329.2	35.89
6.1	37.00	115.8	22.39	225.6	29.22	335.3	36.00
12.2	36.78	121.9	22.78	231.6	29.61	341.4	36.23
18.3	36.61	128.0	23.11	237.7	30.11	347.5	36.23
24.4	36.39	134.1	23.50	243.8	30.50	353.6	36.28
30.5	36.23	140.2	23.72	249.9	30.78	359.7	36.39
36.6	35.89	146.3	24.22	256.0	31.28	365.8	36.50
42.7	35.39	152.4	24.61	262.1	31.72	371.9	36.50
48.8	35.11	158.5	25.00	268.2	32.22	378.0	36.61
54.9	34.78	164.6	25.39	274.3	32.61	384.0	36.61
61.0	34.50	170.7	25.72	280.4	33.22	390.1	36.73
67.1	21.39	176.8	26.11	286.5	33.72	396.2	36.73
73.2	20.89	182.9	26.50	292.6	34.39	402.3	36.73
79.2	20.89	189.0	26.78	298.7	34.89	408.4	36.73
85.3	21.11	195.1	27.22	304.8	35.23	414.5	36.61
91.4	21.28	201.2	27.72	310.9	35.50	420.6	36.28
97.5	21.61	207.3	28.11	317.0	35.73	426.7	36.00
103.6	21.78	213.4	28.39	323.1	35.78	432.8	35.89

Thermal Conductivities

Depth Int (m)	(m)	Lith	$k_{\Theta M} \pm SSD$ $\left(\frac{W}{m^{\circ}C}\right)$	N	$\Phi \pm \Delta\Phi$		$k_{\Theta} \pm \Delta k_{\Theta}$ $\left(\frac{W}{m^{\circ}C}\right)$	
0.0	91.0	S	2.96	1	0.40	0.05	1.57	0.20
91.0	279.0	CS (p)	2.00 *	0	0.20	0.05	1.58	0.17
279.0	389.0	Rhyolite	1.98	1	0.20	0.05	1.56	0.17
389.0	405.0	Bas And	1.80 *	0	0.20	0.05	1.45	0.15
405.0	436.0	Mudflow	2.10	1	0.20	0.05	1.64	0.18

Comments:

Lithologic log: Chapin

Very little sample available.

* No samples available, k_{Θ} measured in similar lithology, different well.

Well 37

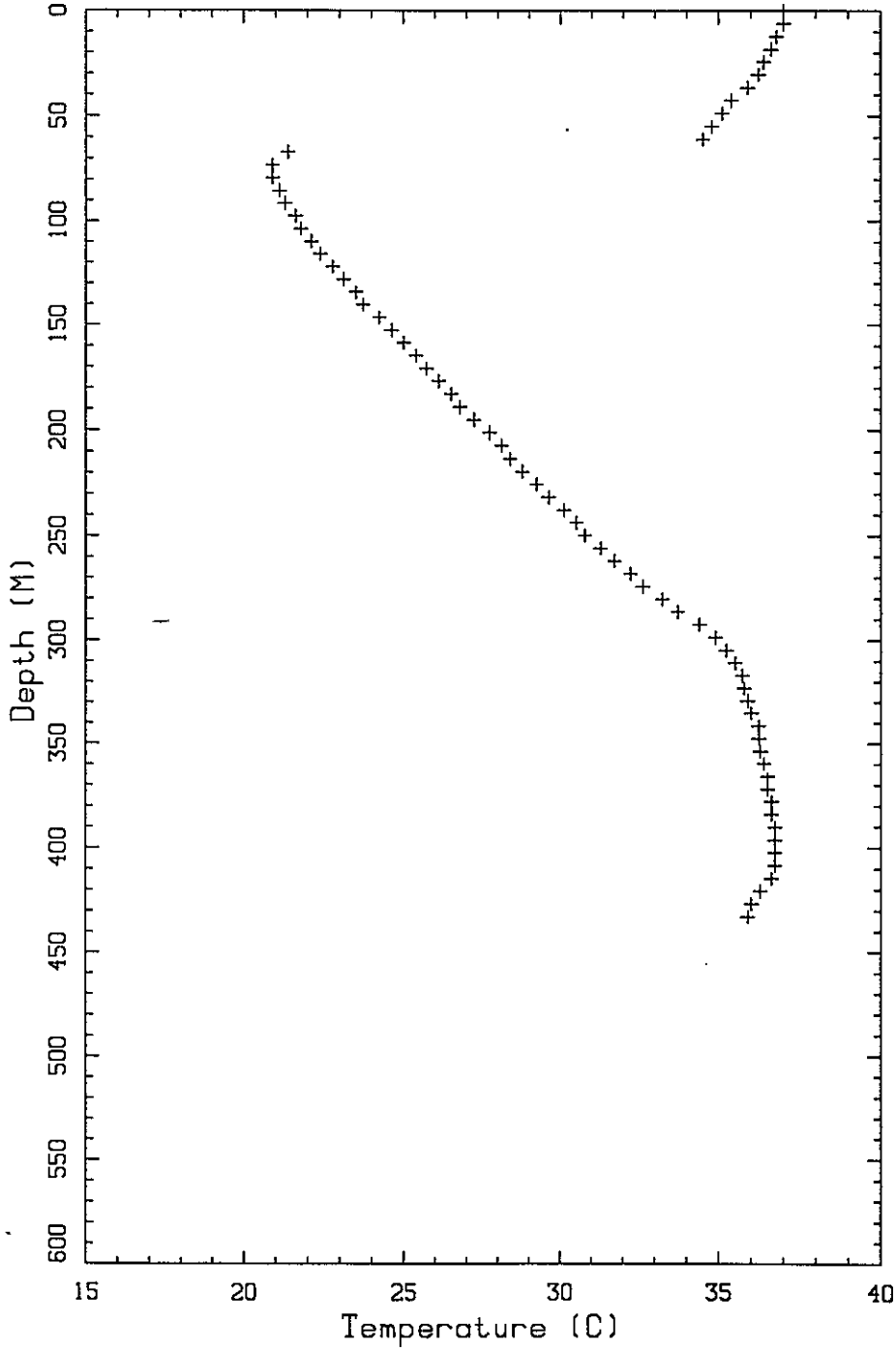
Depth (M)
0
50
100
150
200
250
300
350
400
450
500
550
600
15
20
25
30
35
40
Temperature (C)

Well Number: 38

Subsurface Temperatures

z (m)	T (^{o}C)	z (m)	T (^{o}C)	z (m)	T (^{o}C)	z (m)	T (^{o}C)
19.8	19.17	61.0	21.89	109.7	24.39		
24.4	19.56	70.1	22.45	115.8	24.67		
27.4	19.72	73.2	22.61	121.9	25.00		
30.5	19.95	79.2	22.95	128.0	25.34		
36.6	20.39	85.3	23.34	134.1	25.84		
42.7	20.83	91.4	23.61	140.2	26.17		
48.8	21.17	97.5	23.84	141.7	26.17		
54.9	21.56	103.6	24.11				

Thermal Conductivities

Depth Int (m)	(m)	Lith	$k_{\Theta M} \pm SSD$ $\left(\frac{W}{m^{o}C}\right)$		N	$\Phi \pm \Delta\Phi$		$k_{\Theta} \pm \Delta k_{\Theta}$ $\left(\frac{W}{m^{o}C}\right)$	
9.0	50.0	C,S & G	2.64	0.19	4	0.30	0.10	1.70	0.31
55.0	131.0	S & M	2.69	0.24	4	0.40	0.05	1.49	0.15
133.0	142.0	C & S	2.46	0.00	2	0.30	0.10	1.62	0.31

Comments:
Lithologic log: Chapin, driller's log

Well Number: 39

Subsurface Temperatures

z (m)	T (°C)	z (m)	T (°C)	z (m)	T (°C)	z (m)	T (°C)
3.0	21.00	19.8	19.11	42.7	19.72	73.2	20.89
6.1	19.72	24.4	19.28	48.8	19.95	79.2	21.11
9.1	19.06	27.4	19.33	54.9	20.22		
12.2	19.00	30.5	19.39	61.0	20.39		
15.2	19.00	36.6	19.56	70.1	20.72		

Thermal Conductivities

Depth Int (m)	(m)	Lith	$k_{\Theta M} \pm SSD$ $\left(\frac{W}{m^\circ C}\right)$		N	$\Phi \pm \Delta\Phi$		$k_\Theta \pm \Delta k_\Theta$ $\left(\frac{W}{m^\circ C}\right)$	
0.0	79.0	S,G & M	2.76	0.28	6	0.30	0.05	1.75	0.19

Comments:
Lithologic logs: Chapin, driller's log

Well 38

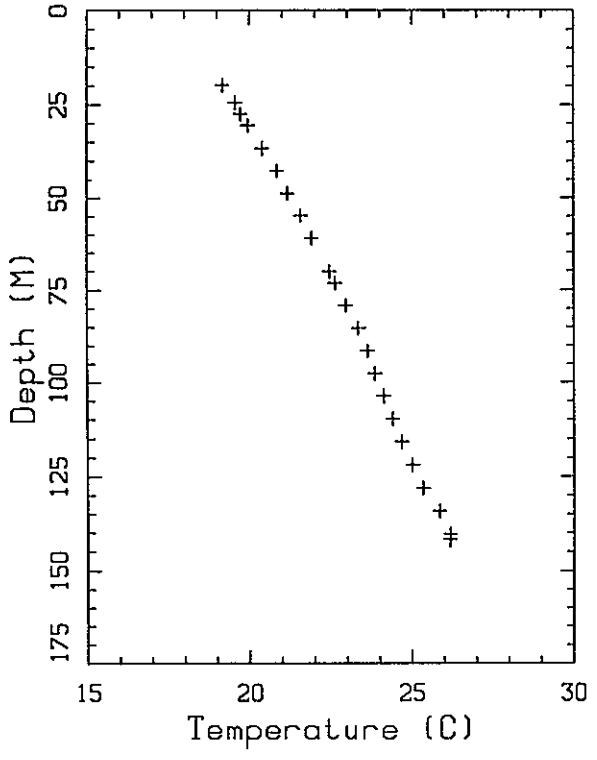

Well 39

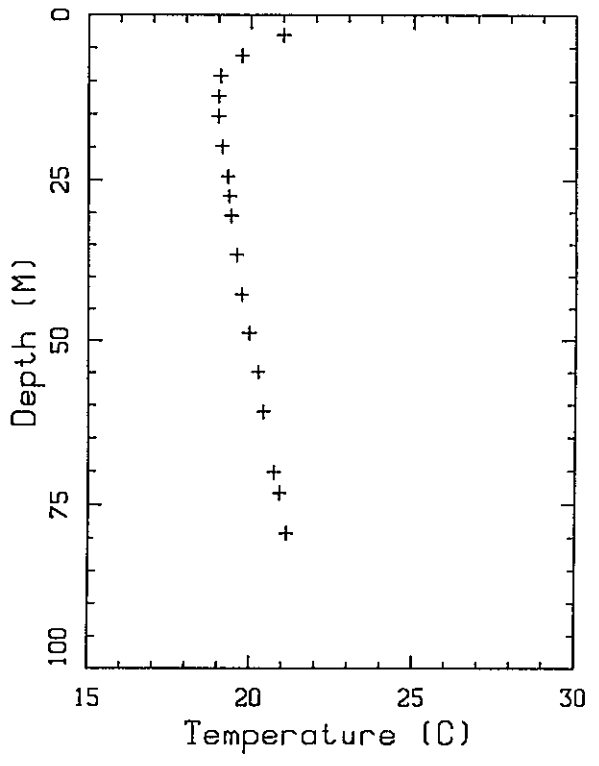

Well Number: 40

Subsurface Temperatures

z (m)	T ($^\circ C$)	z (m)	T ($^\circ C$)	z (m)	T ($^\circ C$)	z (m)	T ($^\circ C$)
3.0	20.28	24.4	21.28	54.9	24.11	91.4	27.39
6.1	18.33	27.4	21.56	61.0	24.84	97.5	27.89
9.1	18.78	30.5	21.89	70.1	25.56	103.6	28.22
12.2	19.67	36.6	22.67	73.2	25.95	109.7	28.78
15.2	20.00	42.7	23.22	79.2	26.61	115.8	29.00
19.8	20.72	48.8	23.56	85.3	27.06	121.9	29.22

Thermal Conductivities

Depth Int (m)	(m)	Lith	$k_{\Theta M} \pm SSD$ $\left(\frac{W}{m^\circ C}\right)$		N	$\Phi \pm \Delta\Phi$		$k_\Theta \pm \Delta k_\Theta$ $\left(\frac{W}{m^\circ C}\right)$	
0.0	61.0	S & M	2.77		2	0.40	0.05	1.51	0.21
61.0	73.0	S	3.46		2	0.40	0.05	1.72	0.24
91.0	104.0	S	3.69	0.27	3	0.40	0.05	1.80	0.25
122.0	128.0	S –	3.87		2	0.40	0.05	1.84	0.26
61.0	142.0	S	3.68	0.24	7	0.40	0.05	1.79	0.21

Comments:

Lithologic logs: Chapin, driller's log

Well Number: 41

Subsurface Temperatures

z (m)	T (^{o}C)	z (m)	T (^{o}C)	z (m)	T (^{o}C)	z (m)	T (^{o}C)
3.0	18.60	27.4	18.83	51.8	19.96	76.2	20.90
6.1	16.81	30.5	18.98	54.9	20.04	79.2	21.02
9.1	17.47	33.5	19.12	57.9	20.13	82.3	21.16
12.2	17.92	36.6	19.27	61.0	20.27	85.3	21.29
15.2	18.16	39.6	19.42	64.0	20.41	88.4	21.41
18.3	18.36	42.7	19.53	67.1	20.52	91.4	21.56
21.3	18.53	45.7	19.70	70.1	20.66	94.5	21.68
24.4	18.67	48.8	19.83	73.2	20.78	97.5	21.80

Thermal Conductivities

Depth Int (m)	(m)	Lith	$k_{\Theta M} \pm SSD$ $\left(\frac{W}{m^{o}C}\right)$	N	$\Phi \pm \Delta\Phi$		$k_{\Theta} \pm \Delta k_{\Theta}$ $\left(\frac{W}{m^{o}C}\right)$	
15.0	97.0	MS,S & G	2.67 * 0.26	5	0.30	0.10	1.71	0.31

Comments:
Lithologic logs: Chapin and driller's log
* k_{Θ}: operator values (ok)

Well 40

Well 41

Well Number: 42

Subsurface Temperatures

z (m)	T (°C)	z (m)	T (°C)	z (m)	T (°C)	z (m)	T (°C)
3.0	18.42	27.4	19.38	51.8	20.66	76.2	22.00
6.1	17.35	30.5	19.53	54.9	20.82	79.2	22.16
9.1	18.08	33.5	19.70	57.9	21.00		
12.2	18.44	36.6	19.85	61.0	21.16		
15.2	18.67	39.6	20.02	64.0	21.31		
18.3	18.87	42.7	20.17	67.1	21.47		
21.3	19.07	45.7	20.35	70.1	21.66		
24.4	19.21	48.8	20.50	73.2	21.82		

Thermal Conductivities

Depth Int (m)	(m)	Lith	$k_{\Theta M} \pm SSD$ $\left(\frac{W}{m^\circ C}\right)$		N	$\Phi \pm \Delta\Phi$		$k_\Theta \pm \Delta k_\Theta$ $\left(\frac{W}{m^\circ C}\right)$	
0.0	79.0	MS,S & G	2.39 *	0.15	7	0.30	0.10	1.59	0.27

Comments:
Lithologic logs: Chapin and driller's log
* k_Θ: operator values (ok)

Well Number: 43

Subsurface Temperatures

z (m)	T ($^\circ C$)	z (m)	T ($^\circ C$)	z (m)	T ($^\circ C$)	z (m)	T ($^\circ C$)
9.1	17.83	48.8	19.78	97.5	22.48	146.3	25.32
12.2	18.28	54.9	20.11	103.6	22.81	152.4	25.61
15.2	18.18	61.0	20.47	109.7	23.20		
18.3	18.30	67.1	20.76	115.8	23.56		
24.4	18.60	73.2	21.05	121.9	23.90		
30.5	18.89	79.2	21.32	128.0	24.26		
36.6	19.18	85.3	21.76	134.1	24.65		
42.7	19.50	91.4	22.10	140.2	24.97		

Thermal Conductivities

Depth Int (m)	(m)	Lith	$k_{\Theta M} \pm SSD$ $\left(\frac{W}{m^\circ C}\right)$		N	$\Phi \pm \Delta\Phi$		$k_\Theta \pm \Delta k_\Theta$ $\left(\frac{W}{m^\circ C}\right)$	
12.0	152.0	CS (p)	2.16	0.07	5	0.20	0.05	1.68	0.15

Comments:

Lithologic log: Chapin

Well 42

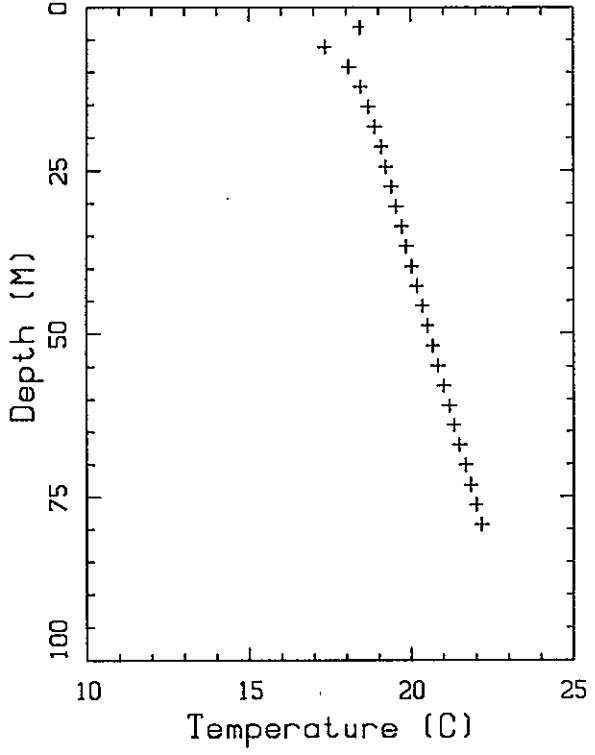

Well 43

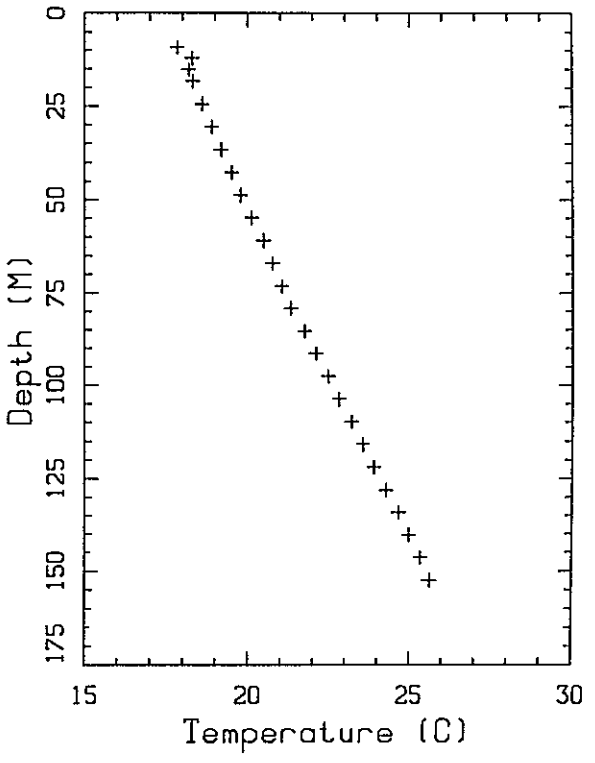

Well Number: 44

Subsurface Temperatures

z (m)	T (°C)	z (m)	T (°C)	z (m)	T (°C)	z (m)	T (°C)
3.0	19.83	27.4	19.92	51.8	20.86		
6.1	17.92	30.5	20.04	54.9	20.98		
9.1	18.67	33.5	20.13	57.9	21.09		
12.2	19.08	36.6	20.27	61.0	21.22		
15.2	19.27	39.6	20.38	64.0	21.33		
18.3	19.42	42.7	20.50	67.1	21.43		
21.3	19.58	45.7	20.62	70.1	21.56		
24.4	19.75	48.8	20.74				

Thermal Conductivities

Depth Int (m)	(m)	Lith	$k_{\Theta M} \pm SSD$ $\left(\frac{W}{m^\circ C}\right)$		N	$\Phi \pm \Delta\Phi$		$k_\Theta \pm \Delta k_\Theta$ $\left(\frac{W}{m^\circ C}\right)$	
12.0	46.0	MS,S & G	2.23 *	0.06	4	0.30	0.10	1.51	0.24
46.0	76.0	MS & S	2.27 *	0.19	6	0.30	0.10	1.53	0.24

Comments:
Lithologic logs: Chapin and driller's log
* k_Θ: values from our lab and from the operator (ok)

Well Number: 45

Subsurface Temperatures

z (m)	T (°C)	z (m)	T (°C)	z (m)	T (°C)	z (m)	T (°C)
3.0	19.53	24.4	19.36	45.7	20.90	67.1	22.45
6.1	17.92	27.4	19.56	48.8	21.12	70.1	22.66
9.1	18.23	30.5	19.79	51.8	21.35	73.2	22.86
12.2	18.53	33.5	20.02	54.9	21.57	75.9	23.03
15.2	18.71	36.6	20.23	57.9	21.82		
18.3	18.91	39.6	20.46	61.0	22.06		
21.3	19.14	42.7	20.68	64.0	22.26		

Thermal Conductivities

Depth Int (m)	(m)	Lith	$k_{\Theta M} \pm SSD$ $\left(\frac{W}{m°C}\right)$	N	$\Phi \pm \Delta\Phi$		$k_\Theta \pm \Delta k_\Theta$ $\left(\frac{W}{m°C}\right)$	
0.0	76.0	G,S & M	2.07 *	0.17	10	0.30	0.05	1.43	0.13

Comments:

Lithologic logs: Chapin and driller's log

* k_Θ: operator values (ok)

Well 44

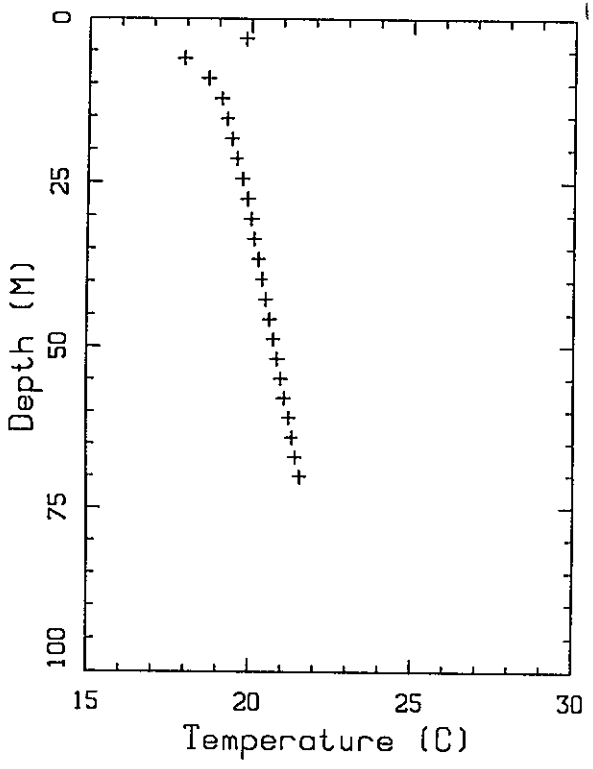

Well 45

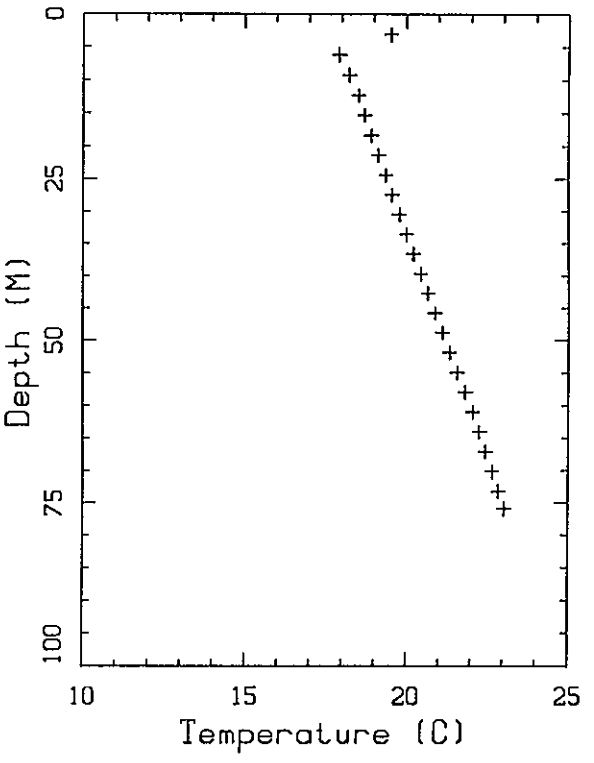

Well Number: 46

Subsurface Temperatures

z (m)	T (^{o}C)	z (m)	T (^{o}C)	z (m)	T (^{o}C)	z (m)	T (^{o}C)
3.0	21.21	36.6	21.49	70.1	23.50	103.6	25.39
6.1	18.83	39.6	21.68	73.2	23.67	106.7	25.56
9.1	19.32	42.7	21.86	76.2	23.85	109.7	25.73
12.2	19.75	45.7	22.03	79.2	24.04	112.8	25.91
15.2	20.02	48.8	22.22	82.3	24.21	115.8	26.08
18.3	20.23	51.8	22.41	85.3	24.37	118.9	26.25
21.3	20.45	54.9	22.59	88.4	24.55	121.9	26.42
24.4	20.66	57.9	22.77	91.4	24.72	125.0	26.59
27.4	20.90	61.0	22.96	94.5	24.89	128.0	27.31
30.5	21.10	64.0	23.14	97.5	25.06	131.1	26.67
33.5	21.31	67.1	23.31	100.6	25.22	134.1	27.07

Thermal Conductivities

Depth Int (m)	(m)	Lith	$k_{\Theta M} \pm SSD$ $\left(\frac{W}{m^{o}C}\right)$		N	$\Phi \pm \Delta\Phi$		$k_{\Theta} \pm \Delta k_{\Theta}$ $\left(\frac{W}{m^{o}C}\right)$	
27.0	134.0	S & G	2.97 *	0.09	5	0.40	0.05	1.58	0.17

Comments:
Lithologic logs: Chapin and driller's log
* k_{Θ}: operator values (ok)

Well Number: 47

Subsurface Temperatures

z (m)	T (^{o}C)	z (m)	T (^{o}C)	z (m)	T (^{o}C)	z (m)	T (^{o}C)
3.0	19.88	24.4	19.34	45.7	19.85	67.1	20.37
6.1	17.99	27.4	19.42	48.8	19.92	70.1	20.42
9.1	18.67	30.5	19.49	51.8	20.00	73.2	20.50
12.2	18.96	33.5	19.58	54.9	20.07	76.2	20.56
15.2	19.05	36.6	19.64	57.9	20.15		
18.3	19.14	39.6	19.71	61.0	20.23		
21.3	19.25	42.7	19.79	64.0	20.31		

Thermal Conductivities

Depth Int (m)	(m)	Lith	$k_{\Theta M} \pm SSD$ $\left(\frac{W}{m^{o}C}\right)$		N	$\Phi \pm \Delta\Phi$		$k_{\Theta} \pm \Delta k_{\Theta}$ $\left(\frac{W}{m^{o}C}\right)$	
0.0	46.0	G & MS	2.16 *	0.16	4	0.30	0.05	1.48	0.13
46.0	76.0	MS & S	2.11 *	0.14	4	0.30	0.10	1.45	0.22

Comments:

Lithologic logs: Chapin and driller's log

* k_{Θ}: values from our lab and from the operator (ok)

Well 46

Well 47

Well Number: 48

Subsurface Temperatures

z (m)	T ($^\circ C$)	z (m)	T ($^\circ C$)	z (m)	T ($^\circ C$)	z (m)	T ($^\circ C$)
6.1	16.49	24.4	17.50	54.9	18.74	85.3	19.76
9.1	16.22	30.5	17.76	61.0	18.90	91.4	19.93
12.2	16.70	36.6	17.99	67.1	19.16		
15.2	17.00	42.7	18.25	73.2	19.37		
18.3	17.17	48.8	18.53	79.2	19.57		

Thermal Conductivities

Depth Int (m)	(m)	Lith	$k_{\Theta M}$ $\pm$ SSD $\left(\frac{W}{m^\circ C}\right)$		N	Φ $\pm$ $\Delta\Phi$		k_Θ $\pm$ Δk_Θ $\left(\frac{W}{m^\circ C}\right)$	
0.0	91.0	S,M & G	3.06	0.14	6	0.30	0.10	1.89	0.36

Comments:
Lithologic Log: Chapin

Well Number: 49

Subsurface Temperatures

z (m)	T ($^\circ C$)	z (m)	T ($^\circ C$)	z (m)	T ($^\circ C$)	z (m)	T ($^\circ C$)
6.1	17.75	21.3	18.46	42.7	19.08	73.2	19.88
9.1	17.32	24.4	18.55	48.8	19.40	79.2	20.02
12.2	17.79	27.4	18.64	54.9	19.40	85.3	20.16
15.2	18.14	30.5	18.74	61.0	19.66	91.4	20.35
18.3	18.29	36.6	18.90	67.1	19.71	91.7	20.39

Thermal Conductivities

Depth Int (m)	(m)	Lith	$k_{\Theta M} \pm SSD$ $\left(\frac{W}{m^\circ C}\right)$		N	$\Phi \pm \Delta\Phi$		$k_\Theta \pm \Delta k_\Theta$ $\left(\frac{W}{m^\circ C}\right)$	
0.0	91.0	G,S & M	2.99	0.03	3	0.30	0.05	1.86	0.20

Comments:
Lithologic Log: Chapin

Well 48

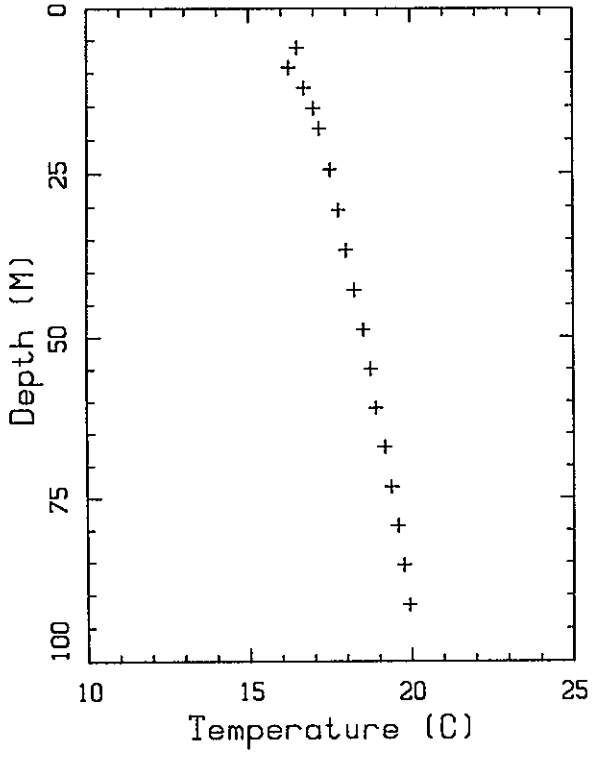

Well 49

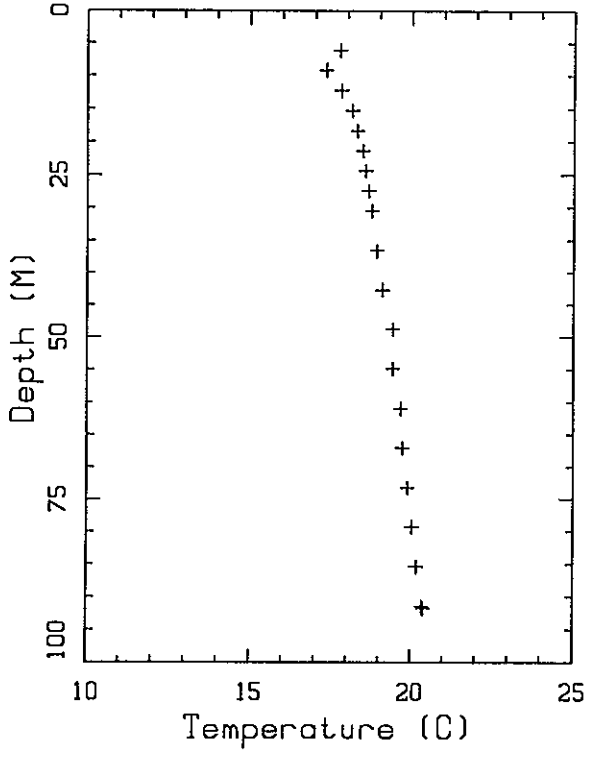

Appendix B

Heat-Flow Determinations

Heat flow determinations and estimates from this study are shown in Table 1 (in text) and in Figure B1.

The heat flow (q) across an interval is equal to the product of the thermal conductivity of that interval (k_Θ) and the temperature gradient across that interval (Γ). Geothermal studies are most often concerned with the vertical temperature gradient as measured from a temperature well log.

$$q = k_\Theta \frac{\partial T}{\partial z} = k_\Theta \Gamma \qquad \text{(B1)}$$

In this study, intervals of relatively constant temperature gradient are selected within the temperature log of each site. The temperature gradient and in-situ thermal conductivity of each interval are determined in order to obtain the heat flow of that interval. If the heat flow of a site is constant with depth (within the uncertainty of the heat-flow determinations), then that value (or a median value of similar heat flow) is recorded in Table 1 for that site.

There are a number of sites in which heat flow varies with depth beyond the limits of measurement uncertainty. It is possible that fluid flow either in the borehole or in the formation is responsible for variation of heat flow with depth, but it is difficult to determine which. Details of well construction are unknown for most wells. We assume that the annulus between the casing and the well bore is not grouted, in which case significant borehole flow is possible.

Some temperature depth profiles are extremely distorted. In wells such as 10, 26, 27 and 33, temperature gradients change dramatically within each well, and some wells contain isothermal zones. We assume that these wells are perturbed

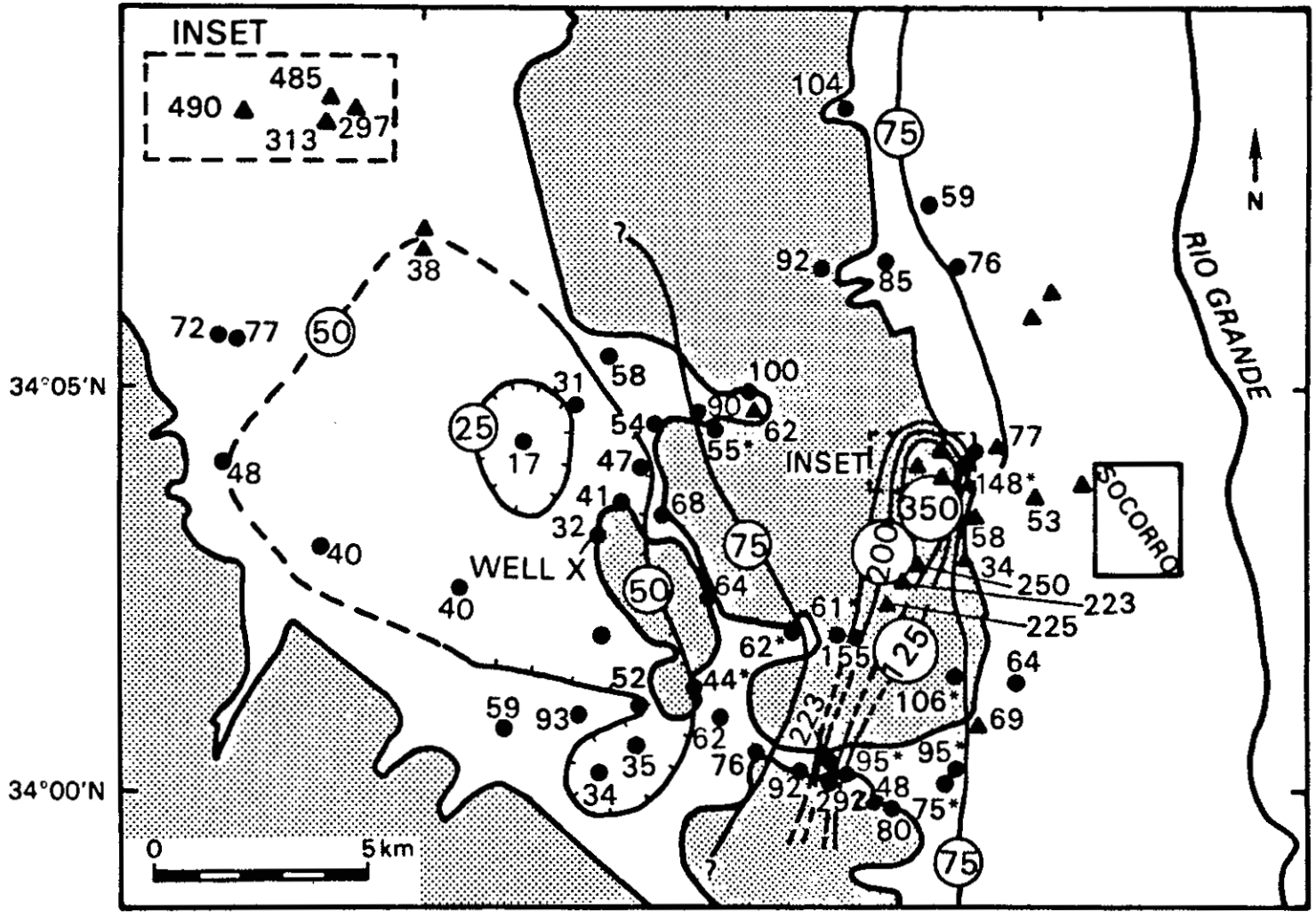

Fig. B1. Heat-flow contour map. Heat flows given in $mW\ m^{-2}$ ($1\ HFU = 41.84\ mW\ m^{-2}$). Note magnified inset of Wood's Tunnel area. The uncertainties of the heat-flow determinations range from 10% to 20%, except for heat-flow estimates (indicated by *) which have higher uncertainty. Circled numbers are contour labels and contours are dashed where data is sparse. Note that contour interval varies between 25 and 150 $mW\ m^{-2}$ depending on location.

by borehole flow. Similar temperature-depth profiles were observed at the Beoware Geothermal field, Nevada; Smith (1983) suggested that these temperature disturbances are produced by thermal fluids welling up in the well bore annulus. It is difficult to determine a representative temperature gradient for such wells. We assume that the bottom-hole temperature or (in one case) the maximum measured temperature is the least likely to be severely perturbed (not unreasonable since these wells generally appear to be perturbed by upward fluid flow). An average geothermal gradient (marked by astericks in Table 1) is calculated for these wells from the bottom hole temperature of the well and an estimated surface temperature. Heat flows estimated from these average gradients are denoted by astericks in Figure B1 and Table 1 (in text).

We have determined surface temperatures in the Socorro area as a function of elevation by extrapolating temperature-depth profiles which appear to be relatively undisturbed and well-behaved near the surface. Temperatures at depths greater than 30 m were used to avoid the effects of annual temperature fluctuation. When a linear temperature-depth profile below 30 m could be readily extrapolated to the surface, the resultant surface temperatures were determined. These temperatures (for the geothermal wells of this study) have been plotted in Figure B2, and a least-mean-square fit line through the data is used to estimate surface temperature as a function of elevation.

In a number of other wells, heat flows vary with depth but without the extreme distortion discussed above. Shallow heat flows are lower than deep heat flows in a number of wells in La Jencia Basin (e.g. 5, 11, 21 and 22), suggesting hydrologic perturbation. Lithologic logs of these wells often indicate that the low heat flows occur in more permeable material which overlies relatively impermeable claystone, suggesting that some near-surface ground-water flow may be influencing temperatures in the uppermost material. It is possible that hydrologic

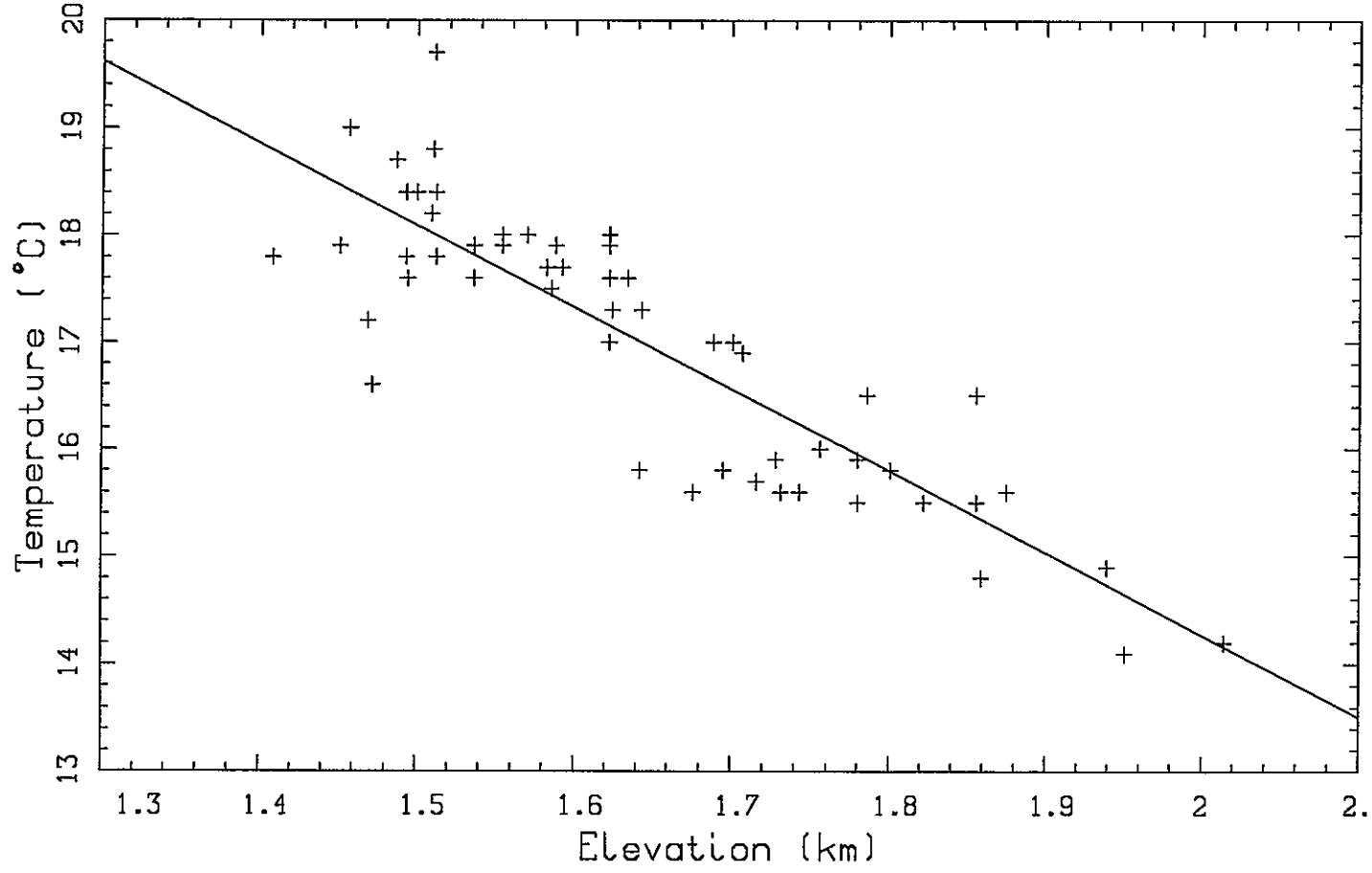

Fig. B2. Extrapolated surface temperatures as a function of temperature from geothermal wells in the Socorro area. Least-mean-square linear fit plotted also:

$$T = -7.63 \times 10^{-3}\, z + 29.55$$

where T is temperature in $^{\circ}C$, and z in elevation in meters.

recharge infiltrates into the upper material (reducing temperature gradients), and then flows laterally on top of the claystone aquitard. Another possibility is that lateral flow of water recharged elsewhere may cool these upper, more permeable rocks. In either case, as discussed in the text, it is unlikely that any significant amount of near surface water flows down into the underlying claystone, and we look to another cause to explain the low heat flows observed in the underlying claystone.

Heat flows in other wells are higher at shallow depths than at greater depths. These higher heat flows tend to be measured in coarse, unsaturated material which is located a substantial distance above the water table. Coarse materials at a given elevation above the water table tend to be drier than fine grained materials (see discussion in Appendix D). We suggest that it is possible that these coarse materials are so dry that their thermal conductivity has been substantially overestimated, and therefore the heat flow in these intervals is actually lower than we have determined.

In all cases where heat flows vary with depth but are not extremely distorted (as in the examples discussed in the two preceding paragraphs), we have assumed that the heat flow from the lowest part of the well is most representative. This is a fairly common assumption in the study of heat-flow. Typically an investigator will assume that the temperatures measured in the deepest part of the well are the least perturbed by near surface hydrologic and other shallow phenomena and that deep temperatures are the most representative of the geothermal regime. Heat flows determined using this assumption are marked by the letter "D" in Table 1.

Uncertainty and error in heat-flow determinations

There are uncertainties and errors associated with both the temperature gradient and the thermal conductivity (k_Θ) of an interval. In order to quantify the uncertainty we use the relationship:

$$\Delta Q = \frac{\partial Q}{\partial k_\Theta} \Delta k_\Theta + \frac{\partial Q}{\partial \Gamma} \Delta \Gamma \tag{B2}$$

from Young (1962), which can be written

$$\frac{\Delta Q}{Q} = \frac{\Delta k_\Theta}{k_\Theta} + \frac{\Delta \Gamma}{\Gamma}. \tag{B3}$$

Temperature Gradient

The uncertainty in the temperature gradient is comprised of the uncertainty in the temperature measurement and in the calculation of the gradient.

The accuracy of temperature measurements made by industry investigators is unknown, so we assume their measurements are as accurate as those in another geothermal studies for which such information in available. In a study of heat flow in Arizona, Shearer (1979) states that the error introduced into temperature gradient determinations by error in his temperature measurements is less than 1%. In addition, a possible systematic error may be introduced by stretching in the cable used to lower the temperature probe, causing temperature gradients to be systematically high by less than 3% (op. cit.). We do not include the systematic cable-stretching error in our uncertainty calculations, instead noting the possibility of such a systematic over-estimation of heat flow.

Temperature gradients are calculated by determining the least-mean-square linear fit to measured temperatures and depths. The uncertainty of this gradient determination is assumed to be the standard deviation of the gradient. We assume

that the random error in the temperature measurement is incorporated into the standard deviation of the gradient.

Thermal conductivity

The uncertainty in k_Θ consists of the uncertainty in the matrix thermal conductivity ($k_{\Theta M}$) and in porosity (Φ). In-situ thermal conductivity is determined by the formula

$$k_\Theta = {k_{\Theta_w}}^{\Phi} \; {k_{\Theta M}}^{1-\Phi} \tag{B4}$$

where k_{Θ_w} in the thermal conductivity of water.

The uncertainty of k_Θ is determined by

$$\Delta k_\Theta = \frac{\partial k_\Theta}{\partial \Phi}\Delta\Phi + \frac{\partial k_\Theta}{\partial k_{\Theta M}}\Delta k_{\Theta M} \tag{B5}$$

and therefore

$$\frac{\Delta k_\Theta}{k_\Theta} = (\ln k_{\Theta_w} - \ln k_{\Theta M})\frac{\Delta\Phi}{\Phi} + (1-\Phi)\frac{\Delta k_{\Theta M}}{k_{\Theta M}} \tag{B6}$$

Matrix thermal conductivities ($k_{\Theta M}$) of samples from most sites were measured in the lab as described in Appendix C. The uncertainty of our $k_{\Theta M}$ measurement ($\Delta k_{\Theta M}$) is assumed to be equal to the reproducibility of the measurements: $\pm 4\,\%$ (Reiter and Hartman, 1971). Where measurements of samples from the site in question are not available, or are of poor quality, higher uncertainties are assigned, as described in Table C1.

The uncertainty in porosity is very difficult to determine. The porosity of claystones has been measured in the lab, but we only have estimates of the porosity of unconsolidated material or substantially fractured rocks in the Socorro area. Uncertainty in porosity introduces most of the uncertainty in the determination of

Table B1: Uncertainty in $k_{\Theta M}$ Data	
$\Delta k_{\Theta M}$ (percent)	Type of $k_{\Theta M}$ data
4%	At least 3 measurement by our lab or by operator whose measurements of $k_{\Theta M}$ are consistent with our lab.
6%	1 or 2 measurements in our lab, or No samples, only measurement available from operator whose $k_{\Theta M}$ values are inconsistent with our lab, or No samples, no measurements available, so we chose typical value for lithologic unit described in lithologic log.
10%	No samples, no measurements, no lithologic logs.

k_Θ. Values of Φ and $\Delta\Phi$ (the uncertainty in Φ) used in this study are listed in Appendix C (for each litholigic unit) and in Appendix A (and for each well). These values were estimated for each type of lithologic unit using tabulated values of Φ from assorted references. (Note the high uncertainties in the porosity of unconsolidated muddy or clayey units.)

Heat-Flow Corrections

The possible influences of a variety of other perturbations upon heat flow in the Socorro area have been considered.

Diurnal and annual periodic surface temperature variation is negligible ($\approx$0.1 %) for depths greater than 22 m (Minier, 1987). In this study, we usually neglected any data from depths shallower than 30 m. The effect of long term

climatic changes could be of greater magnitude (Minier, 1987), but would tend to systematically effect all data, without changing the nature of the anomalies observed in the Socorro area.

The influence of local topography was modeled (for a purely conductive system, with no heat advection by fluid). We found that the terrain correction near the east front of the Socorro mountain block is about 10 - 15%, which is far smaller than the heat-flow variation observed in the Socorro area. The only areas at which the terrain correction is significantly greater is near the tops of local peaks, where no heat-flow data have been obtained. Terrain corrections have not been applied to data from the Socorro area in this study.

The effects of thermal refraction were also modeled (for a purely conductive system). Thermal refraction was found to have a substantial effect. It was found that the upfaulted block of Precambrian rocks in the Socorro mountain block, at Wood's Tunnel, could produce a variation in conductive heat flow of about a factor of two. Thermal refraction has been included in our modeling of conduction and advection in the Socorro hydrothermal system.

We also considered the effects of sedimentation and erosion on heat flow. The natural effect of these processes would be to reduce heat flows in areas of extensive sedimentation, such as La Jencia Basin and the Socorro Basin, and elevate heat flows in areas of uplift and erosion, such as the Socorro mountain block. The thermal effects of sedimentation and erosion are determined using the solution for transient heat conduction in a moving solid (Carslaw and Jaeger, 1946, second edition, Chapter 15.2). We found that a reasonable erosion or sedimentation rate for the Socorro area of about 1000 m in 5 million years would produce a variation in heat flow of less than 10%. (Note that most of the lowest heat flows of eastern La Jencia Basin are found in areas where subsidence has been

negligible in the last 5 million years.) No erosion or sedimentation corrections have been applied to the Socorro area data in this study.

Appendix C

Thermal Conductivity

Thermal conductivities of lithologic samples were measured in the laboratory using the system presented by Reiter and Hartman (1971). This system is applied to drill cutting fragments by the technique of Sass et al. (1971). Drill cuttings are packed into cells and vacuum flooded with water. The thermal conductivity of the packed cell is measured. and a correction is made to account for the influence of the cell and the influence of water in the voids within and between chips (Sass et al., 1971). The resultant value ($k_{\Theta M}$) is the thermal conductivity of the sample's matrix material (without porosity). It is necessary to apply a correction for the in-situ porosity of the geologic material in order to determine the in-situ thermal conductivity (k_{Θ}).

If it is assumed that the in-situ pore space is entirely filled with water of thermal conductivity $k_{\Theta W}$ (0.61 $W\, m^{o}\, C^{-1}$), then the relationship between in-situ and matrix thermal conductivities is as follows:

$$k_{\Theta} = (k_{\Theta M})^{1-\Phi}\ (k_{\Theta W})^{\Phi} \tag{C1}$$

where Φ is in-situ porosity (Woodside and Messmer, 1961).

Both matrix porosity (intergranular porosity) and fracture porosity may contribute to in-situ porosity. In-situ porosity is often obtained from geophysical logs, but none exist for the Socorro geothermal sites. Porosity is very difficult to determine for geologic units in the Socorro area, and is a source of considerable uncertainty in thermal conductivity determinations for this study.

In this study we assume that matrix porosity is dominant in unconsolidated sediments and moderately indurated claystones of the Upper Popatosa Formation (these claystone become ductile when wet, so presumably most fractures would

close). We assume that fracture porosity is dominant in Tertiary volcanic rocks and the well indurated sediments of the Lower Popatosa.

The matrix porosity of competent rock can be measured in the lab. Relatively large samples are best, such as pieces of core, but measurements can be made on drill cuttings. In this study the matrix porosity of claystone cuttings was measured by flooding the claystones with oil in a density bottle. Oil was used because the claystone cuttings showed a strong tendency to swell in water. Swelling in situ would be suppressed by lithostatic pressure, and swelling in thermal conductivity measurement is inhibited by applied pressure. Therefore, porosity measured from a swelled sample would probably not be representative of in situ conditions, or appropriate for corrections to our thermal conductivity measurements. Porosities of 11-22 % were measured in moderately indurated claystone chips. Morris and Johnson (1967) list porosity ranges of 41.2 to 45.2 % for claystone and 1.4 to 9.7 % for shale. If our measurements are correct, Popatosa claystones must be considerably more consolidated or altered than the claystones measured by Morris and Johnson.

We did not oven-dry samples as part of our porosity measurement process because we had not done so as part of the thermal conductivity measurement. Perhaps measured porosities would have been higher had we done so, but the results would not have been applicable as a porosity correction for our thermal conductivity measurements.

The in-situ matrix porosity of incompetent materials is not well estimated by laboratory measurements of drill cutting samples. There is likely to be preferential loss of certain materials from the samples, and the in-situ compaction would be very difficult to duplicate. In situ porosity of near-surface sediments in the Socorro area has been estimated at 40-45% (Ibrahim, 1962), and we use this as an

upper limit for the porosity of unconsolidated sediments.

Fracture porosity cannot be measured in the laboratory, unless sample pieces are large enough to contain a representative number of fractures. Drill cuttings give no information about fracture porosity. We could find no measurements of the porosity of volcanic rocks in the Socorro area, so we obtained representative values and ranges of values from the general literature.

Lithologic logs by Chapin and Osbourn were used in conjunction with our own observation of cuttings and operator lithologic logs to determine the lithology of drill cuttings. We have summarized the lithology by listing the lithologic components of the interval in descending order of contribution. For example: 'Sand, Mud and Gravel' would be a muddy sand with some gravel.

Porosities used in our porosity corrections, and the estimated uncertainty in porosity values are listed in Table C1.

We were forced to to assume a fairly wide range of possible porosities for clayey unconsolidated materials, which introduces considerable uncertainty into heat-flow determinations for sites in such material.

In addition to the problem of in-situ porosity, there also remains the problem of saturation. Equation (C1) was obtained assuming that the pore space is entirely filled with water in-situ. That is not necessarily the case; the water table in the Socorro area is quite deep in places (up to 120 m) and large depth intervals of some geothermal wells are above the water table (unfortunately water levels are not known in most of the geothermal wells in this study). We find, however, that the variation of thermal conductivity with saturation is probably not important, except in a few wells at shallow depths. The value of in-situ thermal conductivity that Sanford (1977) estimated for unsaturated volcanic breccia using thermal diffusivity is very close to the value we obtain for volcanic breccia from the same

Table C1: Assumed Porosity of Geologic Materials	
Material	Porosity (%)
Gravel Boulders Gravel, sand and mud Gravel, mud and sand Sand, gravel and mud Sand, mud and gravel	30 ±5
Sand Sand and mud	40 ±5
Clay Mud Mudstone (poorly indurated) Clay and sand Mud and sand Mudstone and sand	30 ±10
Claystone Claystone and gravel	20 ±5
Sandstone Claystone and Sandstone Claystone and Sand	25 ±5
Well-indurated Conglomerate or Mudflow	20 ±5
Lava flow Welded Tuff	20 ±5

location using the technique of Reiter and Hartman (1971), assuming complete saturation ($\approx$1.7 $W\ m^{o}\ C^{-1}$). Therefore, it seems likely that little error is introduced by calculating and using the saturated thermal conductivity for these materials. In addition, temperature gradients measured in many Socorro geothermal wells do not appear to change greatly above and below the water table and so thermal conductivities probably do not vary greatly either.

De Vries (1963) has found that vapor transport of heat in the unsaturated zone can act to keep the thermal conductivity of soils relatively constant with

moisture content, and relatively close to the saturated k_Θ unless the soil is very dry. In general, fine-grained materials tend to have a higher moisture content at a give elevation above the water table than coarse materials (Freeze and Cherry, 1979). Many of the heat-flow sites of this study are drilled in clays and clayey materials which would tend to have relatively high moisture contents, and therefore saturation variation would tend to have less influence on thermal conductivity. However, there are a few sites drilled in very coarse material where the water table is quite deep, in which temperature gradients are significantly higher at shallow depths. Temperature gradients in these wells (e.g. 3 and 4) are higher in the shallow gravels and sand above the water table than temperature gradients below the water table. In these cases the heat flows determined above the water table are considered suspect.

Thermal conductivities had previously been measured for two sets of industry geothermal data by the industrial operator. We measured the thermal conductivities of test groups of samples from these data sets to compare our thermal conductivity values to those measured by the operator. For one set of data, the $k_{\Theta M}$ we measured were in agreement with those measured by the operator. We used operator data from this data set in our results, and did not measure the $k_{\Theta M}$ of all available samples ourselves. Values of $k_{\Theta M}$ measured by the other operator were not as reliable, tending to be low. We measured the thermal conductivity of all the samples available for this set of data, but in some case we had no samples from these wells, and were forced to rely on operator values. These operator values which we suspect to be low are so marked in Appendix A.

The thermal conductivities we measured were generally quite low. Except for the Precambrian rock of Wood's Tunnel (thermal conductivity of 3.1 $W\, m^0\, C^{-1}$ measured by Reiter and Smith, 1977), all samples were of Tertiary volcanic and sedimentary rocks. The thermal conductivities of these Tertiary

rocks are almost all less than 2.0 $W\ m^{o}\ C^{-1}$, and more than half are less than 1.7 $W\ m^{o}\ C^{-1}$.

Porosity measurement

Matrix porosity of Popatosa claystones was measured using a density bottle with a medium of oil (Mazola). A density bottle has a tight fitting top with a fine hole through which excess fluid escapes. When the top is properly fitted (sealed) the volume of its contents are known with a very high degree of accuracy, and therefore density calculations can be made with corresponding accuracy.

Oil was used because the claystones swell in contact with water, and also because it appears that oil soaks into claystone chips more slowly than water does. The largest drill cuttings of claystone were selected in order to reduce errors due to surface effects. The samples were placed in a density bottle and weighed. Oil was poured in rapidly filling the bottle completely, and the bottle sealed without allowing time for oil to soak into the pores (the matrix porosity) of the claystone chips. The bottle full of samples and oil was weighed. These measurements, combined with the known volume of the bottle, yield the bulk density of the chips, assuming that only negligible amounts of oil soaked into the matrix porosity of the chips. We cut open chips that had been soaked in oil for a short amount of time and observed that only a very thin layer of the chip was saturated by the oil.

In order to determine bulk porosity from bulk density it is necessary to know the solid density of the material (we use the term "solid density" in this discussion instead of "matrix density" to avoid confusion with "matrix porosity"). We measure solid density in two different ways.

After performing the bulk density measurement described above, we left the chips in oil for several days until oil soaked all the way through the chips. The

density bottle was then topped off with more oil, sealed and reweighed. The solid density of the material can be determined from these measurements, by assuming that the pore space of the chips has been entirely filled with oil. A second technique for measuring solid density is to grind dry chips into a very fine powder (presumably eliminating all matrix porosity). The powder is put in the density bottle and weighed. The density bottle is filled with oil and the bottle is agitated to release trapped air. When all the air has escaped from the sample, the density bottle is topped off with oil, sealed and weighed. These two methods yield comparable values for solid density.

APPENDIX D

Numerical Modeling

Finite difference techniques have been applied to model the Socorro hydrothermal system in steady state. First, the ground-water flow system is modeled. The governing equation is

$$\frac{\partial}{\partial x}\left(k_{HX}\frac{\partial h}{\partial x}\right)+\frac{\partial}{\partial z}\left(k_{HZ}\frac{\partial h}{\partial z}\right) = 0 \qquad \text{(D1)}$$

where h is the hydraulic head, and k_{HX} and k_{HZ} are the hydraulic conductivities in the x (horizontal) and z (vertical) directions.

Hydraulic conductivity is allowed to vary with position, and to be anisotropic. Water density and viscosity are assumed to remain constant, and not to vary with temperature; the free convection and temperature-caused viscosity variation are not modeled. The governing equation is applied to a block-centered grid (illustrated in Figure D1). Note that the first index, i, denotes the vertical coordinate, and j denotes the horizontal. We obtain

$$\frac{\left(k_{HX}\frac{\partial h}{\partial x}\right)_{i,j+\frac{1}{2}}-\left(k_{HX}\frac{\partial h}{\partial x}\right)_{i,j-\frac{1}{2}}}{\Delta x}+$$

$$\frac{\left(k_{HZ}\frac{\partial h}{\partial z}\right)_{i+\frac{1}{2},j}-\left(k_{HZ}\frac{\partial h}{\partial z}\right)_{i-\frac{1}{2},j}}{\Delta z} = 0 \qquad \text{(D2)}$$

where

$$(k_{HX})_{i,j\pm\frac{1}{2}} = \frac{2\,k_{HX}(i,j)\,k_{HX}(i,j\pm1)}{k_{HX}(i,j)+k_{HX}(i,j\pm1)} \qquad \text{(D3a)}$$

$$(k_{HZ})_{i\pm\frac{1}{2},j} = \frac{2\,k_{HZ}(i,j)\,k_{HZ}(i\pm1,j)}{k_{HZ}(i,j)+k_{HZ}(i\pm1,j)} \qquad \text{(D3b)}$$

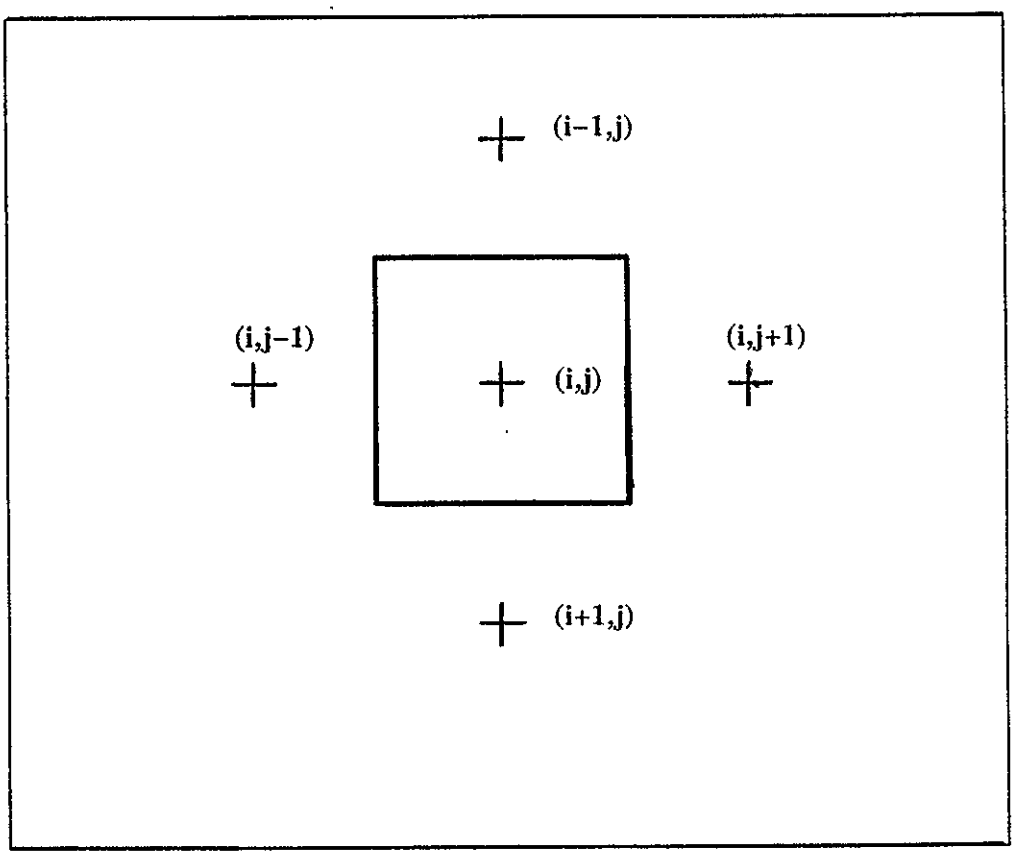

Fig. D1. Block-centered grid used in finite difference modeling.

and

$$\left(\frac{\partial h}{\partial x}\right)_{i,j\pm\frac{1}{2}} = \frac{\pm(h(i,j\pm1) - h(i,j))}{\Delta x} \tag{D4a}$$

$$\left(\frac{\partial h}{\partial z}\right)_{i\pm\frac{1}{2},j} = \frac{\pm(h(i\pm1,j) - h(i,j))}{\Delta z} \tag{D4b}$$

Heads are calculated at each point by direct solution, using the heads from the previous iteration and the heads calculated at the current iteration, where available. Iteration continues until the convergence criterion is met. The convergence criterion is:

$$\sum_{i=1}^{m}\sum_{j=1}^{n} \left| h(i,j)_{k-1} - h(i,j)_k \right| < C \tag{D5}$$

where k is the iteration number, and C is a convergence factor chosen to be less than 1% of the total head change across the system.

When the head distribution has converged, finite difference techniques are employed to model the temperatures of the system, in steady state. The governing equation is

$$\frac{\partial}{\partial x}\left(k_\Theta \frac{\partial T}{\partial x}\right) + \frac{\partial}{\partial z}\left(k_\Theta \frac{\partial T}{\partial z}\right) - \rho_F \, c_F \left(v_X \frac{\partial T}{\partial x} + v_Z \frac{\partial T}{\partial z}\right) = 0 \tag{D6}$$

where ρ_F and c_F are the density and specific heat of water (assumed constant in this model) and k_Θ is the thermal conductivity of the saturated porous medium (which may vary with position but is assumed isotropic in this formulation). v_X and v_X are the volumetric fluid fluxes in the x (horizontal) and z (vertical) direction, which are determined by Darcy's law:

$$v_X = -k_{HX} \frac{\partial h}{\partial x} \qquad v_Z = -k_{HZ} \frac{\partial h}{\partial z} \tag{D7}$$

In terms of the block centered grid of Figure D1, the governing equation is

$$\frac{(k_\Theta \frac{\partial T}{\partial x})_{i,j+\frac{1}{2}} - (k_\Theta \frac{\partial T}{\partial x})_{i,j-\frac{1}{2}}}{\Delta x} + \frac{(k_\Theta \frac{\partial T}{\partial z})_{i+\frac{1}{2},j} - (k_\Theta \frac{\partial T}{\partial z})_{i-\frac{1}{2},j}}{\Delta z}$$

$$- \frac{\rho_F c_F \left[(v_X T_w)_{i,j+\frac{1}{2}} - (v_X T_w)_{i,j-\frac{1}{2}}\right]}{\Delta x}$$

$$- \frac{\rho_F c_F \left[(v_Z T_w)_{i+\frac{1}{2},j} - (v_Z T_w)_{i-\frac{1}{2},j}\right]}{\Delta z} = 0 \qquad \text{(D8)}$$

where the fluid flow rates (v_X and v_Z) are defined by equation D7 and D4a and D4b, and where

$$(k_\Theta)_{i,j\pm\frac{1}{2}} = \frac{2\, k_\Theta\,(i,j) k_\Theta(i,j\pm1)}{k_\Theta(i,j) + k_\Theta(i,j\pm1)} \qquad \text{(D9a)}$$

$$(k_\Theta)_{i\pm\frac{1}{2},j} = \frac{2\, k_\Theta\,(i,j) k_\Theta(i\pm1,j)}{k_\Theta(i,j) + k_\Theta(i\pm1,j)} \qquad \text{(D9b)}$$

$$(\frac{\partial T}{\partial x})_{i,j\pm\frac{1}{2}} = \pm\frac{[T(i,j\pm1) - T(i,j)]}{\Delta x} \qquad \text{(D10a)}$$

$$(\frac{\partial T}{\partial z})_{i\pm\frac{1}{2},j} = \pm\frac{[T(i\pm1,j) - T(i,j)]}{\Delta z} \qquad \text{(D10b)}$$

T_w is an upstream weighted temperature, used in advective terms to improve convergence. We have developed a system which allows us to apply weighting only when modeling a system for which the temperatures will not converge otherwise,

and allows us to apply just enough upstream weighting to obtain convergence. The upstream weighted temperatures are calculated by

$$(T_w)_{i,j-\frac{1}{2}} = T(i,j-1)\beta_X + T(i,j)[1-\beta_X] \quad \text{(D11a)}$$

$$(T_w)_{i,j+\frac{1}{2}} = T(i,j+1)[1-\beta_X] + T(i,j)\beta_X \quad \text{(D11b)}$$

$$(T_w)_{i-\frac{1}{2},j} = T(i-1)\beta_Z + T(i,j)[1-\beta_Z] \quad \text{(D11c)}$$

$$(T_w)_{i+\frac{1}{2},j} = T(i+1)[1-\beta_Z] + T(i,j)\beta_Z \quad \text{(D11d)}$$

where

$$\beta_X = \frac{v_X}{|v_X|}\alpha + .5 \quad \text{(D12a)}$$

$$\beta_Z = \frac{v_Z}{|v_Z|}\alpha + .5 \quad \text{(D12b)}$$

If $\alpha = 0$, no upstream weighting is applied; and $\alpha = .5$ for full upstream weighting. When temperatures did not converge with $\alpha = 0$, increasing values of α were tried until convergence was obtained.

Temperatures are calculated at each point, by direct solution, using the temperature values of surrounding grid points from the previous iteration and the present iteration where available. Iteration continues until convergence is achieved, using the same type of criteria given in Equation D5, applied to temperatures.

Model Verification

The numerical codes developed as part of this study were verified by testing against a number of analytical solutions. First, the code was tested against the analytical solution for one dimensional conduction/ convection presented by Bredehoeft and Popadapolous (1965). We found that the temperature field and temperature gradients produced by the numerical model matched those of the

analytical solution for fluid flow velocities less than $10^{-6}\,m\,s^{-1}$ (using a grid spacing of 100 m). (Velocities obtained in modeling of the Socorro hydrothermal system are generally $<10^{-8}\,m\,s^{-1}$.)

Additional verification used more complex analytical solutions. The numerical code was tested against an analytical solution that we developed for the horizontal flow of anomalously cool fluid in the presence of a basal heat-flow boundary condition, and upper-boundary constant temperature (i.e. the fluid flow is perpendicular to basal heat flow). We also tested our program against an analytical approximation for the temperature field produced by two-dimensional heat and fluid transport in a closed basin, developed by Domenico and Palauskias (1973) which is only valid at low velocities and temperature gradients. In both cases, the numerical code reproduced the analytical solutions quite well, and we were satisfied that the numerical code accurately simulated heat and fluid transport.

The computer code presented here is based on a code written by Gerry Clarkson for transient heat conduction. A copy of the fluid flow and heat transport numerical code developed in this study follows. These codes were developed by M. Barroll in 1988 and 1989.

```
c   g3ha.f
c finite difference, block centered grid
c solution to head equation.  double precision.
c Hydraulic conductivity (k) may vary with position and be anisotropic.
c Boundaries may be fixed flow, fixed head, or a combination of the two.
c
c Input files from gfa.f
c       gfa.dat
c       boundh.dat
c Output files
c       gfn.dat  (updated version of gfa.dat:  to restart program
c               where you left off and continue iterations, mv gfn.dat
c               to gfa.dat and then restart g3ha.)
c       g3ha.out  ( commented output: this is what you look at)
c       contour.out ( data file containing system dimensions and head
c               data which can be contoured by contour.f)
c
        real k(105,205),l,pi,ky(105,205)
        dimension t(105,205),h(105,205),xh(105,205)
        dimension tn(105,205)
        common/aa/m,n,delx,dely,acon,bcon,np,alf
        common/bb/gam,to
        double precision h,t,delh,ts
        character *10 filnx,filny,tkf

        open(unit=21,file='gfa.dat')
        open(unit=15,file='g3ha.out')

c input: md: # of grid points vertically, nd: # of horizontally,
c both md and nd exclude mirror points, so the system the computer
c deals with is md+2 by nd+2
c  yo: height of true system (m) (excluding
c mirror points), l: width, excluding mirror points
c niter1r:  max number of additional h iterations per run of g3head,
c conv: h convergence criteria (<.01) sum(abs(delh between steps))
c niter2r:  max number of additional t iterations per run of g3temp,
c conv2: t convergence criteria (<.01) sum(abs(delt between steps))
c to: temp at surface (C), gamm: background temp gradient (C/km), tcond: thermal
c conductivity (W/mC)
c np: output criteria, np =1 to output all values, np=2, ever other val, etc
c acon,bcon: head parameters used in analytical head solutions for test cases
c iter1: number of head iterations already performed before this run.
c h(m,n): initial hydraulic head distribution (m) mxn matrix
c k(m,n): hydraulic conductivity matrix (m/s)
c t(m,n): temperatures (c)
c iter2 number of temp iterations.already performed before this run.

        read(21,*)md,nd,yo,l,niter1r,conv,niter2r,conv2
        read(21,*)to,gamm,tcond,np,acon,bcon,iter1,del
        read(21,*)tkf
```



```
        read(21,*)nakx,naky
        write(6,*)md,nd,yo,l,niter1r,conv,niter2r,conv2
c true number of grid points needed including mirror points
        m=md+2
        n=nd+2
        if(nakx.eq.1)then
        read(21,*)xkx
        write(*,*)xkx
        do 105 i=1,m
        do 105 j=1,n
105     k(i,j)=xkx
        else
        read(21,*)filnx
        open(unit=22,file=filnx)
        do 106 i=1,m
106     read(22,*)(k(i,j),j=1,n)
        close(unit=22)
        end if
        write(*,*)' entered kx'
        if(naky.eq.1)then
        read(21,*)xky
        write(*,*)xky
        do 107 i=1,m
        do 107 j=1,n
107     ky(i,j)=xky
        else
        read(21,*)filny
        open(unit=22,file=filny)
        do 108 i=1,m
108     read(22,*)(ky(i,j),j=1,n)
        end if
        write(*,*)' entered ky'
        do 15 i=1,m
15      read(21,*)(h(i,j),j=1,n)
        do 17 i=1,m
17      read(21,*)(t(i,j),j=1,n)
        read(21,*)iter2
        close(unit=21)
c maximum total number of head iterations allowed
        niter=iter1+niter1r
        write(*,*)' entered all data'

c  *********************************************

c convert C/km to C/m
        gam=gamm/1000.
c block widths
        delx=l/nd
        dely=yo/md
c hydraulic conductivity
```

```
      pi=3.14159
c density of water kg m-3
      rho=1000.
c specific heat of water
      c=4185.
      alf=tcond/(rho*c)
c a constant that may be used in analytical solutions

c  *****************************************

c calculate surface temperature: half way between top & 2nd row of
c grid points
      ts=(t(1,1)+t(2,2))/2.

      write(15,*)' surface temp: ',ts
      write(15,*)' '
      write(15,*)' temperature gradient (C/km) ',gamm
      write(15,*)' '
      write(15,*)' thermal conductivity (W/C*m**2): ',tcond
      write(15,*)' thermal diffusivity (m**2/s): ',alf
      write(15,*)' '
      write(15,*)' hydraulic conductivity: ',k(1,1)
      write(15,*)' '
      write(15,*)' horiz x: ',l,' m ;  dx= ',delx,' m; n= ',n
      write(15,*)' '
      write(15,*)' vert  y: ',yo,' m ;  dy= ',dely,' m; m= ',m
      write(15,*)' '
      write(15,*)' acon,bcon  (m) ',acon,bcon
      write(15,*)' '
c     bb=cosh(pi*yo/l)
c     write(15,*)' cosh(pi*yo/xl) = ',bb
      write(15,*)' '
      write(15,*)' '
      write(15,*)' '


c  *****************************************
c  set head boundary conditions
      call boundh(1,h,l,k,ky)
c     do 888 i=1,m
c888  write(6,*)(h(i,j),j=1,n)
c Numerical soln for head distribution
c Start iterating, stop when heads have converged (stopped changing)
c or when number of iterations performed this run exceed niterlr
      iter=iterl
10    continue
c     write(15,*)' call solveh'
      call solveh(h,k,ky,delh)
      iter=iter+1
```



```
c set boundary conditions for head
c     write(15,*)' call boundh 2'
      call boundh(2,h,l,k,ky)
      mm=mod(iter,100)
      if(mm.eq.0)then
c check against analytical solution (simple test cases)
c     call anlyt(l,h,l,yo,iter,delh)
c mass convergence calculations
      xleft=0.0
      xright=0.0
      do 88 i=2,m-1
      xleft=xleft-k(i,1)*(h(i,2)-h(i,1))*dely/delx
88    xright=xright-k(i,n)*(h(i,n)-h(i,n-1))*dely/delx
      xtop=0.0
      xbot=0.0
      do 89 j=2,n-1
      xtop=xtop-ky(2,j)*(h(2,j)-h(1,j))*delx/dely
89    xbot=xbot-ky(m-1,j)*(h(m,j)-h(m-1,j))*delx/dely
      dsum=xleft-xright+xtop-xbot
c left is the net mass coming into system through the left hand side
c right is the the mass leaving the system through the right hand
c side, dsum is the difference.  If top and bottom have no flow
c boundary conditions, dsum should be very small
      write(*,*)' left= ',xleft,'  right= ',xright,' dsum= ',dsum
      write(*,*)' top ',xtop,'  bot ',xbot
      write(15,*)' left= ',xleft,'  right= ',xright,' dsum= ',dsum
      write(15,*)' top ',xtop,'  bot ',xbot
      end if
      mn=mod(iter,50)
      if(mn.eq.0)then
      write(6,*)' iter: ',iter,'  delh= ',delh
      end if
      if(delh.gt.conv.and.iter.lt.niter)goto 10

c  *****************************************
c output to file gflow33n.dat which is identical to gflow33
c except that it contains updated h values and iter value
c so calculations can be continued from where the last
c run left off by moving gflow33n.dat to gflow33.dat

      open(unit=22,file='gfn.dat')
      write(22,*)md,nd,yo,l,niterlr,conv,niter2r,conv2
      write(22,*)to,gamm,tcond,np,acon,bcon,iter,delh
      write(22,*)tkf
      write(22,*)nakx,naky
      if(nakx.eq.1)then
      write(22,*)xkx
      else
      write(22,*)filnx
      end if
```

```
      if(naky.eq.1)then
      write(22,*)xky
      else
      write(22,*)filny
      end if

      do 42 i=1,m
42    write(22,*)(h(i,j),j=1,n)

      do 45 i=1,m
45    write(22,*)(t(i,j),j=1,n)
      write(22,*)iter2
      close(unit=22)
      open(unit=17,file='contour.out')
      ymin=0.0
      xmin=0.0
      mo=m-1
      no=n-1
      write(17,*)mo,no,ymin,xmin,yo,l
      do 47 i=1,m-1
      do 47 j=1,n
47    tn(i,j)=(h(i,j)+h(i+1,j))*.5
      do 48 i=1,m-1
      do 48 j=1,n-1
48    xh(i,j)=(h(i,j)+h(i,j+1))*.5
      do 52 i=1,m-1
52    write(17,*)(xh(i,j),j=1,n-1)
      close(unit=17)

c output to regular output file

      write(15,*)' '
      write(15,*)' iter: ',iter,'  delh= ',delh
      write(15,*)' '
      write(15,*)' hydraulic heads: numerical'
      do 50 i=2,m-1,np
      write(15,*)' '
50    write(15,*)(h(i,j),j=1,n,np)
c     call anlyt(2,h,l,yo,iter,delh)

c  ****************************************

99    continue
      close(unit=15)
      stop
      end


c  ************************************
c  ** Numerical calculations ************
```



```
      subroutine solveh(h,k,ky,delh)
      common/aa/m,n,delx,dely,acon,bcon,np,alf
      real k(105,205),ky(105,205)
      dimension h(105,205)
      double precision h,kkk,dx2,dy2,delh,xh,kip,kim,kjp,kjm,a

      delh=0.0
      dx2=delx*delx
      dy2=dely*dely
      do 200 i=2,m-1
      do 200 j=2,n-1
      xkx=k(i,j)
      xky=ky(i,j)
      kip=dble(2.*xky*ky(i+1,j)/((xky+ky(i+1,j))*dy2))
      kim=dble(2.*xky*ky(i-1,j)/((xky+ky(i-1,j))*dy2))
      kjp=dble(2.*xkx*k(i,j+1)/((xkx+k(i,j+1))*dx2))
      kjm=dble(2.*xkx*k(i,j-1)/((xkx+k(i,j-1))*dx2))
      kkk=kip+kim+kjp+kjm

      xh=h(i,j)
      a=kip*h(i+1,j)+kim*h(i-1,j)+kjp*h(i,j+1)+kjm*h(i,j-1)
      h(i,j)=a/kkk
      delh=dabs(xh-h(i,j))+delh

200   continue

      return
      end

c  **** head boundary conditions *********************

      subroutine boundh(nc,h,l,k,ky)
      common/aa/m,n,delx,dely,hl,hr,np,alf
      real pi,hl,hr,lh(205),rh(205),th(205)
      real k(105,205),ky(105,205)
      double precision h(105,205)
      real bh(205),l

c     set boundary conditions
      open(unit=16,file='boundh.dat')
c na? = 1 for fixed head bc
c     2 for fixed flow bc
c ?h( ) are arrays containing the fixed head or flow values
c nh??  are indexes for use with mixed boundary conditions (I haven't
c tried to  use these)
      read(16,*)na1,nh11,nh21,nf11,nf21
      read(16,*)(lh(i),i=1,m)
      read(16,*)na2,nh12,nh22,nf12,nf22
      read(16,*)(rh(i),i=1,m)
```

```
      read(16,*)na3,nh13,nh23,nf13,nf23
      read(16,*)(th(i),i=1,n)
      read(16,*)na4,nh14,nh24,nf14,nf24
      read(16,*)(bh(i),i=1,n)
      close(unit=16)

c     write(6,*)na1,lh(1),lh(m),na2,rh(1),rh(m)
c     write(6,*)na3,th(1),th(n),na4,bh(1),bh(n)
c left hand sid
      if(na1.eq.1)then
      do 50 i=1,m
50    h(i,1)=2.*lh(i)-h(i,2)
      end if
      if(na1.eq.2)then
      do 60 i=1,m
60    h(i,1)=h(i,2)+delx*lh(i)/k(i,1)
      end if
      if(na1.eq.3)then
      do 70 i=nh11,nh21
70    h(i,1)=2.*lh(i)-h(i,2)
      do 72 i=nf11,nf21
72    h(i,1)=h(i,2)+delx*lh(i)/k(i,1)
      end if

c right hand side
      if(na2.eq.1)then
      do 80 i=1,m
80    h(i,n)=2.*rh(i)-h(i,n-1)
      end if
      if(na2.eq.2)then
      do 90 i=1,m
90    h(i,n)=h(i,n-1)-delx*rh(i)/k(i,n)
      end if
      if(na2.eq.3)then
      do 95 i=nh12,nh22
95    h(i,n)=2.*rh(i)-h(i,n-1)
      do 92 i=nf12,nf22
92    h(i,n)=h(i,n-1)-delx*rh(i)/k(i,n)
      end if

c top:
      if(na3.eq.1)then
      do 100 i=1,n
100   h(1,i)=2.*th(i)-h(2,i)
      end if
      if(na3.eq.2)then
      do 110 i=1,n
110   h(1,i)=h(2,i)+th(i)*dely/ky(1,i)
      end if
      if(na3.eq.3)then
```



```
      do 120 i=nh13,nh23
120   h(1,i)=2.*th(i)-h(2,i)
      do 121 i=nf13,nf23
121   h(1,i)=h(2,i)+th(i)*dely/ky(1,i)
      end if

c bottom
      if(na4.eq.1)then
      do 130 i=1,n
130   h(m,i)=2.*bh(i)-h(m-1,i)
      end if
      if(na4.eq.2)then
      do 140 i=1,n
140   h(m,i)=h(m-1,i)-bh(i)*dely/ky(m,i)
      end if
      if(na4.eq.3)then
      do 160 i=nh14,nh24
160   h(m,i)=2.*bh(i)-h(m-1,i)
      do 162 i=nf14,nf24
162   h(m,i)=h(m-1,i)-bh(i)*dely/ky(m,i)
      end if

      return
      end
```

```
c                       g3ta.f
c finite difference, block centered grid, solution to temperature
c equation.  double precision.
c Hydraulic conductivity and thermal conductivity can vary
c Hydr. cond. can be anisotropic
c Upstream weighting optional
c Input files:
c       gflow33.dat, General info input: dimensions, initial conditions
c               The original gflow33.dat file is created by gflowf.f
c               and then altered by g3head.f to contain the correct
c               steady state heads.  Output from g3head is gflow33n.dat.
c               mv gflow33n.dat gflow33.dat and then run g3temp.
c       boundh.dat, Head boundary data (just for output)
c       boundt.dat, Temperature boundary data (created by gflowf.f)
c       tk.dat: contains thermal conductivity matrix
c Output files
c       gflow33n.dat: updated gflow33.dat.  To continue iteration of
c               temperature solution mv gflow33n.dat gflow33.dat
c               and run g3temp.f again
c       g3temp.out:  Commented output: this is what you look at
c       contt.out: Data file containing system dimensions and
c               temperatures.  This can by contoured by contour.f
c       qs.dat: Data file containing surface temperature gradients
c               These can be plotted using david.f

        real k(105,105),l,pi,ky(105,105)
        dimension t(105,105),h(105,105),vx(105,105),vy(105,105)
        dimension gsn(105),xx(105),yy(105),tc(105,105),te(105,105)
        dimension tk(105,105)
        common/aa/m,n,delx,dely,np
        common/bb/tk
        double precision delt,h,t,delh,ts,vx,vy,gsn
        character *10 filnx,filny,tkf

        open(unit=21,file='gfa.dat')
        open(unit=15,file='g3ta.out')

c input: m: # of rows, n: # of cols,(excluding mirror points)
c yo: height of true system (m)  l: width, (excluding mirror points)
c niter1r:  max number of iterations per run of g3head.f,
c conv: convergence criteria (<.1)
c niter2r: max number of iterations per run of g3temp.f
c conv2: convergence criteria (<.01)
c to: temp at surface (C), gamm: background temp gradient (C/km), tcond: thermal
c conductivity (W/mC)
c acon,bcon: head parameters used in analytical solutions
c iter1: number of head iterations already performed
c delh: convergence of heads achieved (must be small)
c h(m,n): hydraulic head distribution (m) mxn matrix
c k(m,n): hydraulic conductivity matrix (m/s)
```



```
c t(m,n): initial temperatures (C)
c iter2: number of temperature iterations performed
        read(21,*)md,nd,yo,l,niter1r,conv,niter2r,conv2
        read(21,*)to,gamm,tcond,np,acon,bcon,iter1,delh
        read(21,*)tkf
        read(21,*)nakx,naky
c       write(6,*)md,nd,yo,l,niter1r,conv,niter2r,conv2
        m=md+2
        n=nd+2

        if(nakx.eq.1)then
        read(21,*)xkx
        do 105 i=1,m
        do 105 j=1,n
105     k(i,j)=xkx
        else
        read(21,*)filnx
        open(unit=22,file=filnx)
        do 106 i=1,m
106     read(22,*)(k(i,j),j=1,n)
        close(unit=22)
        end if
        if(naky.eq.1)then
        read(21,*)xky
        do 107 i=1,m
        do 107 j=1,n
107     ky(i,j)=xky
        else
        read(21,*)filny
        open(unit=22,file=filny)
        do 108 i=1,m
108     read(22,*)(ky(i,j),j=1,n)
        end if
        do 15 i=1,m
15      read(21,*)(h(i,j),j=1,n)
        do 17 i=1,m
17      read(21,*)(t(i,j),j=1,n)
        read(21,*)iter2
        close(unit=21)

        open(unit=21,file='weight')
c bet is upstream weighting factor,  0 < bet < .5, 0 is no upstream
c weighting,  .5 is fully upstream weighting.  Upstream weighting
c will improve convergence of solution when convection is dominant.
        read(21,*)bet
        close(unit=21)

c Thermal conductivity data
        open(unit=21,file=tkf)
        do 200 i=1,m
```

```
200     read(21,*)(tk(i,j),j=1,n)
        close(unit=21)

c allow temp iteration to progress for niter2r more beyond the
c previous iter2
        niter2=iter2+niter2r

c  *****************************************

        gam=gamm/1000.
        delx=l/nd
        dely=yo/md
        pi=3.14159
c  *****************************************

c Output to regular output file
        ts=(t(1,1)+t(2,2))/2.
        write(15,*)' output g3ta.out'
        write(15,*)' '
        write(15,*)' upstream weighting,  bet= ',bet
        write(15,*)' (0<bet<.5,  0 mean no weighting)'
        write(15,*)' '
        write(15,*)' surface temp: ',ts
        write(15,*)' '
        write(15,*)' temperature gradient (C/km) ',gamm
        write(15,*)' '
        write(15,*)' thermal conductivity (W/C*m**2): ',tcond
        rc=4185000.0
        alf=tcond/rc
        write(15,*)' thermal diffusivity (m**2/s): ',alf
        write(15,*)' '

c  *****************************************

        write(15,*)' '
        write(15,*)' horiz x: ',1,' m ;  dx= ',delx,' m; n= ',n
        write(15,*)' '
        write(15,*)' vert  y: ',yo,' m ;  dy= ',dely,' m; m= ',m
        write(15,*)' '
        write(15,*)' acon,bcon  (m) ',acon,bcon
        write(15,*)' '
        do 887 j=2,n-1
887     xx(j)=(j-2)*delx+.5*delx
        do 888 i=2,m-1
888     yy(i)=(i-2)*dely+.5*dely
        write(15,*)' hydraulic conductivity: '
        write(15,*)' '
        write(15,*)' kx  '
        write(15,*)' '
        write(15,919)(xx(i),i=2,n-1,np)
```



```
919     format(7(f10.1,x))
        do 14 i=2,m-1,np
        write(15,*)' '
14      write(15,9)(k(i,j),j=2,n-1,np)
        write(15,*)' '
        write(15,*)' ky'
        do 18 i=2,m-1,np
        write(15,*)' '
18      write(15,9)(ky(i,j),j=2,n-1,np)
9       format(7(e10.3,x))
        write(15,*)' '
        write(15,*)
        write(15,*)' thermal conductivity'
        do 899 i=2,m-1,np
899     write(15,*)(tk(i,j),j=2,n-1,np)

        write(15,*)' '
        write(15,*)' Solution for Heads: iter: ',iter1,'  delh= ',delh
        write(15,*)' '
        write(15,*)' hydraulic heads: numerical'
        xe=0.
        write(15,908)xe,(xx(j),j=2,n-1,np)
        do 44 i=2,m-1,np
        write(15,*)' '
44      write(15,908)yy(i),(h(i,j),j=2,n-1,np)

c  *****************************************
c  *****************************************

c output to restart file, gflow33n.dat.   to use restart file
c it must be renamed 'gflow33.dat':  input file
        open(unit=22,file='gfn.dat')
        write(22,*)md,nd,yo,l,niter1r,conv,niter2r,conv2
        write(22,*)to,gamm,tcond,np,acon,bcon,iter1,delh
        write(22,*)tkf
        write(22,*)nakx,naky
        if(nakx.eq.1)then
        write(22,*)xkx
        else
        write(22,*)filnx
        end if
        if(naky.eq.1)then
        write(2,*)xky
        else
        write(22,*)filny
        end if

        do 42 i=1,m
42      write(22,*)(h(i,j),j=1,n)
```

```
c  ****************************************

c use darcy's law to find velocities given the heads and hydraulic
c conductivities
        call vell(h,k,ky,vx,vy)
c boundary conditions for temperature
        call boundt(1,t,ts)

c  ****************************************
c Start iterating temperature solution where restart (if any) left off

        iter=iter2
        call gradn(t,gsn)
60      continue
        iter=iter+1
c solve for temperatures numerically
        call solvet2(iter,t,vx,vy,delt,bet)
c set boundary conditions
        call boundt(2,t,ts)

c  ****************************************

        mm=mod(iter,10)
        if(mm.eq.0)then
c numerical surface grad
        call gradn(t,gsn)


        write(15,*)' '
        write(15,*)' surface grad, numerical'
        write(15,908)(gsn(i),i=2,n-1,np)
        end if

c  ****************************************

c       write(6,*)delt,conv2,iter,niter2
c Check convergence: if we have not converged and have not yet
c  exceded maximum allowed iteration, iterate again, goto 60
        if(delt.gt.conv2.and.iter.lt.niter2)goto 60
c Otherwise, write out present results and stop
        write(15,*)' '
        write(15,*)' '
        write(15,*)' ********************************************'
        write(15,*)' Iteration: ',iter,'  Convergence factor:',delt
        write(15,*)' '

889     continue

        xiter=float(iter)
        write(15,*)' Temps: numerical solution '
```



```
        write(15,908)xiter,(xx(j),j=2,n-1,np)
        do 909 i=2,m
        write(15,*)' '
909     write(15,908)yy(i),(t(i,j),j=2,n-1,np)
        write(15,*)' '

c put surface temp grad and heat flow into an output file for plotting
c by david.f and into regular output file
        open(unit=17,file='qs.dat')
c       write(17,*)n-2
        write(15,*)' surface grad, degC/km'
        do 913 i=2,n-1
913     write(17,*)xx(i),gsn(i)
        write(17,*)' '
        write(15,*)'      x       grad        x         grad        x
     c    grad'
        do 912 i=2,n-1,3
912     write(15,902)xx(i),gsn(i),xx(i+1),gsn(i+1),xx(i+2),gsn(i+2)
        do 914 i=2,n-1
        gsn(i)=gsn(i)*tk(1,i)
914     write(17,*)xx(i),gsn(i)
        write(17,*)' '
        close(unit=17)
        write(15,*)' '
        write(15,*)' '
        write(15,*)' surface heat flow, mW/m**2'
        write(15,*)'      x        HF         x          HF          x
     c     HF '
        do 915 i=2,n-1,3
915     write(15,902)xx(i),gsn(i),xx(i+1),gsn(i+1),xx(i+2),gsn(i+2)
902     format(3(2x,f9.2,x,f9.2))
908     format(7(f10.3,x))
        close(unit=15)

        call gradn(t,gsn)

c adjust temperature matrix for contour output, and output to
c data file set up to use in 'contour.f'
        open(unit=17,file='contt.out')
        xmin=0.
        ymin=0.
        mo=m-1
        no=n-1
        write(17,*)mo,no,ymin,xmin,yo,l
        do 82 i=1,m-1
        do 82 j=1,n
82      tc(i,j)=(t(i,j)+t(i+1,j))*.5
        do 83 i=1,m-1
        do 83 j=1,n-1
83      te(i,j)=(tc(i,j)+tc(i,j+1))*.5
```

```
      do 85 i=1,m-1
85    write(17,*)(te(i,j),j=1,n-1)
      close(unit=17)

c last parameters for restart file
      do 86 i=1,m
86    write(22,*)(t(i,j),j=1,n)
      write(22,*)iter
      close(unit=22)

99    continue
      stop
      end


c  ****************************************
c Numerical calculation of temperature values

      subroutine solvet2(iter,t,vx,vy,delt,bet)
      dimension tk(105,105)
      dimension t(105,105),vx(105,105),vy(105,105)
      common/aa/m,n,delx,dely,nh
      common/bb/tk
      double precision t,delt,tcon,tht,th,th11,th12,th2,th3
      double precision tconi,dx,dy,vx,vy,vim,vip,vjm,vjp
c density of water 1000 kg m-3
c specific heat of water 4185
      rc=4185000.0
      delx2=delx*delx
      dely2=dely*dely
      dx=dble(delx)
      dy=dble(dely)

c eps is an small adjustment to avoid zero velocities
            eps=.1e-15
            delt=0.0
            do 700 i=2,m-1
            do 700 j=2,n-1
            th=t(i,j)

            vim=vy(i-1,j)
            vip=vy(i,j)
            vjm=vx(i,j-1)
            vjp=vx(i,j)

            vyo=vip+eps
            sy=vyo/abs(vyo)
            b=.5+sy*bet
            xb=1.-b
```



```
            vxo=vjp+eps
            sx=vxo/abs(vxo)
            c=.5+sx*bet
            xc=1.-c
            aim=2.*tk(i,j)*tk(i-1,j)/((tk(i,j)+tk(i-1,j))*rc)
            aip=2.*tk(i,j)*tk(i+1,j)/((tk(i,j)+tk(i+1,j))*rc)
            ajm=2.*tk(i,j)*tk(i,j-1)/((tk(i,j)+tk(i,j-1))*rc)
            ajp=2.*tk(i,j)*tk(i,j+1)/((tk(i,j)+tk(i,j+1))*rc)

            tconi=(ajm+ajp)/delx2+(aim+aip)/dely2
            tcon=tconi+(vjp*c-vjm*xc)/dx+(vip*b-vim*xb)/dy
c           th1=ajm*t(i,j-1)+ajp*t(i,j+1)+aim*t(i-1,j)+aip*t(i+1,j)
            th11=(ajm*t(i,j-1)+ajp*t(i,j+1))/delx2
            th12=(aim*t(i-1,j)+aip*t(i+1,j))/dely2
            th2=(-vjp*xc*t(i,j+1)+vjm*c*t(i,j-1))/dx
            th3=(-vip*xb*t(i+1,j)+vim*b*t(i-1,j))/dy
            tht=th11+th12+th2+th3
            t(i,j)=tht/tcon
            delt=dabs(th-t(i,j))+delt
700         continue
      mn=mod(iter,10)
      if(mn.eq.0)then
      write(6,*)' iter = ',iter,'   delt = ',delt
      write(15,*)' ********************************'
      write(15,*)' ********************************'
      write(15,*)' iter = ',iter,'   delt = ',delt
      write(15,*)' last line of t'
      write(15,908)(t(m-1,j),j=2,n-1,np)
908   format(7(f10.3,x))
      end if
      return
      end

c  ****************************************
c  numerical calculation of groundwater velocities using Darcy's law

      subroutine vell(h,k,ky,vx,vy)
      dimension h(105,105),vx(105,105),vy(105,105)
      common/aa/m,n,delx,dely,np
      real k(105,105),ky(105,105)
      double precision h,vx,vy,kkk,vr,vl,vu,vb,vt
c calculate velocities
c units: m
c     write(6,*)m,n,delx,dely,alf,k(1,1)
      do 50 i=1,m
      do 50 j=1,n
      vx(i,j)=0.0
50    vy(i,j)=0.0
```

D14

```
      do 51 i=1,m-1
      do 51 j=1,n-1
      kkk=dble(2.*k(i,j)*k(i,j+1)/(k(i,j)+k(i,j+1)))
51    vx(i,j)=-kkk*(h(i,j+1)-h(i,j))/delx

      do 52 i=1,m-1
      do 52 j=1,n-1
       kkk=dble(2.*ky(i,j)*ky(i+1,j)/(ky(i,j)+ky(i+1,j)))
52    vy(i,j)=-kkk*(h(i+1,j)-h(i,j))/dely


      write(15,*)' '
      write(15,*)' vx '
      do 55 i=1,m-1,np
      write(15,*)' '
55    write(15,9)(vx(i,j),j=1,n-1,np)
      write(15,*)' '
      write(15,*)' vy '
      write(15,*)' '
9     format(7(e10.3,x))
      do 56 i=1,m-1,np
56    write(15,9)(vy(i,j),j=1,n-1,np)
c mass conservation check
      vr=0.0
      vl=0.0
      vt=0.0
      vb=0.0
      do 58 i=2,m-1
      vl=vl+vx(i,1)*dely
58    vr=vr+vx(i,n-1)*dely
      do 59 j=2,n-1
      vu=vu+vy(1,j)*delx
59    vb=vb+vy(m-1,j)*delx
      vt=vr-vl-vu+vb
      write(15,*)' '
      write(15,*)' mass conservation '
      write(15,*)' fluxes:  left side: ',vl
      write(15,*)'         right side: ',vr
      write(15,*)'           top side: ',vu
      write(15,*)'        bottom side: ',vb
      write(15,*)' sum: (pos: source) : ',vt
      write(15,*)' '
      return
      end

c  ******************************************
c  ** Numerical calculations of temp gradient

      subroutine gradn(t,gsn)
      dimension t(105,105),gsn(105)
```



```
      common/aa/m,n,delx,dely,np
      double precision t,gsn

      do 80 j=1,n
      dt=sngl(t(2,j)-t(1,j))
80    gsn(j)=dt*1000./dely
c     write(15,*)' '
c     write(15,*)' surface grads (C/km) numerical'
c     write(15,*)(gsn(j),j=2,n-1,np)
      return
      end


c  **** temp B C calculation subroutines *********************

      subroutine boundt(nc,t,ts)
      dimension tk(105,105)
      common/aa/m,n,delx,dely,np
      common/bb/tk
      real pi,lh(105),rh(105),th(105)
      double precision t(105,105)
      real bh(105)

      if(nc.eq.1)then
      open(unit=16,file='boundh.dat')
      read(16,*)na1,nh11,nh21,nf11,nf21
      read(16,*)(lh(i),i=1,m)
      read(16,*)na2,nh12,nh22,nf12,nf22
      read(16,*)(rh(i),i=1,m)
      read(16,*)na3,nh13,nh23,nf13,nf23
      read(16,*)(th(i),i=1,n)
      read(16,*)na4,nh14,nh24,nf14,nf24
      read(16,*)(bh(i),i=1,n)
      close(unit=16)
      write(15,*)' '
      write(15,*)' head boundary conditions '
      write(15,*)'a,b,c,d,e: a=1 for fixed h, 2 for fixed grad'
      write(15,*)' b-e are indices for mixed b.c. s'
      write(15,*)' vector = values for h or grad along boundary'
      write(15,*)'  '
      write(15,*)' left hand side'
      write(15,*)na1,nh11,nh21,nf11,nf21
      write(15,*)(lh(i),i=1,m)
      write(15,*)' right hand side'
      write(15,*)na2,nh12,nh22,nf12,nf22
      write(15,*)(rh(i),i=1,m)
      write(15,*)' top '
      write(15,*)na3,nh13,nh23,nf13,nf23
      write(15,*)(th(i),i=1,n)
      write(15,*)' bottom'
```

```
      write(15,*)na4,nh14,nh24,nf14,nf24
      write(15,*)(bh(i),i=1,n)
      end if
c     set boundary conditions
      open(unit=16,file='boundt.dat')
      read(16,*)na1,nh11,nh21,nf11,nf21
      read(16,*)(lh(i),i=1,m)
      read(16,*)na2,nh12,nh22,nf12,nf22
      read(16,*)(rh(i),i=1,m)
      read(16,*)na3,nh13,nh23,nf13,nf23
      read(16,*)(th(i),i=1,n)
      read(16,*)na4,nh14,nh24,nf14,nf24
      read(16,*)(bh(i),i=1,n)
      close(unit=16)

      if(nc.eq.1)then

      write(15,*)' '
      write(15,*)' temperature boundary conditions '
      write(15,*)'a,b,c,d,e: a=1 for fixed t, 2 for fixed grad'
      write(15,*)' b-e are indices for mixed b cs'
      write(15,*)' vector = values for t or HF along boundary'
      write(15,*)'  '
      write(15,*)' left hand side'
      write(15,*)na1,nh11,nh21,nf11,nf21
      write(15,*)(lh(i),i=1,m)
      write(15,*)' right hand side'
      write(15,*)na2,nh12,nh22,nf12,nf22
      write(15,*)(rh(i),i=1,m)
      write(15,*)' top '
      write(15,*)na3,nh13,nh23,nf13,nf23
      write(15,*)(th(i),i=1,n)
      write(15,*)' bottom'
      write(15,*)na4,nh14,nh24,nf14,nf24
      write(15,*)(bh(i),i=1,n)
      end if
c left hand side
      if(na1.eq.1)then
      do 50 i=1,m
50    t(i,1)=2.*lh(i)-t(i,2)
      end if
      if(na1.eq.2)then
      do 60 i=1,m
60    t(i,1)=t(i,2)-delx*lh(i)/tk(i,2)
      end if
      if(na1.eq.3)then
      do 70 i=nh11,nh21
70    t(i,1)=2.*lh(i)-t(i,2)
      do 72 i=nf11,nf21
72    t(i,1)=t(i,2)-delx*lh(i)/tk(i,2)
```



```
      end if

c right hand side
      if(na2.eq.1)then
      do 80 i=1,m
80    t(i,n)=2.*rh(i)-t(i,n-1)
      end if
      if(na2.eq.2)then
      do 90 i=1,m
90    t(i,n)=t(i,n-1)+delx*rh(i)/tk(i,n-1)
      end if
      if(na2.eq.3)then
      do 95 i=nh12,nh22
95    t(i,n)=2.*rh(i)-t(i,n-1)
      do 92 i=nf12,nf22
92    t(i,n)=t(i,n-1)+delx*rh(i)/tk(i,n-1)
      end if

c top: constant head
      if(na3.eq.1)then
      do 100 i=1,n
100   t(1,i)=2.*th(i)-t(2,i)
      end if
      if(na3.eq.2)then
      do 110 i=1,n
110   t(1,i)=t(2,i)-th(i)*dely/tk(2,i)
      end if
      if(na3.eq.3)then
      do 120 i=nh13,nh23
120   t(1,i)=2.*th(i)-t(2,i)
      do 121 i=nf13,nf23
121   t(1,i)=t(2,i)-th(i)*dely/tk(2,i)
      end if

c bottom
      if(na4.eq.1)then
      do 130 i=1,n
130   t(m,i)=2.*bh(i)-t(m-1,i)
      end if
      if(na4.eq.2)then
      do 140 i=1,n
140   t(m,i)=t(m-1,i)+bh(i)*dely/tk(m-1,i)
c     write(*,*)(tk(m-1,i),i=1,n)
      end if
      if(na4.eq.3)then
      do 160 i=nh14,nh24
160   t(m,i)=2.*bh(i)-t(m-1,i)
      do 162 i=nf14,nf24
162   t(m,i)=t(m-1,i)+bh(i)*dely/tk(m-1,i)
      end if


      return
      end
```

APPENDIX E

Model System

The system modeled is shown in Figure 14, in the test, and Figure E1. The model is a simplified, generalized, cross section of La Jencia Basin and the Socorro mountain block, extending into the Socorro Basin. The cross-section is taken approximately perpendicular to water table elevation contours (see Figure 7 in text) and therefore should roughly parallel the major ground-water flow direction (except in the Socorro Basin in which ground water flows southward, roughly perpendicular to the cross section). Temperatures and heads produced by the model for the "Socorro Basin" (to the right of unit B) should be disregarded. The system has been extended into Socorro Basin solely to avoid placing potentially restrictive head, temperature, or flux boundary conditions at the eastern frontal fault zone of the Socorro mountain block, an important but highly uncertain boundary. Setting boundary conditions a few kilometers away from the frontal fault, out in the basin where we assume that temperatures are largely controlled by the Rio Grande flow system, places fewer unnecessary constraints on the Socorro hydrogeothermal system.

Boundary conditions

The boundary conditions for the system are somewhat complex, partly because we are not modeling a complete, closed hydrologic system (Fig E1). Boundary conditions for closed systems are often "no flow" of water and "no flow" of heat. In this study, water (and probably heat as well) enters the system through the western boundary in central La Jencia Basin. Most recharge in the Socorro area occurs further west in and near the Magdalena Mountains. Water

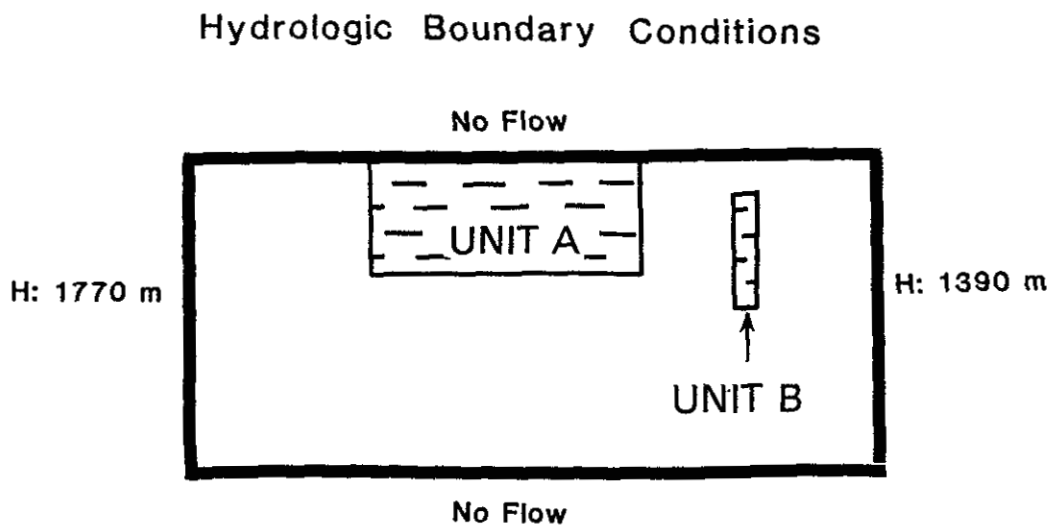

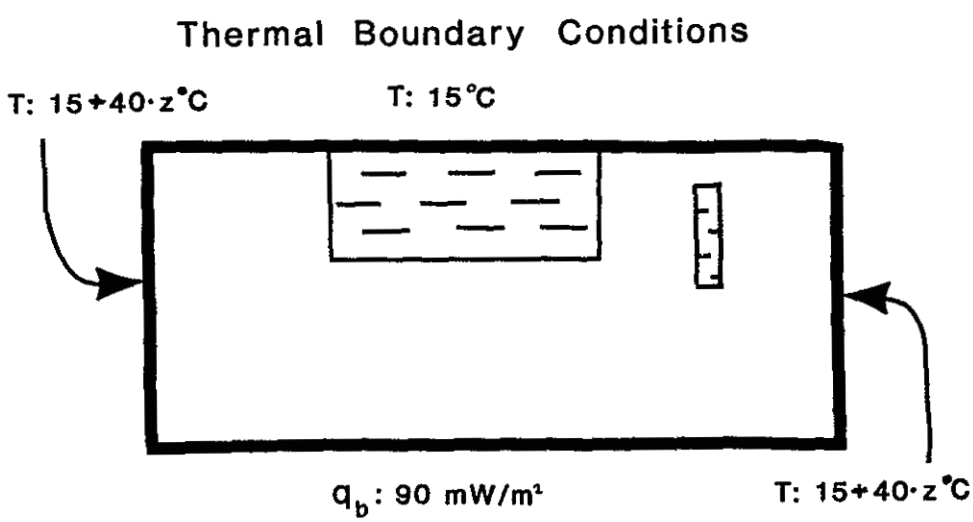

Fig. E1. Boundary conditions for head and temperature used in the majority of the models presented in this study.

leaves the system through the eastern boundary into the Socorro Basin (and in reality, leaves the system in the third dimension, flowing southward, once it reaches the Rio Grande ground-water flow system in Socorro Basin).

Head boundary conditions

Fixed head boundary conditions are applied to the right and left-hand boundaries of the system; the heads are constant with depth and equal to the water table elevation. This may not be entirely accurate, heads in La Jencia Basin near the western recharge zone probably decrease with depth, but sensitivity analysis shows that the model is not greatly influenced by these boundary conditions. No-flow boundary conditions are assumed on the top and bottom ($dh/dz = 0$), equivalent to an impermeable bottom boundary and a top surface with no hydrologic recharge. (When a reasonable--i.e. small-- amount of surface recharge is incorporated, surface heat flows are slightly reduced throughout the model, but the trends in the surface heat flows and subsurface temperatures are unchanged).

Temperature boundary conditions

Temperatures at the upper boundary of the system are fixed at $15^{o}\,C$. Any variation of temperature with elevation is neglected. The lower boundary condition is constant basal heat flow. Generally, 90 $mW\,m^{-2}$ was employed as the basal heat flow, a reasonable value for the Rio Grande rift (Reiter et al., 1986). Sensitivity analysis indicates that the surface heat-flow profile is relatively insensitive to the basal heat flow, indicating that any extra basal heat input into the system is swept out of the system by advection in the subsurface.

When modeling temperatures, we do not wish to restrict heat from entering and leaving the system through the left and right-hand boundaries. In order to

allow this, these boundary are given fixed temperatures which vary linearly with depth. Temperatures along the eastern and western boundaries increase with depth at a gradient of 40 $^{o}C/km$, equivalent to a vertical heat flow of 60 $mW\,m^{-2}$ (given the system thermal conductivity of 1.5 $W\,(m^{o}K)^{-1}$). This is a reasonable heat flow for the locations in the Socorro area to which the boundaries correspond: west-central La Jencia Basin, and central Socorro Basin. Note that this heat flow (60 $mW\,m^{-2}$) is lower than the basal heat-flow boundary condition of the model. This is because the heat flows observed in west-central La Jencia Basin and central Socorro Basin are lower than typical Rio Grande rift heat flows (75 $-100\ mW\,m^{-2}$, Reiter et al, 1986). Heat flow in these areas is probably perturbed by ground-water flow elements not modeled in the present system such as recharge at and near the Magdalena Mountains and ground-water flow associated with the Rio Grande. These boundary conditions have little influence on model results, and the difference between the vertical heat flow on the sides and input at the base (30 $mW\,m^{-2}$) is much smaller than the variation in heat flow we are attempting to model.

Thermal conductivity (k_{Θ})

Thermal conductivities in the model are chosen to be consistent with values measured in the study area. All Tertiary material in the Socorro area appears to have fairly similar k_{Θ}, within the range of about 1.4 $-2.0\ W\,(m^{o}K)^{-1}$. Simplifying, we chose a value of 1.5 $W\,(m^{o}K)^{-1}$ to represent all Tertiary material, including volcanic rocks, sedimentary rocks and unconsolidated sediments. Reiter and Smith (1977) measured the k_{Θ} of Precambrian rock at Wood's Tunnel to be 3.07 $\pm .28\ W\,(m^{o}K)^{-1}$. In this study we use a value of 3.0 $W\,(m^{o}K)^{-1}$ for all Precambrian rock.

Hydraulic conductivity (k_H)

The only hydraulic conductivity information available for the Socorro area is from pump tests in Socorro Basin alluvial fill, for which Hantush (1961) obtained values between $1.0 - 2.0 \times 10^{-4}$ $m\ s^{-1}$. No k_H data exist for the alluvium, fanglomerates or claystones of La Jencia Basin, or for the Tertiary volcanic rocks or for Precambrian rocks of the Socorro area. Hawkins and Stephens (1980) provide an extensive list of k_H data for materials similar to those found in the Socorro area, from numerous other studies; there are a very wide range of values for each type of material.

Because so little hydrologic and subsurface structural information are available from the Socorro area, we were forced develop a greatly simplified hydrogeologic model of the hydrologic system. For the purposes of our model, the system is divided into two types of material. Relatively permeable aquifer materials form one group. This group includes fanglomerates, gravels, sands and muds of the upper Popatosa Formation fanglomerate facies, the Sierra Ladrones Formation and Quaternary alluvium. Also included among the relatively permeable materials are the fractured, well-indurated sediments and volcanics of the lower Popatosa Formation, cauldron-related volcanic units and any other volcanics rocks, and (possibly) fractured Precambrian rocks. The second type of hydrogeologic material consists of less permeable clays and claystones, which are considered to act as an aquitard unit in the Socorro area. The larger part of this aquitard is comprised of the upper Popatosa claystone facies; however, there are some more recently deposited clays in central La Jencia Basin (Anderholm, 1987).

We obtained k_H values for clay from Freeze and Cherry (1979, Table 2.2) and Morris and Johnson (1967). These sources give a value of $\approx 10^{-9}$ $m\ s^{-1}$ as

an upper limit for the hydraulic conductivity of clays. Numerical modeling sensitivity analysis shows that the choice of k_H for the aquitard has no influence on the model results, as long as the aquitard k_H is less than 0.01 times the k_H of the aquifer.

The k_H of the aquifer materials could easily range from $10^{-4}\ m\ s^{-1}$ (the value obtained by Hantush (1961) for Socorro Basin) to $10^{-8} m\ s^{-1}$ (the low end of the range of k_H for fractured igneous rocks, from Freeze and Cherry, 1979, Table 2.2). In choosing a single value, k_{HA}, for the aquifer materials in our model, we considered the fact that the net hydraulic conductivity of a system of units in series is controlled by the units of the lowest k_H. The system we hypothesize (Figure E1) involves a sedimentary aquifer in series with a volcanic aquifer (flow in the aquitard in negligible), so the net k_{HA} of the combined aquifer is controlled by the k_H of the volcanic rocks. Numerical modeling shows that the choice of k_{HA} is very important to the model results (as shown in Figure 17 of the text). In most models we used a value of $2.0 \times 10^{-7}\ m\ s^{-1}$ for k_{HA}, because this value usually produced a net hydraulic flux through the system comparable with that expected from recharge estimates (see text).

Model output

The model generates hydraulic heads and temperatures at each nodal point in the model. These nodal points are not on the boundary of the system, because boundaries are halfway between nodal points (see Figure D1). Head and temperature fields are contoured after readjusting the field so that heads and temperatures are defined at the system boundaries.

The model-generated surface heat flows that are plotted in Figures 15 and 17 - 24 are the heat flows at the upper surface of the model. These heat flows

are calculated using the difference between temperatures at nodes just below the top surface and just above the top surface of the model system. The top surface of the model system corresponds to the water table, so the heat flow at the top surface corresponds to the heat flow at or above the water table. We suggest that it is reasonable, in most cases, to compare these model-generated surface heat flows to the heat flows observed in the Socorro area. In most areas (in the model and in the Socorro area) heat flows do not vary substantially with depth, and therefore the exact depth in the model at which the heat flow is calculated is unimportant. Model generated heat flows vary most with depth in the hydrologic window. Corresponding data from the hydrologic window of the Socorro area are from wells that are almost entirely above the water table, therefore it is appropriate to model these heat flow with heat flows from the water table of the model system.

Additional Models

Results from additional model variations (illustrated in Figure E2) are shown in Tables E1 and E2. These tables are similar to Table 2 in the text. Brief descriptions of the distinguishing features of each model are given in the first column, followed by the net hydrologic flow through each model, and then the minimum and maximum heat flow produced in each model simulation.

The variation of the base model tabulated here include the addition of recharge to the model system, variation of the hydraulic head boundary condition, variation of hydraulic conductivity within the aquifer, variation of the aquitard thickness, variation of the total thickness of the system, and variation in the basement topography and aquifer geometry. The majority of these models produce surface heat-flow profiles that are very similar to the surface heat flow

profile produced by the base model. The most notable exception is case Beta in which unit B is extended downward to the base of the model, cutting off most of the fluid flow.

Table E1, Further Comparison of Selected Models

Model	Q_H $m^2\ s^{-1} \times 10^{-5}$	q_{min} $mW\ m^{-2}$	q_{max} $mW\ m^{-2}$
Base Model ($k_{HA} = 2 \times 10^{-7}$)	1.3	14.6	177
Add recharge (a and b)			
($0.25\ in\ yr^{-1} = 2 \times 10^{-10}\ m\ s^{-1}$)	1.3	10.6	≈155
($0.50\ in\ yr^{-1} = 4 \times 10^{-10}\ m\ s^{-1}$)	1.4	7.5	120
($0.50\ in\ yr^{-1} = 4 \times 10^{-10}\ m\ s^{-1}$)			
On left quarter of model	1.4	7.1	156
Head on left boundary			
varies: $\frac{\partial h}{\partial z} = -6.6 \times 10^{-3}$ (c)	1.2	10.5	143
Thinner Unit A			
750 m (d)	1.4	15.9	169
600 m (e)	1.4	24.2	154
Sediments have higher			
k_H than volcanics (f)			
$\frac{k_{HS}}{k_{HV}} = \frac{1 \times 10^{-6}}{1 \times 10^{-7}}$	0.92	11.8	113
$\frac{k_{HS}}{k_{HV}} = \frac{1 \times 10^{-6}}{2 \times 10^{-7}}$	1.7	10.2	143
Smaller system, Depth: 2km			
Same aquitards as base (g)			
$k_{HA} = 2 \times 10^{-7}\ m\ s^{-1}$	0.68	26	148
$k_{HA} = 5 \times 10^{-7}\ m\ s^{-1}$	1.70	25	198
$k_{HA} = 8 \times 10^{-7}\ m\ s^{-1}$	2.70	26	223
Estimated Q_H from recharge: $0.81 - 1.1 \times 10^{-5}\ m^2\ s^{-1}$			

Table E1. Further Comparison of Selected Models. This table contains abbreviated descriptions and results from a set of additional variations upon the base model. The models are illustrated in Figure E2; the letters in parenthesis refers to the figure labels in E2. Q_H is the net hydraulic flux through the model, q_{min} and q_{max} are the minimum and maximum surface heat flows produced by the model.

Table E2, Further Comparison of Selected Models

Model	Q_H $m^2\ s^{-1} \times 10^{-5}$	q_{min} $mW\ m^{-2}$	q_{max} $mW\ m^{-2}$
Base Model: $k_{HA} = 2 \times 10^{-7}\ m\ s^{-1}$	1.3	14.6	177
Beta: Constrictive unit B $k_{HA} = 1 \times 10^{-7}\ m\ s^{-1}$ (h)	0.0002	60	60
Del: Short system, No Unit B, $k_{HA} = 2 \times 10^{-7}\ m\ s^{-1}$ (i)			
$q_b = 60 mW\ m^{-2}$	1.1	18.2	109
$q_b = 75 mW\ m^{-2}$	1.1	18.2	110
$q_b = 90 mW\ m^{-2}$	1.1	18.2	112
Eps: Del with finer grid, $\Delta x = \Delta z = 75\ m$ (i), $q_b = 60\ mW\ m^{-2}$	1.1	18.0	112
Theta: 5 km deep system, No Unit B, $k_{HA} = 2 \times 10^{-7}\ m\ s^{-1}$ (j)	2.0	17.1	106
Kap: 7 km deep system, basement topography, No Unit B, $k_{HA} = 2 \times 10^{-7}\ m\ s^{-1}$ (k)	2.1	19.8	173
Lam: Kap with Unit B, $k_{HA} = 1 \times 10^{-7}\ m\ s^{-1}$ (l)	1.1	23.8	246
Mu: 5 km deep system, basement topography, Unit B, $k_{HA} = 2 \times 10^{-7}\ m\ s^{-1}$ (m)	2.1	28.3	141
Estimated Q_H from recharge: $0.81 - 1.1 \times 10^{-5}\ m^2\ s^{-1}$			

Table E2. Further Comparison of Selected Models. This table contains abbreviated descriptions and results from a set of additional variations upon the base model. The models are illustrated in Figure E2; the letters in parenthesis refers to the figure labels in E2. Q_H is the net hydraulic flux through the model, q_{min} and q_{max} are the minimum and maximum surface heat flows produced by the model.

Figure E2.

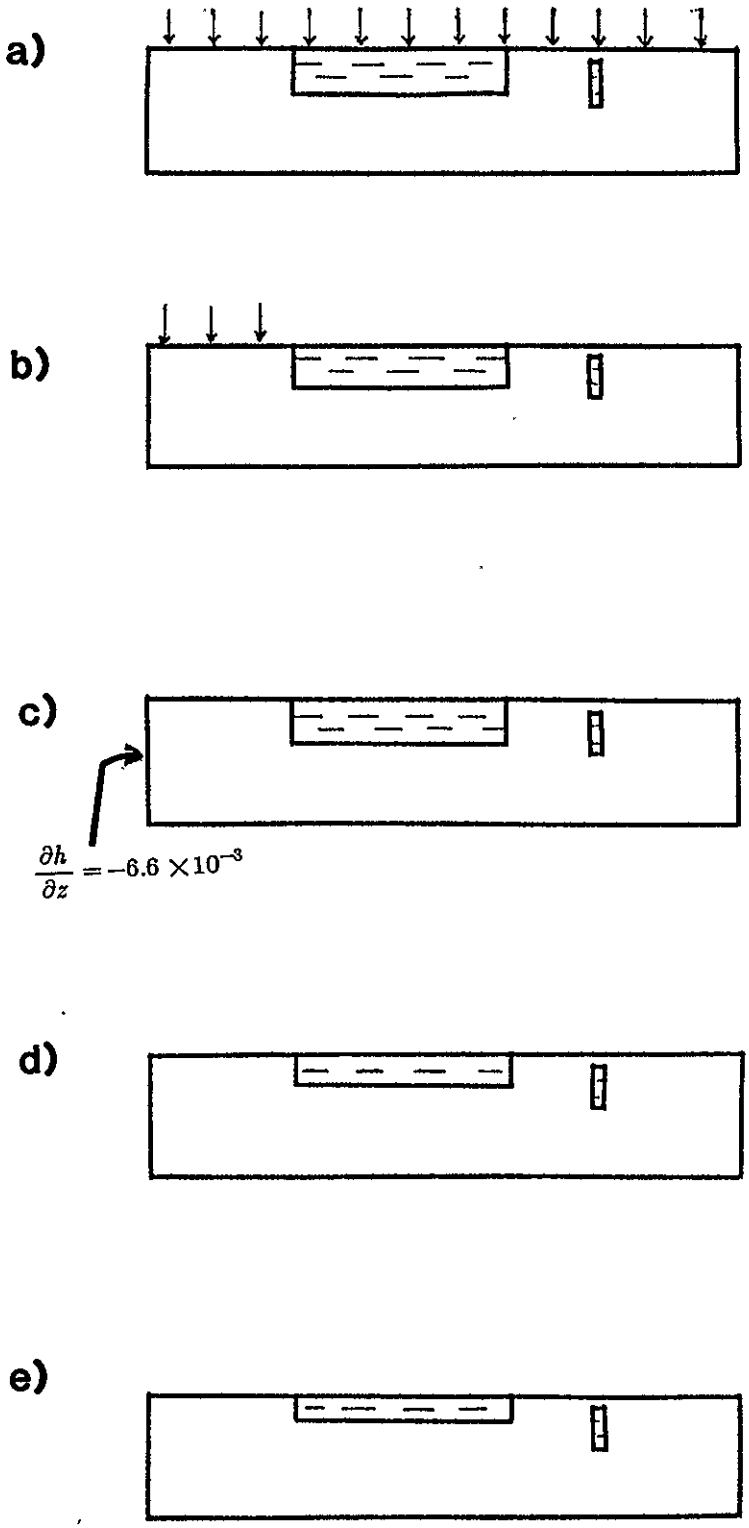

f)

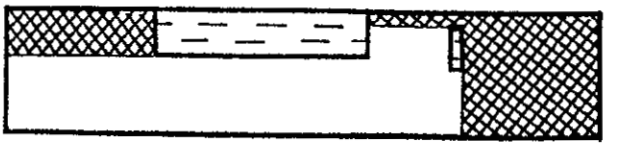

g)

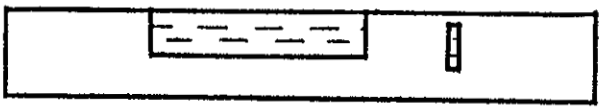

h)

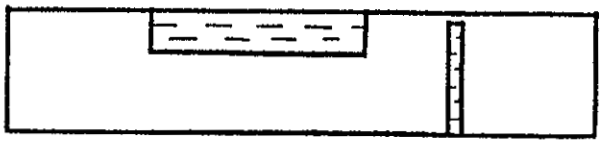

i)

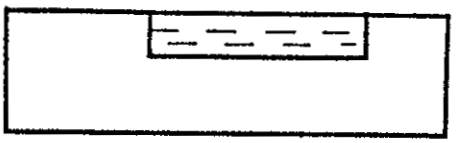

j)

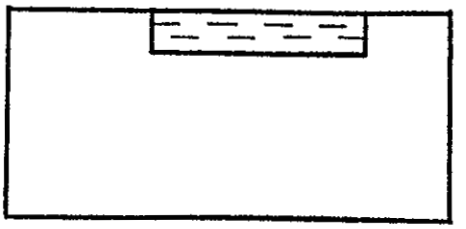

k)

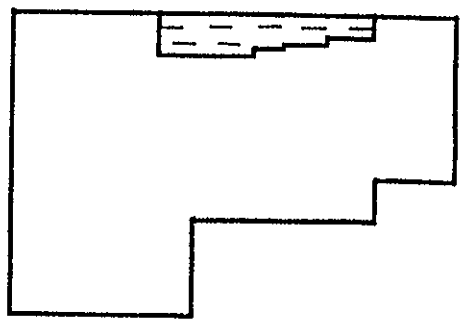

l)

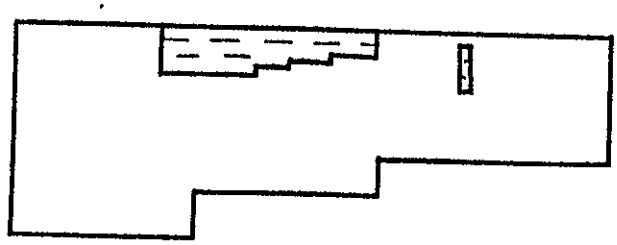

m)

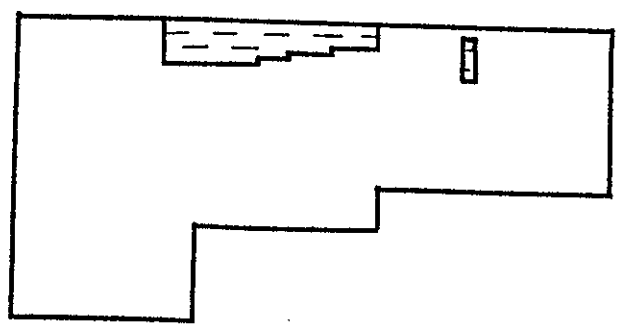

Caption for Figure E2.

These figures illustrate the models tabulated in Table E1 and E2.

a) This model is the same as the base model with the addition of surface recharge all accross the top of the model. (2×10^{-10} m s^{-1} or 4×10^{-10} m s^{-1}).

b) This model is the same as the base model with the addition of surface recharge only accross the top one-quarter of the system.

c) This model is the same as the base model with a change in the hydraulic head boundary condition on the left-hand side. Instead of a constant head (h =1770 m, base model) on the left-hand side, heads vary with depth (h =1770 m -6.6×10^{-3} z).

d) In this model the unit A aquitard is thinner than in the base model. Unit A is 750 m thick instead of 1050 m thick.

e) In this model The unit A aquitard is thinner than in the base model. Unit A is 600 m thick instead of 1050 m thick.

f) In this model, the parts of the aquifer that represent gravels and fanglomerates (hatch-marked areas) are given a high hydraulic conductivity (k_{HS}) than the parts of the aquifer which represent volcanic rocks (plain areas, k_{HV}).(k_{HS}/k_{VS} =10 or 5; k_{HS} =1 $\times 10^{-6}$ m s^{-1}).

g) This system is not as deep than the base model, only extending to a total depth of 2 km (instead of 3 km). Otherwise the geometries of the aquifer and aquitard units are the same. A variety of k_{HA} values were used.

h) Beta. This system similar to the base model except that the unit B aquitard extends to the bottom of the system, and the hydraulic conductivity of the aquifer is somewhat lower (k_{HA} =1 $\times 10^{-7}$ instead of 2 $\times 10^{-7}$). The basal heat flow into this system is 60 mW m^{-2}. Almost no fluid flow occurs in this model, and therefore no fluid induced geothermal anomaly results.

i) Del. This system is not as wide as the base model, and the unit B aquitard is not included. Eps: same as Del, except that the grid spacing is twice as fine. (Del: Δx =Δz =150 m and in Eps: Δx =Δz =75 m).

j) Theta. This system is the same as Del, except deeper. The total depth of Theta is 5 km, while the total depth of Del is 3 km.

k) Kap. Similar to Theta and Del, this is a deep system that does not include unit B, but does include profound basement topography. Total depth is 7 km. The unit A aquitard has variable thickness representing the probably change in the depth of the base of unit A from west to east. The right-hand

step in the basement represents the upfaulting of the hydrologic window block, while the left-hand step represents the possible margin of the Sawmill Canyon caldera.

l) Lam. Similar to Theta and Kap, this system is 5 km deep and includes the unit B aquitard, as well as basement topography and variation in the thickness of unit A.

m) Mu. Similar to Lam and Kap, this system is 7 km deep and includes the unit B aquitard, as well as basement topography and variation in the thickness of unit A.

Appendix F

Heat balance

Heat balance calculations can be used to show whether the observed heat output is indicative of anomalous heat sources or whether it could be caused by hydrologic circulation. A heat balance study by Ingebritsen et al. (1989) in the Cascade Range shows that "ground-water circulation sweeps sufficient heat out of areas where rocks younger than 6 Ma are exposed to account for the anomalously high advective and conductive heat discharge measured in older rocks at lower elevations". Ingebritsen et al. (1989) suggest that the anomalously high heat flow observed in this area is not due to midcrustal magma, as other investigators have postulated, but may be caused instead by regional ground-water flow.

In this study, we perform a heat balance calculation for the Socorro area in order to determine whether the heat output observed at the surface is so large as to require the influence of anomalous heat sources (such as upper crustal magma) either within or near the system. Alternatively, if the observed heat output could be provided by a basal heat flow typical of the Rio Grande rift, that would suggest that the thermal effects of crustal magma are not observed at the surface in the Socorro hydrothermal system. This would not preclude the existence of upper crustal magma. Magmatic heat could be masked by subsurface ground-water advection having no surface expression within the study area, or magma could be of such small volume, or have been emplaced so recently as to have no thermal expression at the surface at this time.

In order to make a heat balance calculation, a three dimensional system must be defined. Figure F1 shows the system we have chosen in which to balance heat input and output; this system is quite different from the two dimensional system

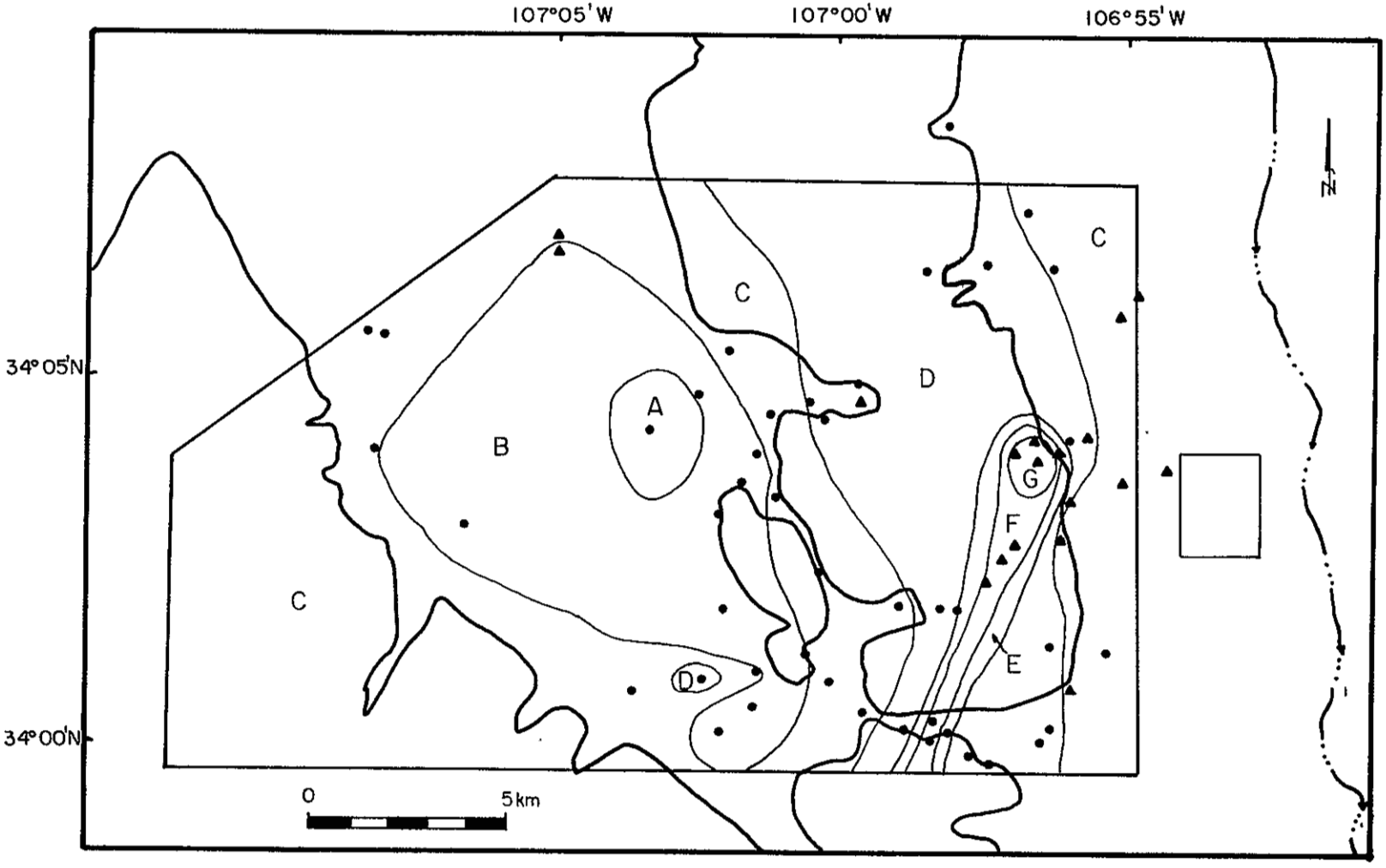

Fig. F1. System as defined for heat balance calculations is shown by five sided polygon in this figure. Heat-flow contours are included, and the areas between contour lines are labeled A through G. These areas are used in calculating the total surface heat flux (Table F1).

which is modeled elsewhere in this study. The areas of geothermal interest are southern La Jencia Basin and the Socorro mountain block. The hydrologic system which includes these areas is somewhat larger, and not entirely well defined. Recharge occurs largely in and near the Magdalenas. We assume that there is a hydrologic divide in the Magdalena Mountains which separate the Socorro hydrothermal system to the east from another ground-water system to the west, and we assume this divide is a ridge in the northern Magdalena Mountains. The northern and southern boundaries to the flow system are somewhat arbitrary; we choose system boundaries to be roughly parallel to the ground-water flow passing through the northern end of the Magdalena Mountains and passing through Socorro Canyon, although it is possible that some ground water leaves the system through these boundaries. We chose the eastern boundary of the system near the eastern front of the Socorro mountain block, at which point ground water either discharges at springs, or flows into the Socorro Basin ground-water system as underflow. The bottom boundary at the system is generally defined as being below the zone of ground-water circulation.

Heat Conduction

Conventional tectonic heat flow (q_z) is the vertical convective heat flow per unit area, defined by

$$q_z = -k_\Theta \frac{\partial T}{\partial z} \tag{F1}$$

where k_Θ is the thermal conductivity of the material through which the heat flow is determined. In order to perform a heat balance calculation we must determine the total heat conducted out of the system by integrating the vertical heat flow over the area of the system:

$$Q = \int q_z \, dA \tag{F2}$$

We performed this intergration graphically using a contour map of heat-flow determinations (Figure F1). A representative heat flow within a contour interval (q_i) was determined, sometimes by taking a simple average of the values within the interval. The area of the interval (A_i) was determined by superimposing the contour map on a fine grid and counting the grid blocks within the contour interval. The net heat flux (Q_Θ) was determined by

$$Q_\Theta = \sum_i q_i A_i \qquad \text{(F3)}$$

The average basal heat flow (q_b) is determined by dividing the total heat output by the surface area of the system; it represents the average basal heat input required to produce the observed heat output. A sample calculation is shown in Table F1. Several repetitions of this process led to total heat outputs between 23 and 27 $\times 10^6$ W, and a q_b of 70 to 80 $mW\ m^{-2}$.

These calculations were made assuming that the heat flow in the eastern Magdalena Mountains (where no measurements exist) is represented by heat flows measured in western La Jencia Basin (included in zone C, Figure F1). In the sample calculation of Table F1, heat flow in the eastern Magdalena Mountains has been assumed to be 70 $mW\ m^{-2}$. Uncertainty in the heat flow of this area introduces the most uncertainty into these calculations. For example, if the average heat flow of zone C were 60 $mW\ m^{-2}$ (instead of 70 $mW\ m^{-2}$), the average conductive heat flow would be 70.3 $mW\ m^{-2}$ (instead of 75.5 $mW\ m^{-2}$).

The net heat conducted into the system is unknown. It is unlikely that any heat-flow measurements in the Socorro area penetrate below the zone of hydrologic perturbation. It is reasonable to assume that the background heat flow in the Socorro area is within the range of heat flows typical of the Rio Grande rift: i.e., 75 to 100 $mW\ m^{-2}$ (Reiter et al, 1986), but there is also the possibility of

Table F1: Graphical Intergration of Conductive Heat Flow				
Sample Calculation				
Zone	Heat-Flow Range	q_i	Area	Net Heat
	$mW\ m^{-2}$	$mW\ m^{-2}$	$m^2 \times 10^6$	$W \times 10^6$
A	17 - 25	22	4.6	.10
B	25 - 50	40	70.7	2.83
C	50 - 75	70	169.4	11.86
D	75 - 125	100	71.9	7.19
E	125 - 200	160	4.9	.78
F	200 - 350	250	5.8	1.45
G	350 - 490	400	1.5	.60
Totals			328.8	24.81
Average Heat Flow:75.5 $mW\ m^{-2}$				

Table F1. Sample calculation of numerical integration of conducted surface heat flow. Zones consist of the areas between temperature contours as shown in Fig. F1, q_i is the typical heat flow estimated for zone i, "Net Heat" is the product of q_i and the area of zone i, "Totals" are the total area of the system as shown in Fig. F1, and the total heat conducted out of this system.

anomalous heat input from magma in the upper crust.

Heat Advection

Fluid flow can transport heat in or out of the system by advection. The amount of heat transported by advection (Q) depends on the difference in temperature between fluid entering and leaving the system, and the fluid flow rate.

$$Q = \rho\, c\, V\, (T_{out} - T_{in}) \qquad \text{(F4)}$$

where ρ is the fluid density ($10^3\ kg\ m^{-3}$), c is the specific heat of the fluid ($4.185 \times 10^3\ J\ m^{-1o} K^{-1}$), V is the volumetric fluid flow rate ($m^3\ s^{-1}$), and T_{in} and T_{out} are the fluid inflow and outflow temperatures.

The heat advected out of the system by the Socorro thermal springs (Q_S) can be estimated fairly easily. For the purposes of this study, the Socorro thermal springs consist of Socorro Springs and Sedillo Springs. We neglect nearby Cook Springs; discharge from Cook Springs appears to be much cooler and of much less quantity than that of Socorro and Sedillo springs (Table F2).

We estimate the average inflow temperature from the mean annual air temperatures. Gabin and Lesperance (1977) give a mean annual air temperature of $11.1^o\ C$ for the town of Magdalena at 2000 m elevation. We suggest an average inflow water temperature of $10 - 13^o\ C$. Using these values T_{out} and T_{in}, and values of spring discharge from Table F2 for V, we obtain a range of values for Q_S of 1.8 to $2.5 \times 10^6\ W$.

Preliminary Heat Balance

A simplified heat balance for the Socorro system is illustrated in Figure F2. In this preliminary model we assume that heat output equals the sum of net surface heat conduction ($Q_\Theta = 24.8 \times 10^6\ W$) and heat advection by thermal springs ($Q_S \approx 2.2\ W \times 10^6$). In steady-state conditions

$$Q_{in} = Q_{out} = Q_\Theta + Q_S = \approx 27 \times 10^6\ W \qquad \text{(F5)}$$

The average basal heat flow (q_b) that would produce this much heat is obtained by dividing Q_{in} by the area of the system ($3.28 \times 10^8\ m^2$). In this case $q_b = 82\ mW\ m^{-2}$. Addition of the heat advected by the thermal springs into the problem has added 6 $mW\ m^{-2}$ to the value of q_b determined using conductive heat output alone ($\Delta q_b = 6\ mW\ m^{-2}$).

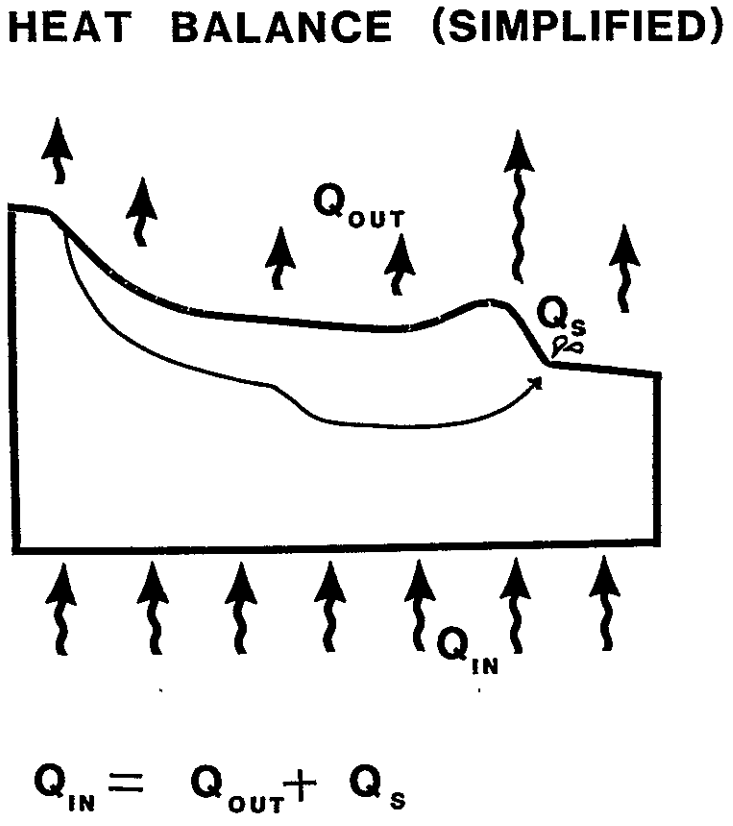

Fig. F2. Simplified heat balance. This figure represents a generalized cross section from the Magdalena Mountains to Socorro Basin. Long thin line represents ground water flowing from the Magdelena Mountains to discharge at the Socorro thermal springs. Fat arrows represent conductive heat flow. Q_{out} is the net heat conducted out of the top surface of the system, Q_{in} is the net heat conducted into the base of the system, Q_s is the heat convected out of the system by the thermal springs.

Table F2; Hydrologic Flow Information			
Flow component	Discharge	Recharge	Temperature
	$m^3\ s^{-1}$	$m^3\ s^{-1}$	^oC
Socorro Springs	0.0167 - 0.0189 (1)		32 - 34 (1,3)
Sedillo Springs	0.0060 - 0.0069 (1)		32 - 33 (1,3)
Cook Springs	0.0003-0.0006 (3)		13 - 19 (3)
Other Springs	0.0018 (4)		13 - 16 (4)
Magdalena Mnt.		0.162 (2)	10 - 13 (5)
Soc.-Lem. Mnt.		0.016 (2)	
Underflow	0.150 - 0.153 (5)		32 - 40 (5)
Sources of data indicated by #in parentheses:			
1 Gross and Wilcox, 1983			
2 Anderholm, 1987			
3 Summers, 1976			
4 Clark and Summers, 1971			
5 Estimates made as part of this study			

Table F2. Hydrologic information from the Socorro area. The magnitude and temperature of discharge and recharge components are listed.

So far, our estimates of q_b obtained from surface heat output are not anomalously high. Heat flows in the Rio Grande rift are typically between 75 and 100 $mW\ m^{-2}$, and so a value of 82 $mW\ m^{-2}$ for the Socorro area certainly does not suggest the presence of anomalous crustal heat sources. However, this estimate of q_b is a minimum value. The calculations described above neglect the considerable amount of heat which may be advected out of the system by hydrologic underflow. This heat would not be observed at the surface within the system (Fig

F1).

Hydrologic Balance

In order to make a more complete accounting of the heat balance in the Socorro area, it is necessary to estimate the hydrologic underflow out of the system. We have no measurements of subsurface hydrologic flux out of the system, nor any measurements of the temperature of deep subsurface waters, and so we cannot estimate the heat transported by underflow with any degree of confidence. In the following discussion we estimate the the possible thermal effects that a large amount of underflow could have.

In order to estimate the maximum reasonable hydrologic underflow, we employ a simplistic hydrologic balance of the Socorro geothermal system, illustrated in Figure F3. The recharge from the Magdalena Mountains (R_M) plus the smaller recharge component associated with the Socorro mountain block (R_S) constitutes the hydrologic input into the system (we neglect the possibility of ground-water underflow entering the system from west of the Magdalena Mountains). Hydrologic outflow consists of surface discharge from springs within the system (D_S), which includes all springs listed in Table F2, and subsurface flow (underflow) out of the system (D_U). We neglect ground-water withdrawal by pumpage in La Jencia Basin, probably a very small quantity.

Under steady-state conditions

$$R_M + R_S = D_S + D_U \tag{F6}$$

Values for R_M, R_S and D_S are obtained from Table F2. Applying Equation (F5) we obtain a value of 0.15 $m^3\ s^{-1}$ for D_U. In all probability, not all underflow leaves the system through the eastern boundary (as Figure F3 implies); underflow may also leave through the northern and southern boundaries. The

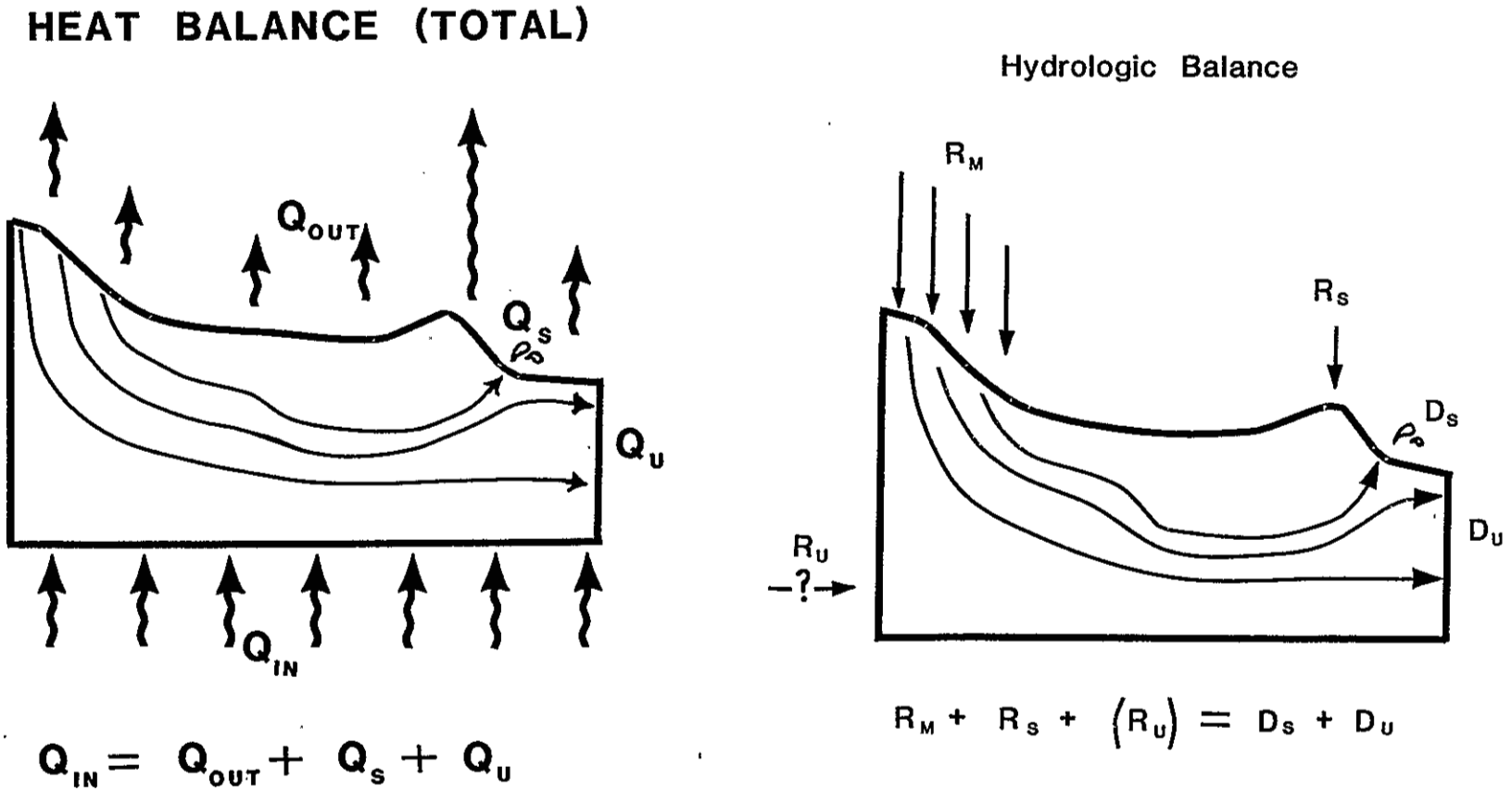

Fig. F3. More complete heat balance and hydrologic balance. Q_{out}, Q_{in} and Q_s are defined in the caption of Fig. F2. Q_u is the heat convected out of the system by hydrologic underflow. R_M, R_S and R_U represent recharge to the system by precipitation in the Magdalena Mountains, precipitation in the Socorro mountain block and underflow from beneath the Magdelena Mountains respectively (R_U is neglected in the calculations in the text.)

location at which underflow leaves the system does not influence these calculation (except as the depth of underflow affects its temperature), but underflow that does not pass through the Socorro mountain block would not influence a thermal anomaly associated with that mountain block.

The heat advected out of the system by underflow (Q_U) depends on the net flux and temperature of the fluid, according to Equation F4 (where T_{in} and T_{out} are the average temperatures at which the underflow enters and leaves the system). The temperature at which water enters the system is the temperature of recharge (both in the Magdalena Mountains and in the Socorro mountain block), which can be estimated using mean annual surface temperatures. We suggest a range of 10 to 15 ^{o}C for T_{in}. We have no way of measuring or even estimating to any degree of accuracy the average temperature at which underflow leaves the system. A range of values for the heat advected out of the system by underflow is shown in Table F3 for a variety of inflow and outflow temperatures. Also shown is the change in average basal heat flow associated with the heat advected out of the system by underflow (Δq_b):

$$\Delta q_b = \frac{Q_U}{AREA} \tag{F7}$$

When the possible heat output due to underflow is included in the heat balance, the average basal heat flow estimate ranges from 111 to 139 $mW\,m^{-2}$ (Table F4). These values of q_b are sufficiently high that they suggest the possibility of anomalous heat sources within or below the system. Unfortunately the estimate of heat transported by underflow is not based on any actual measurements of subsurface flow rates or deep subsurface temperatures (below 600 m). We can only reguard these estimates as a guide to the heat that could be transported by a large rate of underflow.

Table F3: Possible Heat Transport by Underflow			
T_{in}	T_{out}	Q_U	Δq_b
^oC	^oC	$W \times 10^6$	$mW\ m^{-2}$
15	30	9.4	29
10	30	12.6	48
10	35	15.7	48
10	40	18.8	57

Table F3. Possible heat transport by underflow. T_{in} and T_{out} are the assumed temperatures of inflow (recharge) and outflow (underflow out of the system). Q_U is the net heat that underflow would transport out of the system, Δq_b is the change in average basal heat flow that would be required when Q_U is included in the heat balance.

Table F4 summarizes our heat balance calculations; q_b increases as additional components of heat outflow are included.

Summary

In conclusion, heat balance calculations involving the Socorro hydrothermal system indicate that a basal heat flow of $\approx 82\ mW\ m^{-2}$ could produce the heat observed at the surface in the Socorro area. Surface heat output includes surface heat conduction and heat advected out of the system by thermal springs, both of which quantities can be estimated with some degree of accuracy. The resulting value of basal heat flow ($82\ mW\ m^{-2}$) is consistent with background heat-flow determinations for the Rio Grande rift of $75 - 100\ mW\ m^{-2}$ (Reiter et al., 1986), and does not indicate the necessity of anomalous crustal heat sources to explain the heat flows observed or the existence of thermal springs near Socorro. We conclude that if there are anomalous heat sources in the upper crust in the Socorro

Table F4: Summary of Heat Balance Calculation				
Conduction	Springs	Underflow	Total	Basal
Q_Θ	Q_S	Q_U	Q_{total}	q_b
$W \times 10^6$	$W \times 10^6$	$W \times 10^6$	$W \times 10^6$	$mW\ m^{-2}$
24.8			24.8	76
24.8	2.2		27.0	82
24.8	2.2	9.5	36.5	111
24.8	2.2	12.6	39.6	120
24.8	2.2	15.7	42.7	130
24.8	2.2	18.8	45.8	139

Table F4. Summary of heat balance calculations. Q_Θ, Q_S and Q_U are the net heat transported out of the system by conduction, by advection at the thermal springs and by advection of heat by (possible) underflow. Q_{total} is the sum of these three terms, and q_b is the average basal heat flow that would by required to produce the total heat output (Q_{total}).

area, the heat from these bodies is not observed at the surface in the Socorro area.

However, heat balance calculations are not complete until we include advective transport of heat out of the system in the subsurface (by underflow). No information exists concerning to the quantity or temperature of underflow, so we can only estimate what effect underflow could have, when certain assumptions are made. Assuming a large rate of underflow (equal to the rate of recharge to the system minus the rate of discharge at springs), a substantial amount of heat would be advected out of the Socorro system, sufficient to mask anomalously high heat input to the system.

This dissertation is accepted on behalf of the faculty of the Institute by the following committee:

Marshall Cates

Advisor

Allan R. Sanford

Fred W. Phillips

Allan Gilpatrin

John Wm. Schulz

Aug 30 1989

Date

Map 1

LOCATION MAP: SOCORRO GEOTHERMAL DATA

BARROLL, 1989

NM

0 1 2 3 4 5
km

SCALE 1 62,500

LEMITAR MOUNTAINS

* POLVADERA PEAK

SOCORRO BASIN

LA JENCIA BASIN

* NORTH PEAK

* STRAWBERRY PEAK

NOGAL CANYON

SOCORRO PEAK *

RIO GRANDE

WATER CANYON

BLUE CANYON

SOCORRO CANYON

MAGDALENA MOUNTAINS

CHUPADERA MOUNTAINS

NM TECH

SOCORRO

COOK SPRINGS

SOCORRO SPRINGS

SEDILLO SPRINGS

34°10'
34°05'
34°00'

107°15' 107°10' 107°05' 107°00' 106°55' 106°50'

Plate 2

NOGAL CANYON

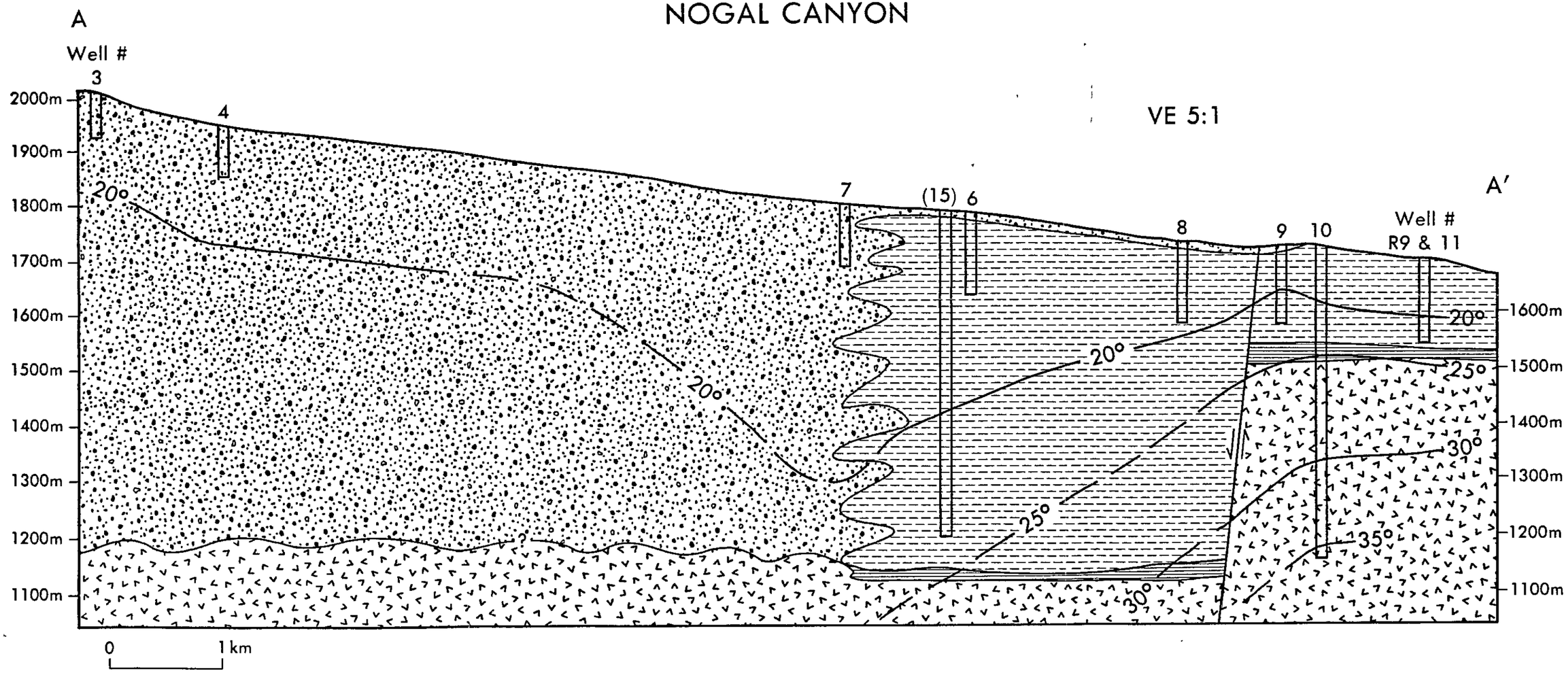

Plate 3

BLUE CANYON

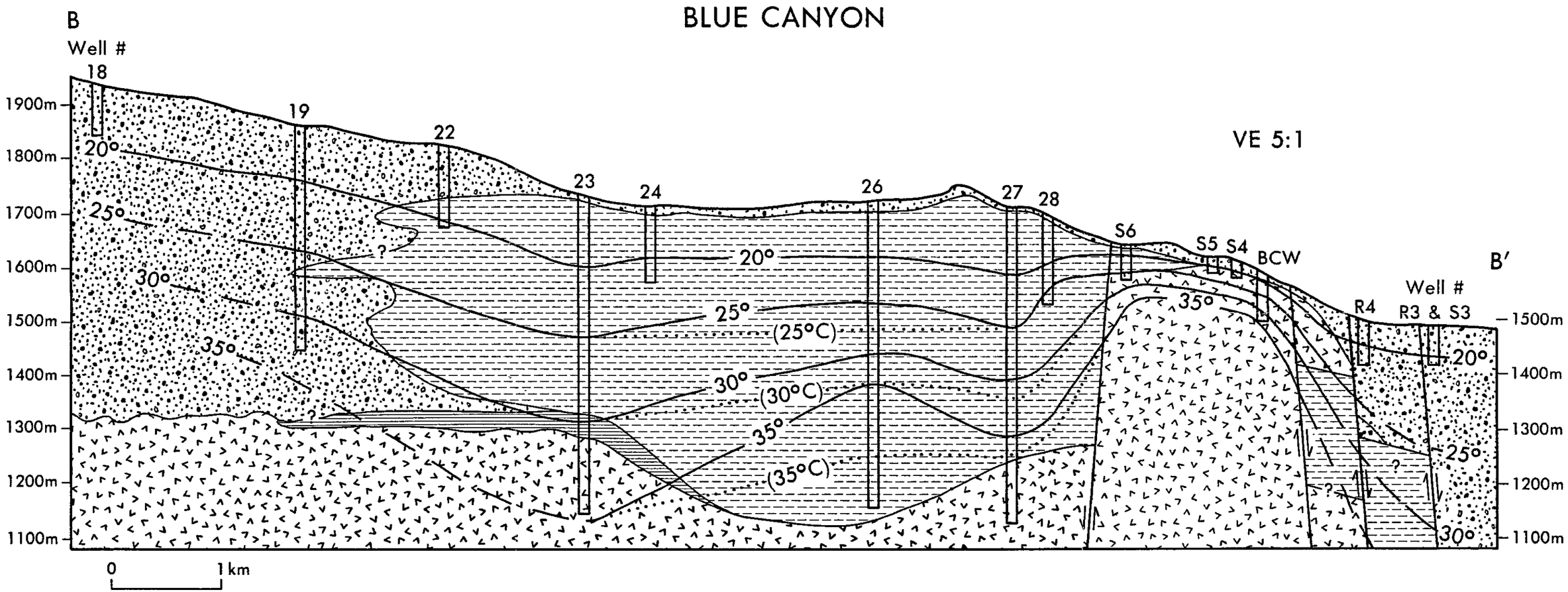

Plate 4

SOCORRO CANYON

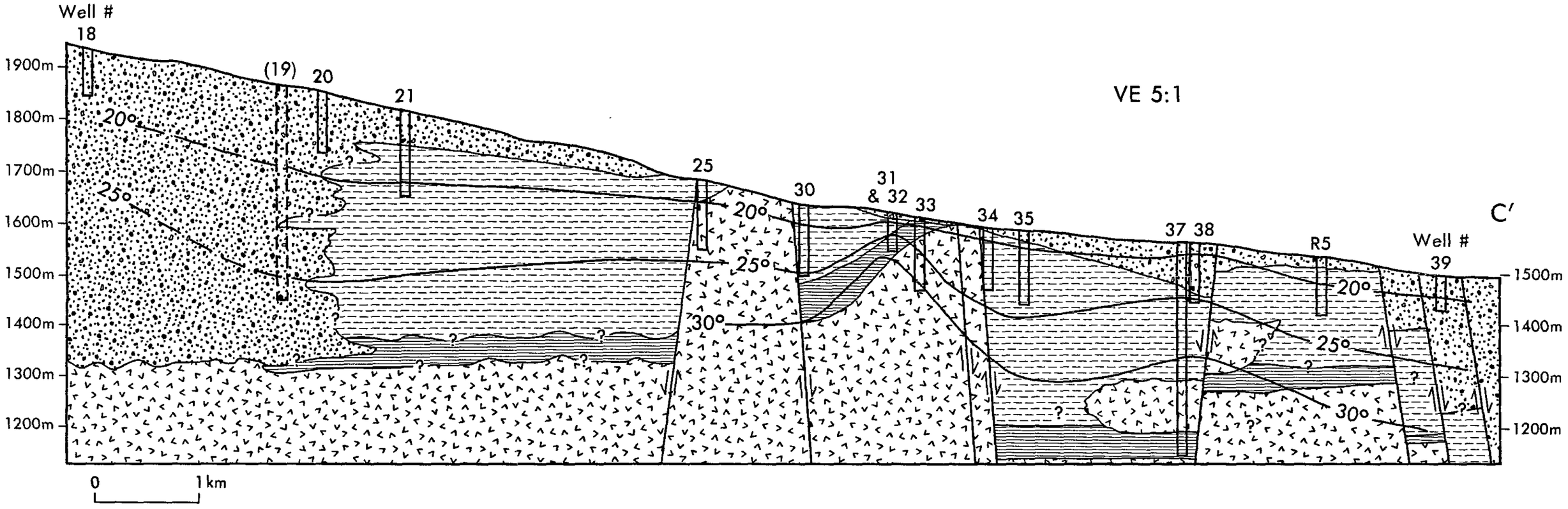

Plate Captions

Plate 1. Map of the Socorro Geothermal area. Wells shown with circles are from the industrial geothermal data set obtained between 1978 and 1980. Wells shown with triangles are from earlier studies. Numbers or letters and numbers are for well identification. Identification codes beginning with R are from Reiter and Smith (1977). Identification codes beginning with S are from Sanford (1977).

Plate 2. Cross-section AA' of observed subsurface temperatures and generalized geology of Nogal Canyon. Vertical rectangles indicate well control (of temperature and, in most cases, lithology). Well 15 is marked by parentheses because it is somewhat out of the line of cross section. Geology after Chamberlin, 1980, and Chapin and Foster (unpublished lithologic logs). Key to lithologic units found in Figure 9.

Plate 3. Cross-section BB' of observed subsurface temperatures and generalized geology of Blue Canyon. Vertical rectangles indicate well control (of temperature and, in most cases, lithology). Geology after Chamberlin, 1980, and Chapin and Foster (unpublished lithologic logs). Key to lithologic units found in Figure 9.

Plate 4. Cross-section CC' of observed subsurface temperatures and generalized geology of Socorro Canyon. Vertical rectangles indicate well control (of temperature and, in most cases, lithology). Well 19 is marked by parentheses and dashed lines because it is somewhat out of the line of cross section and is used only for lithologic control. Geology after Chamberlin, 1980, and Chapin and Foster (unpublished lithologic logs). Key to lithologic units found in Figure 9.